MCAM in Melanoma Metastasis: The Role of Putative Endocytosis Motifs

Jake Harfield

School of Pharmacy and Biomedical Sciences, CHIRI Biosciences Research Precinct, Faculty of Health Sciences, Curtin University, GPO Box U1987, Perth, Western Australia.

Keywords: MCAM, metastasis, melanoma, recycling

Declaration

To the best of my knowledge and belief this thesis contains no material previously published by any other person except where due acknowledgment has been made.

This thesis contains no material which has been accepted for the award of any other degree or diploma in any university.

Jake Harfield

30 August 2021

Abstract

Melanoma cell adhesion molecule (MCAM) is a marker of melanoma metastasis andcontributes to melanoma progression. Cell surface expression of MCAM is integral toits function, but how MCAM is sorted and recycled through the cell is unknown. Twoputative endocytosis/sorting motifs have been identified in the intracellular domain of MCAM. Transduction of wild-type MCAM, and MCAM containing disruptive mutations in these sorting motifs, into an MCAM-negative cell line, produced cells with differences in morphology and spreading behaviour on matrix proteins. Disruption of the sorting motifs did not affect surface expression of MCAM but enhanced the directional motility of cells compared to the WT-expressing cell line. Both WT and MT MCAM consistently co-localised with F-actin and moesin in protrusions and structures resembling cytoskeletal stress fibres. Furthermore, both mutant cell lines consistently produced a structure believed to be the WRAMP (Wnt-receptor-actin-myosin-polarity) structure, which has been described by others to contribute to melanoma migration. Exploration into the recycling of MCAM showed significant co-localisation with Rab7-positive late endosomes, but not with early/recycling endosomes or lysosomes, suggesting that MCAM may be rescued from late endosomes. Preliminary investigations also suggested that retromer, a keyplayer in endosomal sorting, may not play a major role in MCAM trafficking. Further elucidating the role of MCAM in melanoma metastasis, as well as the recycling/sorting pathways involved, may identify new therapeutic targets for metastatic melanoma.

Acknowledgements

I would like to acknowledge every person who taught, guided, and supported me throughout the generation of this thesis. First and foremost is my primary supervisorDr Danielle Dye who oversaw my first steps in a research laboratory and without whom I would not have the skills and ability I have today. I would also like to sincerelythank my excellent co-supervisor Professor Deirdre Coombe. Together Danielle and Deirdre have a formidable wealth of knowledge and passion for science that I am grateful to have been able to tap into.

I would also like to thank all the members of the lab who trained and supported me throughout the last two or more years – especially Beverly Kinnear, Tenielle George,Catherine LeGrand-Heck, and Jess Murray. My sincere thanks also go to Dr Connie Jackaman for all the guidance and training on the confocal microscope and Jeanne Edmands for her assistance in flow cytometry and sorting.

Finally, and with sufficient cheesiness, I would like to thank my beautiful partner Jamie Pitcher for the endless emotional support she has given me over the last two years. I guess I should also acknowledge the first cause that led to this thesis being written - my mother Sarah and father Zo; without whom I would not be the man I amtoday (or literally here at all!).

This research is supported by an Australian Government Research Training (RTP) Scholarship.

Abbreviations

◦C	Degrees Celsius
AA	Amino acid
ACTAB	Beta actin
AGRF	Australian genome research facility
ALCAM	Activated leukocyte cell adhesion molecule
AKT	Protein kinase B
ANOVA	Analysis of variance
AP-2	Apetala 2
ATF-3	Activating transcription factor 3
BAR	Bin/Amphiphysin/RVS
BCA	Bicinchoninic acid assay
BCAM	Basal cell adhesion molecule (Lutheran protein)
BSA	Bovine serum albumin
c-myb	Cellular myb
CAM	Cell adhesion molecule
CArG	Geranylgeranyl pyrophosphate synthase
cDNA	Coding DNA
CRE	Cyclic adenosine monophosphate response element
CREB	Cyclic adenosine monophosphate response element-binding protein
CSC	Cargo selection complex
DAPI	4’6-diamidine-2’-phenylindole
DEPC	Diethyl pyrocarbonate
DMEM	Dulbecco’s modified eagle medium
DNA	Deoxyribonucleic acid
ECM	Extracellular matrix
EDTA	Ethylenediaminetetraacetic acid
EE	Early endosome

EMT	Endothelial-mesenchymal transition
EPC	Endothelial progenitor cells
ER	Endoplasmic reticulum
ERM	Ezrin-radixin-moesin
ERULS	Ezrin-rich uropod-like structure
FAK	Focal adhesion kinase
FC	Flow cytometry
FCS	Foetal calf serum
FERM	4.1-ezrin-radixin-moesin
FGF-4	Fibroblast growth factor 4
FITC	Flourescein Isothiocyanate
G-CSF	Granulocyte-colony stimulating factor
Gal	Galectin
GAPDH	Glyceraldehyde 3-phosphate dehydrogenase
GFP	Green fluorescent protein
GTP	Guanosine 5'-triphosphate
GD	Grantham deviation
GV	Grantham variation
HBS	HEPES buffered saline
HEPES	4-(2-hydroxyethyl)-1-piperazineethanesulfonic acid
HIV	Human immunodeficiency virus
HRP	Horse radish peroxidase
IgSF	Immunoglobulin superfamily
ICAM-1	Intercellular adhesion molecule 1
ICD	Intracellular domain
Id-1	Inhibitor of DNA binding 1
IF	Immunoflourescence
IgG	Immunoglobulin G
INR	Initiator element

IQGAP1	IQ motif containing GTPase activating protein 1
kDa	Kilodalton
LA	LL623-624AA
LB	Luria-Bertani
LE	Late endosome
mA	MilliAmperes
MAPK	Mitogen-activated protein kinase
MCAM	Melanoma cell adhesion molecule
MCAM-S	MCAM short isoform
MCAM-L	MCAM long isoform
MCS	Multiple cloning site
MFI	Mean fluorescent intensity
MDCK	Madin-Darby Canine Kidney
MLCK	Myosin light-chain kinase
MMP	Metalloproteinase
MPR	Mannose-6-phosphate receptor
mRNA	Messenger ribonucleic acid
MT	Mutant
MVB	Multi-vesicular body
MyoD	Myoblast determination protein 1
MSH	Melanocyte stimulating hormone
NCAM	Neural cell adhesion molecule
ND	Not determined
NFκB	Nuclear factor kappa-light-chain-enhancer of activated B cells
NGF	Nerve growth factor
NK	Natural killer cells
O/N	Overnight
PAR-1	Protease-activated receptor 1
PBS	Phosphate buffered saline

PBS/BSA	PBS/0.5% w/v BSA
PBST	PBS/0.1% v/v Tween-20
PCR	Polymerase chain reaction
PECAM-1	Platelet endothelial cell adhesion molecule 1
PFA	Paraformaldehyde
PI3K	Phosphoinositide 3-kinase
PKC	Protein kinase C
PMA	Phorbol 12-myristate 13-acetate
PROVEAN	Protein variation effect analyser
PVDF	Polyvinylidene difluoride
qPCR	Quantitative polymerase chain reaction
RE	Recycling endosome
RE	Restriction enzyme
RGP	Radial growth phase
RhoA	Ras homolog family member A
RhoB	Ras homolog family member B
RNA	Ribonucleic acid
RPMI	Roswell Park Memorial Institute
RT	Room temperature
SCRIB	Protein scribble homolog
SDHA	Succinate dehydrogenase complex subunit A
siRNA	Small interfering RNA
sMCAM	Soluble MCAM
SNX	Sorting nexin
SP1	Specificity protein 1
TBP	TATA-binding protein
TGN	Trans-Golgi network
VANGL2	Vang-like protein 2
VE	Vascular endothelial
VEGF	Vascular endothelial growth factor

VEGFR	Vascular endothelial growth factor receptor
VGP	Vertical growth phase
VPS	Vacuolar protein sorting
UCOE	Ubiquitously acting chromatin opening elements
UV	Ultraviolet
WB	Western blot
WRAMP	Wnt-receptor-actin-myosin-polarity
WT	Wild type
YA	Y641A

TABLE OF Contents

CHAPTER I:

Introduction and Literature Review

1. Melanoma Biology and Epidemiology

Melanoma was first described in 1787 by John Hunter, and the term melanoma was coined by Sir Robert Carswell from the Greek "*melas*" meaning black, and "*-oma*" denoting growth.Melanoma is a malignant tumour that arises from the uncontrolled proliferation of melanocytes, which are melanin-producing neural-crest-derived cells located in the epidermis of the skin, hair follicles, and in the choroidal layer of the eye (Abdel-Malek et al. 1999; Abdel-Malek et al. 1995; Lerner and McGuire 1964; Tsatmali et al. 2002). Cutaneous melanoma is the most common form of melanoma and is a particularly aggressive form of skin cancer.

1.0.1 Epidemiology

The incidence of melanoma has risen faster than almost all other cancers (Ferlay et al. 2015; Kosary et al. 2014; Rigel and Carucci 2000), as have hospitalisations arising from patients suffering from melanoma (Australian Institute of Health and Welfare 2016). Australia has the second-highest rate of melanoma worldwide (35/100,000 per year) and it remains the fourth most commonly diagnosed cancer in Australia as of 2016 (Australian Institute of Health and Welfare 2016). Furthermore, due to its tendency to metastasise, melanoma is the deadliest form of skin cancer and is responsible for 80% of skin cancer related deaths (Australian Institute of Health and Welfare 2016; Duggan et al. 2016; Estecha et al. 2009; Gloster and Brodland 1996; Linos et al. 2009; Miller and Mihm 2006).

Melanoma is classified according to tumour thickness and ulceration at diagnosis, with stage 0, I and II referring to tumours that have not spread beyond the skin. Stage III melanoma indicates tumour cells have spread to lymph nodes and in stage IV, melanoma cells have spread to organs, such as brain, liver or lungs (Gershenwald et al. 2017); which is known as metastatic melanoma (MM). Following excision of a primary lesion, approximately 30% of patients then develop metastasis in distant organs; including up to 15% of patients with very thin primary tumours (< 1mm) (Sandru et al. 2014).

1.0.2 Melanoma treatment

Prior to the recent introduction of targeted and immunotherapies, the only treatment for metastatic melanoma available was decarbazine, which has an objective response rate of 13-30%, with a median overall survival of 9.1 months (Eggermont and Kirkwood 2004). As of 2011, a number of new treatments became available; including immunotherapies, targeted therapies and most recently an oncolytic viral therapy (Lee et al. 2017). Targeted therapies include kinase inhibitors (vemurafenib, dabrafenib, trametinib) which are indicated for the 50% of patients whose tumours harbor a mutation in the *BRAF* gene, leading to constitutive activation of the mitogen-activated protein kinase (MAPK) pathway. Unfortunately, some patients are

intrinsically resistant to BRAF inhibitors; and the majority of patients who do respond to treatment, become resistant in less than 12 months (Griffin et al. 2017).

Immunotherapies include monoclonal antibodies (mAbs) that target cytotoxic T-lymphocyte-associated-protein-4 (CTLA-4) and programmed cell death receptor-1 (PD-1) (Lee et al. 2017). These immunotherapies suppress inhibitory receptors on T cells and restore an anti-tumour immune response (Seidel et al. 2018). Used alone, mAbs targeting PD-1 (pembrolizumab and nivolumab) have an objective response rate (ORR) of 33-43% and mAbs targeting CTLA-4 (tremelimumab and ipilimumab) have an ORR of 10.7 - 19% in metastatic melanoma (Seidel et al. 2018). However, when used together, nivolumab and ipilimumab demonstrated an ORR of 57.6%, and 52% overall survival at five years. However, despite this marked improvement in outcomes, many patients do not show a durable response to immunotherapy (Larkin et al. 2015; Larkin et al. 2019). In addition, treatment-related toxicities remain a problem, particularly in patients receiving combination PD-1/CTLA-4 treatment (Buchanan et al. 2021).

In 2015, the Food and Drug Administration (FDA, USA) also approved the use of an oncolytic virus, tamilogene laherparepvec (T-VEC); which is genetically modified to enable selective replication inside tumour cells. Although the exact mechanism of action of T-VEC is not completely understood, it is believed tumour cell lysis and release of tumour antigens help augment tumour-specific immunity (Kohlhapp and Kaufman 2016). T-VEC has also been trialled in combination with anti-PD1 immunotherapy, with a phase 1b trial reporting an ORR of 48-57% (Long et al. 2016).

Additional immunotherapies in clinical trial for melanoma include a mAb targeting lymphocyte activation gene-3 (LAG3), which is another immune checkpoint receptor; and cytokine therapies such as interleukin-2 (IL-2) (Buchanan et al. 2021). IL-2 stimulates CD8 T cells and natural killer (NK) cells, but can also stimulate regulatory T cells, which reduces anti-tumour activity. Thus new-generation IL-2 based therapies aim to preferentially activate CD8 T cells and NK cells only (Buchanan et al. 2021). Finally, T cell re-direction is also being explored using a new class of biologicals, immune mobilising monoclonal T-cell receptors against cancer (immTACs), which bind tumour-associated antigens on cancer cells and assist to recruit T cells to the tumour (Buchanan et al. 2021).

1.1 Malignant Change and Metastasis

1.1.1 Malignant Change

Ultraviolet (UV) light is the primary environmental risk factor for transformation of melanocytes to a melanoma. Under normal conditions, keratinocytes produce melanocyte stimulating hormone (MSH) in response to UV-induced DNA damage. MSH binds to the melanocortin 1 receptor on melanocytes, inducing the production of melanin (the pigment that protects against further UV-related DNA damage) (Seyfried and

Huysentruyt 2013). However, UV exposure can also cause DNA damage in melanocytes, oxidative stress and inflammation; all of which contribute to the early stages of melanoma tumorigenesis (Leonardi et al. 2018).

Melanoma metastasis is linked to both cellular mutations and alterations in the microenvironment, which culminate in protein expression changes favourable to invasion and intravasation (Chiriboga et al. 2016; Falzone et al. 2016; Guarneri et al. 2017; Lee et al. 2014; Moro et al. 2014; Sandri et al. 2016). Mutations are frequently observed in both tumour suppressor genes and proto-oncogenes. Tumour suppressor genes often inactivated in melanocytic transformation include *PTEN, NF1, CDKN2A* and *p53,* while the proto-oncogenes *BRAF*, *NRAS, KIT* often harbour activating mutations (Hodis et al. 2012; Krauthammer et al. 2012). Additionally, mutations within thetelomerase reverse transcriptase (*TERT*) core promoter are highly elevated in metastatic melanoma and is likely to be a major tumorigenic mechanism (Chappell et al. 2011). Cumulatively, these genetic changes often activate the two major signalling pathways involved in cell proliferation and survival: the mitogen-activated protein kinase (MAPK) and phosphatidylinositol 3-kinase/protein kinase B (PI3K/AKT) pathways (Wang et al. 2007). Indeed, up to 90% of melanoma display increased MAPK activation (Cohen et al. 2002; Gray-Schopfer et al. 2007). The increased activation of MAPK is often associated with *BRAF* mutations, which are found in ~50% of cutaneous melanoma (Curtin et al. 2005). Other driver mutations in melanoma include variations in *NRAS* (seen in 15-30% of tumours) (Maertens et al. 2013), *NF1* (10-15%) (Beadling et al. 2008; Whittaker et al. 2013), and *KIT* (2- 8%) (Handolias et al. 2010; Liu et al. 2014). For an extensive review on thegenetic and molecular abnormalities underpinning the malignant transformation of melanocytes, see (Testa et al. 2017).

The accumulation of mutations in tumour suppressor and proto-oncogenes over time may eventually produce a malignant cell capable of uncontrolled proliferation. However, additional changes are necessary to enable a complete metastatic phenotype, including the immunological state and anatomical site. TNF and IL-6, two pro-inflammatory cytokines, maymodulate melanoma aggressiveness. TNF is thought to upregulate the activity of metalloproteinases (MMP) in the skin (Han et al. 2001; Rossi et al. 2018). The MMPs, especially MMP-2 and MMP-9, degrade the extracellular matrix (ECM) and allow tumour intravasation (Falzone et al. 2016; Moro et al. 2014). In addition to MMP-2 and MMP-9, MMP-12, MMP-14, and MMP-19 have also been implicated in melanoma aggressiveness (Gong et al. 2018; Salemi et al. 2018; Zhang et al. 2015) However, the role of TNF is controversial as it has been reported to both inhibit and promote cancer growth (Rossi et al. 2018).

Further signalling pathways implicated in the progression of melanoma include Wnt signalling, the Notch pathway, endothelins, and SOX proteins (Liu et al. 2014) Angiogenesis also plays central role in supplying blood to the tumour and ensuring its continued development, with VEGF a key player in melanoma angiogenesis (Dewing et al. 2012).

The uncontrolled cellular proliferation of melanocytes thus results in the formation of benignnevi, which may lay dormant for years before accumulating the mutations which produce a primary melanoma tumour.

1.1.2 Metastasis: Invasion, Intravasation, and Extravasation

Metastasis is believed to be the primary causative factor in ~90% of cancer-related deaths (Chaffer and Weinberg 2011). Metastasis is the process by which cancer cells spread beyond the primary tumour to distant tissues or organs (Australian Institute of Health and Welfare 2016), and is predominantly a linear cascade through threemajor processes: invasion, intravasation, and extravasation. Invasion involves cells detaching from the primary tumour and invading the surrounding tissue. In melanoma, tumour cell invasion occurs in two phases. First, during the radial growth phase (RGP), melanocytes acquire a proliferative and survival phenotype. Following this, during the vertical growth phase (VGP), cells invade downwards through the dermis and hypodermis (Elder 2006). Primary melanoma cells then intravasate into blood or lymphatic vessels, where they must evade detection by the immune system to allow dissemination to distal sites. Finally, the cells extravasate from the vessels and invade surrounding tissue, before proliferating to form a secondary tumour (Seyfried and Huysentruyt 2013).

1.2 Cell Adhesion Molecules

Cell adhesion molecules (CAMs) are a large family of transmembrane glycoproteins categorised into four structurally and functionally distinct subfamilies: integrins, selectins, cadherins, and the immunoglobulin superfamily (IgSF) (Fig. 1). The function of CAMs is integral to tissue homeostasis, regulating development, differentiation, migration, and tissuemaintenance (Homrich et al. 2015). They function by directly modulating the interaction between cells and neighbouring cells or the ECM, as well as playing a role in signal transduction (Cohen et al. 1997). Changes inthe expression of CAMs has been linked to metastasis in multiple cancers (Farahani et al. 2014), where their aberrant or altered expression can disrupt tissue homeostasis or produce malignant cell phenotypes.

1.2.1 Immunoglobulin superfamily

This review will focus on the largest and most diverse family of CAMs, the IgSF, which contains over 765 members (Wai Wong et al. 2012). IgSF proteins mediate calcium-independent adhesion and are categorised by the presence of one or more Ig-like domains in the extracellular region (Homrich et al. 2015). IgSF members often interact with other Ig-like domains via their *N*-terminal domains, as well as with integrins and carbohydrates, thereby coordinating both homophilicand heterophilic interactions (Wai Wong et al. 2012). The *C*-terminal domain often interacts with the cytoskeleton, or cytoskeletal adaptor

proteins, as well as signalling complexes. Multiple IgSF members have been identified as markers of cancer metastasis including melanoma cell adhesion molecule (MCAM), neural cell adhesion molecule (NCAM), platelet endothelial cell adhesion molecule (PECAM-1), activated leukocyte cell adhesion molecule (ALCAM), intercellular adhesion molecule (ICAM-1) and L1 cell adhesion molecule (L1CAM) (Wai Wong et al. 2012).

Figure 1. Cell adhesion molecule classes

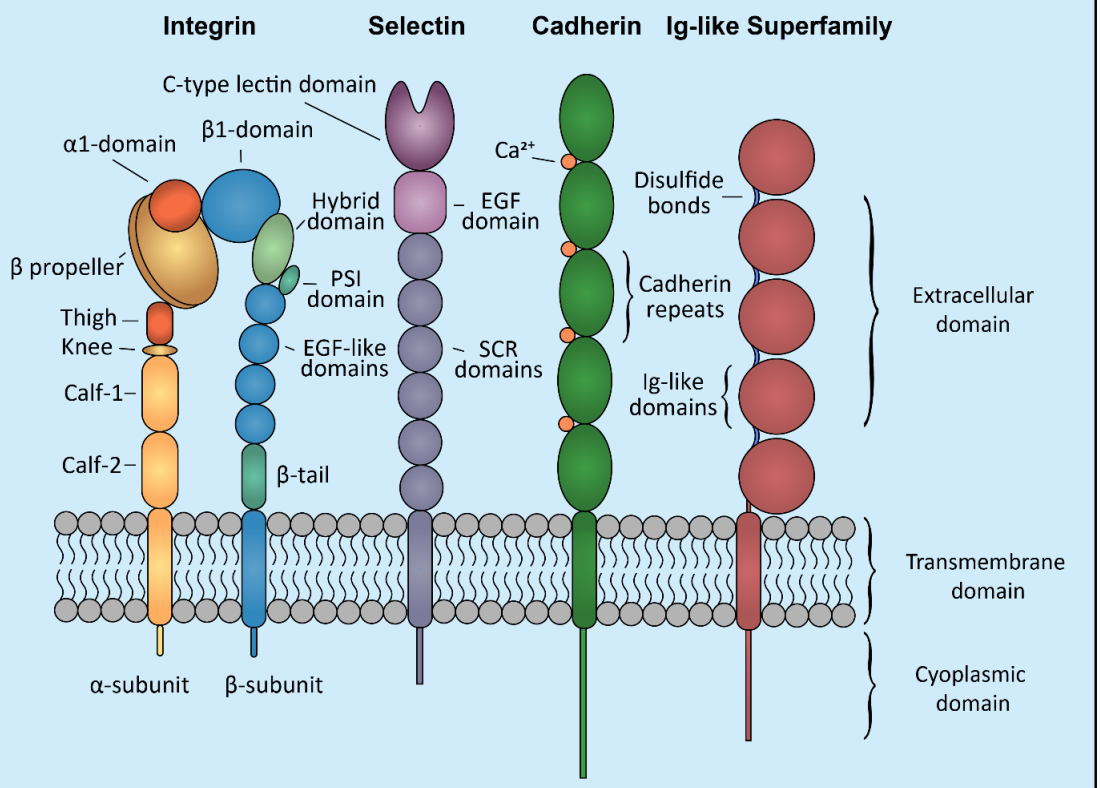

Figure 1. Protein structure of cell adhesion molecule classes. From left to right: Integrins, selectins, cadherins, and the immunoglobulin-like superfamily. PSI = plexin-semaphorin-integrin, EGF = laminin-epidermal growth factor, SCR = short consensus repeat, Ig = immunoglobulin.

1.2.2 Integrins

Integrins are large heterodimeric transmembrane proteins which are primarily involved in the linkage of the intracellular cytoskeleton to the ECM via large signalling complexes (Campbell and Humphries 2011). Integrins are composed of covalently bound α- and β- subunits and respond to the pericellular environment through a complex receptor activation mechanism, which acts through conformational changes in the structure of the receptor (Campbell and Humphries 2011). There are eighteen α-subunits and eight β-subunits, comprising 24 integrin heterodimers with varying functions and affinities (Howe and Addison 2012). β1-integrin is the most common β-subunit and is found in half of the possible heterodimers. Furthermore, and importantly, the β1-integrin subunit is most commonly found in the heterodimers upregulated in

tumours and is involved in ECM binding (Howe and Addison 2012). Aberrant and modified integrin expression and function has been noted in melanoma and is thought to contribute to progression (D'Onofrio et al. 2008; Kramer et al. 1991). Furthermore, possible coordination between MCAM and β1-integrin has been hypothesised, with expression of the chicken homolog of MCAM (HEMCAM) associated with downregulation of β1-integrin expression (Alais et al. 2001). Further, a similar finding was described in human SB2 melanoma cells transfected withMCAM, where MCAM expression was associated with a modest decrease in β1-integrin expression (Dye 2007).

1.3 Melanoma Cell Adhesion Molecule (MCAM)

1.3.1 Background

MCAM (CD146/Mel-CAM/S-endo1/Muc18/gicerin/HEMCAM) is a member of the IgSF and isassociated with many cancers, including melanoma, breast, pancreatic, prostate, gastric, ovarian, lung and kidney cancers, osteosarcoma, Kaposi sarcoma, Schwann cell tumours, and leiomyosarcoma (Stalin et al. 2017). MCAM was discovered as a marker for melanoma metastasis due to itsexpression in melanoma but not in primary melanocytes (Lehmann et al. 1989) and has since been linked to poor prognosis in melanoma, lung cancer, and digestive system cancers (Rapanotti et al. 2017; Stalin et al. 2017; Zeng et al. 2017). The 5- year survival rate of patients with MCAM-positive melanoma is 40%, whereas for MCAM- negative tumours it is 95% (Dye et al. 2013). Furthermore, MCAM is thought to be expressed in 70-90% ofmelanoma tumours (Pearl et al. 2008). Like other CAMs, MCAM modulates a diverse range of homeostaticcell functions including cell adhesion, migration, invasion, proliferation, survival, and angiogenesis, and thereby directly promotes tumour progression (Johnson et al. 1997; Stalin et al. 2016; Xie et al. 1997; Zheng et al. 2016).

1.3.2 Gene Structure

The MCAM receptor consists of three domains: intracellular, transmembrane, and the extracellular domain containing five Ig-like domains (V1-V2-C2-C2-C2) (Fig. 2). *MCAM* is a ~14kb gene located at chromosome 11 q23.3 with a 3.3 kb mRNA and 1.94 kb coding region (Kuske and Johnson 1999; Lehmann et al. 1989). The coding region contains sixteen exons, thirteen of which encode the five Ig-like domains, with the remaining three encoding the intracellular and transmembrane domains (Fig. 2A). The V1 Ig-like domain is encoded by three exons; however, the remaining Ig-like domains are encoded by two exons. In these, the splice junctions lie between the β-sheets that form the Ig-like domains (Sers et al. 1993)(Fig. 2A). Furthermore, *MCAM* contains three poly(A) signals which are found at the fifth and fifteenth exons and result in alternative splicing and the formation of up to three isoforms – MCAM-Long (MCAM-L), MCAM-short (MCAM-S), and soluble MCAM (sMCAM)(Sers et al. 1993). *MCAM* is highly conserved between human, chicken, mouse, and

zebrafish: the coding sequence (CDS) of human *MCAM* shares ~73.8% identity with chicken MCAM and ~80.6% identity with mouse MCAM (Yang et al. 2001).

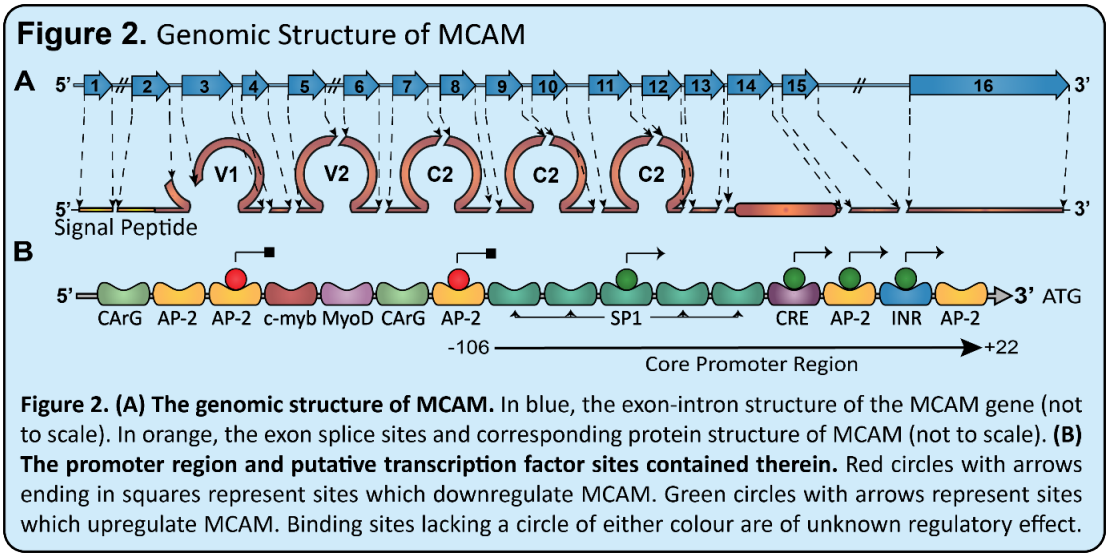

Figure 2. (A) The genomic structure of MCAM. In blue, the exon-intron structure of the MCAM gene (not to scale). In orange, the exon splice sites and corresponding protein structure of MCAM (not to scale). **(B) The promoter region and putative transcription factor sites contained therein.** Red circles with arrows ending in squares represent sites which downregulate MCAM. Green circles with arrows represent sites which upregulate MCAM. Binding sites lacking a circle of either colour are of unknown regulatory effect.

1.3.3 Gene Regulation

MCAM contains a TATA- and CAAT-box absent core promoter region (Sers et al. 1993). This core promoter region contains many putative transcription factor binding sites: Activator protein 2 (AP-2), specificity protein 1 (SP1), initiator element (INR), c-myeloblastosis (c-myb), myoblast determination protein 1 (MyoD), geranylgeranyl pyrophosphate synthase (CArG), and a cyclic-AMP response element (CRE)(Sers et al. 1993)(Fig. 2B). In total, the promoter region contains four AP-2 binding sites. The one found at -23 bp was found to upregulate reporter activity, while the two further upstream (-131 and -302) are thought to have a down-regulatory effect (Mintz-Weber and Johnson 2000). Furthermore, there are five Sp1 sites which are thought to be necessary for MCAM transcription, as deletion of all putative locations in the promoter region reduced core promoter activity by 80% (Mintz-Weber and Johnson 2000). Additionally, the INR initiator sequence is also linked to MCAM expression through basic helix-loop-helix (bHLH) regulatory factors, which may downregulateMCAM expression through phorbol 12-myristate 13-acetate (PMA) stimulation or upregulate MCAM expression via forskolin stimulation (Rummel et al. 1996). Importantly, deletion of the INR sequence completely abrogated MCAM expression (Karlen and Braathen 2000). Finally, MCAM expression may be modified byactivation of the G-couple protein receptor, protease-activated receptor 1 (PAR-1). PAR-1 appears to stimulate platelet activation factor (PAF) and PAF-receptor (PAF-R) expression. Then, PAF/PAF-R signalling mediates MCAM transcription via activation of the c-AMP responsive element-binding protein (CREB) and SP1 (Melnikova et al. 2009).

1.3.4 Protein Structure

MCAM is an approximately ~113 kDa, heavily glycosylated single-span transmembraneprotein. The MCAM protein is organised into three distinct domains mentioned above: an extracellular domain (ECD) 558 amino acids (AA) long which consists of five Ig-like domains (V1-V2-C1-C1- C1), a transmembrane domain 24 AA long, and an intracellular domain (ICD) existing in two isoforms (Fig. 3). The Ig-like domains of the MCAM protein are β-sheets stabilised bydisulphide bonds lying between the sheets (Fig. 3). Two isoforms, MCAM-L and MCAM-S, differ in the length of their intracellular domains, with MCAM-L containing 64 AA and MCAM-S containing 21 AA (Taira et al. 1995). The MCAM protein shows a high level of conservation between species (Table 1). The intracellular domain of MCAM-L contains an ezrin-radixin-moesin (ERM) binding motif, two putative endocytosis motifs - the dileucine (EEMGLL) and tyrosine(YIDL) motifs, and two putative protein kinase C (PKC) sites (Fig. 3A). The MCAM-S intracellular domain is much shorter in comparison and contains the ERM motif, a single PKCsite, and a PDZ-binding domain (Wang et al. 2020) (Fig. 3B).

The intracellular domain of both long and short isoforms of MCAM is highly conserved at theamino acid level (Table 1). Mouse, chicken, and zebrafish intracellular domains display higher homology to the human intracellular domains than the total protein sequence does. This suggests that there may be higher functional importance in the intracellular tail. In addition,all putative domains in the intracellular tail of human isoforms are conserved in the mouse and chicken proteins.

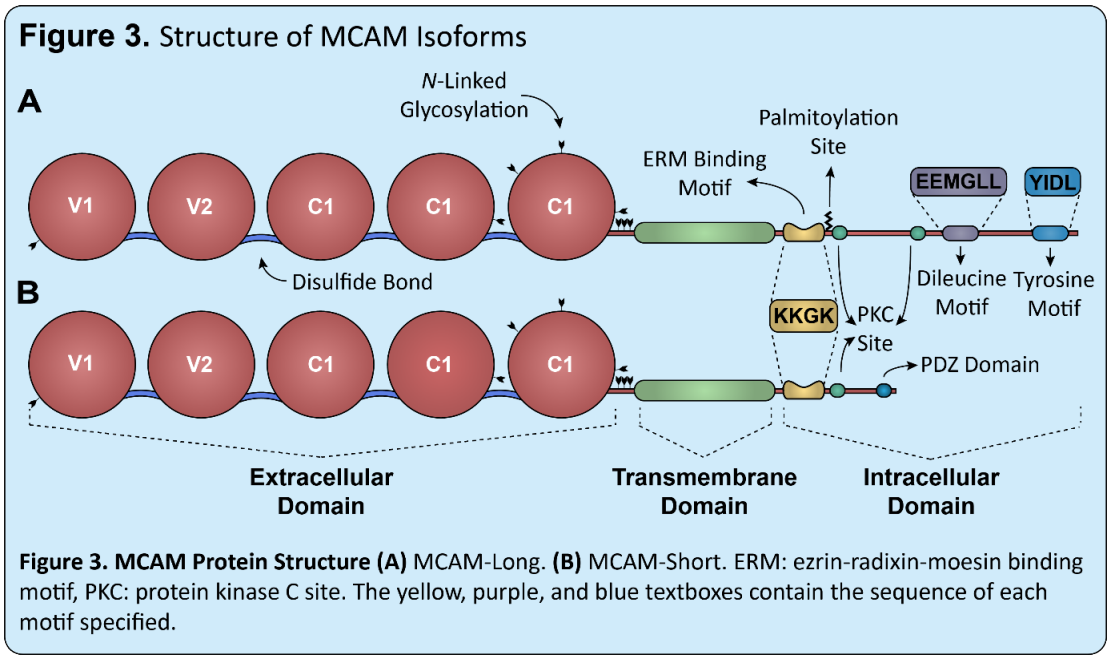

Figure 3. MCAM Protein Structure (A) MCAM-Long. **(B)** MCAM-Short. ERM: ezrin-radixin-moesin binding motif, PKC: protein kinase C site. The yellow, purple, and blue textboxes contain the sequence of each motif specified.

Table 1. Conservation of mouse, chicken and zebrafish full length MCAM and intracellular tail protein sequences compare to the human isoforms

Isoform	Mouse	Chicken	Zebrafish
MCAM-L	76.2%	36.6%	32.1%
MCAM-L tail	90.8%	69.2%	54.7%
MCAM-S	75.3%	36.4%	31.8%
MCAM-S tail	91.3%	69.6%	56.5%

MCAM is highly glycosylated. The theoretical mass of MCAM is ~70 kDa, which suggests thatover 30% of its true mass results from glycosylation of the protein. The glycosylation occurs in the extracellular domain where there are predicted to be eight *N*-glycosylation sites (Wang et al. 2020) (Fig. 3). These are located at positions 58, 418, 449, 467, 508, 518, 527, and 544 (Wu et al. 2001). Six of these sites are conserved in the mouse protein, indicating the importance of glycosylation in the function of MCAM (Lei et al. 2015). Various other post-translational modifications of MCAM are thoughtto occur including sialylation of the extracellular domain (Jouve et al. 2013; Lehmann et al. 1987), and ubiquitination (Tang et al. 2015), palmitoylation (Wang et al. 2015) and phosphorylation (Xu et al. 2019) of the intracellular domain.

The third isoform of MCAM is a soluble, cleaved protein (sMCAM) consisting entirely of the extracellular domain. sMCAM appears to be generated in endothelial cells by MMP- mediated cleavage at the transmembrane region (Bardin et al. 2009; Bardin et al. 1998; Boneberg et al. 2009; Ouhtit et al. 2017). However, chicken sMCAM appears to be produced by alternative splicing rather than MMP-mediated cleavage (Vainio et al. 1996)It is important to determine whether alternative splicing also plays a role in the production of sMCAM in human cells.

1.3.5 Dimerisation and Binding

Interestingly, the binding behaviour of MCAM remains contentious in the literature. MCAM undergoes heterophilic binding with various cellular and ECM molecules, and these interactions will be discussed in Section 1.6. However, whether MCAM undergoes inter- cellular homophilic binding is controversial. One group has presented data suggesting that neuronal cells over-expressing chicken MCAM displayed increased aggregation compared tocontrol cells, and produced longer neurites when cultured on an MCAM-Fc chimeric proteinsubstrate (Taira et al. 2004, 2005; Taira et al. 1995; Taira et al. 1998; Taira et al. 1999). A critique of these studies suggested that the findings may be a result of heterophilic interactions between MCAM and an unknown ligand on the neuronal cells (Hiroi et al. 2003). In studies of human MCAM, evidence of homophilic binding of MCAM is yet to be produced. An early study of MCAM reported that MCAM contributed to cell-cell adhesion viainteraction with an unknown, heterophilic ligand (Johnson et al. 1997). Furthermore, surface

plasmon resonance experiments found that human sMCAM had no binding capacity for immobilised MCAM (Bardin et al. 2009).

Despite the lack of evidence for *trans*-homophilic binding, MCAM does form *cis*-dimers on the cell surface, and this function is thought to be integral to its involvement in various signalling complexes (Bu et al. 2007; Zhuang et al. 2010). This is discussed in further detail in Section 1.6.1 with regards to specific binding partners.

1.3.6 Expression and Localisation

MCAM is expressed in a wide range of normal tissues, such as endothelial and neuronal cells, playing a functional role in homeostasis and normal cell function. MCAM is often expressed in stem and embryonic tissues and is associated with stem-like characteristics. Table 2 summarises the expression and function of MCAM as reported in the literature.

1.3.7 Endocytosis and Recycling

The internalisation of membrane proteins occurs for many reasons including nutrient uptake, signal transduction and regulation, regulation of the cell membrane composition, and the homeostatic turnover of membrane proteins (Aguilar and Wendland 2005). Surface receptor levels influence cell-celland cell-matrix interactions as well as normal cell behaviour. Thus, transport of membrane proteins to and from the surface is essential for cell function.

Little is known about the endocytosis and recycling of MCAM, although it contains two putative endocytosis/sorting motifs (Fig. 3). The dileucine motif conforms to the structure of the [DE]XXXL[LI] consensus motif while the tyrosine motif conforms to the YXXØ consensus motif (Ø stands for a residue with a bulky hydrophobic side chain, and X stands for any aminoacid)(Bonifacino and Traub 2003). These motifs are involved in the internalisation and sorting of proteins to endosomal and lysosomal compartments, as well as basolateral targeting (Bonifacino and Traub 2003). Interestingly Y641G (which forms part of the YXXØ consensus motif), has also recently been identified as a site of MCAM phosphorylation in endothelial cells following growth factor stimulation (Xu et al. 2019); although it not yet clear whether these two putative functions are mutually exclusive.

Table 2. Expression and function of MCAM in normal tissue

Location	Isoform		References
Mesenchymal stem cells	ND	Increased differentiation and migration	(Espagnolle et al. 2014; Fayazi et al. 2015; Russell et al. 2010; Sacchetti et al. 2007; Tormin et al. 2011; Xu et al. 2009)
Human Endothelial Cells	ND	Cell-cell interactions/ angiogenesis	(Bardin et al. 2001; Bardin et al. 2009; Bardin et al. 1998; Yan et al. 2003)
	MCAM-L	Vascular stabilisation	(Kebir et al. 2010; Stalin et al. 2013)
	MCAM-S	Angiogenesis	(Kebir et al. 2010)
	sMCAM	Angiogenesis	(Bardin et al. 2009; Bardin et al. 1998; Bardin et al. 2003; Harhouri et al. 2010)
Pericytes	ND	ND	(Espagnolle et al. 2014; Shih et al. 1994)
Hair Follicles	ND	ND	(Shih et al. 1994)
Keratinocytes	ND	Adhesion/ inflammation marker	(Weninger et al. 2000)
Smooth muscle	ND	ND	(Shih et al. 1994)
Neurological tissue	ND	Neurite extension	(Shih et al. 1994; Taira et al. 2005; Taira et al. 1995)
Trophoblast	ND	Marker for differentiation/ Limits migration	(Shih et al. 1998; Shih et al. 1994; Shih and Kurman 1996)
	sMCAM	Defective trophoblast invasion	(Pasquier et al. 2005)
B-lymphocytes	ND	ND	(Elshal et al. 2005)
T-lymphocytes, TH17 cells	ND	Increased adhesion to endothelium/ activation marker	(Elshal et al. 2007; Elshal et al. 2005; Kamiyama et al. 2012; Pickl et al. 1997)
Follicular Dendritic Cells	ND	ND	(Bardin et al. 1996)
NK cells	ND	Maturation	(Despoix et al. 2008)

1.3.7.1 Endocytosis

Endocytosis occurs via either clathrin-dependent, caveolin-dependent, or clathrin/caveolin- independent mechanisms (Fig. 4)(Doherty and McMahon 2009; Kawauchi 2012). Clathrin-dependent endocytosis is more broadly understood than clathrin-independent mechanisms and involves over 50 known components (Kaksonen and Roux 2018). The process of clathrin-dependent endocytosis is summarised as follows:first, endocytic coat proteins (such as clathrin) cluster at the cell surface, along with receptors targeted for internalisation. Next, a clathrin-coated pit forms whereby the plasma membraneis invaginated via enveloping coat proteins (Kaksonen and Roux 2018). Following this, the neck of the invagination is constricted and excised, forming a clathrin-coated vesicle containing the cargo receptors which is subsequently trafficked to early endosomes (Kaksonen and Roux 2018). Caveolin-dependent endocytosis involves the coating of membrane invaginations with caveolin rather than clathrin. Furthermore, there are multiple clathrin/caveolin-independent pathways of endocytosis, including RhoA, Flotillin, Cdc42, and Arf6 mediated endocytosis, as well as micropinocytosis (Mayor et al. 2014).

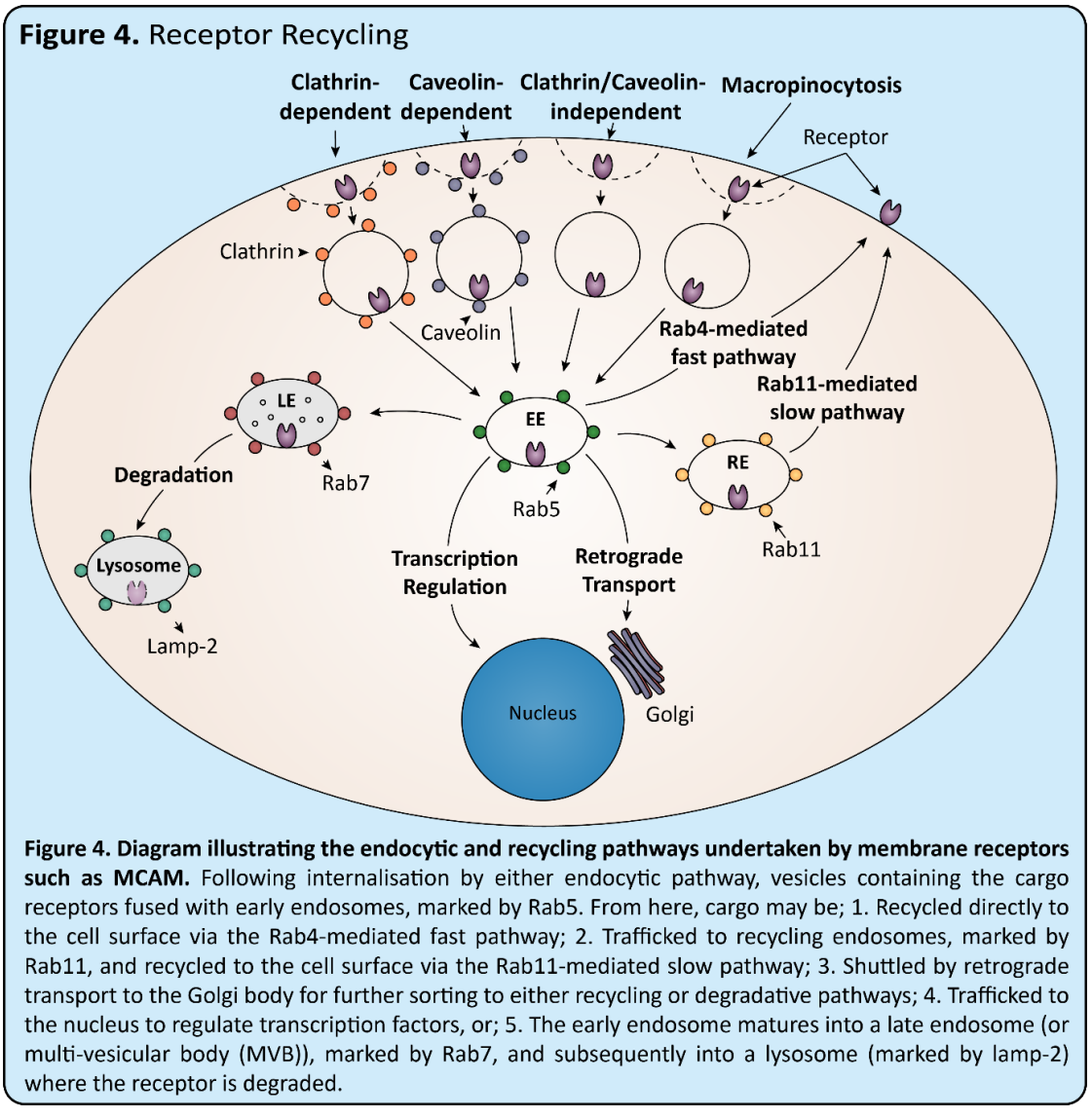

Figure 4. Diagram illustrating the endocytic and recycling pathways undertaken by membrane receptors such as MCAM. Following internalisation by either endocytic pathway, vesicles containing the cargo receptors fused with early endosomes, marked by Rab5. From here, cargo may be; 1. Recycled directly to the cell surface via the Rab4-mediated fast pathway; 2. Trafficked to recycling endosomes, marked by Rab11, and recycled to the cell surface via the Rab11-mediated slow pathway; 3. Shuttled by retrograde transport to the Golgi body for further sorting to either recycling or degradative pathways; 4. Trafficked to the nucleus to regulate transcription factors, or; 5. The early endosome matures into a late endosome (or multi-vesicular body (MVB)), marked by Rab7, and subsequently into a lysosome (marked by lamp-2) where the receptor is degraded.

The mechanism by which MCAM is internalised into the cell is unknown, however, as many other members of the IgSF are endocytosed via the clathrin-mediated pathway, it has been speculated that this is most likely the pathway by which MCAM is internalised (Dye 2007; Kamiguchi and Lemmon 1997; Minana et al. 2001; Thelen et al. 2008). Data suggests the clathrin-mediated pathway is at least partially accountable for the endocytosis of MCAM, as sucrose-mediated blockade of the clathrin-mediated pathway reduced MCAM internalisation (Dye 2007).

Following the endocytosis of membrane receptors, cargo-containing vesicles are trafficked to early endosomes (Xu et al. 2017). The cargo is then either: trafficked directly to the cell surface; to late endosomes followed by lysosomes for degradation; to recycling endosomes for signalling or re-expression on the cell surface; to the Golgi via retrograde transport; or to the nucleus to regulate transcription factors (Fig. 4)(Xu et al. 2017). The recycling of membrane receptors is integral to their function and is necessary for the maintenance of receptor expression on the cell surface. The sorting of receptors through either recycling or degradative pathways determines their expression level and therefore has a direct link to cell phenotype, such as cell adhesion and migration (Burd and Cullen 2014; Cullen and Korswagen 2011).

Receptors can be recycled to the cell surface from the early endosomes via the Rab4-mediated fast pathway, or from the recycling endosomes via the Rab11-mediated slow pathway (Fig. 4)(Grant and Donaldson 2009). The pathway that MCAM takes to be recycled is not known, however, it has been postulated that the dileucine motif is necessary for this process to occur (Dye 2007). Furthermore, both Rab4 and Rab11 have been shown to co-localise with MCAM under various conditions in melanoma cells (Dye et al. 2009; Witze et al. 2008).

1.3.7.2 Endosomal Sorting

Endosomal sorting is also regulated by the retromer complex, which has been described as a "master conductor" of this process (Burd and Cullen 2014). Retromer regulates the sorting and recycling of proteins from endosomes to the *trans*-Golgi network (TGN) (retromer-mediated retrograde transport) and plasma membrane (retromer-mediated recycling)(Vagnozzi and Pratico 2019; Zhang, Huang, et al. 2018), and is a complexsystem which involves many accessory proteins. The sorting nexins (SNXs) are an integral part of the retromer complex, and contribute to retromer-membrane associations (Burd and Cullen 2014). AllSNXs have a SNX-phox-homology (SNX-PX) domain but vary in their C-terminal domains (Zhang, Huang, et al. 2018)(Fig. 5).

Figure 5. Structure of Retromer Components and Sorting Nexins

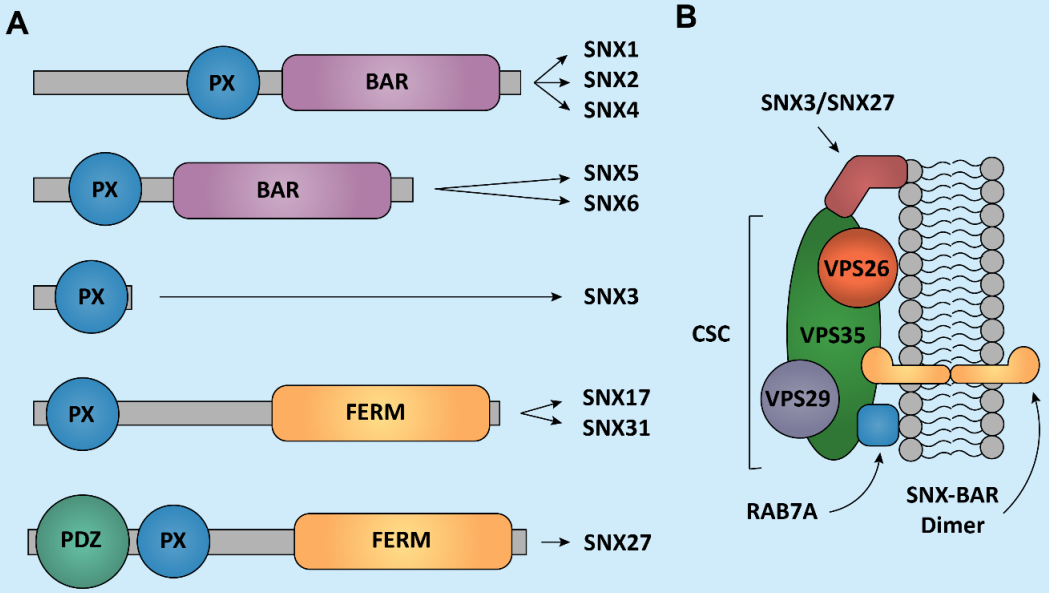

Figure 5. (A) Sorting nexins and retromer. **(B)** Representation of the retromer subcomplexes. The cargo selection complex (CSC) containing VPS26, VPS29, and VPS35 interacts with either the SNX-BAR membrane deformation complex (SNX1/2 and SNX5/6), or another sorting nexin such as SNX3 or SNX27. RAB7A stabilises the interaction between retromer and the plasma membrane.

Retromer consists of two sub-complexes: the core retromer, or cargo selection complex (CSC), which consists of a trimer of vacuolar protein sorting (VPS) associated proteins VPS26,VPS29 and VPS35, and the membrane deformation complex, which is composed of different combinations of SNXs that regulate membrane deformation, tubule formation, and play a role in cargo selection (Burd and Cullen 2014). The most common retromer complex is the SNX-BAR-retromer, comprised of heterodimers of SNX1-SNX2 or SNX5-SNX6 (Vagnozzi and Pratico 2019). These SNXs contain a C-terminal BIN/Amphiphysin/RVS (BAR) domain (Vagnozzi and Pratico 2019). Finally, an accessory protein is required to stabilise the CSC upon membrane interactions, such as SNX3 and RAB7A (Vagnozzi and Pratico 2019). Other retromer complexes include the SNX27-retromer, which contains a C-terminal FERM (4.1/ezrin/radixin/moesin) domain, and the SNX3-retromer (Harterink et al. 2011; Steinberg et al. 2013; Temkin et al. 2011; Zhang et al. 2011).

Each retromer complex takes part in distinct and overlapping cargo sorting pathways, and recent studies suggest that components of the complex can also act individually (McNally and Cullen 2018). Plasma membrane proteins are a principal cargo for retromer-mediated recycling, however, few studies have explored its role in cancer. The SNX-FERMs, SNX17, SNX27 and SNX31, mediaterecycling of cargo via an NPx[Y/F] motif recognition (where x is any residue), although SNX27also sorts proteins containing a PDZ ligand. SNX17 mediates the recycling of over 200 cell surface proteins, including many integrins and receptors, but does not interact with the CSC (McNally et al. 2017). Interestingly, SNX31 appears to be upregulated during melanoma metastasis and has been described as a driver mutation, yet it is silenced

during *in vitro* cell culture (Hodis et al. 2012; Tseng et al. 2014). Furthermore, SNX4 mediates the sorting of the transferrin receptor away from the degradation pathway (Johannes and Popoff 2008).

1.4 MCAM in Cancer

MCAM is highly expressed in multiple cancers, and in many of these is a marker for metastasis or poor prognosis. Table 3 contains a non-exhaustive list of cancers in which MCAM has beeneither associated with poor prognosis or directly implicated in tumourigenicity. Interestingly,after an extensive literature review, only two examples were found where MCAM expression was associated with an anti-metastatic phenotype: pancreatic cancer (Zheng et al. 2016) and breast cancer (Shih et al. 1997).

MCAM appears to be involved in all steps of metastasis. In the early stages of metastasis, MCAM expression is often involved in epithelial-mesenchymal transition (EMT) and increased invasion of tumour cells. For instance, in melanoma, MCAM appears to contribute to the transition from the RGP to the VGP. This transition is one of the early steps in melanoma progression and has been described as an “EMT-like” process (Zigler et al. 2011). However, MCAM is also often implicated in the later stages of metastasis, including extravasation, angiogenesis, and secondary tumour formation (Schlagbauer-Wadl et al. 1999). The following sections will expand upon the role of MCAM in cancer, with a specific focus on its role in melanoma, and how these effects are mediated.

1.5 MCAM interaction Partners and Signalling Pathways

1.5.1 VEGF/VEGFR-2

Angiogenesis is defined as the process by which new blood vessels are formed (Adair and Montani 2010). It is necessary to provide nutrients to a tumour once it reaches a critical mass, and thereby promotes tumour growth and survival (Yadav et al. 2015). Pro-angiogenic factors are usually required to promote angiogenesis, and vascular endothelial growth factor VEGF is the predominant family of pro-angiogenic factors (Jiang et al. 2012), of which VEGF-A is the founding member (Holmes and Zachary 2005; Tugues et al. 2011). The cognate receptors for VEGF are the vascular endothelial growth factor receptors, VEGFR-1, VEGFR-2, and VEGFR-3 (Tugues et al. 2011). VEGF-A is the primary ligand for VEGFR-2 and therefore muchof the literature focuses on the mechanism by which their interaction promotesangiogenesis (Tugues et al. 2011).

Table 3. MCAM expression in various cancers and its reported effects.

Cell line/Tissue	Isoform	Effect	References
Melanoma	*ND*	*In vitro* – increasedinvasion, motility *In vivo* – poor prognosis	(Dye et al. 2013; Rapanotti et al. 2017; Stalin et al. 2017; Watson-Hurst and Becker 2006; Zeng et al. 2017)
	sMCAM	Increased angiogenesis,survival	(Stalin et al. 2013)
Prostate Cancer	ND	Increased invasiveness, metastasis	(Liu et al. 2008; Wu et al. 2011; Zoni et al. 2019)
Breast Cancer	ND	*In vitro* – increasedmotility, tamoxifenresistance *In vivo* – poor prognosis	(Garcia et al. 2007; Imbert et al. 2012; Liang et al. 2017; Zabouo et al. 2009)
Ovarian Cancer	ND	*In vitro* - Increasedinvasion, proliferation, survival *In vivo* – Poor prognosis	(Aldovini et al. 2006; Wu et al. 2012; Zeng et al. 2017)
Osteosarcoma	ND	*In vitro* – Potentialmarker for metastasis *In vivo* – Increased invasion, pulmonary metastasis	(McGary et al. 2003; Schiano et al. 2012)
Gastric Cancer	*ND*	*In vitro* – EMT *In vivo* – Poor prognosis	(Liu et al. 2012)
Non-Small Cell Lung Cancer / Lung Adenocarcinoma	ND	*In vivo* – Poor prognosis	(Kristiansen et al. 2003; Oka et al. 2012; Zhang et al. 2014)
Pancreatic Cancer	ND	increased invasiveness *In vivo* – Low expression associated with poor prognosis	(Zheng et al. 2016)
Uterine Leiomyosarcoma	ND	*In vivo* – Increasedlymph node metastasis, poor prognosis	(Zhou et al. 2015)
Hepatocellular Carcinoma	ND	*In vitro* – Increased invasion, motility, EMT transition *In vivo* – Increased invasion, poor prognosis	(Jiang et al. 2016)
Squamous Cell Carcinoma	ND	*In vivo* – Increased lymph node metastasis, poor prognosis	(Li et al. 2014)
Colorectal Cancer	*ND*	*In vivo* – Marker for liver metastasis	(Tian et al. 2013)
Malignant Rhabdoid Tumour	*ND*	*In vitro* – Marker for tumourigenicity	(Nodomi et al. 2016)

VEGFRs often require a co-receptor to form signalling complexes (Tugues et al. 2011). MCAM is a co- receptor for VEGFR-2, and the interaction between MCAM and VEGFR-2 appears to be essential for VEGF-mediated phosphorylation and subsequent activation of VEGFR-2 (Zheng et al. 2009). This phosphorylation leads directly to the activation of the PI3K-AKT, nuclear factor kappa- light-chain-enhancer of activated B cells (NFκB), and p38 MAPK pathways, promoting angiogenesis and enhancing tumour survival (Halt et al. 2016). The mechanism is summarised as follows: An MCAM dimer forms a complex with a VEGFR-2 molecule on the cell surface via interactions between their extracellular domains (Fig. 6). The formation of this complex leads to the recruitment of VEGF and the phosphorylation and activation of VEGFR-2. Following this, ERM proteins (cytoskeletal linkers) are recruited to the intracellular tails of MCAM/VEGFR-2, forming a cytoskeletal/signalling complex which then transduces the downstream pro-angiogenic activation of the AKT, NFκB, and p38 MAPK pathways (Zheng et al. 2009) (Fig.6).

Figure 6. VEGFR-2 and MCAM Interaction

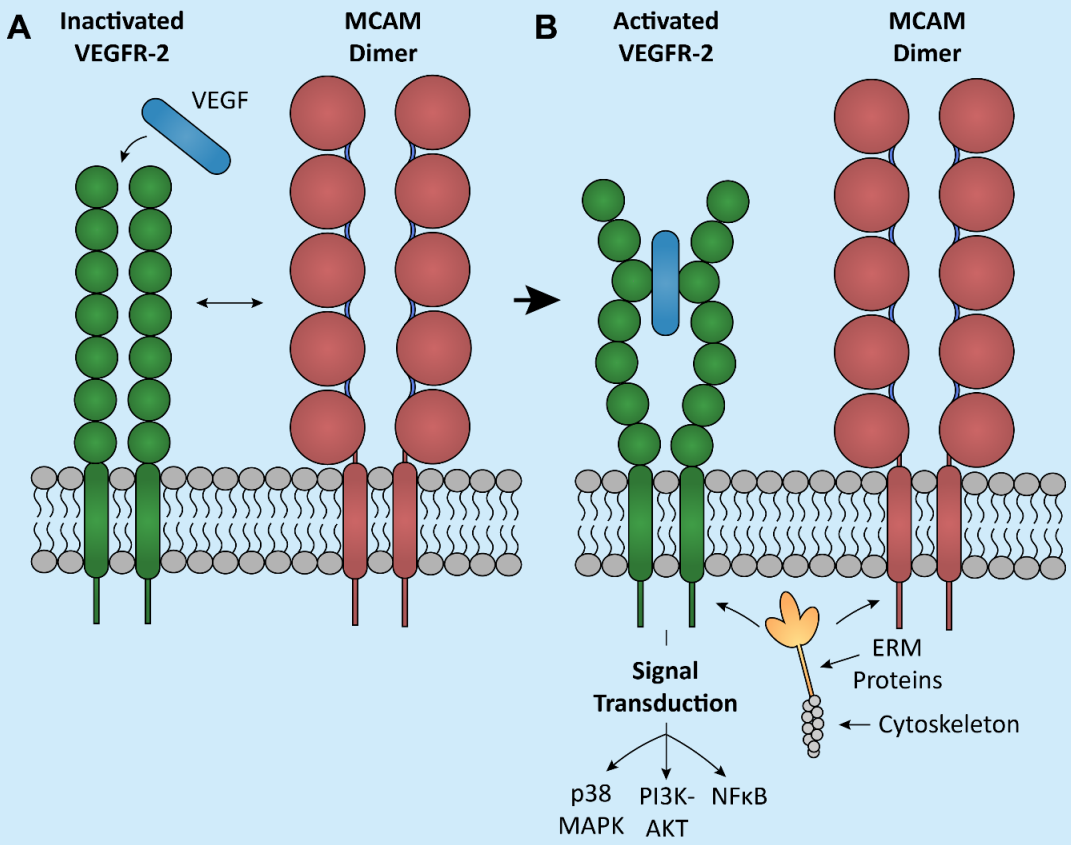

Figure 6. MCAM-VEGFR-2 interaction. (A) An MCAM dimer on the cell surface interacts with a VEGFR-2 dimer through their extracellular domains. VEGF-A is recruited, which binds and activates the VEGFR-2 receptor. **(B)** The activated VEGFR-2/MCAM complex recruits ERM proteins and cytoskeleton, forming a signalling complex which transduces signals which activate the p38-MAPK/PI3K-AKT/NFκB pathways.

The interaction between MCAM and VEGFR-2 has been confirmed in subsequent studies (Jiang et al. 2012; Zhuang et al. 2010). One study found that treatment of cells with an anti-MCAM blocking antibody (AA98) prevented the MCAM-VEGFR-2 interaction and inhibited VEGF-mediated endothelial tube formation by ~50% (Jiang et al. 2012). Additionally, it was found that MCAM was necessary for VEGF- mediated vessel permeability in endothelial cells (Jiang et al. 2012). Finally, MCAM knockdown also resulted in a ~50% reduction in microvasculature density in Matrigel plugs which had been implanted into a mouse model (Jiang et al. 2012). These data are supported by So *et al* (2010) who found that knockdown of chicken MCAM MCAM also displayed a similar reduction in tumour angiogenesis (So et al. 2010).Interestingly, data suggests that MCAM dimerization and the NFκB pathway may be involvedin a positive feedback system. Bu et al (2007) found that MCAM dimerization was associatedwith activation of NFκB (Fig 6)(Bu et al. 2007), and that chemical inhibition of NFκB, in turn, reduced MCAM dimerization. This suggests a positive feedback system by which the NFκB pathway promotes MCAM-expression and/or dimerization (and thus the interaction of MCAM with VEGFR-2), which in turn activates the NFκB pathway. A similar feedback pathway may involve reactive oxygen species (ROS)-mediated dimerisation of MCAM (Zhuang et al. 2010).

Figure 6. VEGFR-2 and MCAM Interaction

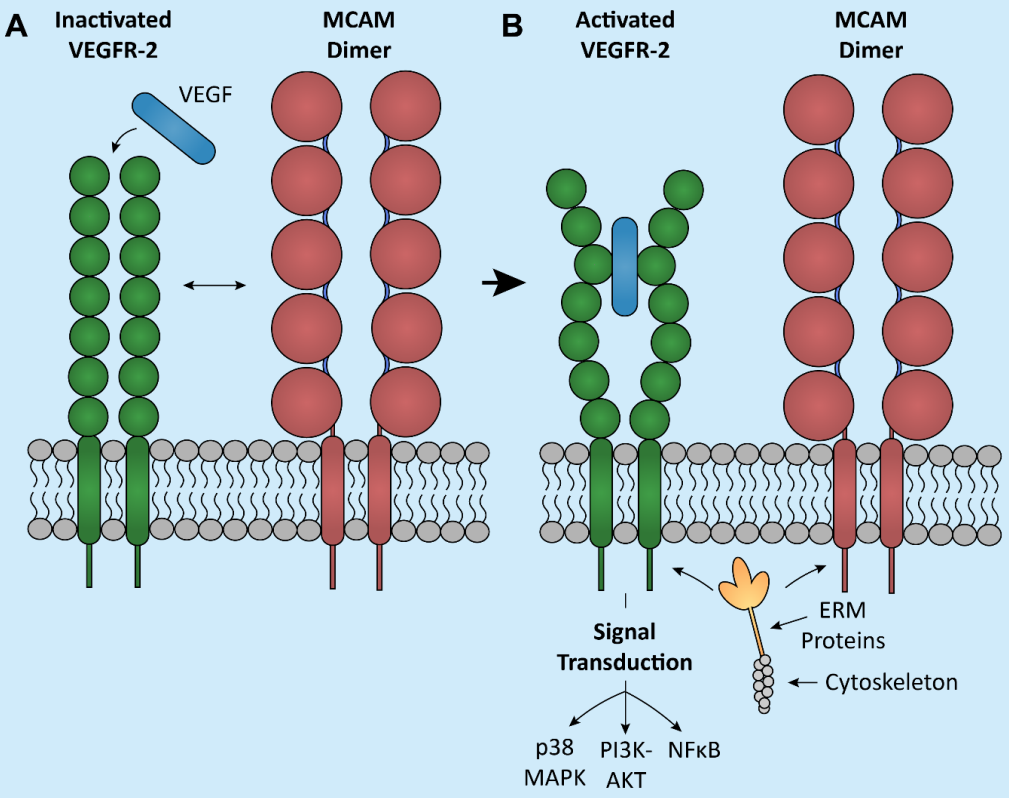

Figure 6. MCAM-VEGFR-2 interaction. (A) An MCAM dimer on the cell surface interacts with a VEGFR-2 dimer through their extracellular domains. VEGF-A is recruited, which binds and activates the VEGFR-2 receptor. **(B)** The activated VEGFR-2/MCAM complex recruits ERM proteins and cytoskeleton, forming a signalling complex which transduces signals which activate the p38-MAPK/PI3K-AKT/NFκB pathways.

The small GTP-binding protein Rac1 and NOX4 (NADPH oxidase 4) are activated via VEGFR-2 signalling. This leads to the release of ROS species that induced MCAM dimerisation, which in turn may activate more VEGFR-2 receptors (Zhuang et al. 2010). These mechanisms illustrate how MCAM and VEGFR- 2 constitute a pro-angiogenic signal transduction system in endothelial cells, contributing tothe vascularisation and growth of tumours.The interaction between MCAM and VEGF/VEGFR has also been associated with transendothelial migration, whereby melanoma cells migrate across the surface of an endothelial layer (Bardin et al. 2009). This is required for melanoma cells to intra- and extravasate (Section 1.3.2). Following

VEGF treatment of endothelial cells, MCAM appears to stimulate the phosphorylation of focal adhesion kinase (FAK), which subsequently leads to the phosphorylation of vascular endothelial (VE)-cadherin and opening of endothelial junctions,enabling migration of melanoma cells (Bardin et al. 2009). Furthermore, MCAM knockout in endothelial cells also reduced the capacity for melanoma cells to transmigrate (Bardin et al. 2009).

Interestingly, it is yet to be confirmed whether MCAM and VEGF/VEGFR also interact in melanoma cells. In addition, there is some controversy in the literature regarding VEGFR2 expression in melanoma. A number of studies have found VEGFR2 expression on ~ 80% of melanoma cells, whereas in a recent study, where antibody specificity was demonstrated by immunofluorescence, immunoblot, knock-down and knock-in experiments, only 7% of melanoma cells expressed VEGFR2 (Molhoek et al. 2011). Thus, VEGFR2-MCAM interaction may contribute tomelanoma metastasis indirectly via endothelial cell activation rather than occur in melanoma cells themselves.

1.5.2 Galectins

As previously mentioned, MCAM is highly glycosylated and contains eight *N*-glycosylation sites in its extracellular domain (Section 1.5.4). Galectin-3 (Gal-3), a galactoside-binding protein, interacts directly with MCAM via *N*-linked glycan structures (Colomb et al. 2017; Zhang, Zheng, et al. 2018). Gal-3 appearsto bind predominantly to the fifth Ig-like domain of MCAM, as deletion of this portion significantly abrogated MCAM-Gal-3 binding (Zhang, Miller, et al. 2019). Gal-3 also interacts directly with VEGFR-2 to form multimers, which stabilise VEGFR2 on the cell surface. When VEGF-A is also bound, Gal-3 binding maintains the VEGR2/VEGFA complex on the cell surface and promotes prolonged angiogenic signaling (Markowska et al. 2011). As MCAM interacts with both Gal-3 and VEGFR-2 directly, it may be possible that Gal-3 contributes to the interaction between MCAM and VEGFR-2. Furthermore, the binding of Gal-3 to MCAM induces MCAM dimerisation, which isrequired for MCAM-mediated activation of VEGFR-2 (Colomb et al. 2017). Additionally, Gal-3-induced dimerisation of MCAM leads to the activation of the PI3K-AKT pathway, as well as IL-6 and granulocyte-colony stimulating factor (G-CSF) production, all of which are implicated in metastatic progression (Colomb et al. 2017).

Galectin-1 (Gal-1) also interacts directly with MCAM (Jouve et al. 2013). *In vitro,* this interaction appears to promote survival in endothelial cells by inhibiting apoptotic pathways (Colomb et al. 2017; Jouve et al. 2013).

1.5.3 Id-1

Inhibitor of DNA binding 1 (Id-1) is a transcription regulator that is associated with cancer progression (Zigler et al. 2011). Activating transcription factor 3 (ATF-3) is a transcription factor which inhibits Id-1 activation. MCAM is thought to downregulate ATF-3 leading to increased activation of Id-1. MCAM-mediated activation of the Id-1 cascade is thought to increaseMMP-2 expression, resulting in increased invasion in melanoma cells (Zigler et al. 2011).

1.5.4 Laminins

Laminin-411 and laminin-421 (laminins 8 and 9) have both been identified as interaction partners of MCAM (Flanagan et al. 2012). These α4-laminins are upregulated during the progression of severalcancers and have been linked to melanoma migration (Ishikawa et al. 2014). Laminin-411 is expressed on thebasement membrane of vascular endothelial cells and may be required for the MCAM- mediated invasion of T-cells into tissues (Flanagan et al. 2012). Blocking MCAM with an anti-MCAM antibody reduced the ability of T-cells to invade or infiltrate endothelial monolayers (Flanagan et al. 2012). In contrast, Ishikawa et al (2014) demonstrated that laminin-421, but not laminin-411, bound MCAM in solid state binding assays. In addition, they found that an anti-MCAM antibody blocked MCAM-mediated migration on laminin-421 but could not achieve the same effect on laminin-411 (Ishikawa et al. 2014). Finally, chicken MCAM interacts directly with NOF (neurite outgrowth factor), which is a member of the laminin family, and this interaction contributes to neurite outgrowth (Taira et al. 2004, 2005; Taira et al. 1994).

1.5.5 Wnt-receptor-actin-myosin-polarity (WRAMP) structure

The trailing edge mechanics of directional cell migration are poorly understood. Generally, Ras homolog gene family, member A (RhoA) and Rho kinase-dependent processes drive cytoskeletal-mediated mechanical force and motility, leading to directional migration of cells (Cramer 2010). Interestingly, many Ca^{2+}-mediated pathways take place at the trailing edge. One example is the phosphorylation of myosin light chain by myosin light-chain kinase (MLCK), aCa^{2+}-dependent enzyme, which results in the degradation of focal adhesions and the releaseof cell-matrix adhesions (Petrie et al. 2009). Such mechanisms often involve a gradient of Ca^{2+} with a higherconcentration at the trailing edge of the cell to a lower concentration at the leading edge (Hahn et al. 1992). A structure has recently been identified which directs cell migration and potentially acts through a

calcium gradient as described above. This structure has been called the wnt-receptor-actin-myosin polarity (WRAMP) and is described below (Witze et al. 2008).

The expression level of Wnt5a positively correlates with melanoma invasiveness (Bittner et al. 2000) and is thought to directly mediate melanoma invasion (Da Forno et al. 2008; Dissanayake et al. 2007; Weeraratna et al. 2002; Ye et al. 2013). The WRAMP mechanism describesone way in which Wnt5a contributes to the motility and invasiveness of melanoma, as follows(Fig. 7). Wnt5a stimulates the internalisation of MCAM (and other receptors) from the cell surface. MCAM is then transported to the rear of the cell, which is thought to occur via Rab4/RhoB-mediated late endosomes (multi-vesicular bodies, MVBs). This process may alsoinvolve coat protein 1β (COP1β)-mediated retrograde transport of MCAM from the Golgi to the ER. A polarised distribution of MCAM, actin, myosin IIB, and other components at the trailing edge of the cell form the WRAMP structure (Witze et al. 2013; Witze et al. 2008). The IQ Motif Containing GTPase Activating Protein 1 (IQGAP1) may play an important role in this process as it interacts directly with MCAM and is a cytoskeletal-linker protein, likely scaffolding MCAM and the actin cytoskeleton and allowing for nucleation of the WRAMP (Witze et al. 2013). The final step involves the endoplasmic reticulum (ER) being recruited to the WRAMP structure (likely involving COP-1β), a rear-membrane retraction, and a localised Ca2+ signal produced by the cortical ER, which stimulates adhesion disassembly, membrane retraction, cytoskeletal contraction, and finally cell migration (Witze et al. 2013; Witze et al. 2008). Interestingly this process appears to be transient and defines the directionality of cell migration, forming at the rear of the cell and then dissipating and re-forming at the new rear as the cell changes direction (Connacher et al. 2017).

Calpain-2 and phosphorylated myosin light chain co-localised at the WRAMP, which suggestthat calcium-dependent enzymes such as Calpain-2 are required for cell movement as part of the WRAMP mechanism. Calpain-2 mediates the proteolysis of focal adhesion proteins such as Talin-1 and leads to focal adhesion disassembly and membrane retraction. Calpain also mediates proteolysis of Filamin-A which binds and stabilises actin filaments, suggesting another mechanism for actin reorganisation and cellular movement following a calcium signal (Witze et al. 2013).

Frizzled-3 (Fz-3), a Wnt5a receptor, also co-localised with MCAM at the trailing edge of the cell, likely following Dishevelled-mediated Wnt signalling (Witze et al. 2013). Cytoskeletal dynamics proteins such as gelsolin and Filamin-A were also localised to the WRAMP structure. Filamin-A crosslinks actin filaments while gelsolin is involved in microfilament turnover. Focal adhesion proteins Talin-1 and kindlin-3, which enable actin-ECM interactions, were also present (Witze et al. 2013). Microtubule dynamics proteins were present, including the nuclear migration protein, Nuclear Distribution C, Dynein Complex Regulator (nudC). Furthermore, MAPK1 waspresent, which functions to disassemble focal adhesions via the phosphorylation of calpain, followed by proteolysis of focal adhesion proteins such as Talin-1 (as described above) (Witze et al. 2013).

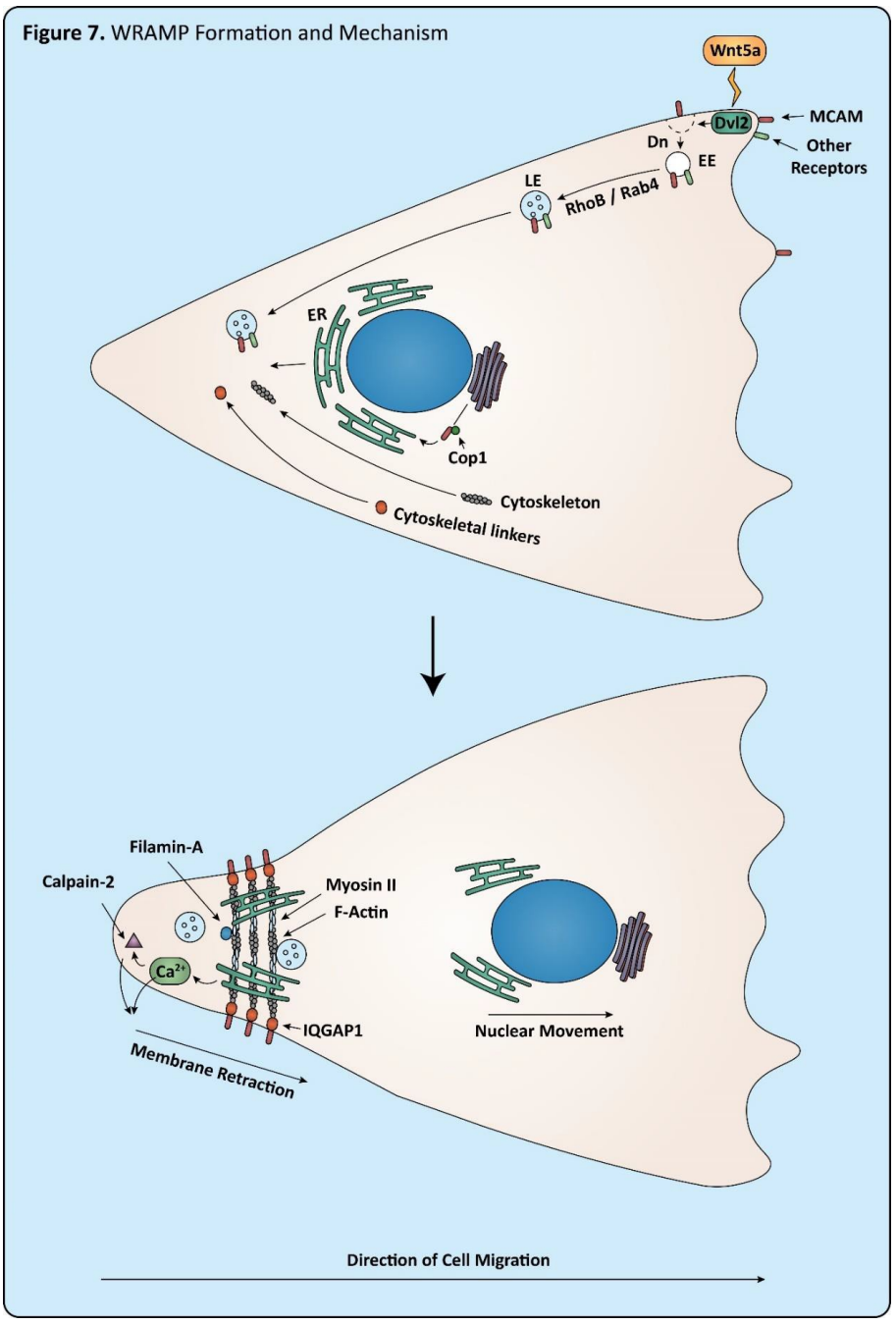

Figure 7. WRAMP-mediated directional cell migration. Upon stimulation by Wnt5a, receptors including MCAM are endocytosed via a dynamin-dependent pathway. This is thought to be triggered by Wnt5a-Dishevelled2-Frizzled-3 signalling. Upon endocytosis into early endosomes, receptors aretrafficked from the leading edge to the trailing edge of the cell via late endosomes (MVBs), avoidinglysosomal degradation. This is thought to be mediated by RhoB and Rab4 trafficking. MCAM may also be trafficked via retrograde transport mediated by COP1β (binding the KKGK motif in the intracellular tail of MCAM) to the ER in the WRAMP structure. Simultaneously, various componentsare recruited to the trailing edge of the cell including: cortical ER, cytoskeleton (F-actin / Myosin IIB),cytoskeletal linkers/dynamics proteins (IQGAP1/Filamin-A/Talin-1/others), microtubule dynamics proteins (NudC), ER trafficking proteins (COP1β), and various other components and enzymes (calpain-2/MAPK1). In the WRAMP structure, IQGAP1 and potentially other proteins are thought tolink MCAM to the cytoskeleton. Cytoskeletal dynamics result in drawing the rear membrane into proximity with the cortical ER. Next, there is a localised calcium release followed by membrane retraction. The calcium release may activate local enzymes including Calpain-2 which cleavesFilamin-A linkages. Furthermore, calpain-2 may result in the proteolysis of Talin-1, causing detachment from the ECM. Meanwhile, the nucleus is undergoing nucleokinesis, and the cell is migrating forwards.

Finally, Wnt5a appears to stimulate the depalmitoylation of MCAM at the residue cysteine 590 in its intracellular tail (Wang et al. 2015). Palmitoylation is the addition of fatty acyl moieties to cysteines, and acts to tether proteins to membranes. This process is reversible, and the addition and removal of palmitate allows proteins to move to and from membranes in a dynamic manner (Conibear and Davis 2010). This depalmitoylation of MCAM, occuring via the depalmitoylation- mediating enzyme APT1, results in MCAM being incorporated into the WRAMP structure at the rear of the cell (Wang et al. 2015). Mutation of C590 to a glycine, inhibiting palmitoylation, resulted in an increase of polarised MCAM at the trailing edge of the cell, suggesting that palmitoylationmaintains symmetrical MCAM expression and that depalmitoylation may be necessary for its transport to the WRAMP structure (Wang et al. 2015).

A375 melanoma cells, which migrate via an amoeboid-like "blebbing", have been found to form a structure reminiscent of the WRAMP, termed the ezrin-rich uropod-like structure (ERULS) (Lorentzen et al. 2011). The ERULS forms as the back of the cell and contains co-localised ezrin, F-actin,myosin light chain, β1-integrin, and phosphatidylinositol (4,5)-bisphosphate (Lorentzen et al. 2011). Additionally, moesin was also reported to co-localise with F-actin and myosin IIB in a similarstructure associated with RhoA-mediated migration in melanoma cells (Estecha et al. 2009). Whether MCAM is associated with these structures was not explored, however, another structure containing MCAM, moesin, SCRIB, and VANGL2 has been described in differentiating myotubes. In myotubes, asymmetric distribution of MCAM anchors the rear of the cell and enables myotube elongation (Moreno-Fortuny et al. 2017). Interestingly, MCAM interacts with various cytoskeletal linkers including IQGAP1 (Witze et al. 2013), ezrin, radixin, moesin (Luo et al. 2012), and hShroom1 (Dye et al. 2009). Hence, MCAM may consistently play a role in rear-directed mechanisms of cellular migration and polarisation.

1.5.6 Moesin

As mentioned above, moesin co-localises with a rear-polarised structure similar to ERULS which is associated with cellular migration and is also known to localise at the leading edge of migrating melanoma cells. MCAM directly interacts with moesin (Luo et al. 2012) resulting in the recruitment of RhoGDI1. This activates RhoA and leads to enhanced melanoma migration (Luo et al. 2012). MCAM and moesin appear to co-localise at the cell membrane within cell protrusions at the leading edge of the cell (Luo et al. 2012). Furthermore, moesin requires its FERM domain for interaction with MCAM and moesin localisation is altered following MCAM knockdown (Luo et al. 2012), which also reduces the migratory capacity of the cells. Interestingly, MCAM-L is highly expressed in the microvilli of lymphocytes and is correlated with increasingamount and length of these microvilli via cytoskeletal rearrangements (Guezguez et al. 2007).

1.5.7 PI3K-AKT Pathway

MCAM has been linked to the PI3K-AKT pathway through multiple lines of evidence. The PI3K-AKT pathway is often overexpressed in cancer and results in the downstream inhibition of apoptosis and activation of proliferation (Hemmings and Restuccia 2012). AKT is highly activated in melanoma, while it is not in normal melanocytes (Li et al. 2003), similar to MCAM. In both melanoma and prostate cancercells, MCAM and AKT have been reported to be involved in a positive feedback loop, with AKT activation upregulating MCAM and vice-versa, resulting in the inhibition of apoptosis (Li et al. 2003). As mentioned above, the interaction between MCAM and VEGFR-2 stimulates the downstream activation of the PI3K-AKT pathway. Interestingly, MCAM- mediated AKT activation could be prevented by blocking MCAM with the AA98 antibody (Jiang et al. 2012) or by MCAM-knockout (Jiang et al. 2012; Zeng et al. 2014). This suggests that the AA98 antibody blocks the interactionbetween MCAM and VEGFR-2, leading to enhanced cell survival. Furthermore, the interaction between Gal-3 and MCAM also results in activation of the AKT pathway (Colomb et al. 2017). However, at least one study found no change in phospho-AKT levels following the siRNA knockdown of MCAM (Watson-Hurst and Becker 2006), and no link between MCAM and the PI3K-AKT pathway has beenidentified in various other cancers, suggesting that the MCAM-AKT pathway may be cell line specific (Ma et al. 2010).

1.5.8 FAK/FYN

MCAM also induces the phosphorylation and activation of FAK, paxillin, and Pyk2, which results in the association of the tyrosine kinase FYN with the cytoplasmic tail of MCAM (Anfosso et al. 1998).These findings presented early evidence that MCAM initiates an outside-in signalling cascade. MCAM may also be necessary for VEGF-mediated FAK activation in melanoma cells, which has been linked with increased trans-endothelial migration (Jouve et al. 2015).

1.5.9 Other

Fibroblast growth factor 4 (FGF4) is another known interaction partner of MCAM, though little is known about this interaction. Gao et al. found that MCAM played a role in apical-basal polarity and planar cell polarity via interactions with FGF4. Here, MCAM was found to induce lumenogenesis and ciliogenesis through an MCAM-FGF4-NFAT signalling pathway,as well as by a separate MCAM-mediated activation of JNK (Gao et al. 2017).

1.6 Aims

MCAM is highly expressed and associated with metastasis in multiple cancers. Despite recent advances in understanding intracellular signalling and trafficking, much remains unknown about the mechanisms of

MCAM-mediated cell invasion. Specifically, the molecular interactions of the intracellular tail of MCAM are not yet completely understood. There is evidence that the dileucine and tyrosine motifs modulate the metastatic potential and cell phenotype in melanoma cell lines. These two domains represent relatively understudied facets of the MCAM molecule more generally. Further, investigations into other cell surface molecules (including integrins) have shown that the endocytosis/sorting of the molecule is integral to their function in cell migration. These mutations were chosen as those most likelyto cause an abrogation of function in the endocytosis motifs without affecting the conformation or other functions of MCAM.

Since MCAM appears to have such a prominent role in metastasis, by introducing these mutations we hope to discover novel data regarding how MCAM traffics through the cell. We hope to lay the groundwork for potentially uncovering novel interaction partners and pathways by which MCAM contributes to metastasis in melanoma, which could in turn lead to novel targets and therapeutic breakthroughs.

We hypothesize that the two putative endocytosis motifs in the cytoplasmic tail of MCAM play a major role in the metastatic potential of melanoma, and that this is mediated by their effect on the sorting and recycling of MCAM throughout the cell.

The overall goal of this thesis was to investigate the role of two putative endocytosis motifs in the intracellular tail of MCAM. Specific aims were:

1. To generate Colo239F melanoma cell populations expressing wild-type MCAM, and MCAM containing disruptive mutations in the putative endocytosis motifs.
2. To explore the effect of wild-type and mutant MCAM expression on the metastatic phenotype of melanoma cells *in vitro,* including the effect of MCAM expression on other cell surface proteins
3. To determine whether the subcellular localisation of MCAM is altered by the disruptive mutations in the putative endocytosis motifs.
4. To investigate the expression of retromer components in melanoma cells, as a preliminary inquiry into the potential role of retromer in the intracellular sorting of MCAM

CHAPTER II:

Experimental Procedures

2.0 Experimental Procedures

2.1 Vector construction

Constructs were previously generated in pGEM-T-easy (Promega, Madison, WI) containing full-length wild-type (WT) MCAM using primers which introduced *Bam*HI and *Eco*RI restriction enzyme (RE) sites compatible with the multi cloning site of pLVX-EF1α-IRES-Puro(pLVX) (Clontech, Mountain View, CA) (Table 4). pGEM-MCAM was used for site-directed mutagenesis to construct mutants (MT) LL623-624AA (MCAM-LA) or Y641A (MCAM-YA) usingPhusion high fidelity DNA polymerase (New England Biolabs [NEB], Ipswich, MA) and non-overlapping primers containing the required base changes to be introduced (Table 4). Briefly,pGEM containing the MCAM insert (20 ng) was amplified in a 25 µl reaction using 1 µM site directed primers, 200 µM dNTPs, 1 x Phusion HF buffer and 1 unit of Phusion DNA polymerase. Cycle conditions were 98°C for 30 seconds (s), followed by 25 cycles of 98°C for10s, 60°C for 20s and 72°C for 20s. The use of non-overlapping primers produced a linear fragment which was further modified using the Kinase, Ligase and DpnI treatment kit (NEB) as per the manufacturer's instructions. The kinase and ligase treatment enabled recircularization of the linear fragment and the DpnI treatment digested any parental, non- mutated plasmid DNA. These new MT constructs were transformed and amplified as described below (Section 2.2).

Table 4: Primer sequences for MCAM expression vector construction and site directed mutagenesis

Primer name	Primer sequence (5'-3')
MCAM_pLVXF (EcoR1)	**GAATTC**AGCATGGGGCTTCCCAGGCTG*
MCAM_pLVXR (BamH1)	**GGATCC**CTAATGCCTCAGATCGATGT*
MCAM-L L623A L624A_F	GAGATGGGCGCCGCGCAGGGCAGCAGCGG
MCAM-L L623A L624A_R	TTCTGGGAGCTTATCTGAC
MCAM-L Y641A_F	GGAGAGAAAGCCATCGATCTGAGGC
MCAM-L Y641A_R	CTGGTCTCCCGGAGCCCTC

Restriction enzyme sites are shown in bold and MCAM sequence is underlined

WT and MT inserts were released from pGEM-T-easy using *Bam*HI/*Eco*RI double digest (HighFidelity [HF] enzymes from NEB) and separated by 1.5% agarose gel electrophoresis in Tris- Acetate-EDTA (TAE) buffer. WT and MT MCAM DNA bands were excised from the agarose following visualisation on a UV transilluminator and purified from the agarose using the ISOLATE II PCR and Gel Kit (Bioline, London, UK), as per the manufacturer's instructions. ThepLVX-EF1α-IRES-Puro (pLVX) expression vector (Clontech, Mountain View, CA) was also prepared by *Bam*HI/*Eco*RI double digest, gel separation and purification, as described above.

Following purification, MCAM fragments were ligated into the *Bam*HI/*Eco*RI sites of the multiple cloning site (MCS) of pLVX-EF1α-IRES-Puro (pLVX) (Clontech, Mountain View, CA). Vector: insert molar ratios of 1:1 and 3:1 were used in 10 µl ligation reactions containing T4 DNA Ligase (NEB), according to the manufacturer's protocol. Sequence and plasmid information for the pLVX-MCAM constructs are described in Chapter 3. Full nucleotide and protein sequence of MCAM are shown in Appendix 1.

2.2 Transformation and bacterial culture

WT and MT pLVX-MCAM constructs were transformed into chemically competent L10 Gold *E. coli* (kindly provided by Dr Carl Mousley, Curtin University). Plasmid DNA (10 - 100 ng) wascombined with 50 µl XL10 Gold *E.coli* and incubated on ice for 20 minutes (min), heat shocked at 42^{o}C for 30s, and allowed to recover for 5 min on ice. The entire volume was plated on Luria-Bertani (LB)-Agar plates containing 100 µg/ml ampicillin and incubated at 37˚C overnight (O/N). Single colonies were picked and amplified in 5 mL LB containing 100 µg/ml ampicillin at 37˚C with agitation O/N. Plasmid DNA was extracted using the ISOLATE II Plasmid Mini Kit (Bioline, London, UK), according to the manufacturer's instructions. Constructs were confirmed by sequencing (Australian Genome Research Facility [AGRF], Victoria, Australia). Sequence analysis is further explained in Chapter 3.

2.3 Cells and maintenance

Cells used, and their maintenance media and supplements are shown in Table 5. Cells were grown to 70-80% confluence before sub-culture. Culture media was aspirated, and cells washed using 2 mL Phosphate Buffered Saline (PBS) (Sigma Aldrich, St. Louis, MO). Cells wereincubated with 500 µL 0.05% v/v Trypsin-EDTA (TE) (Gibco, Thermo Fisher Scientific, Waltham, MA) at 37˚C until detached, before being recovered into 5 mL culture media and counted using a Particle Counter Z2 (Beckman Coulter, Fullerton, CA). Cells were re-seeded such that cells would be 80% confluent after 48-72 h culture. This cell number differed for each cell, according to cell size and growth rate. All tissue culture plasticware was from Nunc (Thermo Fisher Scientific).

2.4 Cell harvesting for experimental procedures

Cells were washed and trypsinised as above, resuspended in culture media, then pelleted by centrifugation at 200 g for 5 min. Cells were resuspended in 1 mL media for counting or washed in 3 mL PBS followed by centrifugation at 200 g for 5 min depending on the experiment.

2.5 Colo239F puromycin kill curve

To determine the concentration of puromycin optimal for selecting transduced Colo239F cells, cells were seeded into a 24-well plate at 10 x 10^5 cells/well in 2 mL culture media and grown for 48 h. Puromycin was added to duplicate wells (0-1 µg/mL) and cells observed over 72 hours, with the puromycin-containing media changed daily. From this, 0.3 µg/mL puromycin (90% cell death after 72 h at 37˚C) was chosen as the best concentration for selection. Following recovery from selection, transduced cells were maintained in medium containing 0.075 µg/mL puromycin.

Table 5: Cells used in this study.

Cell line	Origin	Notes	Growth Media
Melanoma			
Colo239F	Metastatic site –	MCAM negative,unmodified	RPMI
Colo239F-WT	Derived from Colo239F	MCAM positive	RPMI
Colo239F-LA	Derived from Colo239F	MCAM positive,LL623-624AA	RPMI
Colo239F-YA	Derived from Colo239F	MCAM positive,Y641A	RPMI
Colo239F-Neg	Derived from Colo239F	MCAM negative,control	RPMI
SB2	Primary melanoma	MCAM negative	DMEM
SB2 14.1	Derived from SB2	MCAM positive	DMEM
A2058	Metastatic site – lymph node	MCAM positive,unmodified	RPMI
MM253[#]	Metastatic site – lymph node	MCAM positive,unmodified	RPMI
MM96L	Metastatic site – lymph node	MCAM positive,unmodified	RPMI
SkMEL-28[*]	Metastatic site – lymph node	MCAM positive,unmodified	DMEM
Other			
Hek293T[*]	Kidney		DMEM

All cells used were adherent. RPMI: Roswell Park Memorial Institute; DMEM: Dulbecco's Modified Eagle Medium (Both Gibco, Life Technologies). All media were supplemented with 10% FBS,10mM Hepes, 2mM L-glutamine, 1mM sodium pyruvate. [*]A2069, SkMEL-28 and Hek293 cells are listedin the American Tissue Type Culture Collection (ATCC); [#] MM253 cells are listed in the European Collection of Authenticated Cell Cultures. SB2 cells were kindly provided by Dr Stèphane Karlen (Switzerland) and the Colo239F by a colleague.

2.6 Transfection and transduction

HEK293T cells were seeded into a 6 well plate at 1.0 x 10^6 cells/well in Opti-MEM media (Gibco) with 2 mM L-glutamine (Gibco) and incubated for 24 hours, then transfected with either MCAM-WT, MCAM-LA, or MCAM-YA; and the psPAX2 packaging vector and pMD2.G envelope vector. psPAX2 and pMD2.G were both gifts from Didier Trono (Addgene plasmid# 12260; http://n2t.net/addgene:12260; RRID:Addgene_12260 and Addgene plasmid # 12259; http://n2t.net/addgene:12259; RRID:Addgene_12259, respectively).

Transfection was performed according to the Invitrogen Lentiviral production workflow using Lipofectamine 3000 reagent (Invitrogen, Carlsbad, CA). Briefly, for each well to be transfected, the pLVX-MCAM expression vector was combined with the psPAX2 packaging vector, and pMD2.G envelope vector at a 5:3:2 ratio (2, 1.2 and 0.8 µg respectively) in 250 µlof Opti-MEM (Tube A), while 7 µl of Lippfectamine3000 was also diluted in 250 µl of Opti- MEM (Tube B). The contents of Tubes A and B were combined and incubated at room temperature (RT) for 15 mins before being added dropwise to the HEK293T cells. After 6 hours, the media was removed and replaced with fresh OptiMem transfection media. Lentiviral supernatant was collected at 24 - 48 h post-transfection, clarified by centrifugation at 500 g for 5 min and stored at -80°C.

For transduction, Colo239F cells seeded at 2.5 x 10^5 cells/well in a 6-well plate in normal growth media and incubated for 24 hours. Lentiviral supernatant was filtered through a 45 µM syringe filter (Millex, Millipore, Sigma Aldrich) and volumes of 1 mL, 0.5 mL, or 0.2 mL were used to infect the Colo239F cells (removing an equal volume of culture media). Cells were incubated O/N at 37°C and 5% CO_2. Viral supernatant media was aspirated and replacedwith normal growth media 24 h post-infection. Puromycin (0.3 µg/mL) was then added to thegrowth media to select for transduced cells. Media containing 0.3 µg/mL puromycin was replaced daily for 72-96 hours, after which it was replaced with media was containing 0.075 µg/mL puromycin as a maintenance dose. Colo239F cells surviving selection were expandedand assessed for MCAM expression via flow cytometry, immunofluorescence and western blot analysis.

2.7 Antibodies

For a full list of primary, secondary, and control antibodies, as well as their working concentrations refer to Tables 6 and 7.

Table 6: Primary antibodies used in this study for immunofluorescence (IF), flow cytometry (FC), and western blotting (WB)

Target	Antibody	Concentration	Source
CD146	Mouse monoclonal IgG2a (CC9 cl.19)	IF: 1 µg/mL WB: 1 µg/ml FC: 10 µg/mL	Dr. Andrew Zannettino
CD146-ICD	Rabbit monoclonal IgG (EPR3208)	IF: 1 µg/mL	Abcam
Rab4	Rabbit monoclonal IgG (EPR3043)	IF: 2.5 µg/mL	Abcam
Rab7a	Mouse monoclonal IgG2b (Rab7-117)	IF: 2 µg/mL WB: 1 µg/mL	Abcam
VPS35	Goat polyclonal IgG	IF: 0.6 µg/mL WB: 1 µg/mL	Abcam
COP1ß	Rabbit polyclonal IgG	IF: 9 µg/ml	Abcam
Calnexin	Rabbit polyclonal Ig	IF: 6 µg/ml	Abcam
ß1-Integrin	Mouse monoclonal IgG1 (P5D2)	IF: 1 µg/mL WB: 1 µg/mL	Abcam
Rab11	Rabbit polyclonal IgG	IF: 1 µg/mL	Invitrogen
Golgin97	Mouse monoclonal IgG1 (CDF4)	IF: 1 µg/mL	Invitrogen
αVinculin	Mouse monoclonal IgG1 (hVIN-1)	IF: 1/200	Ascites, Sigma
Lamp-1	Mouse monoclonal IgG1 (H4A3)	IF: 1 µg/mL	Developmental Studies Hybridoma Bank
Lamp-2	Mouse monoclonal IgG1 (H4B4)	IF: 1 µg/mL	Developmental Studies Hybridoma Bank
ß1-Integrin	Mouse monoclonalIgG1 (P5D2)	IF: 1 µg/mL	Developmental Studies Hybridoma Bank
ß-Tubulin	Mouse monoclonal IgG1 (E7)	IF: 1 µg/mL	Developmental Studies Hybridoma Bank
Moesin	Rabbit polyclonal IgG	IF: 1 µg/mL	Sigma
Galectin-3	Rat monoclonal IgG2a (Mac-2M3/38)	IF: 1 µg/mL	Developmental Studies Hybridoma Bank

Table 7: Secondary and isotype antibodies used in this study for immunofluorescence (IF), flow cytometry (FC), and western blotting (WB).

Target	Antibody	Concentration	Source
Isotype controls			
Mouse IgG2a		IF: 1 µg/mL FC: 10 µg/mL	Zymed, Thermo Fisher Scientific
Mouse IgG1		IF: 1 µg/mL	Zymed, Thermo Fisher Scientific
Rabbit IgG		IF: 1 µg/mL	Zymed, Thermo Fisher Scientific
Rat IgG		IF: 1 µg/mL	Zymed, Thermo Fisher Scientific
Secondary antibodies			
Anti-mouse IgG1 AlexaFluor 488		IF: 1/400	Invitrogen, Thermo Fisher Scientific
Anti-mouse IgG2a AlexaFluor 546		IF: 1/400	Invitrogen, Thermo Fisher Scientific
Anti-mouse IgG AlexaFluor 488		IF: 1/400	Invitrogen, Thermo Fisher Scientific
Anti-rabbit IgG AlexaFluor 488		IF: 1/400	Invitrogen, Thermo Fisher Scientific
Anti-rat IgG AlexaFluor 488		IF: 1/400	Invitrogen, Thermo Fisher Scientific
Anti-mouse IgG HRP		WB: 1/1000	DAKO, Glostrup, Denmark
Anti-mouse IgG FITC		FC: 1/40	DAKO, Glostrup, Denmark

HRP: horse radish peroxidase; FITC: fluorescein isothiocyanate

2.8 Flow cytometry

2.8.1 Single colour cell surface analysis

Flow cytometry was used to assess MCAM surface expression in Colo239F cells. Cells were harvested as above using 2.5 mM mM ethylenediaminetetraacetic acid (EDTA) in PBS, counted, and resuspended at 3.0 x 10^6 cells/ml in PBS/0.25% v/v BSA/1 mM EDTA(PBS/BSA). 1.5 x 10^5 cells (50 µl) were then aliquoted into round-bottomed tubes. Cells were labelled with primary antibody or isotype control (Tables 6, 7) diluted in 50 µl PBS/BSA and incubated for 30 min on ice. Cells were then washed with 3 ml PBS/BSA and centrifuged at 200 g for 5 min at 4˚C. The wash buffer was removed and cell pellet resuspended in 50 µl species-specific FITC-conjugated antibody (Table 6) in PBS/BSA for 30 min on ice in the dark,then washed with PBS/BSA, followed by PBS, as above. Dead cells were labelled with Zombie-NIR (Biolegend, San Diego, CA) diluted 1:2400 in PBS, then washed as above. Cells were resuspended in 100 µL PBS/BSA containing 1% v/v paraformaldehyde in PBS (PFA/PBS), thenstored on ice in the dark. Samples were processed on the Attune® Acoustic Focusing Flow Cytometer (Applied Biosystems, Foster City, CA) or the BD LSRFortessa™ cell analyser (BD Biosciences, Becton Dickinson, Franklin Lakes, NJ). Data was analysed using FlowJo v10 (TreeStar, Ashland, OR). Cell populations were gated via forward/side scatter to exclude cell debrisand for live cells, with 10 000 - 50, 000 events collected per sample. Fluorescence intensity was expressed as geometric mean of the gated populations.

2.8.2 Single colour total cell analysis

Flow cytometry was also used to analyse protein expression in permeabilised cells. Cells were harvested as in section 2.8.1. Cells were then fixed in 4% PFA on ice for 15 mins, pelleted at 200 g for 5 min, then resuspended at 3.0 x 10^6 cells/ml in permeabilisation buffer (PBS/0.5% BSA/0.1% saponin (Sigma Aldrich) and incubated on ice for 10 min. 1.5 x 10^5 cells (50 µl) were then aliquoted into round-bottomed tubes and labelled with primary or isotype control antibodies diluted in permeabilisation buffer for 30 min on ice. Cells were then washed in 4 mL permeabilisation buffer and collected by centrifugation at 200 *g* for 5 min at4˚C. Subsequently, cells were incubated with species-specific FITC-conjugated antibody in permeabilisation buffer for 30 min on ice in the dark, then washed as above. Finally, the cells were resuspended in 100 µL PBS/BSA containing 1% v/v paraformaldehyde in PBS (PFA/PBS), then stored on ice. Samples were analysed as in section 2.8.1.

2.8.3 Cell sorting

Cell sorting was used to collect MCAM-positive and MCAM-negative cell populations of Colo239F cells transduced with MCAM-WT, MCAM-LA and MCAM-YA. Each cell population underwent a preliminary and final sort to increase the purity of the positive cell populations.For setting gates: 2.5 x 10^5 cells were aliquoted into two round bottom tubes and labelled with anti-MCAM CC9 or mouse IgG2a isotype control antibody in sorting buffer (phenol red free RPMI/1 mM glutamine/1 mM NaP/1 mM HEPES/5% v/v FCS/25 mM sucrose) for 30 min on ice. Cells were washed with 3 mL sorting buffer followed by centrifugation at 200 *g* for 5 min at 4˚C. For sorting: 5.0 x 10^6 cells were added to nine consecutive sterile round bottom tubes, labelled with anti-MCAM antibody CC9, and washed as above. All cells were then incubated with α-mouse FITC antibody in sorting buffer, followed by Zombie-NIR as describedabove (section 2.8.1). Samples for sorting were combined and processed on a FACSJazz™ cellsorter (BD Biosciences, Becton Dickinson, Franklin Lakes, NJ). MCAM-negative and MCAM- positive cell populations were gated and sorted, before being returned to cell culture for expansion and further analyses.

2.9 Immunofluorescent staining

Glass coverslips (10 mm^2 diameter, Number 1 thickness) were UV (ultraviolet) sterilised and coated with 1 µg/cm^2 collagen I (Sigma Aldrich) in PBS in a 24-well plate O/N at 4ºC, before being washed with PBS. Cells were then seeded onto the coverslips at 1.5 x 10^5 cells per wellland grown to 70-80% confluence in normal media at 37°C and 5% CO_2. Cells for migrating cellstains were allowed to grow to 90% confluence and then a wound was created by dragging ap1000 pipette tip along the surface of the coverslip. The medium was then replaced and cellsallowed to migrate for 8 – 16 hours.

Prior to staining, cells were washed with warm HEPES buffered saline (HBS; 150 mM NaCl, 10 mM HEPES, 1mM MgCl2, 1 mM CaCl2), fixed with 4% PFA in HBS for 15 min at RT, and permeabilised with 0.1% v/v Triton X-100 (AMRESCO, Inc., Solon, OH) in HBS for 3 min at 4°C.Cells were rinsed with 3 x 1 mL HBS before incubation in blocking buffer (HBS, 10% v/v goat serum [Sigma-Aldrich], 1% v/v BSA) at 4°C overnight or 1 h at RT. Primary antibody was diluted in 2% v/v goat serum in HBS and 150 µL was added per coverslip and incubated for 1h at RT. Coverslips were washed with 3 x 1 mL HBS for 5 mins. Secondary antibody was dilutedin 2% v/v goat serum in HBS and 150 µL was added per coverslip and incubated at RT for 45 mins. Coverslips were washed 3 x 5 mins with HBS. 4’,6-Diamidine-2’-phenylindole dihydrochloride (DAPI; Sigma-Aldrich) was diluted to 1 µg/mL in HBS and 150 µL was added to the coverslips for 10 mins at RT. Coverslips were washed twice with HBS and mounted onglass slides using Vectashield mounting media (Vector Laboratories, Burlingame, CA). All imaging was performed using a Nikon A1 confocal microscope and analysis performed usingNIS-Elements Viewer (Nikon, Tokyo, Japan) and ImageJ (National Institutes of Health, Bethesda, Maryland, USA).

2.10 Migration and Cell Spreading Assays

2.10.1 Random Motion Motility Assay

Cells were seeded at 3.0 x 10^3 cells/well in 10 wells of a 96-well plate in normal growth medium and incubated at 37°C and 5% CO_2 for 30 min. The Tokai Hit® INU Stage Top Incubator and INUG2A Control Unit were used to perform live cell imaging on the Nikon A1 confocal microscope. Cells were incubated at 37°C and 5% CO_2 for 16-20 h, with phase contrast images taken at 30 min increments. Images were converted to .avi format and processed using Fiji (ImageJ) by utilising the manual tracking plug-in. Approximately 10 cells were tracked per well, with 10 wells analysed per cell population (100 cells in total). Cells were excluded from tracking if they had not spread out on the plastic, if they were unidentifiable from neighbouring cells, and if they remained stationary. Analysis was performed by calculating the total distance travelled and the distance from starting point toend point along a straight line.

2.10.2 Wound Healing Assay

Cells were seeded at 5.0 x 10^3 cells/well in 10-20 wells of a 96-well plate in normal growth medium and incubated at 37°C and 5% CO_2 O/N. Wounds were created using the IncuCyte® WoundMaker™. Cells were then rinsed 2x with 0.1 mL PBS and incubated in normal media with mitomycin C (0.3 µM) (Sigma Aldrich) O/N, which was previously shown in our laboratory to inhibit Colo239F proliferation. This allowed cell movement/invasion into the wound to be assessed without the potential confounder of cell proliferation. Cells were thenvisualised as in section 2.10.1.

2.10.3 Cell Spreading Assay

Cell adhesion assays were performed in 96-well plates. Nine wells were coated with 30 µL ofmatrix proteins diluted in PBS (Table 8) at 2 µg/cm^2 O/N at 4°C. Wells were washed twice with PBS. Cells were seeded at 2.0 x 10^3 cells per well in spreading media (RPMI/20 mM HEPES/2 mM L-glutamine/0.2% (w/v) BSA/ 1mM $MgCl_2$/0.1 mM $CaCl_2$). Cells were visualisedat 37°C and 5% CO_2 for 5 h and imaged at 100 x magnification every 15 min using the Nikon A1 confocal microscope. Quarter fields of view for each well were analysed and the percentage and length of cells which had spread were calculated at two time points (1 h, 2 h) using Fiji (ImageJ). For cell length, 50-500 cells per cell type were measured.

Table 8. Matrix proteins used to coat 96-well plates in spreading assays.

Matrix Protein	Source
Collagen Type I from calf skin	Sigma Aldrich, St. Louis, Missouri, USA
Collagen Type IV from human placenta	
Fibronectin I	
Laminin I from Engelbreth-Holm-Swarm murine sarcoma	

2.11 Cell lysate preparation

Cells were harvested (Section 2.4) and either stored at -80°C as pellets or processed immediately. Cell lysates were prepared by adding 100 µL lysis buffer (PBS/1% v/v NP40 [Sigma-Aldrich] containing 1x Complete Protease Inhibitor [Roche, Basel, Switzerland]) to thecell pellets. Lysates were incubated on ice for 30 min, centrifuged at 10,000 *g* at 4°C for 20 min, and supernatants collected.

2.12 BCA assay

Total protein content of lysates was measured using a bicinchoninic acid assay (BCA) (ThermoFisher) according to the manufacturer's instructions. Duplicate standard curves were produced in a 96-well plate and diluted lysates were measured against the curve. Standards and samples were both diluted in lysis buffer and 200 µL of BCA solution was added to eachwell. The plate was incubated at 37°C for 30 min and absorbance measured at 562 nm on theEnSpire Multinode Plate Reader (Perkin Elmer, Waltham, MA). Data were analysed in Excel.

2.13 SDS-PAGE, western blot and membrane staining

Samples were prepared by mixing equal volumes of lysate and 2x SDS loading buffer (4% SDS, 20% glycerol, 0.01% bromophenol blue, 100M Tris-HCl, pH 6.8; all from Sigma Aldrich) and boiling for 5 min at 95°C. Samples were separated via 10% SDS PAGE gel using a mini-gel apparatus (Hoefer, Holliston, MA) at 25 mA for 3 h. The SDS-PAGE running gel contained 10% 37.5:1 acrylamide/bis (Bio-Rad), 375 mM Tris-HCl, pH 8.8, 0.1% SDS; and the stacking gel contained 4% acrylamide/bis, 125mM Tris-HCl, pH 6.8, 0.1% SDS. Both were polymerised with the addition of ammonium persulfate and Temed. Following gel electrophoresis, samples were transferred onto a polyvinylidene difluoride (PVDF) membrane (MilliporeSigma, Burlington, MA) using a wet transfer system (GE Healthcare, Chicago, IL) at150 mA for 1 h. The membrane was blocked using blocking buffer (5% w/v skim milk powderin PBS, 0.1% v/v Tween-20 [PBST]; Sigma Aldrich) at RT for 1 h or O/N at 4°C. Primary antibodies were diluted in blocking buffer and incubated with the membrane a RT for 1 h or overnight at4°C. The membrane was washed 3 x with 5 mL PBST (5 min/wash). Species-specific HRP- labelled

secondary antibodies diluted in PBST were incubated with the membrane for 45 min at RT with agitation. Finally, the membrane was washed as above then rinsed with PBS. The membrane was developed using Clarity™ Western ECL Blotting substrate (Bio-Rad, Hercules,CA) and imaged on the ChemiDoc™ MP Imaging System using Image Lab Software version 6.01 (Bio-Rad).

2.14 Co-immunoprecipitation of MCAM and β1-integrin

Cells were harvested as above using 2.5 mM EDTA and washed twice in ice-cold PBS. The cell pellet was resuspended in lysis buffer (PBS/1% NP40 v/v) at 5 x 10^7 cells per mL, lysed on icefor 30 min, then pelleted at 10,000 *g* at 4°C for 30 min. 50 µL Protein G sepharose beads (Sigma Aldrich) were washed in 200 µL ice-cold PBS 3x by centrifugation at 100 *g* for 3 min then kept on ice. Supernatant collected from the lysate was incubated with the pre-washed Protein G beads end-over-end for 2 h at 4°C. Beads were then pelleted and pre-cleared supernatant collected and split equally between two 1.5 mL tubes. Anti-MCAM-ICD and anti-rabbit IgG isotype antibodies were diluted first in lysis buffer then added to separate lysates at a final concentration of 1 µg/mL, then incubated for 1 h end-over-end at 4°C. Protein G beads (100 µL per sample) were washed 3 x 3 min with PBS at 100 *g.* The lysates and beads were combined and incubated O/N end-over-end at 4°C. Samples were pelleted as above, supernatant was collected to check for unbound proteins, and beads were washed 2 x 3 minwith lysis buffer and 1 x 3 min with ice-cold PBS to remove unbound (non-specific) proteins. Samples and pre-collected supernatants were then processed according to section 2.12.

2.15 RNA extraction and cDNA synthesis

Biological replicates (n=5) from each melanoma cell line (Table 4) were harvested and pelleted, then stored at -80˚C until use. Cell pellets were lysed with 1 mL TRI Reagent® (Sigma-Aldrich), transferred to a 1.5 mL microtube and mixed vigorously with 0.2 mL chloroform for 15 s. After resting for 5 min at RT, samples were centrifuged at 12,000 g at 4˚C for 30 min. The aqueous layer containing RNA was transferred to a new tube, mixed with 0.5 ml isopropanol and stored at -20˚C for 20 min, followed by centrifugation at 12,000 g at 4˚C for 30 min. The supernatant was eluted, and the pellet was washed in 0.5 mL 70% v/v ethanol, then centrifuged at 8,000g for 10 min. The ethanol was removed, and the samples air dried for 1 h before resuspension in 50 µL RNAse-free water. RNA concentration and purity was determined using the Nanodrop™ 1000 spectrophotometer (ThermoFisher Scientific). 500 ng of RNA was used for cDNA synthesis using the Tetro cDNA Synthesis Kit (Bioline) using random hexamer and Oligo (dT) primers; total reaction volume 20 µl. Thermocycling conditions were: 10 mins at 25°C, 1h at 42°C, 10 mins at 65°C. 5 µL cDNA was diluted 1:10 in DEPC-treated water for use in qPCR; with the remainder stored neat at -20˚C.

2.16 Quantitative Real-Time PCR (qPCR)

All qPCRs were conducted using the 2x SensiFAST™ Sybr® No-ROX (Bioline) reaction mix, according the manufacturer's instructions. Reference genes analysed included beta-actin (*ACTB*), succinate dehydrogenase complex subunit A (*SDHA*), TATA-binding protein (*TBP*) and glyceraldehyde 3-phosphate dehydrogenase (*GAPDH*). Target genes including the sorting nexins (SNX) *SNX1-6, SNX17, SNX27, SNX31*; *vacuolar* protein sorting-associated proteins *VPS26A, VPS26B, VPS29, VPS35,* and Ras-related protein *Rab7A* were analysed (see Table 9 for oligo sequences, annealing temperatures and amplification efficiency data). qPCR was performed using 7.5 µL 2x SensiFAST™ Sybr ® No-ROX, 1 µL 1:10 diluted cDNA, and 1 µL of each primer at 10 µM. Cycle conditions were: 95°C for 2 min followed by 40 cycles of 95°C for 10s, annealing step for 15s (see Table 9 for primer-specific annealing temperatures), and72°C for 20s. Melt curve analysis was performed at 95°C for 15 s, followed by 55°C to 95°C, over 5 min at 0.5°C increments.

Primer efficiency was assessed using serial dilutions of pooled cDNA and plotting the Ct valueof the dilutions against a log scale of the dilution factor, then using the slope of the line to determine efficiency using the formula $(10^{(-1/slope)}-1) \times 100$ (see Appendix 2 for efficiency graphs). Melt curve analysis was performed to determine a single amplicon for all experiments and amplicons were also electrophoresed for a subset of samples to confirm anamplicon of the expected size (data not shown). Data were analysed by the delta-delta-Ct (ΔΔCt) method (Schmittgen and Livak 2008). Ct values were normalised against the geometric mean of the housekeeping gene/s Ct for each sample, and then against the average ΔCt of the SB2 cell line for each gene (used as a control sample due to being MCAM-negative and non- metastatic).

2.17 siRNA knockdown

Pre-validated siRNA constructs were chosen to knockdown VPS35 and SNX3 and AllStars Negative Control siRNA (Qiagen) was used as a control. A lipofectamine only control was alsoused. siRNA and lipofectamine master mixes were prepared by adding either 12.5 uL of siRNA(10 uM) or lipofectamine to 162.5 uL Opti-MEM media (Gibco) per sample. The siRNA and lipofectamine master mixes were mixed and incubated at RT for 20 min. MM253 cells were seeded at 6.0 x 10^4 cells/well into a 6-well plate containing 2 mL normal culture media and, while they were still in suspension prior to adhering, the siRNA/lipofectamine master mix was added. Transfected cells were incubated 48 h at 37°C and 5% CO_2 and then assessed forknockdown of VPS35 or SNX3 via western blot.

Table 9: Target and reference gene primers used in q-PCR.

Gene	Forward primer (5'-3')	Reverse Primer (5'-3')	Efficiency (%)	Annealing Temp
SNX1	AAGCACTCTCAGAATGGCTTC	CGGCCCTCCGTTTTTCAAG	108.52	66˚C
SNX2	TCTGCTCCCGTGATCTTTGAT	AAACCAAGAAAGTCGCTGAATCT	90.94	60 ˚C
SNX3	CCAAGCCGCAGAACCTGAAT	GACCCTGATTTCGTAAGTGGTG	120.51	64˚C
SNX4	GAGTCAGAGCTAGAGTAGCAGAT	ATGGCACTCCATTCACTGAAAA	98.65	64˚C
SNX5	TCTGTATCTGTGGACCTGAATGT	GTGGGCAGTGTGGTCTTGT	93.77	60˚C
SNX6	TTTCTTTGAGCACGAACGAACA	GACCTAGACCTTCGATACAGGAG	94.52	60˚C
SNX17	CGCCTACGTGGCCTATAACAT	CAATGGGTCTTGCCGAACAG	87.44	62˚C
SNX27	CAAGTCCGAGTCCGGCTAC	CCTGCTCGAATCAGGTCCA	90.81	64˚C
SNX31	GCACGTTGGAACGAACAG	CTTTCTTGGTGGCGATGTCA	NA	NA
SNX31.2	GGGCAAGCTCTCTGTTGTGAA	TTCGGAGTCCAACCTTACAGT	NA	NA
VPS26A	TTCAGGAAAGGTAAACCTAGCCT	ATTGGCACCGATGTAAGATTCAT	89.31	62˚C
VPS26B	CTGAACGATGCAGAGAGTAGGA	CCCCGTCGTAGAAGAGGAAATA	93.00	64˚C
VPS29	TGCAACAGTTTGCCAGCTAAA	CCTCTGCAACAGGGCTAAGC	118.43	66˚C
VPS35	GTTTTGACTGGCATATTGGAGCA	TCTGGTGTAACTCAGCACAGG	101.22	60˚C
RAB7A	AGACTGCTGCGTTCTGGTATT	ACTTGTCTGTTTTCGAGGTCAAT	82.96	66˚C
TBP	CCCGAAACGCCGAATATAATCC	AATCAGTGCCGTGGTTAGTG	97.99	62˚C
ACTAB	TCCCTGGAGAAGAGCTACG	GTAGTTTGGATGCCACA	103.64	48˚C
SDHA	TGGCATTACGACACCGTG	GCCTGCCGTGGTTAGTG	86.1	50˚C
GAPDH	AAGGGATTTGGTCGTATTGGGC	AGGGATGATGTTCTGGAGAGCC	89.0	58˚C
MCAM-L	CGCTGTCCTCTATTTCCTCTAT	CAACTACAAGTTCGCTCTTACG	121.92	62˚C
MCAM-S	CGCTGTCCTCTATTTCCTCTAT	TTTCTCTCCATCTCCTGCTTC	80.96	60˚C

SNX1, SNX17, SNX27, VPS29 primer sets did not achieve ideal efficiency, so data was interpreted with care and optimisation is ongoing.

2.18 Cell aggregation assay

Cells were harvested using 2.5 mM EDTA and washed with serum-free RPMI. Cells were resuspended in adhesion media (RPMI, 0.5% v/v BSA, 100 mM HEPES, 1 mM sodium pyruvate) at 1.5 x 10^6 cells/mL. 200 uL of the cell suspension was added to a round-bottom tube and incubated at 37°C for 40 min to allow cell aggregation. 100 uL of 4% v/v paraformaldehyde in PBS was then added to prevent further aggregation. Wet mounts of thecells were viewed under the x4 objective lens using an Axiovert S100 microscope and imaged using the MC80 camera unit (Zeiss, Oberkochen, Germany). Aggregate area was measured using the Scion Image beta 4.02 software (2000 Scion Corporation, Frederick, MD).

2.19 Cell network assay

Wells of a 96-well plate were coated with 40 µL of Matrigel (BD Biosciences), diluted 3:1 withcold PBS. The Matrigel was polymerised by incubating at 37°C for 30 min. Cells were then harvested using 2.5 mM EDTA, washed and resuspended in culture media at 2.0 x 10^5 cells/mL. 100 µL of the cell suspension was added to each well. The cells were incubated at 37°C and 5% CO_2 for 24 h and imaged using an Axiovert S100 microscope and imaged using the MC80 camera unit.

2.20 Growth curves

Cells were harvested as above and pelleted at 200 *g* for 5 min, resuspended in 1 mL media, and seeded into each well of a 24 well plate at 1 x 10^4 cells/mL, then incubated at 37°C and 5% CO_2. Wells were harvested in quadruplicate using 0.2 mL TE, resuspended in 0.5-1 mL of growth medium, and counted using the Beckman Coulter® Particle Counter Z2 daily for six days. A growth curve was generated by plotting cell number against time in hours for each cell line assayed. Cell doubling time was calculated from the curve.

2.21 Statistical Analysis

GraphPad Prism™ was used for all statistical analysis. Data was analysed using the d'Agostino's K-Squared test to determine whether it was normally distributed. Normally distributed data was analysed using ANOVA followed by the post-hoc Dunn's multiple comparisons test. Non-normally distributed data was analysed using the non-parametric Kruskal-Wallis followed by the post-hoc Dunn's multiple comparisons test. A $p \leq 0.05$ was considered statistically significant.

CHAPTER III:

Plasmid and Cell Line Generation

3.0 Plasmid and Cell Line Generation

3.1 Introduction

Multiple studies have investigated the role of MCAM by transfecting full-length MCAM into MCAM-negative melanoma cells. MCAM expression is markedly increased as melanocytes undergo transformation into malignant melanoma (Luca et al. 1993), so enforced expression of MCAM is a valuable experimental procedure for exploring the role MCAM plays in melanoma progression. Significantly, this approach allows for MCAM-negative and MCAM-positive cells to be theoretically identical in every other way, controlling for differences between cell populations.

The first study of this type transfected three MCAM-negative melanoma cell lines with full- length MCAM, and found that MCAM increased homotypic adhesion and aggregation between melanoma cells (Johnson et al. 1997). Later, a study by the same group transfected the MCAM-negative SB2 cell line with full-length MCAM and found increased tumorigenicity and metastasis, indicated by increased adhesion, aggregation, and invasiveness of these cells (Xie et al. 1997). Similar findings were established later, where forced expression of MCAM in two MCAM-negative melanoma cell lines showed increased adhesion and formation of tumour clusters (Schlagbauer-Wadl et al. 1999). Later, the role of MCAM-L in melanoma was explored by transfecting full- length MCAM into three cell lines (Dye 2007). This study again found an increase in homotypic adhesion, a decrease in cell-ECM interactions, and increased invasion, suggesting that MCAM may favour collective migration of melanoma cells (Dye 2007).

In non-melanoma cells, MCAM-L and MCAM-S have been transfected into natural killer (NK) cells as well as endothelial cell lines (Guezguez et al. 2006; Guezguez et al. 2007). These studies found that MCAM-L, but not MCAM-S, increased the transendothelial migration of NK cells (Guezguez et al. 2006). These studies also found the dileucine motif in the intracellular tail of MCAM-L was involved in targeting it to the basolateral membrane in endothelial cells, while MCAM-S was targeted to the apical membrane (Guezguez et al. 2007).

The role of MCAM has been well-established in the literature, but specific mechanisms by which MCAM contributes to phenotypic changes in melanoma progression are not completely understood. Furthermore, the role of specific domains in the intracellular tail requires further investigation. Therefore, the MCAM-negative Colo239F human melanoma cell line was chosen to develop cells expressing WT and mutant (MT) MCAM. This cell line was derived from a melanoma on a patient's shoulder (Moore et al. 1980) and was chosen due to its lack of endogenous MCAM expression, to complement work previously completed in our laboratory using the SB2 MCAM negative cell line. To evaluate the role of the putative endocytosis (di-leucine and tyrosine) motifs in the intracellular tail of MCAM, mutations were introduced to replace residues in these motifs with alanine. Alanine was chosen as it contains a chemically inert methyl function group, can mimic the secondary structure of many other amino acids and is unlikely to cause conformational changes. The goal

of this approach was to explore potential loss/gain-of-function changes in the phenotype in these cells, compared to Colo239F cells expressing WT-MCAM, or MCAM- negative Colo239F cells.

Previously, lipid based plasmid transfection was used in our laboratory to introduce MCAM into the SB2 melanoma cells. However, this process had a low success rate and required multiple rounds of selection and single cell cloning (Dye 2007). Considering this, and the technological advances made since 2007, a lentiviral transduction system was chosen to introduce WT and mutant (MT) MCAM sequences into the Colo239F cell line. The lentiviral system chosen utilised the pLVX-EF1α-IRES-Puro transfer vector, which contains an internal ribosomal entry site (IRES) situated between the insertedgene and a puromycin resistance gene, which allows bicistronic expression from a single promoter (Fig. 8). To complement this, the second generation pMD2.G envelope plasmid and psPAX2 packaging plasmid were used.

Furthermore, considering the lack of literature exploring the role of the putative endocytosis/recycling motifs in the function of MCAM, *in silico* analyses were used to explorethe structural stability of the mutations chosen for this study. A previous study suggested that a L623P or Y641G mutation could be associated with increased degradation of the MCAM protein in transfected cell lines (Dye 2007).

The COSMIC (catalogue of somatic mutations in cancer) identifies 375 mutations in nearly 40 000 samples (Tate et al. 2019). Amongst these, three variants at amino acid (AA) 623 were described (L623I, all in colon carcinoma); with none at AA 641, although there were four at AA 643 (D643N and D643Y; in colon, haemopoietic and endometrial cancer)(Tate et al. 2019). The small numbers of mutations described in these residues, and none associated with melanoma, suggests they may be important in MCAM function.

This chapter describes the generation of the plasmid constructs used to transduce the Colo239F cell line with WT and mutant MCAM, as well as the generation and characterisation of stable Colo239F cell populations expressing WT and MT MCAM,

3.2 Supplemental Methods

3.2.1 Prediction of Effect of Amino Acid Substitutions

The MCAM protein sequence (NP_006491.2) was submitted to various software tools along with the amino acid substitutions used in this study (LL623-624AA and Y641A) to predict the effect these mutations might have on the structure and function of the protein. Software utilised included: PolyPhen-2 (Adzhubei et al. 2010), PROVEAN (Protein Variation Effect Analyzer) (Choi and Chan 2015), PMut2017 (López-Ferrando et al. 2017), and Align-GVGD (Tavtigian et al. 2008). In addition, iPTREE-STAB and iMutant 3.0 were used to determine potential effects on protein stability at 37˚C and 7.4 pH (Capriotti et al. 2005; Huang et al. 2007), with parameters were otherwise left at default.

3.3 Results

3.3.1 Construction of lentiviral expression vectors

pLVX-EF1α-IRES-Puro constructs were successfully generated containing MCAM-WT, MCAM-YA (Y641A), or MCAM-LA (LL623-624AA) inserts (described in Section 2.1) and validated by sequencing. The motifs containing targeted amino acids are shown in Fig. 8A. The cropped sequences of successfully generated constructs are shown in Fig. 8B, with the top consensus sequence displaying the LL623-624AA mutation, and the bottom consensus displaying the Y641A mutation. The rest of the intracellular MCAM sequence was unchanged from WT- MCAM (Fig. 8A). Plasmid maps for the pLVX-EF1α-IRES-Puro and pGEM-T-Easy TA cloning vector used are shown in Fig. 8C.

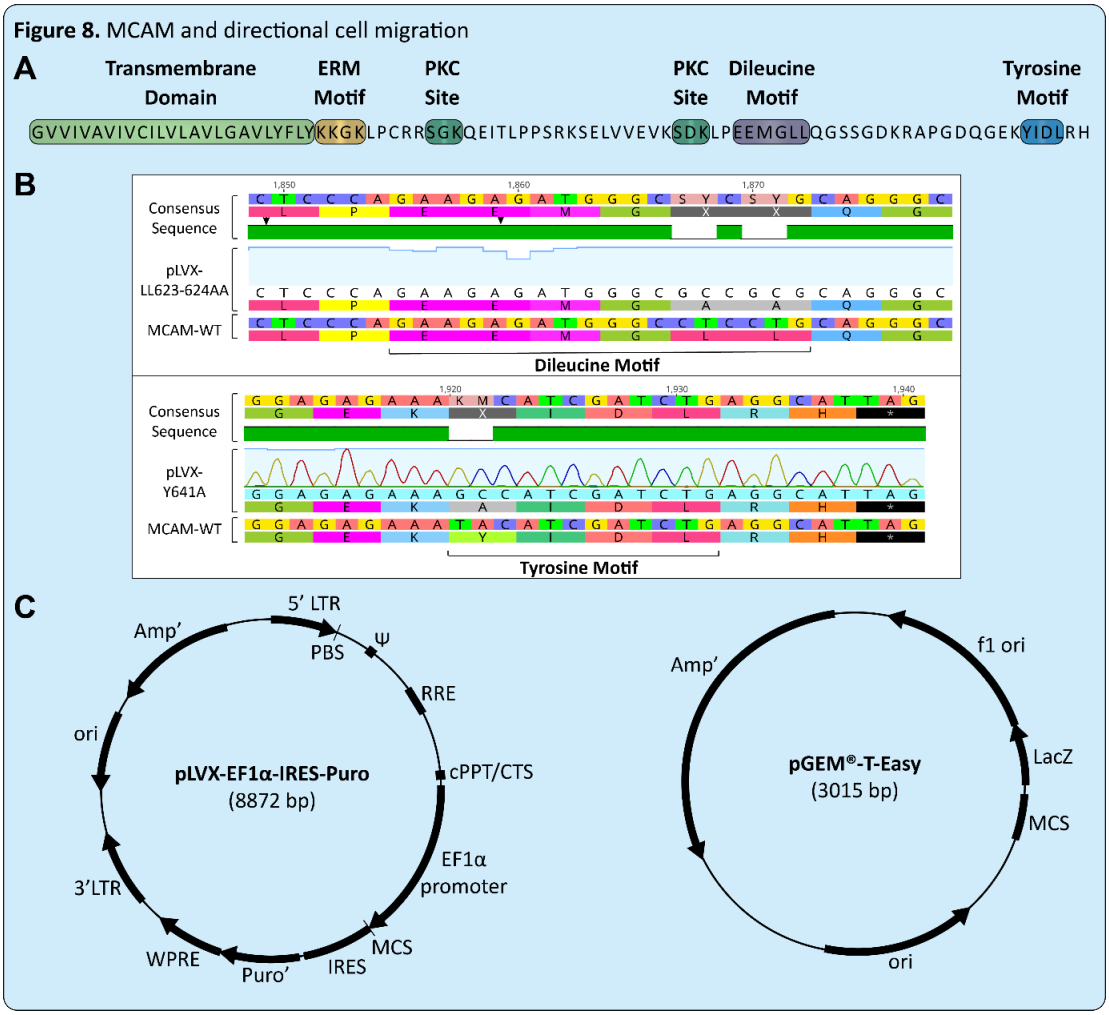

Figure 8. Sequence and plasmid information. (A) Sequence and putative domains in the intracellulartail of MCAM. (B) Sequencing results following insertion of mutant MCAM-LL623-624AA and MCAM-Y641A sequences into pLVX aligned with wild-type MCAM using Geneious™. Gaps in the green consensus sequence indication position of mutations. (C) pLVX-EF1α-IRES-Puro and pGEM-T-Easy plasmid maps (adapted from manufacturer).

3.3.2 Transfection, transduction and flow sorting

Parental Colo239F cells displayed a very low level of endogenous MCAM expression via flowcytometry, with approximately 1.6% cells showing low MCAM expression (Fig. 9A). Following puromycin selection and cell expansion, parental Colo239F cells transduced with either pLVX-WT, pLVX-YA, or pLVX-LA were analysed for MCAM cell surface expression via flow cytometry (Fig. 9).

Colo239F cells transduced with pLVX-WT produced two cell populations displaying bimodal MCAM expression: Colo239F-WT1.1 (28.8%) (data not shown) and Colo239F-WT1.2 (71.5% MCAM-positive) (Fig. 9B). The Colo239F-WT1.2 cells were subjected to cell sorting to produce the MCAM-positive Colo239F-WT2.1 (94.4% MCAM-positive) and MCAM-negative Colo239F-WT2.1-Neg (9.03% MCAM-positive) cells (Fig. 9C-D). The Colo239F-WT2.1 cell population was then subjected to an additional round of cell sorting to produce the final Colo239F-WT3.1 (94.8% MCAM-positive) (Fig. 9E) and Colo239F-WT3.1-Neg (0.42% MCAM-positive) cells (Fig.9F).

Colo239F cells transduced with pLVX-LA also produced a cell population with bimodal MCAM expression: Colo239F-LA1.1 (5.82% MCAM-positive) (Fig. 9G). The Colo239F-LA1.1 cells were then subjected to cell sorting to produce the MCAM-positive Colo239F-LA2.1 (69.9% MCAM- positive) (Fig. 9H) and MCAM-negative Colo239F-LA2.1-Neg (7.07% MCAM-positive) cells (Fig. 9I). As the Colo239F-LA2.1 cell population had two distinct peaks, it was subjected to an additional round of cell sorting to produce a more homogenous MCAM positive population, Colo239F-LA3.1 (92.2% MCAM-positive) (Fig. 9J) and Colo239F-LA3.1-Neg (0.74% MCAM-positive) cell s (Fig. 9K).

Colo239F cells transduced with pLVX-YA produced two cell populations with bimodal MCAM expression: Colo239F-YA1.1 (4.02% MCAM-positive) (Fig. 9L) and Colo239F-YA1.2 (1.82% MCAM-positive) (data not shown). The Colo239F-YA1.1 cells were subjected to cell sorting to produce the MCAM-positive Colo239F-YA2.1 (66.6% MCAM-positive) (Fig. 9M) and MCAM- negative Colo239F-YA2.1-Neg (2.03% MCAM-positive) (Fig. 9N) cells. The Colo239F-YA2.1 cells were then subjected to an additional cell sort to produce the final Colo239F-YA3.1 (79.5% MCAM-positive) cell population (Fig. 9O). For comparison, the native MCAM-expressing human melanoma cell line MM253 is shown in Fig. 9P.

Colo239F-WT3.1, Colo239F-YA3.1, Colo239F-LA3.1, and Colo239F-LA3.1-neg cells lines were chosen for further analysis. These cell populations were maintained in cell culture for 4 weeks and MCAM expression remained stable when cells were grown in a maintenance concentration of 0.075 ug/mL puromycin. Intermediary and final cell populations were all frozen down andstored in liquid nitrogen.

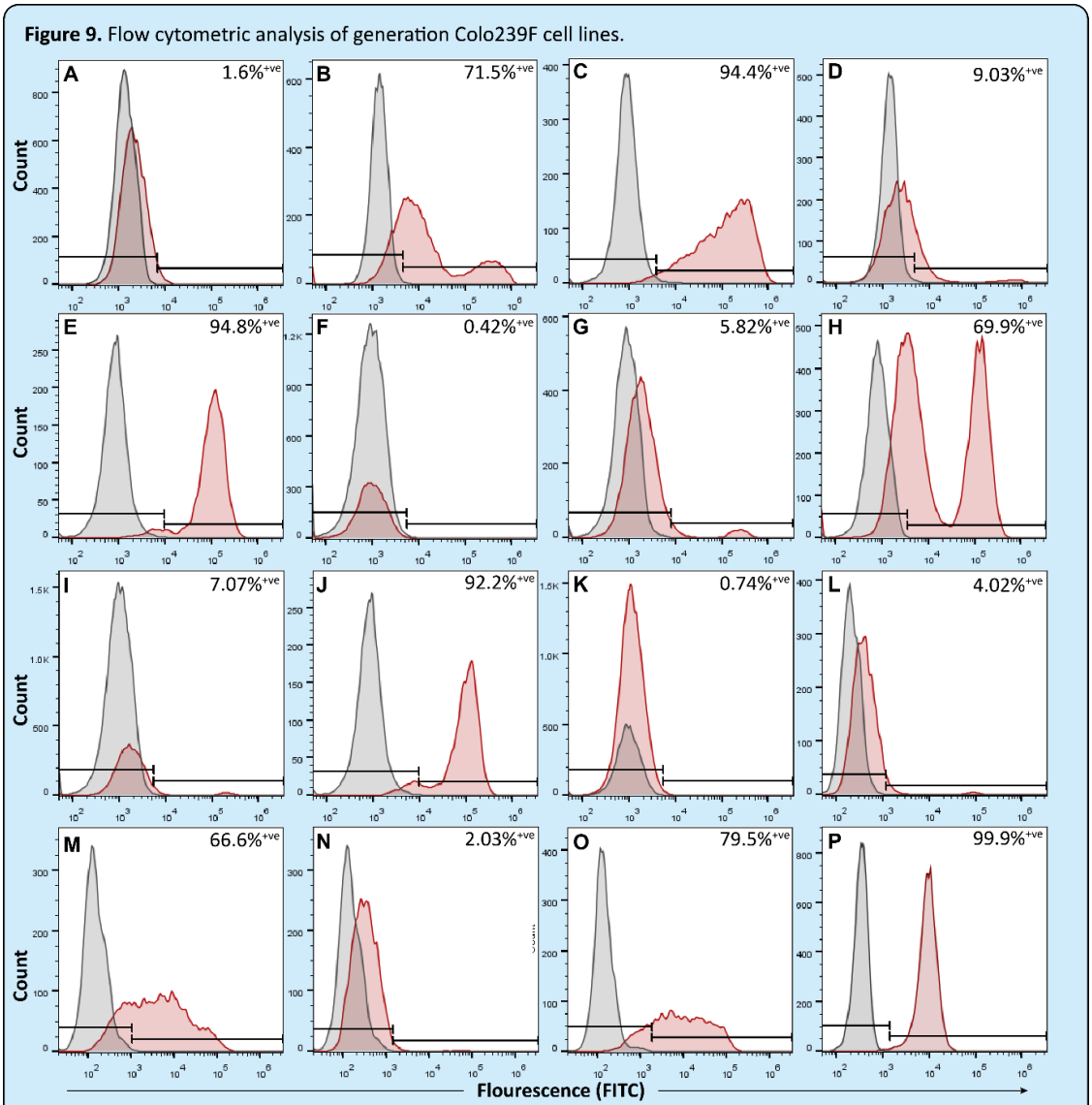

Figure 9. Flow cytometric analysis of generated Colo239F cell lines. (A) Colo239F-parental. **(B)** Colo239F-WT1.1. **(C)** Colo239F-WT2.1. **(D)** Colo239F-WT2.1-Neg. **(E)** Colo239F-WT3.1. **(F)** Colo239F-WT3.1-Neg. **(G)** Colo239F-LA1.1. **(H)** Colo239F-LA2.1. **(I)** Colo239F-LA2.1-neg. **(J)** Colo239F-LA3.1. **(K)** Colo239F-LA3.1-Neg. **(L)** Colo239F-YA1.1. **(M)** Colo239F-YA2.1. **(N)** Colo239F-YA2.1-Neg. **(O)** Colo239F-YA3.1. **(P)** MM253.

3.3.3 Immunofluorescence Analysis

The cellular localisation and expression of MCAM were explored by immunofluorescent staining. Cellular distribution of MCAM was largely consistent between the Colo239F-WT3.1,Colo239F-LA3.1, and Colo239F-YA3.1 cells(Fig. 10C-H). The staining pattern of MCAM was also consistent with the native MCAM-expressing MM253 cells (Fig. 10A-B). MCAM staining appeared throughout the cell, with strong cell surface staining.

3.3.4 Western Blot Analysis

Total cellular MCAM expression was examined by SDS-PAGE and western blot analysis following flow cytometric analyses of cell surface MCAM. Lysates were prepared for the Colo239F-WT3.1, Colo239F-LA3.1, Colo239F-YA3.1, Colo239F-parental and Colo239F-LA3.1-Neg cells, and from two cell populations that naturally express MCAM, MM253 and A2058. Lysates were quantified by BCA protein assay and 10 µg of each lysate was separated by SDS-PAGE. Blots were performed using the anti-MCAM antibody CC9. A strong band at approximately ~113 kDa was identified for each cell population, except for the Colo239F-LA3.1-Neg and Colo239F parental cells, which each had a very faint band at this molecular weight (Fig 10I). This is the approximate size of MCAM protein; indicating that the Colo 239F-MCAM-positive cells strongly express MCAM whereas the MCAM-negative cells expressed MCAM at a very low level, consistent with the flow cytometry data. For comparison, the native MCAM-expressing MM253 and A2058 cell populations are shown.

Figure 10. Analysis of MCAM expression.

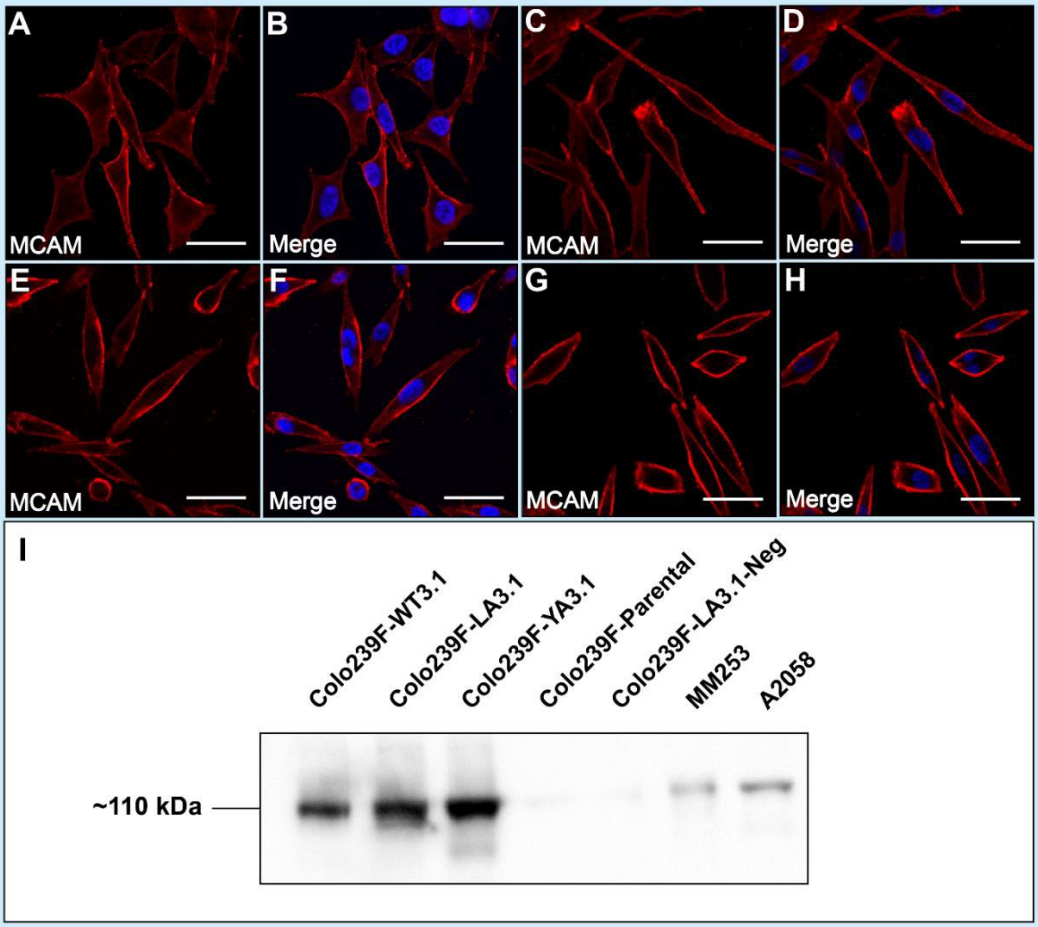

Figure 10. (A-B) MCAM expression in MM253 cells. **(C-D)** MCAM expression in Colo239F-WT3.1 cells. **(E-F)** MCAM expression in Colo239F-LA3.1 cells. **(G-H)** MCAM Expression in Colo239F-YA3.1 Cells. **(I)** Western blot for MCAM using the anti-MCAM CC9 antibody.

3.3.5 *In Silico* Analysis of Mutant MCAM Structure and Function

To explore the potential structural and functional effect of the LL623-624AA and Y641A mutations on MCAM, the protein sequence was analysed using various software tools whichpredict the impact of amino acid substitutions on protein structure and function. The effect of these substitutions on protein stability was also explored using iPTREE-STAB (Table 10).

The results from each of these software tools were largely consistent. PolyPhen-2 predicted each substitution to be probably damaging with a maximum score of 1.000. PMut also predicted that each mutation had a high probability of causing disease and Align-GVGD predicted that each mutation was in the C65 class, which is most likely to interfere with protein function according to its algorithm. The only analysis software which predicted discordant results was PROVEAN, which predicted that L623A and L624A were deleterious toprotein function, but Y641A was neutral. For protein stability, iPTREE-STAB predicted that each mutation would be destabilising to the protein structure.

Table 10. Prediction of amino-acid substitution effect on protein function and structure.

Mutation	PolyPhen-2	PROVEAN	PMut	Align-GVGD	iPTREE-STAB
L623A	Probably Damaging (Score =1.000)	Deleterious (Score = - 2.883)	Disease(0.52)	GV = 0.00, GD= 96.19 Class C65	Destabilising (-1.1575 kcal/mol)
L624A	Probably Damaging (Score =1.000)	Deleterious (Score = - 2.960)	Disease(0.75)	GV = 0.00, GD= 96.19 Class C65	Destabilising (-1.1575 kcal/mol)
Y641A	Probably Damaging (Score =1.000)	Neutral (Score = -1.318)	Disease(0.85)	GV = 0.00, GD= 111.59 Class C65	Destabilising (-1.4725 kcal/mol)

GV = Grantham variation, GD = Grantham deviation

3.4 Discussion

3.4.1 Transduction of Colo239F-parental cells

While the generation of MCAM-WT, MCAM-LA, MCAM-YA, and MCAM-negative cell populations using the lentiviral-based transduction system was ultimately successful, it was time-consuming and labour intensive. Lentiviruses derived from HIV-1, such as pLVX-EF1α- IRES-Puro, have the significant advantage of producing stable and sustained expression of a target protein (Boulaiz et al. 2005). Furthermore, viral methods of transduction are generally more efficientthan non-viral methods of transfection *in vitro* (Boulaiz et al. 2005; Iversen et al. 2005). To date, three generations of HIV-1 based lentivirus systems have been produced (Milone

and O'Doherty 2018). This study utilised the second generation, chosen based on considerations of availability as well as viral titre production capacity (Milone and O'Doherty 2018). The third generation of lentiviral systems sacrifices some viral titre producing capability for greater safety, by separating the packaging system into two separate plasmids (information received from Addgene).

The pLVX-EF1α-IRES-Puro transfer vector contains a puromycin gene which is expressed in a bicistronic manner along with the inserted gene of interest (Fig. 8C). This system should ensure that the gene of interest and the antibiotic resistance gene are always co-expressed. Despite this, significant proportions of the transduced cell populations which survived antibiotic selection were MCAM-negative. This may have occurred for many reasons. The selection protocol and concentration of antibiotic were determined based on the results of a puromycin kill curve experiment (Section 2.5), however, increasing the selection time or concentration of puromycin may have successfully eliminated at least some of the false-positive cells. Antibiotic-resistant but MCAM-negative transductants result from the antibiotic resistance gene remaining active whilst MCAM does not, an issue that should have been mitigated by the use of a bicistronic promoter.

Therefore, the cells may have developed spontaneous resistance to puromycin. For instance, it has been reported that chromosomal rearrangements caused by aneuploidy in cancer cell lines can result in spontaneous multiple resistance at far greater levels than normal (Duesberg et al. 2001). Furthermore, gene silencing following transduction is commonly reported in the literature. PCR analysis could have been performed on the cell populations which were puromycin- resistant but MCAM-negative, to confirm the presence or absence of the coding sequence of MCAM in cellular DNA. However, due to time limitations, this was not pursued.

In addition, gene silencing can occur by multiple mechanisms, including DNA methylation induced silencing. Hypermethylation of transgene promoters has been identified as a targeted cellular approach to silence integrated genes (He et al. 2005) and has been found to affect upto one-third of lentiviral integrations in a porcine model (Hofmann et al. 2006). Recently, it has been discovered that utilising ubiquitously acting chromatin opening elements (UCOEs) in lentiviral vectors may mitigate this issue, as they are resistant to methylation (Zhang et al. 2007). Therefore, it is apparent that epigenetic modifications regulate lentiviral integrations, potentially as a defence against viral infection.

Another mechanism of transgene silencing is RNA silencing/interference (Schepers and Kolter 2001). It is likely that this mechanism evolved as a cellular immune system against viral infection (Elbashir et al. 2001). For instance, microRNA 329 has been found to supress excessive MCAM expression in a mouse model (Wang et al. 2013). A similar mechanism may be occurring in the Colo239F cells in response to enforced MCAM expression. These mechanisms might explain theMCAM-negative, yet antibiotic resistant cells found in this study. However, we did not explore the potential role of miRNA silencing in this study, as the priority was to select the MCAM expressing cells for further analyses.

Furthermore, the calculation of viral titre before transduction was not performed in the interest of limited time and resources. However, properly calculating viral titre before performing the transductions may have ensured more successful infection, and thus integration of our target genes, and avoided the time and labour-intensive process of cell sorting, which was necessary to produce populations of cells with MCAM expression. Two sorts were required to generate populations with homogenous expression profiles similar to native expressers such as the MM253 and A2058 melanoma cell lines (Fig. 9). This was time consuming and limited the time available for subsequent characterisation experiments. The ratio of packaging, envelope, and transfer vectors used to transfect the Hek293T cells may also have been sub-optimal. Having had sufficient success in each transduction to move forward with cell sorting, little optimisation was performed to improve efficiency of the transduction protocol.

The integration of lentiviral transgenes into the genome is random, which presents possible difficulties in ensuring transgene expression, as well as preventing mutagenic effects which might result from a disruptive integration (Smith 2001). Once stable transductants were produced, an homogeneously expressing population was isolated by cell sorting, but single cell cloning was not performed. We choose to use a mixed population to reduce the effect of clonal artefacts, so that we could be more confident that any phenotypic alteration in the cells was due to the expression of MCAM and not to an unintended genomic change.

Interestingly, MCAM-negative but puromycin-resistant cells were far more common in the mutant MCAM transductants than with WT MCAM. As seen in Fig. 9, the proportion of MCAM-positive cells in Colo239F-%T1.1 was 71.5% while Colo239F-LA1.1 and Colo239F-YA1.1 were 7.07% and 4.02%, respectively. More interestingly, this finding mirrors the effect noted in a previous study which sought to transfect the SB2 cell line with MCAM containing similar mutations (Dye 2007). There it was speculated that this effect might be due to regulation at either the nucleic or protein level. A compelling argument is that, since these mutations are rare, and their effect on protein structure or folding is unknown, they may be targeting the mutant MCAM protein for degradation (Dye 2007). The ER and Golgi apparatus identify proteins which are incorrectly folded, and target them for degradation in the lysosomes (Ellgaard and Helenius 2003).

To explore this possibility further, computations were performed *in silico* to determine whetherthe LL623A-624AA and Y641A mutations would be detrimental to protein structure. Indeed, all prediction software used returned a result indicating that these substitutions were likely to be detrimental to protein structure and function (Table 10). Therefore, it is possible the MT proteins may be identified as misfolded and targeted for degradation at a higher rate than the WT protein. Although degradation rate is unlikely to fully explain the differences inexpression in WT versus MT cells, it may be a contributing factor. Degradation rate of WT and MT MCAM could be explored via pulse-chase experiments using radioactive labelled methionine, or by inhibiting protein synthesis with cyclohexamide.

As previously mentioned, (section 1.5.4), these putative endocytic domains are conserved between human, mouse and chicken proteins, suggesting these amino acids play a critical role in MCAM function. In addition, there are very few reported variants in AA623, 624 or 641 of MCAM which suggests these variants may be poorly tolerated by cells. Interestingly, some reports of D643N have been reported (The Cancer Genome Atlas (TCGA)/ Catalogue of Somatic Mutations in Cancer (COSMIC) (Tate et al. 2019); whilst L623I has been reported in three samples of carcinoma of the large intestine. In addition, a mutation at E620Q of the dileucine motif has been recorded in uterine cancer. All these mutations arepredicted to be pathogenic by either PolyPhen or FATTHM (Functional Analysis through Hidden Markov Models)(Shihab et al. 2014).

3.4.2 Characterisation of MCAM expression

The final cell populations generated were shown to express MCAM at levels comparable to native-expressing human melanoma, including MM253 and A2058 cell lines (Fig. 9, 10). By flow cytometry, Colo239F-WT3.1 and Colo239F-LA3.1 cells showed an expression profile similar to MM253 cells, with higher overall expression. The Colo239F-YA3.1 cells showed a more heterogeneous profile, with expression levels similar to the MM253 cells (Fig 9). The percentage of MCAM-positive cells for these cells was: Colo239F-WT3.1 (94.8%), Colo239F- LA3.1 (92.2%), Colo239F-YA3.1 (79.5%), and MM253 (100%). In comparison, the Colo239F- parental, Colo239F-LA3.1-Neg, and Colo239F-WT3.1-Neg cells expressed almost no detectable MCAM via flow cytometry (Fig. 9).

Figure 10A-B shows the comparison between MM253 cells and the MCAM-positive Colo239F cells by immunofluorescent staining. These cells display a consistent expression pattern of MCAM in permeabilized cells, with MCAM concentrated on the cell surface at the peripheries while also showing expression in the centre of the cell. Generally, MM253 cells are much flatter when adhered to a surface than the Colo239F cells, which are raised in their centre. Differences in the plane of the images may explain any slight difference in expression pattern observed in Fig. 10. However, on initial examination, WT and MT MCAM localisation in Colo239F cells appeared broadly similar. Differences in sub-cellular localisation of WT and MT MCAM are described in Chapter 4. Finally, western blot analysis showed a band of ~110 kDa, consistent with the molecular weight of MCAM, in the Colo239F-WT3.1, Colo239F- LA3.1, Colo239F-YA3.1, MM253, and A2058 cells (Fig. 10). In Colo239F-parental and Colo239F-LA3.1-Neg cells, MCAM was barely detectable or undetectable by western blot.

3.5 Conclusion

The first part of this project was to develop MCAM-positive WT and MT cells from the MCAM-negative Colo239F-parental cells. In line with this, the Colo239F-WT3.1, Colo239F-LA3.1, Colo239F-YA3.1, and Colo239F-LA3.1-negative cell populations were generated, expressing wild-type MCAM, MCAM with abrogating mutations in the dileucine and tyrosine motifs, andlow MCAM respectively. These cells expressed MCAM in a stable fashion and were used in a range of experiments to follow (Chapters 4 and 5)

The lentiviral system used to introduce MCAM into these cells was not as efficient as anticipated and required multiple rounds of cell sorting to generate the final transductants. Transduction efficiency and expression levels were variable among transduced cells, and there were large proportions of antibiotic resistant cells which expressed no MCAM. The proper calculation of viral titre, though initially more time-consuming, may have been effective for increasing transduction efficiency. Furthermore, increasing the antibiotic selection time after transduction may have eliminated more non-transduced cells.

CHAPTER IV:

Functional Characterisation

4.1 Introduction

MCAM has known roles in tumourigenicity and metastasis, influencing cell polarity, migration, homotypic adhesion, adhesion to endothelial cells and the ECM, proliferation, spreading, angiogenesis, and signalling (Table 3, Chapter 1). Importantly, as mentioned above, enforced expression of MCAM into MCAM-negative melanoma cells has been reported to increase homotypic adhesion, enhance aggregation, and increase "clumping" in tumours grown in mice (Dye 2007; Johnson et al. 1997; Schlagbauer-Wadl et al. 1999; Xie et al. 1997).

A major part of this project was to characterise the generated Colo239F cell series to explore whether the enforced expression of MCAM in the Colo239F cells would produce a phenotypicchange consistent with the literature, and with that observed in the SB2 melanoma cells, which were previously modified in our laboratory to express MCAM (Dye 2007). A second aim was to explore phenotypic differences between the cell populations expressing WT or MT MCAM,to gain insight into the function of the putative endocytosis motifs (Figures 3 and 8).Functional cell assays included cell morphology assessment, migration, spreading, and proliferation assays. Additionally, immunofluorescence and confocal microscopy was used toexplore whether the sub-cellular localisation or expression of MCAM differed in cells expressing the WT and MT variants.

The role of MCAM in proliferation has been mainly explored in endothelial cells. For instance,MCAM has been shown to activate the PI3K-AKT pathway through interactions with VEGFR-2, which is a signalling cascade that culminates in increased proliferation (Zeng et al. 2014). Furthermore, a similar effect was noted when MCAM bound netrin-1 (a laminin-like protein), leading to the activation of VEGFR-2 and subsequent downstream increase in proliferation (Tu et al. 2015). Further studies in endothelial cells have produced similar results (Jiang et al. 2012; Yan et al. 2003; Zhuang et al. 2010). Increased proliferation correlating with MCAM expression has also been noted in ovarian and prostatecancer (Wu et al. 2012; Zoni et al. 2019), while in melanoma there are conflicting data regarding MCAM and cell proliferation (Alais et al. 2001; Jiang et al. 2012; Satyamoorthy et al. 2001).

Cell adhesion molecules are often involved in cell and tissue morphology (Alford and Taylor-Papadimitriou 1996). Cell adhesionis essential for cell homeostasis, and contributes to regulation of signalling and gene expression (Khalili and Ahmad 2015). Changes in cell adhesion molecule expression are also associated with morphological changes, which in turn are often linked with invasion and metastasis. For instance, the loss of cell adhesiveness often co-occurs with metastasis, allowing for tumour cells to abandon their normal structure/function and invade local tissues (Khalili and Ahmad 2015).

Morphological changes are driven primarily by cytoskeletal reorganisation, and CAMs such as integrins play an essential role in cell adhesion and spreading, and mediate mechanical linkage to the cytoskeleton (Khalili

and Ahmad 2015). Cell spreading also occurs as the result of the interaction between CAMs and the ECM, allowing the cell to adhere to the substrate below it. Interestingly, MCAM appears to modulate the spreading of melanoma cells on substrates such as collagens type I and IV and laminin-111 (Dye 2007); although none of these have been identified as direct ligands of MCAM.

Cell spreading occurs via passive adhesion *in vitro*. During passive adhesion, cells adhereto a substrate, the cell body spreads along the surface, and focal adhesions form between the cell and substrate (Khalili and Ahmad 2015). While the first step of adhesion is driven primarily by electrostaticinteractions, the second step involves integrins as the key player in binding to the ECM, providing a mechanical link between the ECM and cytoskeleton (Khalili and Ahmad 2015). The ECM can consist ofdifferent substrates, and these can alter the spreading kinetics and morphology of different cell types.

Collagen is the most abundant protein in mammals and is composed of three α-chains whichform a helical structure (Ricard-Blum 2011). There are 28 distinct types of collagen, the most abundant of which is collagen type I, a fibril-forming collagen (Henriksen and Karsdal 2016). Collagen type IV, in contrast, is the primary collagen component of the basement membrane which underlies epithelial and endothelial cells (Sand et al. 2016). Cells interact with collagens primarily through β1-integrins (e.g. α1β1,α2β1, α10β1 and α11β1) (Ricard-Blum 2011)

Fibronectin, in contrast, is secreted from cells as a dimer which has binding sites for other ECM components, including collagen, and cell surface receptors (Pankov and Yamada 2002). Again, integrins are the primary cell surface molecules that interact with fibronectin, including those containing the β1-integrin subunit (e.g. α6β1, α8β1 and αVβ1) (Pankov and Yamada 2002). Fibronectin is known to mediate cell adhesion, differentiation, growth, and migration (Pankov and Yamada 2002).

Another important component of the ECM are the laminins, which are a family of 16 glycoproteins present in the basement membrane (Hamill et al. 2009). β1-Integrins are known to interact with various laminin isoforms, primarily through β1-integrins (e.g. α3β1, α4β1, α6β1, α7β1),and are also thought to regulate their deposition to the ECM, contributing to cell adhesion, spreading, and migration (Hamill et al. 2009). Interestingly, MCAM is known to interact with laminin-411 and laminin-421 (previously known as laminin-8 and 9 respectively) and potentially with laminin-332 (laminin-5) (Flanagan et al. 2012; Ishikawa et al. 2014).

Due to the nature of the interactions between CAMs on neighbouring cells, and between cells and the pericellular ECM, they are often directly involved in the mechanisms of cell migration and motility (Huttenlocher and Horwitz 2011; Theveneau and Mayor 2012). CAMs mediate attachment to the ECM at the leading edgeof a cell, and by their linkage to the cytoskeleton, transduce mechanical force to drive cell motility. This is followed by the detachment of CAMs from their ECM ligands at the rear of the cell; all of which enable cell migration (De Pascalis and Etienne-Manneville 2017). MCAM has repeatedly been associated with increased migration and invasion in various cell types (Table 3, Chapter 1). Furthermore, MCAM has

been linked to specific examples of cell migration such as monocyte transendothelial migration and the invasion of lymphocytes into endothelial cell layers (Bardin et al. 2009; Breuer et al. 2018).

The ability of MCAM to influence cell morphology and cell migration is mediated by its interaction with the cell cytoskeleton. F-actin, or filamentous actin, is a helical protein whichforms the cytoskeleton and is crucial to cell morphology, motility, and signaling (Dominguez and Holmes 2011). Importantly, MCAM interacts directly with proteins known as cytoskeletal linkers, which cross-link actin filaments with proteins in the cell membrane. These include the ERM proteins, ezrin, radixin, and moesin (Luo et al. 2012), as well as hShroom1 (Dye et al. 2009) and IQGAP1 (Witze et al. 2013). Recently, the WRAMP structure was described as a mechanism through which MCAM has a direct role in promoting directional cell migration in melanoma and endothelial cells (Connacher et al. 2017; Witze et al. 2013; Witze et al. 2008).

The role of the WRAMP structure in cell migration was covered in detail in section 1.6.1.5. Briefly, Wnt5a-mediated internalisation of MCAM is believed to target MCAM to the rear ofthe cell, where it co-localises with proteins involved in cytoskeletal dynamics and restructuring, microtubule dynamics, and adhesion turnover (Witze et al. 2013; Witze et al. 2008). This structure formsas an antecedent to cell movement and defines the directionality of cell migration (Connacher et al. 2017). When a cell changes direction, the WRAMP disintegrates and re-forms at the new rear of the cell (Connacher et al. 2017). Interestingly, similar mechanisms in melanoma and endothelial cells have been described which involve the actin-linking ERM protein moesin, as well as β1-integrin (Estecha et al. 2009; Lorentzen et al. 2011; Moreno-Fortuny et al. 2017). Taken together, these data provide important evidence that MCAM is involved in dynamic cytoskeletal processes including motility and cell polarity.

Cell polarity and migration are highly dependent upon focal adhesions which are dynamically formed protein complexes that link the ECM to the cytoskeleton and provide traction for the cell (Ridley et al. 2003). Integrins are major players in focal adhesions, adhering to the ECM and acting as mechano-sensors, transmitting force signals through talin and vinculin, and ultimately mediating migration (De Pascalis and Etienne-Manneville 2017). Vinculin itself connects the cytoskeleton to focal adhesions through talin (De Pascalis and Etienne-Manneville 2017). MCAM is reported to induce the phosphorylation of focal adhesion kinase (Anfosso et al. 1998), however, the presence or direct interaction of MCAM with focal adhesion complexes is unknown.

ERM proteins such as moesin are also involved in microtubule dynamics. Solinet et al (2013) found that moesin binding stabilised microtubules at the cell cortex and played a role in spindle formation and cell shape during mitosis (Solinet et al. 2013). Microtubules are also involved in the intracellular transport of molecules and the movement of organelles and vesicles within the cell (Burd and Cullen 2014; Franker and Hoogenraad 2013). However, the potential interplay between MCAM, ERM proteins, and microtubules has not been investigated, including the possibility that MCAM undergoes microtubule-mediated transport throughout the cell.

This chapter describes the observed phenotype of the Colo239F cell series, comparing the MCAM-positive (WT and MT) and MCAM-negative Colo239F cells. Further, it explores cell surface expression of MCAM and β1-integrin, and the subcellular localisation of MCAM in reference to specific cell markers and known interaction partners of MCAM.

4.2 Results

4.2.1 MCAM influences cell size and morphology

To determine whether MCAM expression affects cell morphology in Colo239F cells, the length, height, and total area of cells from each cell population was quantified (Fig. 11 A-B, Table 11). Cells were plated on collagen coated glass coverslips and visualised using phase contrast and anti-β1 integrin immunofluorescence (IF). IF was used to clearly outline the cellmembranes for accurate size analyses. Representative images are shown in Fig. 11C-E. Colo239F-WT cells were significantly shorter on average than the other cell populations ($p \leq 0.001$). Both Colo239F-YA3.1 and Colo239F-LA3.1 were significantly longer on average than the other cell populations ($p \leq 0.001$), with Colo239F-YA3.1 being longer than Colo239F-LA3.1($p \leq 0.05$).

The Colo239F-Parental cells were significantly larger in area than every other population ($p \leq 0.001$). Furthermore, except for the Colo239F-LA3.1-Neg cells, all cells retained the same pattern as for the cell lengths (Fig. 11B, Table 10). Finally, the average height of each cell population was quantified to within 1 µM to determine whether any differences may indicate a change in spreading behaviour due to MCAM expression. All cells were of similar height with the exception of Colo239F-YA3.1, which were smaller (Table 11).

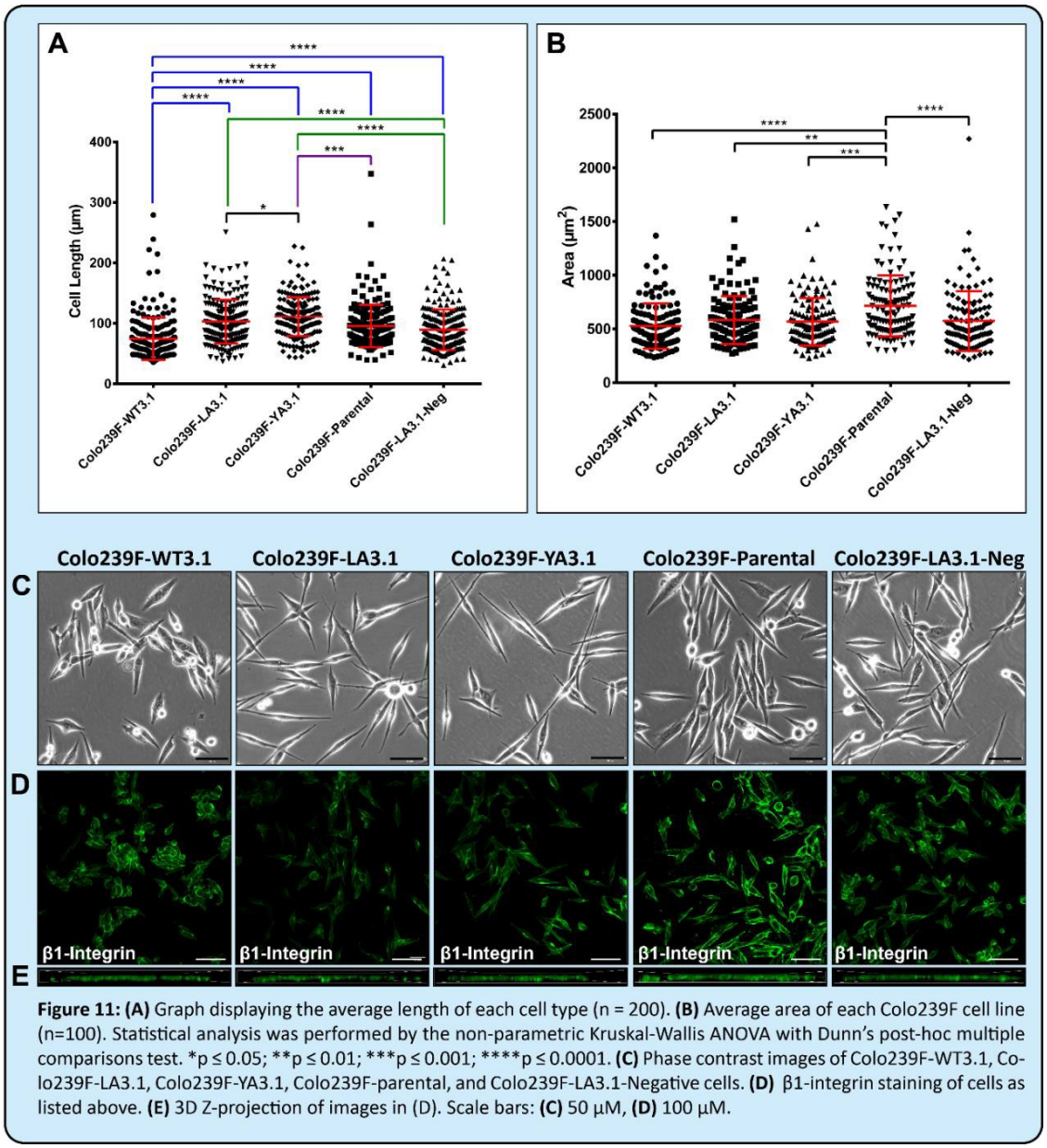

Figure 11: (A) Graph displaying the average length of each cell type (n = 200). **(B)** Average area of each Colo239F cell line (n=100). Statistical analysis was performed by the non-parametric Kruskal-Wallis ANOVA with Dunn's post-hoc multiple comparisons test. *p ≤ 0.05; **p ≤ 0.01; ***p ≤ 0.001; ****p ≤ 0.0001. **(C)** Phase contrast images of Colo239F-WT3.1, Colo239F-LA3.1, Colo239F-YA3.1, Colo239F-parental, and Colo239F-LA3.1-Negative cells. **(D)** β1-integrin staining of cells as listed above. **(E)** 3D Z-projection of images in (D). Scale bars: **(C)** 50 µM, **(D)** 100 µM.

Table 11. Colo239F cell population sizes

Cell Population	Length (µM)	Area (µM^2)	Height (µM)
Colo-239F-WT3.1	74.31 ± 34.97	527.1 ± 210.1	7
Colo-239F-LA3.1	102.7 ± 36.06	583.2 ± 222.1	6
Colo-239F-YA3.1	110.9 ± 31.98	567.8 ± 220.9	4
Colo-239F-Parental	95.65 ± 34.91	715.5 ± 282.9	7
Colo-239F-LA3.1 neg	89.47 ± 33.43	573.8 ± 277.3	6

4.2.2 WT MCAM may contribute to cell proliferation

Proliferation assays were performed on each cell series over a period of six days. Colo239F- WT3.1, Colo239F-YA3.1, Colo239F-LA3.1-Neg, and Colo239F-parental cells were assayed simultaneously and in triplicate, while Colo239F-YA3.1 was assayed against Colo239F-WT3.1 at a different time point according to the same protocol.

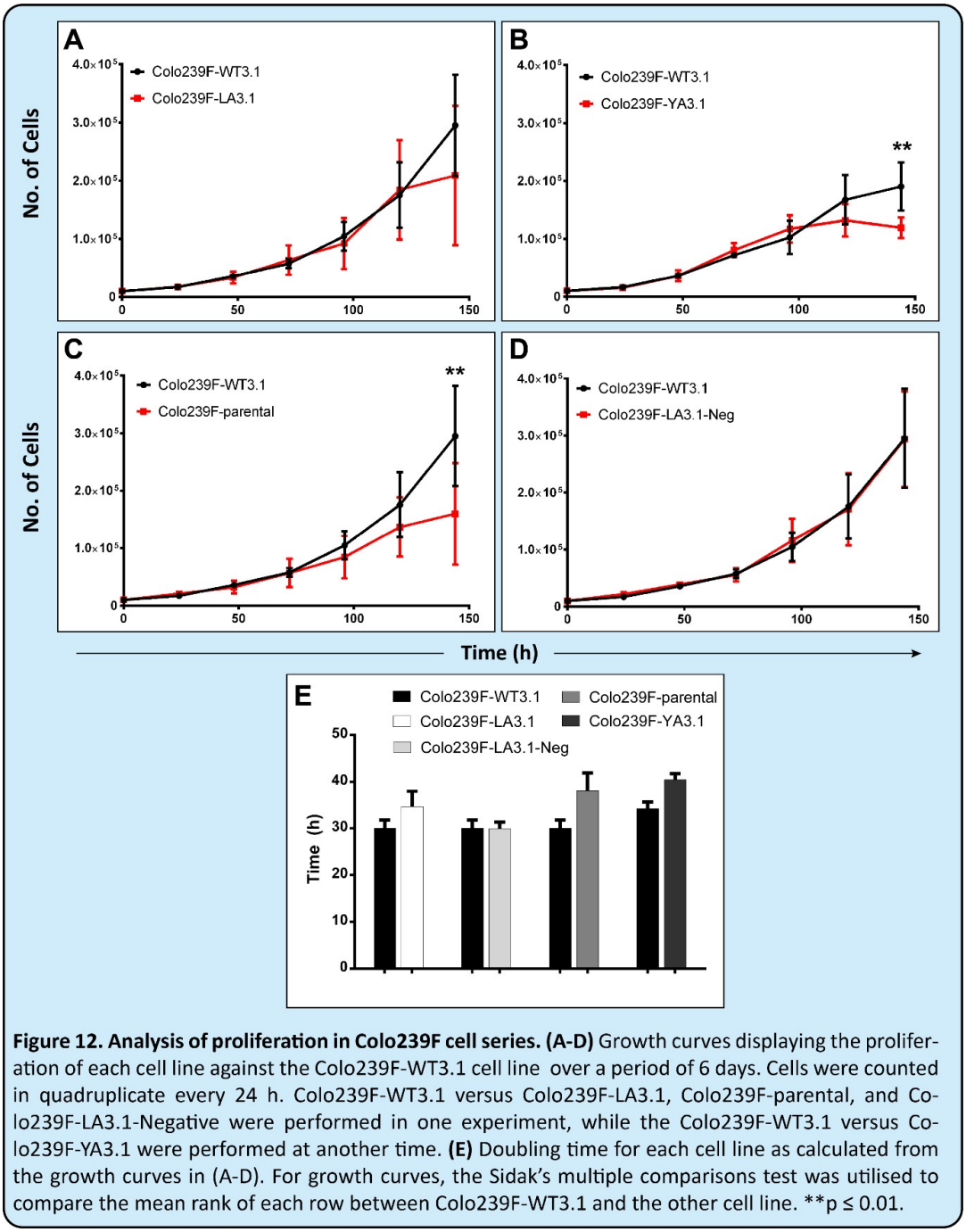

Figure 12. Analysis of proliferation in Colo239F cell series. (A-D) Growth curves displaying the proliferation of each cell line against the Colo239F-WT3.1 cell line over a period of 6 days. Cells were counted in quadruplicate every 24 h. Colo239F-WT3.1 versus Colo239F-LA3.1, Colo239F-parental, and Colo239F-LA3.1-Negative were performed in one experiment, while the Colo239F-WT3.1 versus Colo239F-YA3.1 were performed at another time. **(E)** Doubling time for each cell line as calculated from the growth curves in (A-D). For growth curves, the Sidak's multiple comparisons test was utilised to compare the mean rank of each row between Colo239F-WT3.1 and the other cell line. **p ≤ 0.01.

Colo239F-WT3.1 compared against Colo239F-LA3.1 or Colo239F-LA3.1-Neg cells showed no significant difference in growth rates. All cells had similar proliferation rates until the 96 h mark, at which point Colo239F-WT3.1 and Colo239F-LA3.1-Neg continued to proliferate while Colo239F-LA3.1, Colo239F-YA3.1 and Colo239F-Parental plateaued (Fig. 12A-D). At the 144 h time point, Colo239F-YA3.1 and Colo239F-parental produced a significantly lower count than the Colo239F-WT3.1 cells ($p \leq 0.01$).

Doubling times were calculated based on these growth curves, however, no statistically significant differences between cell types were noted. The doubling times were as follows: Colo239F-WT3.1 (29.99 h ± 1.81 h), Colo239F-LA3.1 (34.64h ± 3.30 h), Colo239F-LA3.1-Neg (29.91 h ± 1.44 h), Colo239F-parental (38.08 h ± 3.79 h). For the experiments comparing Colo239F-WT3.1 to Colo239F-YA3.1, the doubling times were as follows: Colo239F-WT3.1 (34.18 h ± 1.42), and Colo239F-YA3.1 (40.44 ± 2.26 h) (Fig. 12E). The difference between Colo239F-WT3.1 doubling time for each assay indicates a level of inter-experiment variability. Furthermore, while variation was low for the first 72 h, after this point variability in measurements rose considerably, as indicated by the error bars in Fig. 12A-D.

4.2.3 LL623-624AA and Y641A-MCAM promote sustained directional migration in Colo239F cells

As the Colo239-F cells do not form a monolayer in culture, cell migration could not be assessed using a traditional wound healing assay. Instead, a random motility assay was performed on the Colo239F cell series to explore whether the introduction of WT or MT MCAM altered the motility of these cells. Migration distance was calculated via two means: the total distance along the path of migration, and the actual distance the cell travelled fromstart to end. This method provided a metric for determining the directionality of migrating cells in this assay.

Interestingly, Colo239F-LA3.1 and Colo239F-YA3.1 were more motile than the other cell populations and were significantly more motile than Colo239F-WT3.1 ($p \leq 0.0001$, $p \leq 0.05$ respectively) (Fig. 13A-B). Furthermore, when analysing the actual distance travelled by the cell, the Colo239F-LA3.1 and Colo239F-YA3.1 cells were found to sustain their directionality significantly more than the Colo239F-WT3.1 cells ($p \leq 0.001$, $p \leq 0.001$ respectively) (Fig. 13A-B).

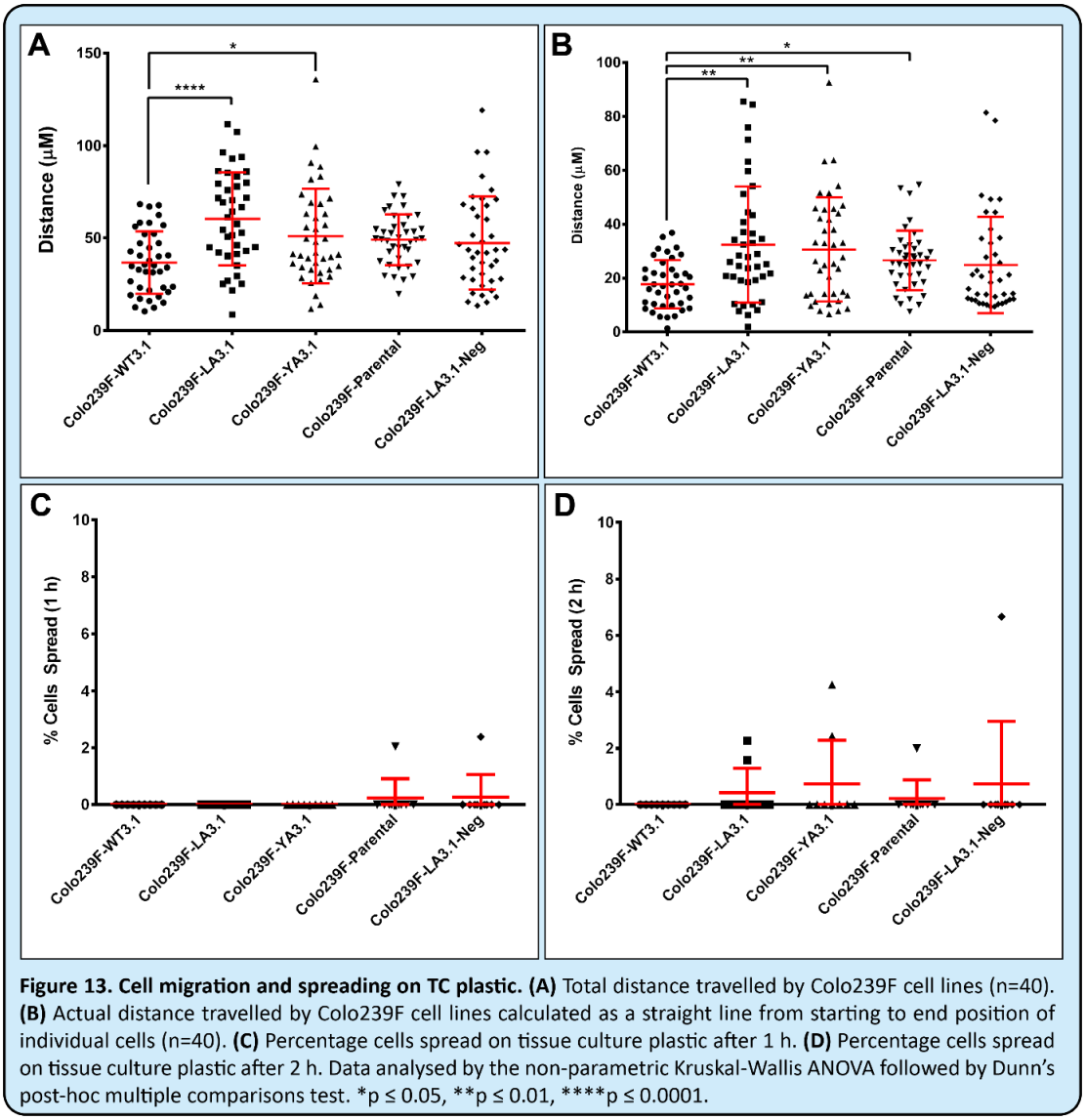

Figure 13. Cell migration and spreading on TC plastic. (A) Total distance travelled by Colo239F cell lines (n=40). **(B)** Actual distance travelled by Colo239F cell lines calculated as a straight line from starting to end position of individual cells (n=40). **(C)** Percentage cells spread on tissue culture plastic after 1 h. **(D)** Percentage cells spread on tissue culture plastic after 2 h. Data analysed by the non-parametric Kruskal-Wallis ANOVA followed by Dunn's post-hoc multiple comparisons test. *p ≤ 0.05, **p ≤ 0.01, ****p ≤ 0.0001.

4.2.4 Colo239F cell series display differences in spreading behaviour on various substrates

The Colo239F cell series was plated on tissue culture plastic and matrix proteins in serum free medium, and allowed to spread for 2 h at 37˚C. These assays were used to determine whether the expression of WT or MT MCAM affected the rate or extent of cell spreading on different substrates. The proportion of cells spread and the extent of cells spreading on eachsubstrate are shown in Figures 14-17; and the data summarized in Tables 12 and 13. On tissueculture plastic, all cells displayed extremely low levels of spreading after 2 h (Fig. 13C-D, Table 12).

Table 12. Percentage of cells spread on tissue culture plastic, collagen type I and IV, fibronectin, and laminin after 1 and 2 h*.

Percentage of cells spread on tissue culture plastic					
Time (h)	**Colo239F-WT3.1**	**Colo239F-LA3.1**	**Colo239F-YA3.1**	**Colo239F-Parental**	**Colo239F-LA3.1-Neg**
1	0 ± 0%	0 ± 0%	0.23 ± 0.64%	0.26 ± 0.75%	0 ± 0%
2	0 ± 0%	0.43 ± 0.82%	0.84 ± 1.52%	0.25 ± 0.66%	0.74 ± 2.09%
Percentage of cells spread on collagen type I					
Time(h)	**Colo239F-WT3.1**	**Colo239F-LA3.1**	**Colo239F-YA3.1**	**Colo239F-Parental**	**Colo239F-LA3.1-Neg**
1	15.32 ± 10.67%	9.04 ± 3.32%	22.89 ± 10.49%	26.01 ± 5.65%	20.64 ± 7.26%
2	38.59 ± 5.67%	28.33 ± 7.89%	38.75 ± 10.72%	45.98 ± 7.46%	40.91 ± 11.05%
Percentage of cells spread on collagen type IV					
Time (h)	**Colo239F-WT3.1**	**Colo239F-LA3.1**	**Colo239F-YA3.1**	**Colo239F-Parental**	**Colo239F-LA3.1-Neg**
1	3.83 ± 3.36%	6.35 ± 4.40%	16.52 ± 11.73%	14.97 ± 6.00%	5.01 ± 4.73%
2	15.17 ±7.64%	18.90 ±5.59%	30.52 ±12.95%	37.15 ±7.77%	16.51 ±3.75%
Percentage of cells spread on fibronectin					
Time (h)	**Colo239F-WT3.1**	**Colo239F-LA3.1**	**Colo239F-YA3.1**	**Colo239F-Parental**	**Colo239F-LA3.1-Neg**
1	51.04 ±11.21%	51.23 ±10.33%	59.24 ±12.84%	64.38 ±12.53%	55.15 ±11.88%
2	67.83 ± 7.80%	70.88 ± 9.48%	75.76 ± 8.70%	72.65 ± 10.98%	68.60 ± 6.60%
Percentage of cells spread on laminin I					
Time(h)	**Colo239F-WT3.1**	**Colo239F-LA3.1**	**Colo239F-YA3.1**	**Colo239F-Parental**	**Colo239F-LA3.1-Neg**
1	35.87 ± 14.56%	9.11 ± 5.31%	35.54 ± 9.11%	14.14 ± 7.56%	2.67 ± 3.37%
2	43.79 ± 10.38%	33.46 ± 7.11%	57.12 ± 8.34%	29.74 ± 11.88%	20.71 ± 5.58%

Cells were seeded at 2.0 x 10^3 cells per well in a 96-well plate and imaged at 100 x magnification at various time points. A quarter field was randomly selected from 9 wells and cells were quantified by number spread and length of cell. Data is presented as mean percentage ± SD.

Table 13. Mean cell length on collagen type I, collagen type IV, fibronectin, and laminin I at 1 and 2 h.

Length (µM) of cells spread on collagen type I					
Time(h)	**Colo239F-WT3.1**	**Colo239F-LA3.1**	**Colo239F-YA3.1**	**Colo239F-Parental**	**Colo239F-LA3.1-Neg**
1	25.93 ± 6.76	23.01 ± 6.06	25.07 ± 6.34	22.69 ± 5.38	22.22 ± 6.59
2	35.31 ± 9.92	33.27 ± 11.15	37.08 ± 12.77	36.57 ± 11.67	31.58 ± 9.83
Length (µM) of cells spread on collagen type IV					
Time(h)	**Colo239F-WT3.1**	**Colo239F-LA3.1**	**Colo239F-YA3.1**	**Colo239F-Parental**	**Colo239F-LA3.1-Neg**
1	3.83 ± 3.57	6.56 ± 4.67	16.52 ± 12.44	14.97 ± 6.37	5.01 ± 50.2
2	15.17 ± 8.10	18.90 ± 5.93	30.52 ± 13.73	37.15 ± 8.24	16.51 ± 3.98
Length (µM) of cells spread on fibronectin					
Time(h)	**Colo239F-WT3.1**	**Colo239F-LA3.1**	**Colo239F-YA3.1**	**Colo239F-Parental**	**Colo239F-LA3.1-Neg**
1	42.64 ± 13.99	53.56 ± 17.62	55.92 ± 18.04	49.10 ± 14.83	44.70 ± 14.18
2	57.50 ± 17.66	71.92 ± 23.50	77.18 ± 24.69	67.56 ± 22.37	57.22 ± 21.88
Length (µM) of cells spread on laminin I					
Time(h)	**Colo239F-WT3.1**	**Colo239F-LA3.1**	**Colo239F-YA3.1**	**Colo239F-Parental**	**Colo239F-LA3.1-Neg**
1	43.01 ± 13.46	37.49 ± 11.61	50.68 ± 18.67	46.70 ± 15.74	35.69 ± 10.75
2	47.85 ± 20.12	58.08 ± 23.36	68.41 ± 23.30	53.69 ± 20.73	48.88 ± 22.23

On type I collagen, after 1 h, significant differences in spreading were noted. The Colo239F- YA3.1 and Colo239F-Parental cells displayed the highest level of spreading, while theColo239F-LA3.1s showed the lowest extent of spreading (Fig. 14A, Table 12). After 2 h, the differences between cells narrowed. However, the pattern seen after 1 h remained, and theproportion of spread Colo239F-LA3.1 cells remained much lower than the other cells (Fig. 14B, Table 12).

The cells displayed dissimilarities in the extent of spreading on collagen type I as measured by cell length. Colo239F-WT3.1 and Colo239F-YA3.1 cells were on average significantly longer than the Colo239F-Parental and Colo239F-LA3.1-Neg cells ($p \leq 0.05$, $p \leq 0.01$ respectively forboth) (Fig. 14C, Table 13). After 2 h, the average length of spread cells had increased by ~10 µM for each cell population. At this point, the Colo239F-LA3.1-Neg cells were significantly shorter than all four other cell populations. The Colo239F-YA3.1 and Colo239F-Parental cells displayed the highest cell length (Fig 14D, Table 13).

To further analyse this data, cell lengths were separated into three categories: short, at under20 µM; medium at 20-30 µM, long at over 30 µM. As expected, after 1 h most cells are eitherin the <20 or 20-30 µM categories, suggesting that the cells are still in the process of spreading at this time (Fig. 14E). Interestingly, the Colo239F-WT3.1 cells displayed ~31% of cells >30 µM, suggesting that this line spread faster on collagen type I than the other cell populations (Fig. 14E). After 2 h, most cells were over 30 µM in length, suggesting that they had finished spreading on this substrate (Fig. 14F). Interestingly, after 2 h the Colo239F- WT3.1s still displayed the highest proportion of cells over 30 µM yet displayed the third- longest cells on average (Fig. 14F). This appears to confirm that they spread faster on collagentype I, but remain morphologically shorter than the other cell populations, which correlates with the data collected on cell morphology in Section 4.2.1.

For cells plated on collagen type IV a distinct pattern in cell spreading was consistent and observable at both 1 and 2 h, and differences were more distinct than in cells plated on collagen type I. At 1h, the Colo239F-YA3.1 cells had a significantly higher proportion of cells spread than every population except Colo239F-Parental (Fig. 15A, Table 12). The Colo239F- WT3.1, Colo239F-LA3.1, and Colo239F-LA3.1-Neg cells displayed the lowest proportion of spread cells on collagen type IV at both time points (Fig. 15A-B). Again, the length of spread cells was quantified. At 1 h, all cells displayed similar cell lengths (Fig. 15C, Table 13). However, after 2 h, the Colo239F-YA3.1 and Colo239F-Parental cells were longer on average.Indeed, the parental cells were significantly longer than both the Colo239F-WT3.1 and Colo239F-LA3.1 cells ($p \leq 0.0001$, $p \leq 0.001$ respectively) and the Colo239F-YA3.1 cells were significantly longer than the Colo239F-LA3.1 cells ($p \leq 0.05$). Interestingly, at 1 h, the Colo239F-WT3.1 cells again displayed the highest proportion >30 µM (Fig. 15E), despite having the least proportion of total cells spread at both time points. Furthermore, the Colo239F-LA3.1 cell population showed a majority of cells at 1 h <20 µM (Fig. 15E). At 2 h, allcell populations again showed most spread cells >30 µM (Fig. 15F).

All cells displayed far greater capacity for spreading on fibronectin I in comparison to the other substrates (Fig. 16). The percentages of spread cells for each population did not differ significantly (Table 12), however, the Colo239F-WT3.1, Colo239F-LA3.1, and Colo239F-LA3.1-Neg cells appeared to spread slowest, while the Colo239F-YA3.1 and Colo239F-Parental cellsspread the fastest (consistent with collagen type I and IV) (Fig. 16A-B). The differences in celllength of spread cells between cell populations are almost identical between 1 and 2 h, withthe differences only becoming more pronounced (Fig. 16C-D, Table 13). The Colo239F-WT3.1and Colo239F-LA3.1-Neg cells were significantly shorter on average than the Colo239F-LA3.1,Colo239F-YA3.1 and Colo239F-Parental cells ($p \leq 0.0001$), while the Colo239F-YA3.1 was significantly longer than all other cells ($p \leq 0.0001$) (Fig. 16D, Table 12). Interestingly, almostzero spread cells had a length of under 20 µM at 1 h, and at 2 h almost zero cells had a lengthof under 30 µM (Fig. 16E-F). This indicates how fast these cells spread on fibronectin compared with collagen types I and IV and laminin I.

On laminin, differences between cell populations were more interesting. After 1 h, Colo239F-WT3.1 and Colo239F-YA3.1 cells spread significantly further than the other three cell populations (Fig. 17A, Table 13). This trend consisted through to the 2 h timepoint, with Colo239F-YA3.1 displaying the highest proportion of spread cells (Table 12), followed by Colo239F-WT3.1, Colo239F-LA3.1, Colo239F-Parental, and finally, Colo239F-LA3.1-Neg (Fig. 17B). Interestingly, despite having a higher proportion of cells spread on laminin I, Colo239F-WT3.1 cells remained relatively short, while Colo239F-YA3.1 cells were the longest (Fig. 17C-D, Table 13). Colo239F-YA3.1 displayed the highest proportion of spread cells >30 µM at both1 and 2 h time points (Fig. 17E, F). The Colo239F-LA3.1-Neg cells appeared significantly shorter when spread than all other cell populations ($p \leq 0.05$ compared with Colo239F-LA3.1,$p \leq 0.0001$ against the others), and displayed the shortest cell length on average. At 2 h, Colo239F-Parental cells had the second-lowest percentage of spread cells (Fig. 17B). This indicates that on laminin I, cells expressing MCAM spread faster than cells which are MCAM-negative.

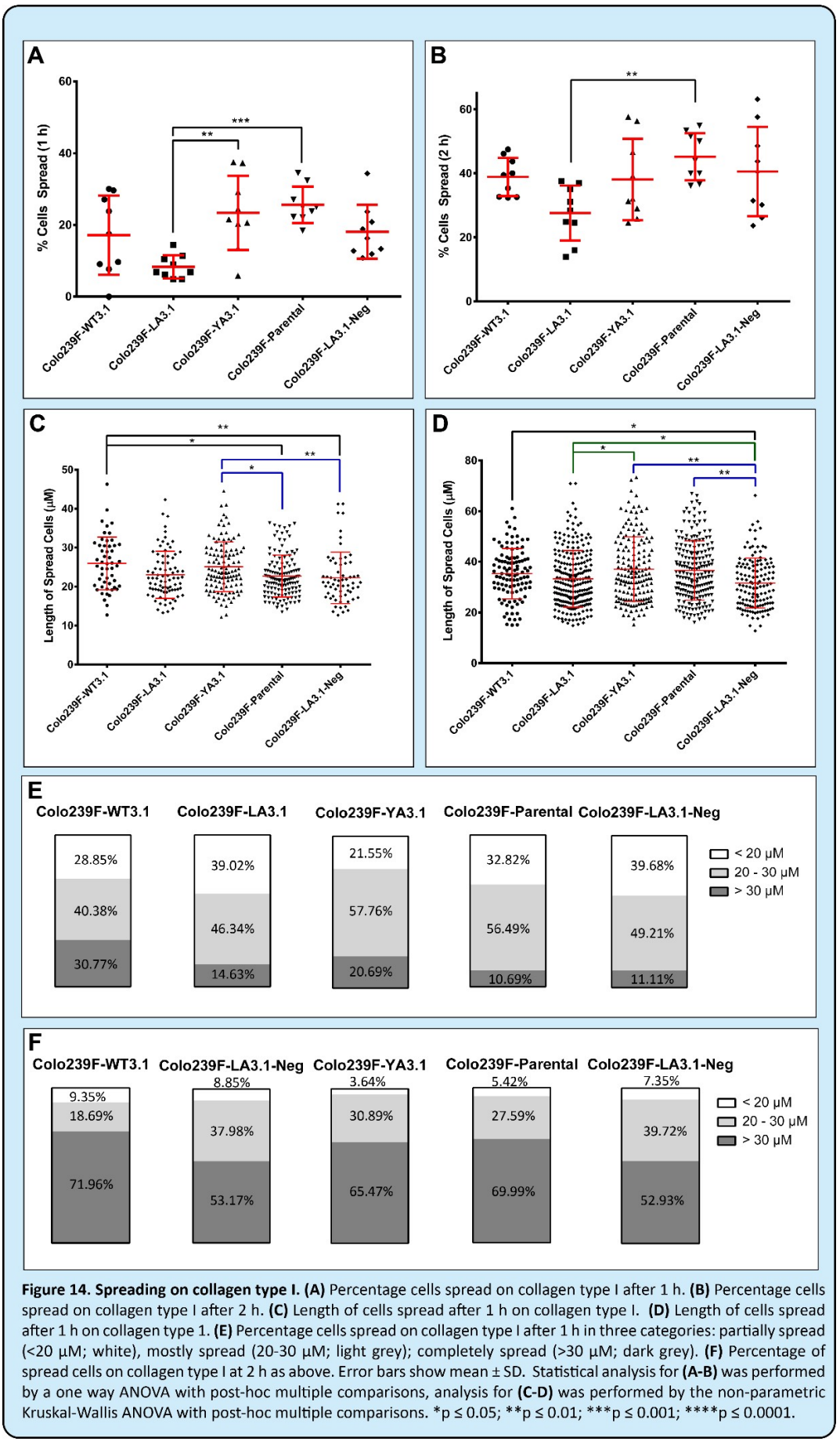

Figure 14. Spreading on collagen type I. (A) Percentage cells spread on collagen type I after 1 h. **(B)** Percentage cells spread on collagen type I after 2 h. **(C)** Length of cells spread after 1 h on collagen type I. **(D)** Length of cells spread after 1 h on collagen type 1. **(E)** Percentage cells spread on collagen type I after 1 h in three categories: partially spread (<20 µM; white), mostly spread (20-30 µM; light grey); completely spread (>30 µM; dark grey). **(F)** Percentage of spread cells on collagen type I at 2 h as above. Error bars show mean ± SD. Statistical analysis for **(A-B)** was performed by a one way ANOVA with post-hoc multiple comparisons, analysis for **(C-D)** was performed by the non-parametric Kruskal-Wallis ANOVA with post-hoc multiple comparisons. *p ≤ 0.05; **p ≤ 0.01; ***p ≤ 0.001; ****p ≤ 0.0001.

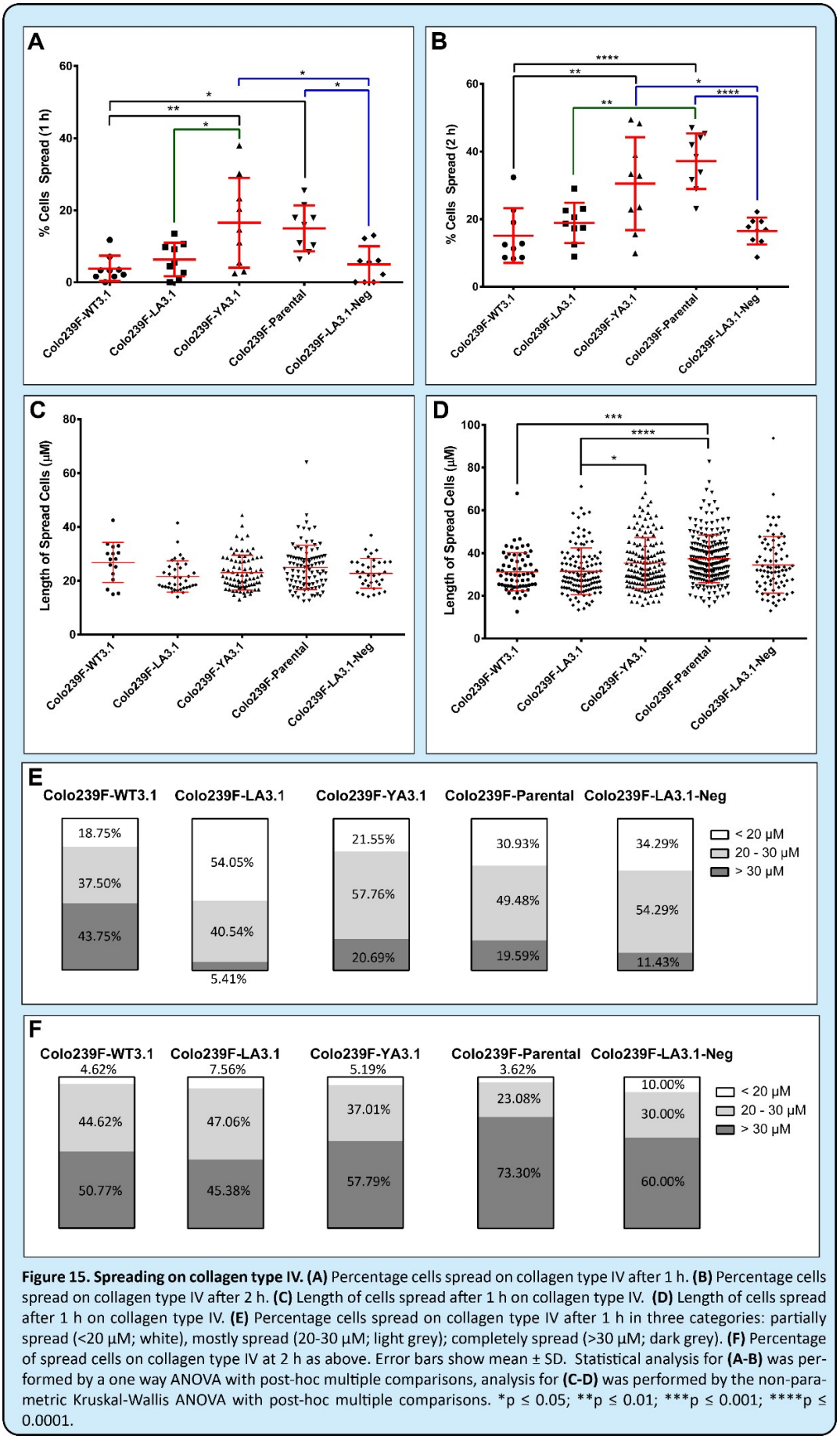

Figure 15. Spreading on collagen type IV. (A) Percentage cells spread on collagen type IV after 1 h. **(B)** Percentage cells spread on collagen type IV after 2 h. **(C)** Length of cells spread after 1 h on collagen type IV. **(D)** Length of cells spread after 1 h on collagen type IV. **(E)** Percentage cells spread on collagen type IV after 1 h in three categories: partially spread (<20 µM; white), mostly spread (20-30 µM; light grey); completely spread (>30 µM; dark grey). **(F)** Percentage of spread cells on collagen type IV at 2 h as above. Error bars show mean ± SD. Statistical analysis for **(A-B)** was performed by a one way ANOVA with post-hoc multiple comparisons, analysis for **(C-D)** was performed by the non-parametric Kruskal-Wallis ANOVA with post-hoc multiple comparisons. *p ≤ 0.05; **p ≤ 0.01; ***p ≤ 0.001; ****p ≤ 0.0001.

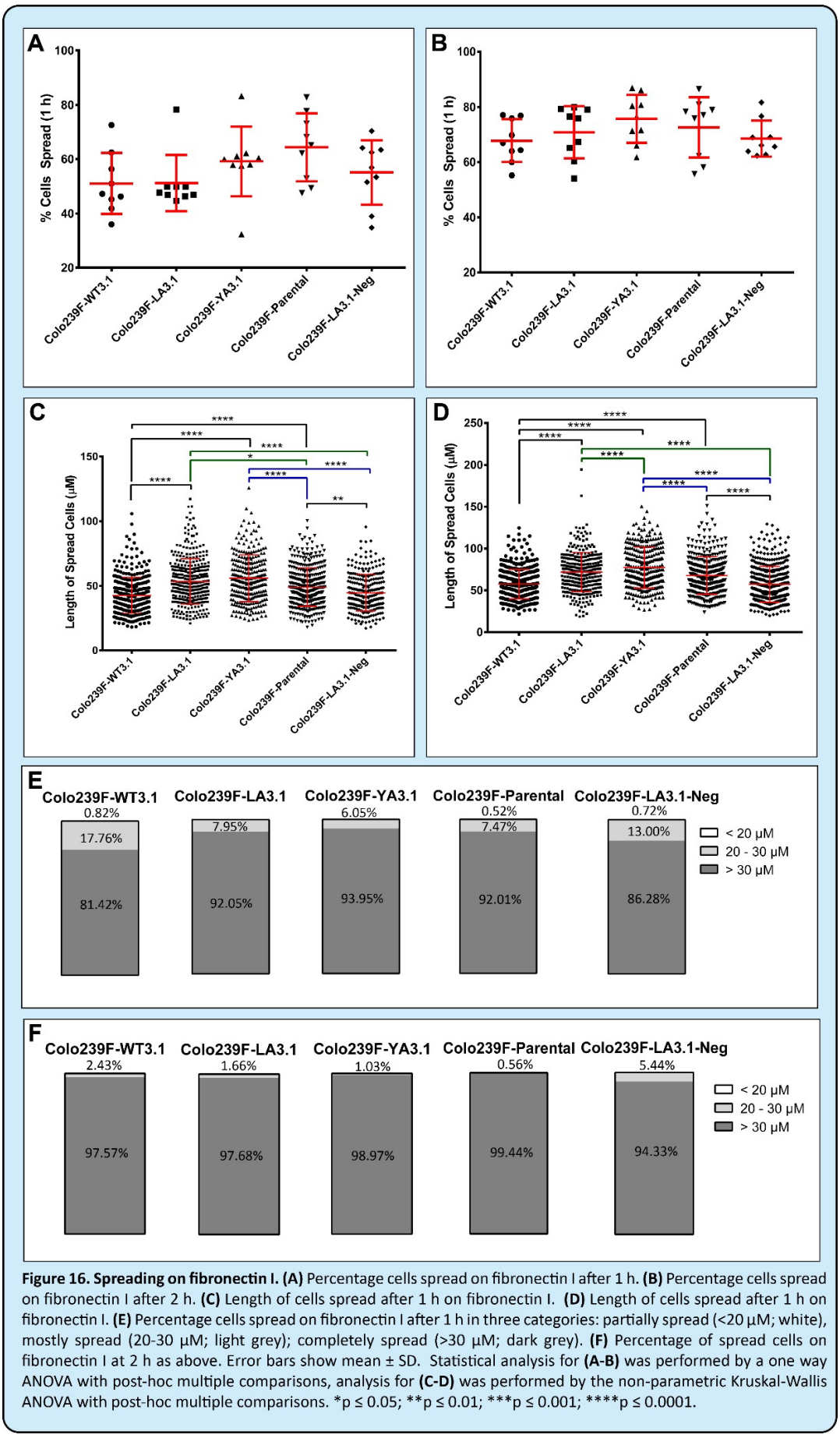

Figure 16. Spreading on fibronectin I. (A) Percentage cells spread on fibronectin I after 1 h. **(B)** Percentage cells spread on fibronectin I after 2 h. **(C)** Length of cells spread after 1 h on fibronectin I. **(D)** Length of cells spread after 1 h on fibronectin I. **(E)** Percentage cells spread on fibronectin I after 1 h in three categories: partially spread (<20 µM; white), mostly spread (20-30 µM; light grey); completely spread (>30 µM; dark grey). **(F)** Percentage of spread cells on fibronectin I at 2 h as above. Error bars show mean ± SD. Statistical analysis for **(A-B)** was performed by a one way ANOVA with post-hoc multiple comparisons, analysis for **(C-D)** was performed by the non-parametric Kruskal-Wallis ANOVA with post-hoc multiple comparisons. *p ≤ 0.05; **p ≤ 0.01; ***p ≤ 0.001; ****p ≤ 0.0001.

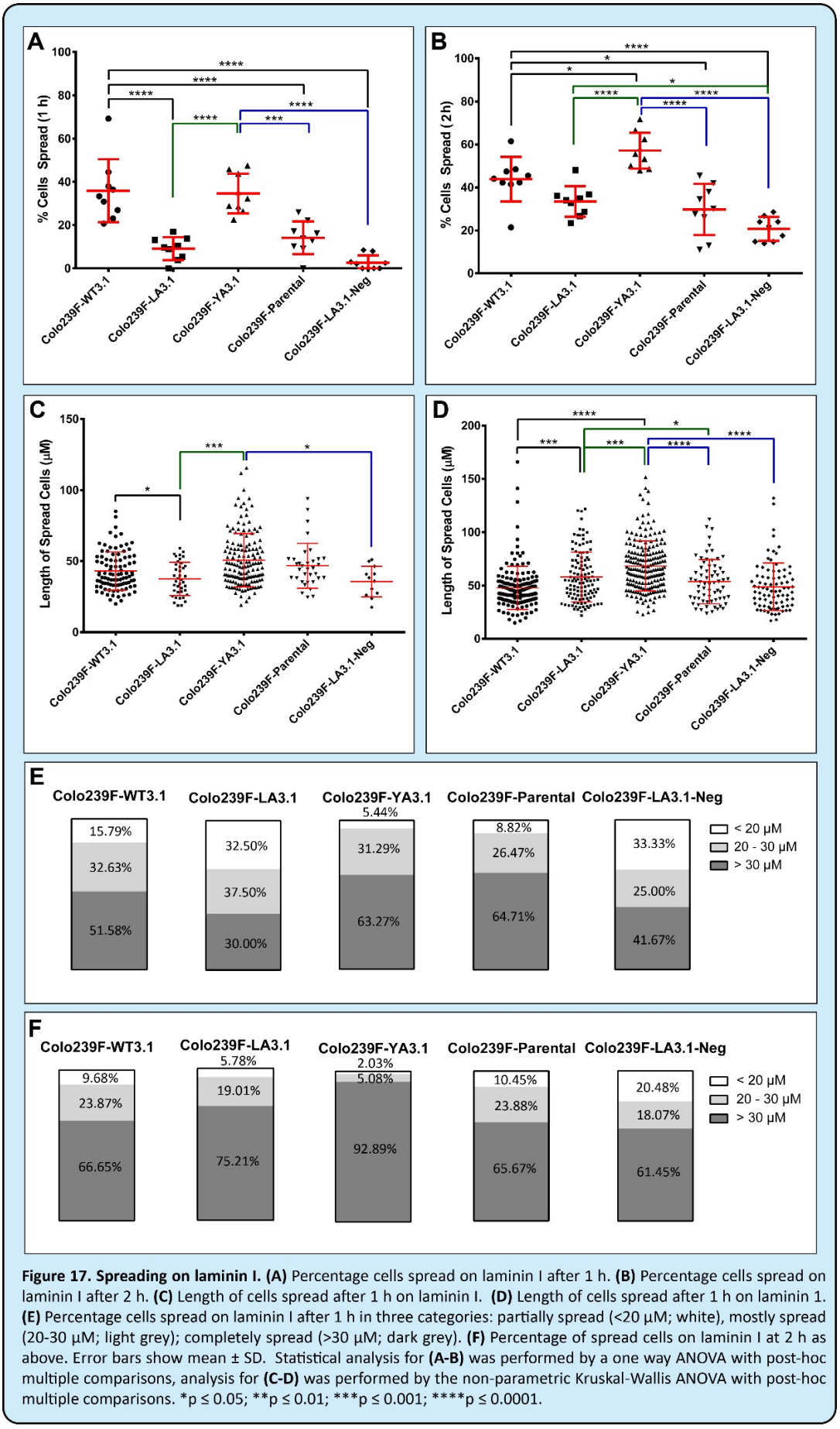

Figure 17. Spreading on laminin I. (A) Percentage cells spread on laminin I after 1 h. **(B)** Percentage cells spread on laminin I after 2 h. **(C)** Length of cells spread after 1 h on laminin I. **(D)** Length of cells spread after 1 h on laminin 1. **(E)** Percentage cells spread on laminin I after 1 h in three categories: partially spread (<20 µM; white), mostly spread (20-30 µM; light grey); completely spread (>30 µM; dark grey). **(F)** Percentage of spread cells on laminin I at 2 h as above. Error bars show mean ± SD. Statistical analysis for **(A-B)** was performed by a one way ANOVA with post-hoc multiple comparisons, analysis for **(C-D)** was performed by the non-parametric Kruskal-Wallis ANOVA with post-hoc multiple comparisons. *p ≤ 0.05; **p ≤ 0.01; ***p ≤ 0.001; ****p ≤ 0.0001.

4.2.5 F-actin, moesin, and β1-integrin co-localise consistently with MCAM in the WRAMP structure

Staining for MCAM in the MT Colo239F-LA3.1 and Colo239F-YA3.1 cells revealed consistent polarised pooling of MCAM. On further observation, this was determined to localise at the rear of the cell and looked similar to the WRAMP structure described by Witze et al. 2008. Interestingly, this consistent polarised pooling of MCAM at the rear of the cell occurred frequently (in approximately 40% of cells) in the Colo239F-LA3.1 and Colo239F-YA3.1 cells but less commonly (in approximately 5-10% of cells) in the Colo239F- WT3.1 cells.

To explore the potential interaction between MCAM and the cytoskeleton, co-staining was performed for MCAM in combination with F-actin and moesin. F-actin staining appeared as either filamentous or small globular structures and was especially strong at the cell periphery, likely due to the planar view of the image (Fig. 18). Extensive co-localisation was noted between MCAM and the actin cytoskeleton at the flanks of the cell (Fig. 18). Interestingly, F-actin strongly and consistently co-localised with MCAM in the WRAMP structure (Fig. 18B-C). Furthermore, moesin also extensively co-localised with MCAM, especially with the WRAMP structure (Fig. 19). Staining with MCAM and β1-integrin also displayed consistent co- localisation (Fig. 20). While it was concentrated on the cell surface and periphery, MCAM and β1-integrin also co-localised extensively in the cytoplasm and specifically in the WRAMP structure (Fig. 20B, C). F-actin and β1-integrin staining in the WRAMP structure appeared to be striated, with MCAM staining strongest closer to the rear, while F-actin and β1-integrin staining were closer to the nucleus (Figs. 18B, 20C).

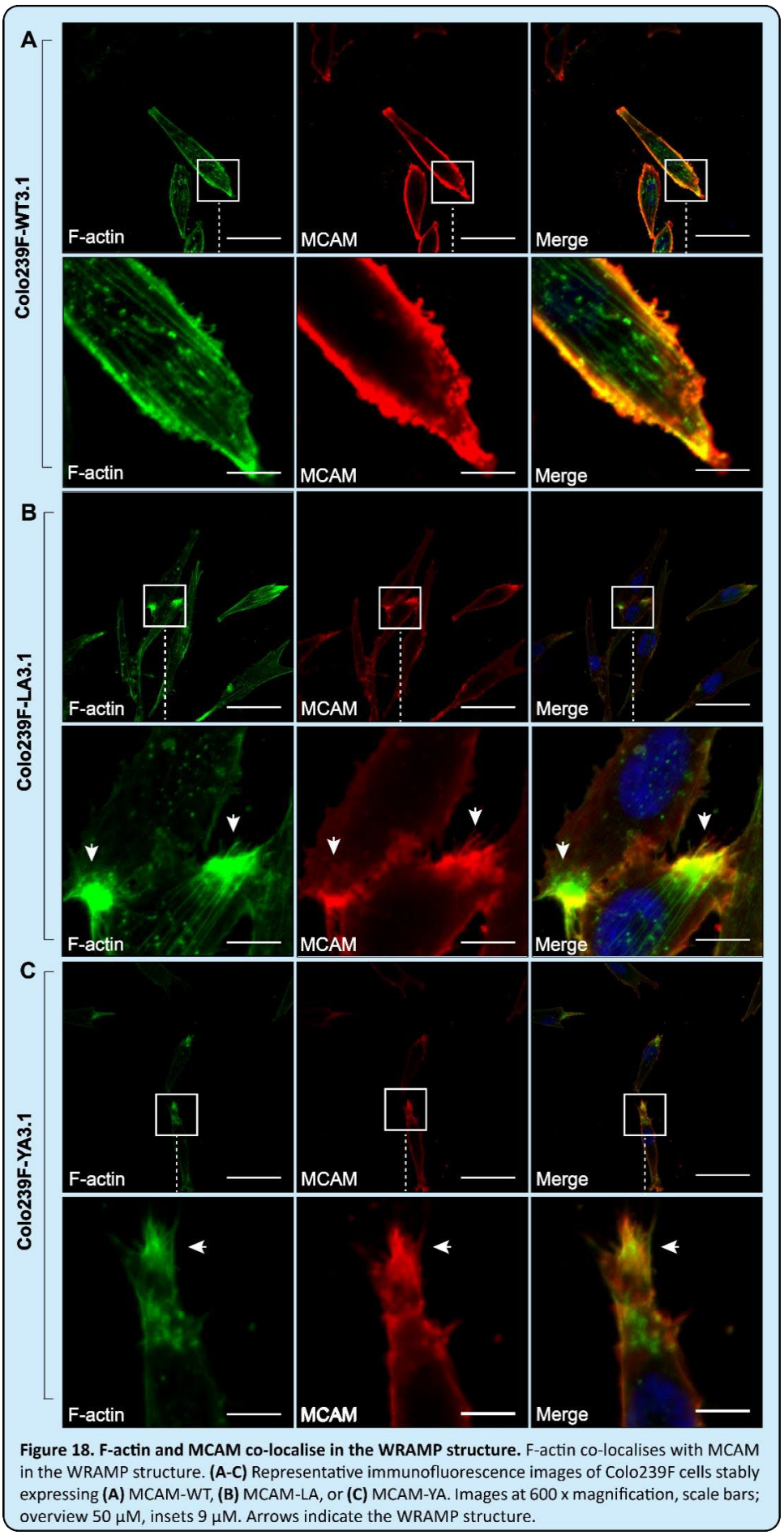

Figure 18. F-actin and MCAM co-localise in the WRAMP structure. F-actin co-localises with MCAM in the WRAMP structure. **(A-C)** Representative immunofluorescence images of Colo239F cells stably expressing **(A)** MCAM-WT, **(B)** MCAM-LA, or **(C)** MCAM-YA. Images at 600 x magnification, scale bars; overview 50 µM, insets 9 µM. Arrows indicate the WRAMP structure.

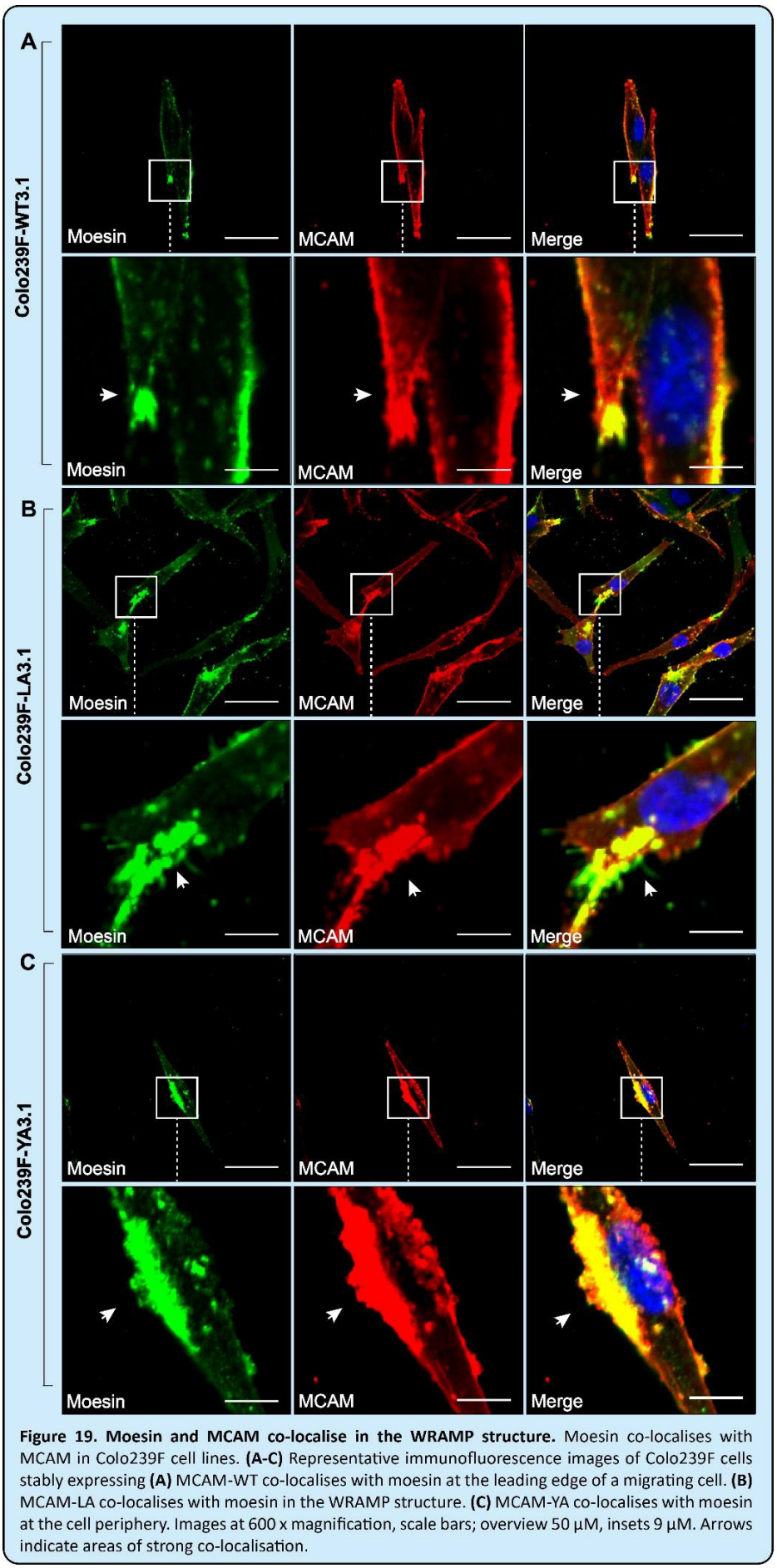

Figure 19. Moesin and MCAM co-localise in the WRAMP structure. Moesin co-localises with MCAM in Colo239F cell lines. **(A-C)** Representative immunofluorescence images of Colo239F cells stably expressing **(A)** MCAM-WT co-localises with moesin at the leading edge of a migrating cell. **(B)** MCAM-LA co-localises with moesin in the WRAMP structure. **(C)** MCAM-YA co-localises with moesin at the cell periphery. Images at 600 x magnification, scale bars; overview 50 µM, insets 9 µM. Arrows indicate areas of strong co-localisation.

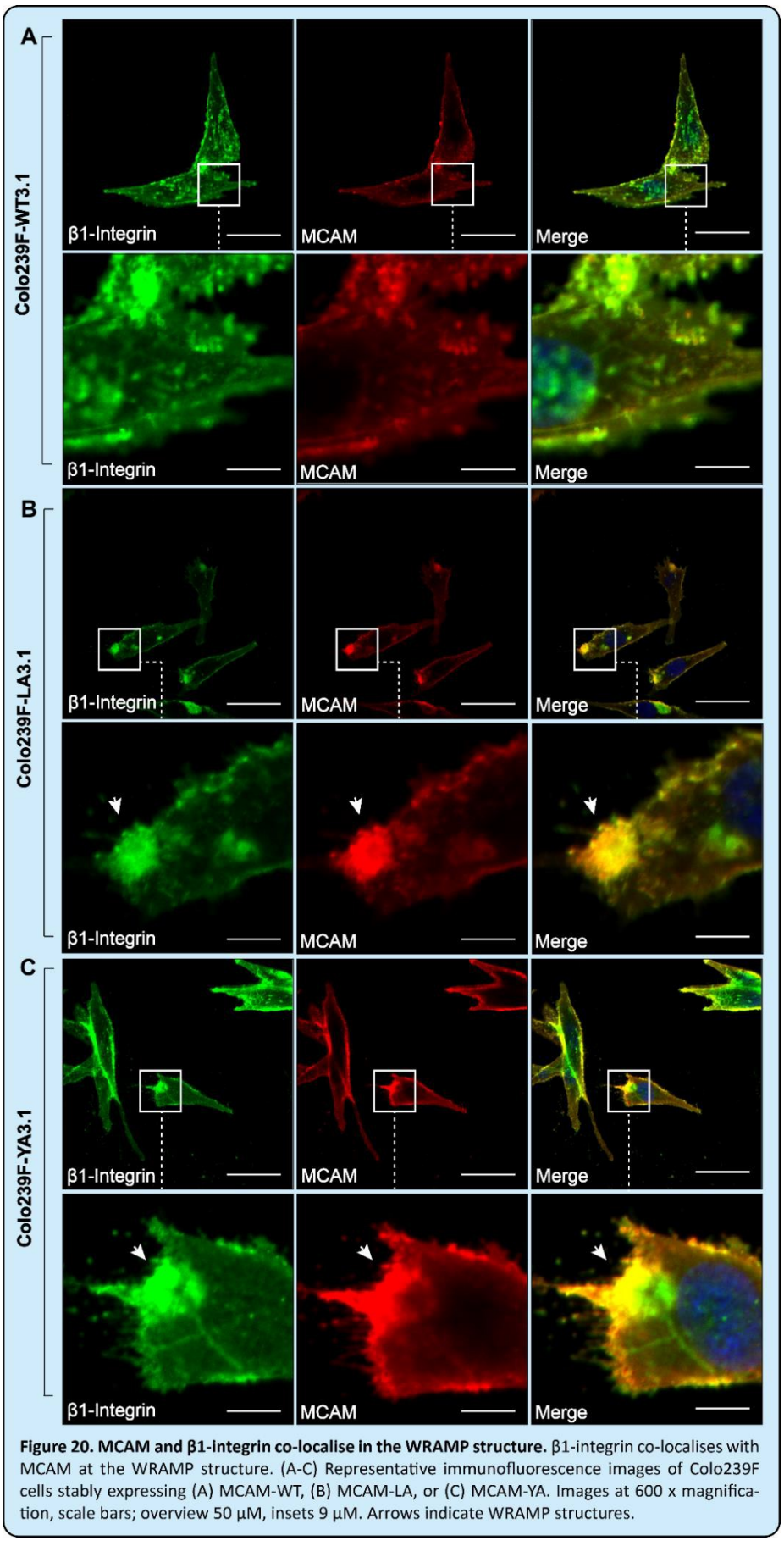

Figure 20. MCAM and β1-integrin co-localise in the WRAMP structure. β1-integrin co-localises with MCAM at the WRAMP structure. (A-C) Representative immunofluorescence images of Colo239F cells stably expressing (A) MCAM-WT, (B) MCAM-LA, or (C) MCAM-YA. Images at 600 x magnification, scale bars; overview 50 µM, insets 9 µM. Arrows indicate WRAMP structures.

4.2.6 MCAM co-localises with F-actin and moesin at cell protrusions

F-actin and MCAM also co-localised strongly at the cell periphery, especially at cellprotrusions (Fig. 21). However, the F-actin fibres which extended through the centres of the cells did not co-localise with MCAM. MCAM and moesin also consistently co-localised throughout the cell, especially at the cell protrusions (Fig. 21A). While representative imagesare from the Colo239F-WT3.1 cells, this was also noted in the MT cells (data not shown).

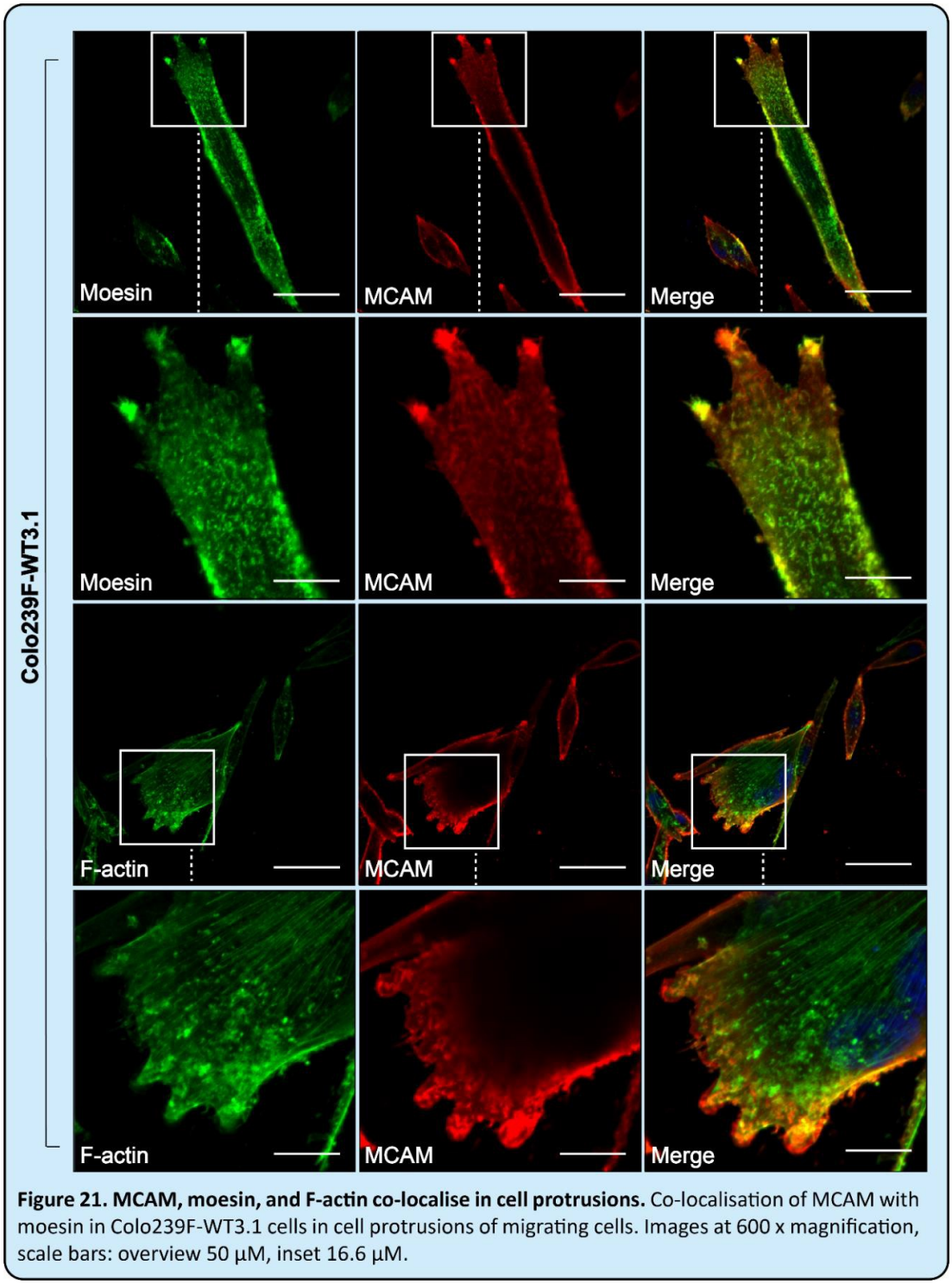

Figure 21. MCAM, moesin, and F-actin co-localise in cell protrusions. Co-localisation of MCAM with moesin in Colo239F-WT3.1 cells in cell protrusions of migrating cells. Images at 600 x magnification, scale bars: overview 50 µM, inset 16.6 µM.

4.2.7 MCAM does not appear to co-localise with microtubules

To assess whether MCAM co-localises with cell microtubules, co-staining was performed withMCAM and β-tubulin (Fig. 22). Very little co-localisation, except at the cell periphery, was noted in Colo239F-WT3.1, Colo239F-LA3.1, or Colo239F-YA3.1 cells.

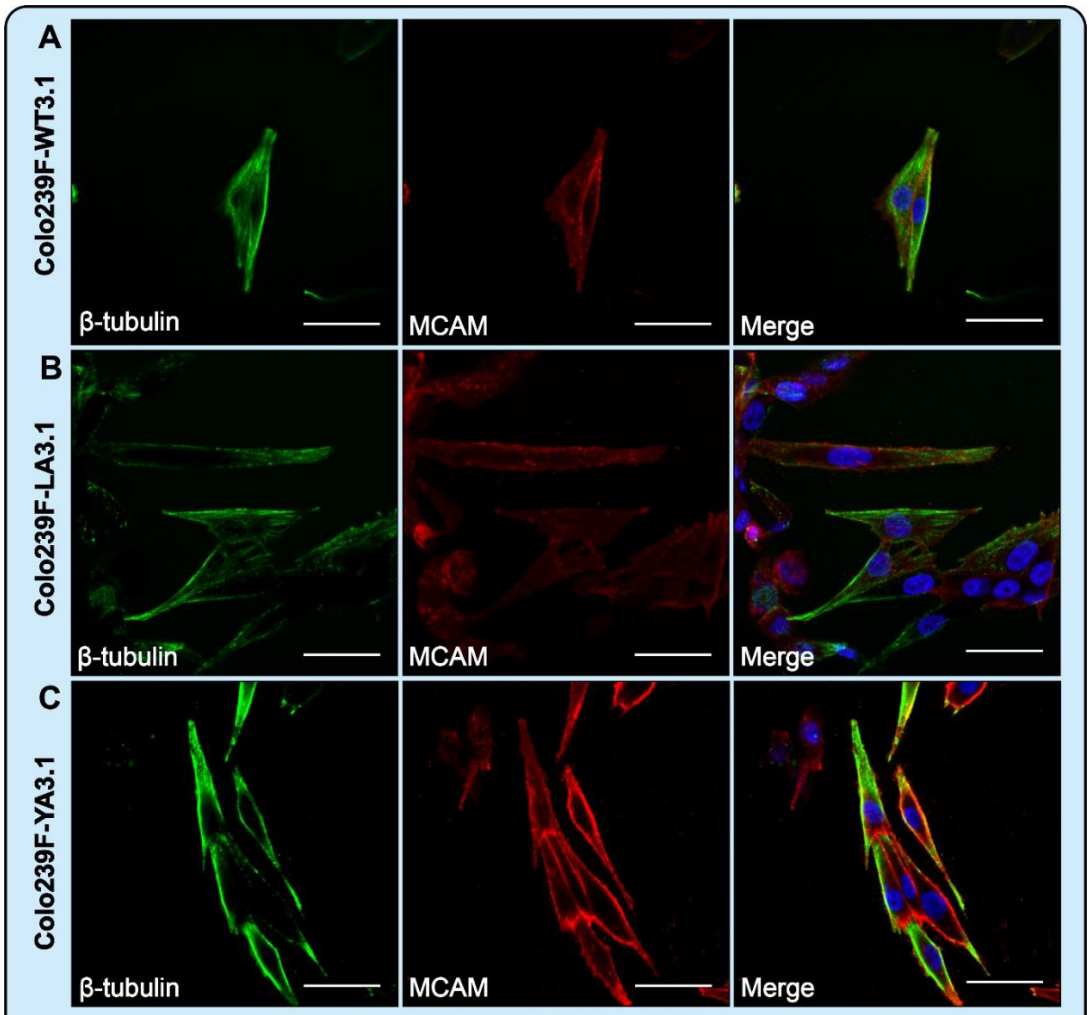

Figure 22. MCAM and β-tubulin do not co-localise in the Colo239F cell series. (A) Co-staining of MCAM with β-tubulin in Colo239F-WT3.1 cells, **(B)** Colo239F-LA3.1 cells, **(C)** and Colo239F-YA3.1 cells indicating limited co-localisation. Images at 600 x magnification, scale bar = 50 µM.

4.2.8 Calnexin and Cop1β are absent from the WRAMP structure

Interestingly, in contrast to previous reports, calnexin and Cop1β co-staining with MCAM displayed a conspicuous lack of staining in the region of the WRAMP structure in Colo239F- LA3.1 and Colo239F-YA3.1 cells (Figs. 23, 24). This effect was more pronounced for calnexin than Cop1β (Fig. 23B, C). Both calnexin and Cop1β staining displayed a punctate pattern withno especially identifiable features. Cop1β staining was stronger in the perinuclear region, probably indicating the Golgi or ER (Fig. 24).

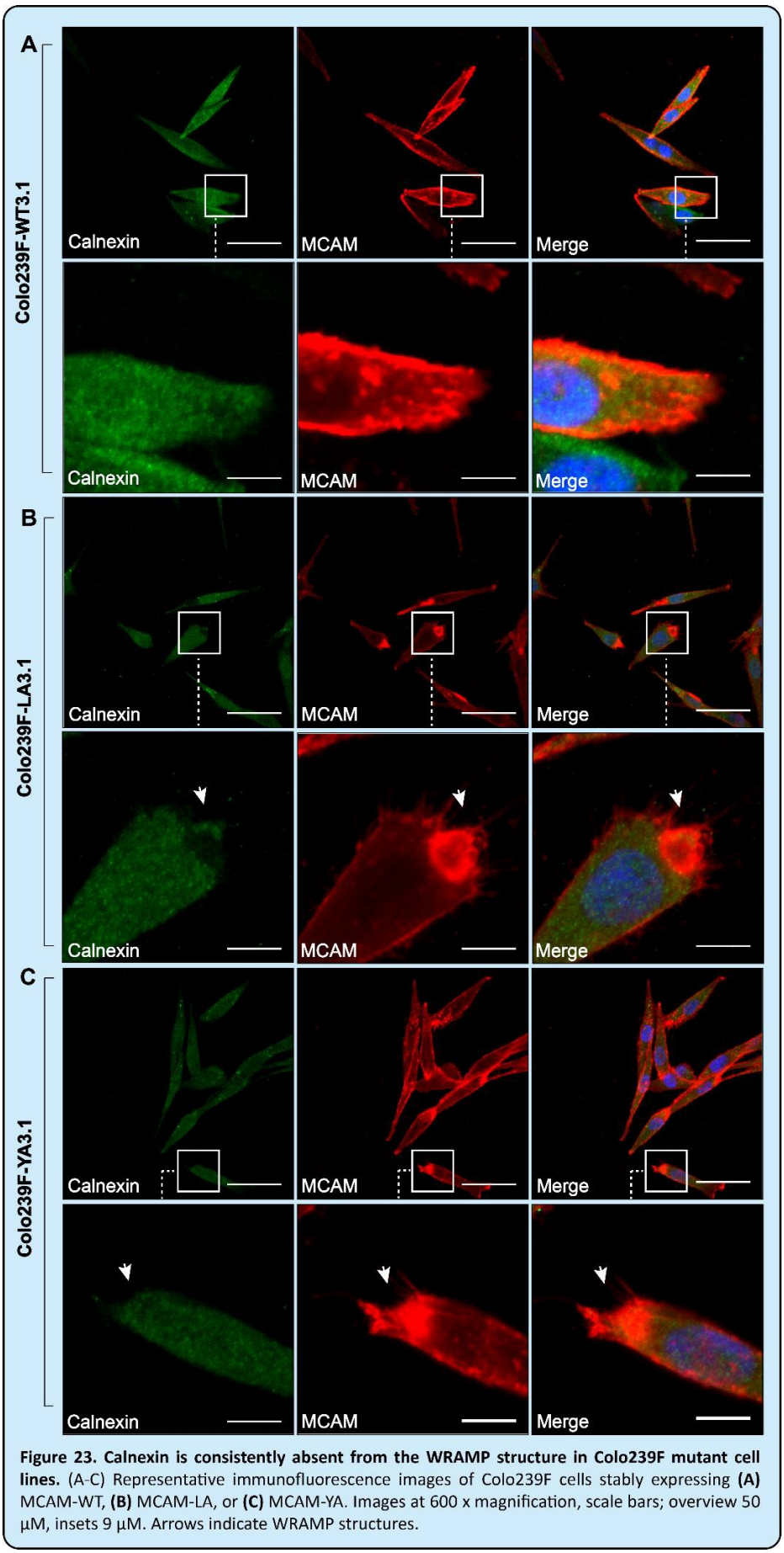

Figure 23. Calnexin is consistently absent from the WRAMP structure in Colo239F mutant cell lines. (A-C) Representative immunofluorescence images of Colo239F cells stably expressing **(A)** MCAM-WT, **(B)** MCAM-LA, or **(C)** MCAM-YA. Images at 600 x magnification, scale bars; overview 50 µM, insets 9 µM. Arrows indicate WRAMP structures.

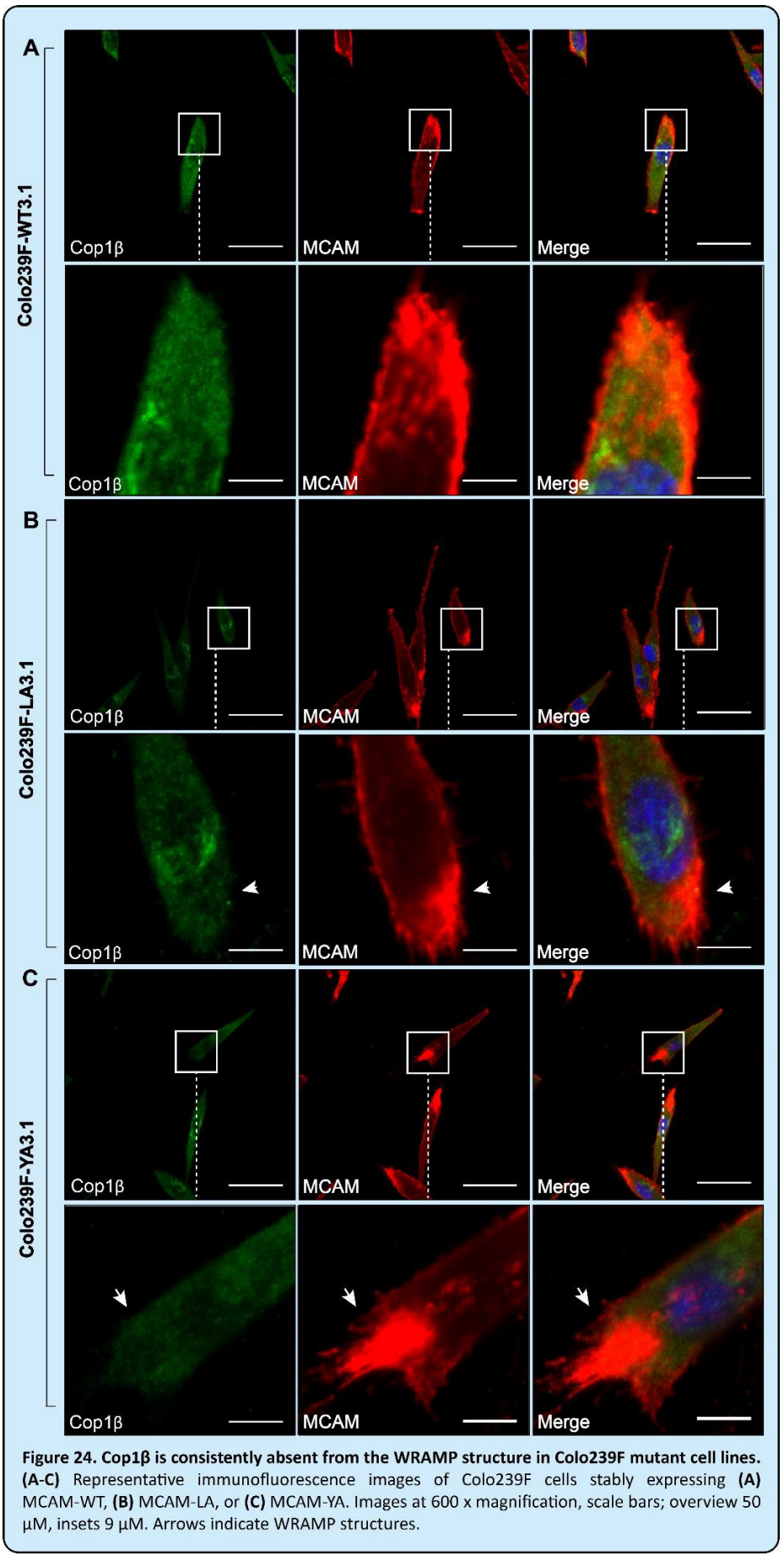

Figure 24. Cop1β is consistently absent from the WRAMP structure in Colo239F mutant cell lines. **(A-C)** Representative immunofluorescence images of Colo239F cells stably expressing **(A)** MCAM-WT, **(B)** MCAM-LA, or **(C)** MCAM-YA. Images at 600 x magnification, scale bars; overview 50 µM, insets 9 µM. Arrows indicate WRAMP structures.

4.2.9 MCAM co-localises with bilateral stress fibre filaments

It was noted that in some cells, MCAM displayed an interesting staining pattern consisting oftwo or more longitudinal filaments extending through the cell either side of the nucleus (Fig.25). On closer inspection, these structures were found to localise to the apical surface of thecell. As they resembled microtubular or cytoskeletal filaments, staining was performed with F- actin and β-tubulin. Interestingly, no co-localisation was identified with β-tubulin. However,F-actin strongly co-localised with MCAM in these structures (Fig. 25B).

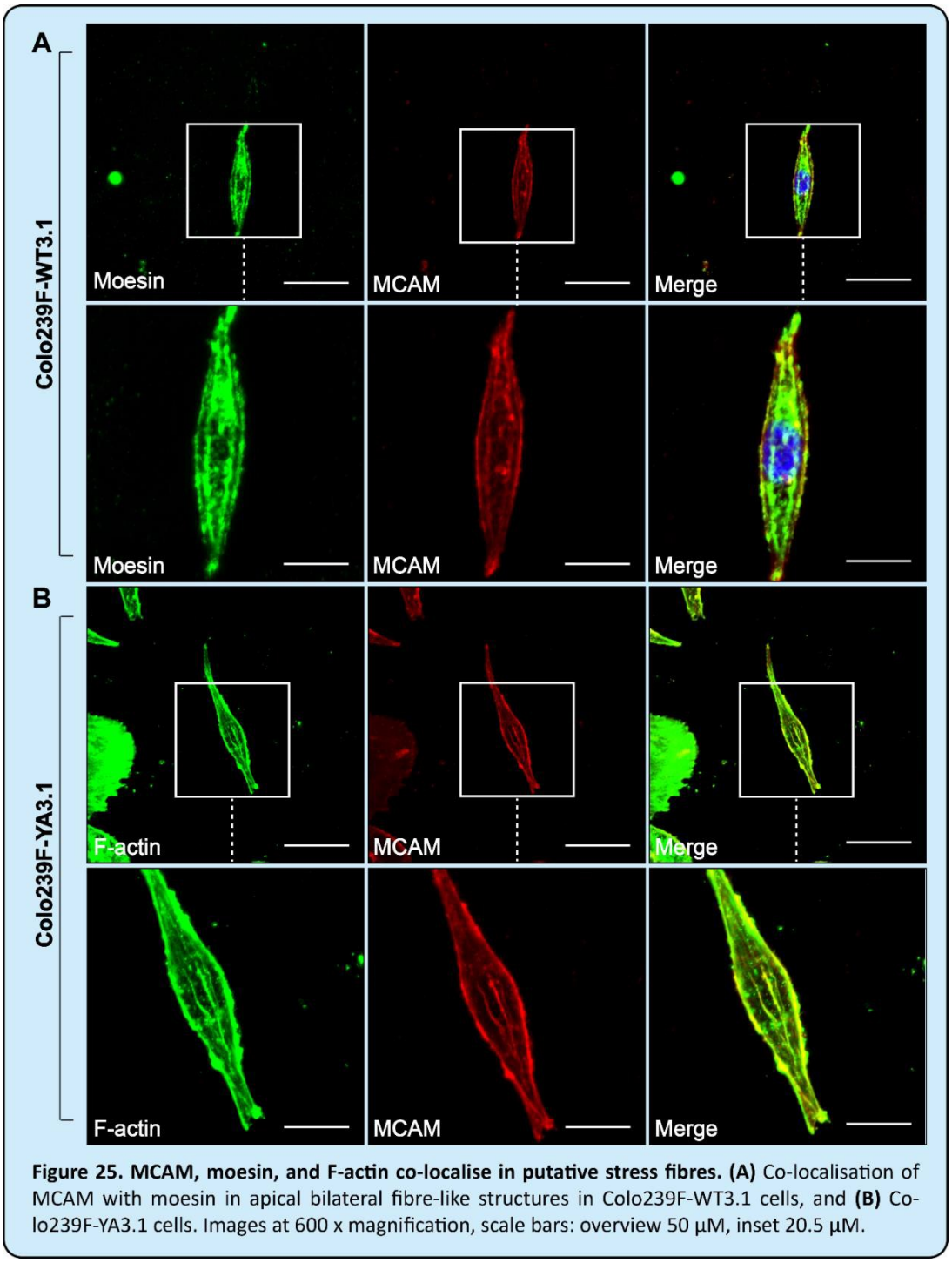

Figure 25. MCAM, moesin, and F-actin co-localise in putative stress fibres. (A) Co-localisation of MCAM with moesin in apical bilateral fibre-like structures in Colo239F-WT3.1 cells, and **(B)** Co-lo239F-YA3.1 cells. Images at 600 x magnification, scale bars: overview 50 µM, inset 20.5 µM.

Furthermore, it was found that moesin (Fig 25A) and Cop1β (Fig 26) also strongly and consistently co-localised with these structures (Fig. 25A). These structures were identified in cells expressing both WT and MT MCAM; representative images from WT and MT cells are displayed.

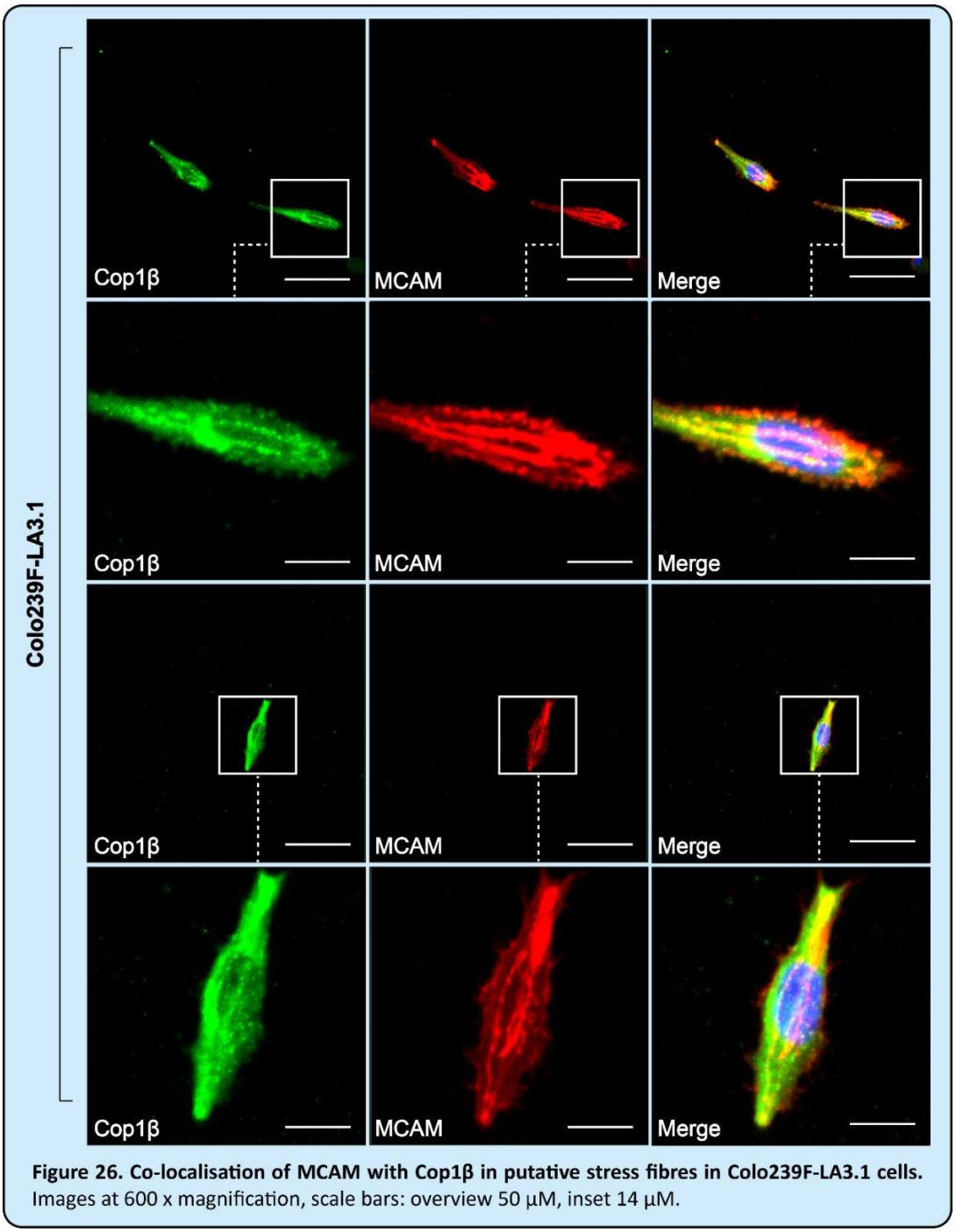

Figure 26. Co-localisation of MCAM with Cop1β in putative stress fibres in Colo239F-LA3.1 cells. Images at 600 x magnification, scale bars: overview 50 µM, inset 14 µM.

4.2.10 MCAM is not present in focal adhesions

To explore whether MCAM was present in focal adhesions, co-staining was performed between MCAM and vinculin (Fig. 27). Vinculin staining was punctate and dispersed throughout the cell, such that focal adhesions could not be identified. A small amount of co-localisation between vinculin and WT MCAM may be present, but there was no co- localisation of vinculin with MT MCAM. Further optimisation of this assay, or staining with phosphorylated paxillin, may clarify the presence or absence of MCAM In focal adhesions. However, due to time constraints, this was not pursued.

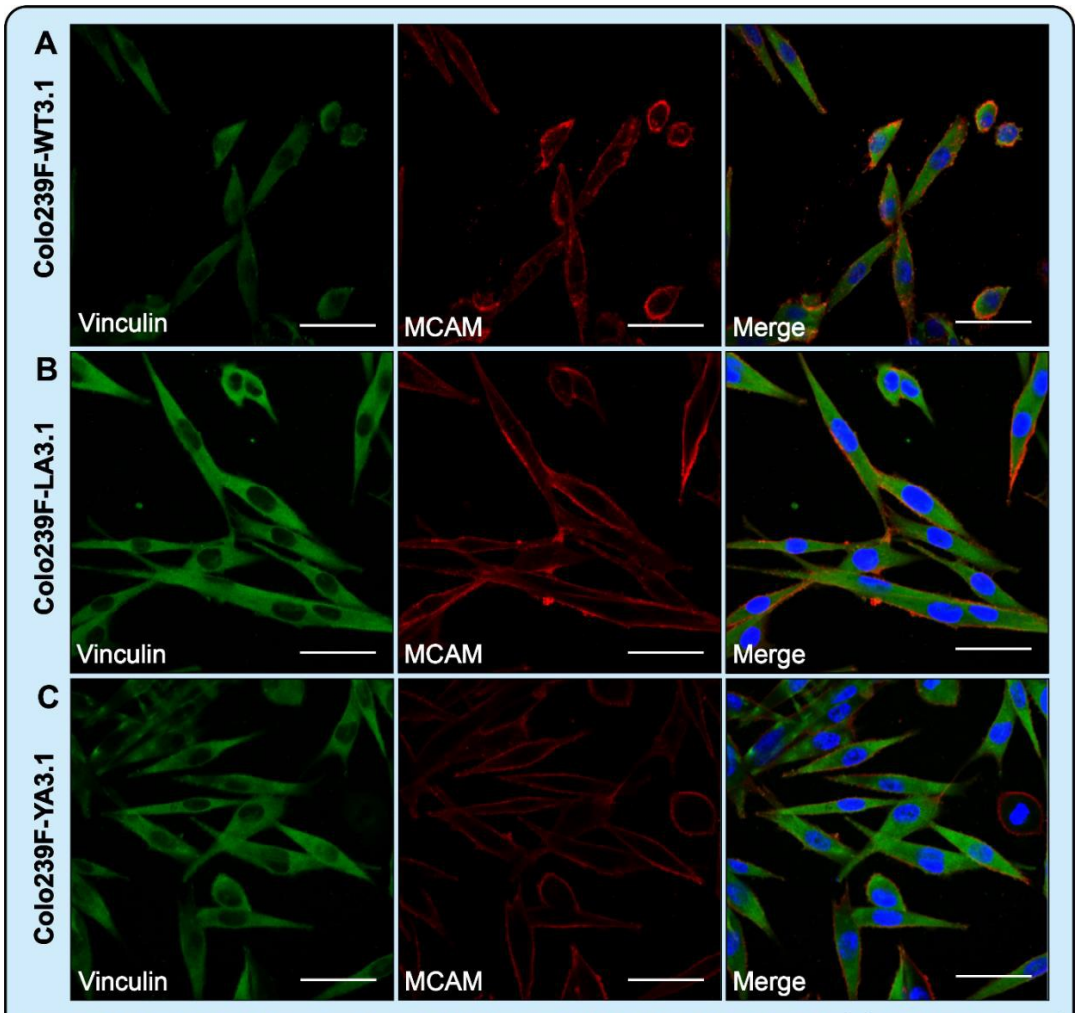

Figure 27. MCAM and vinculin do not co-localise in the Colo239F cell series. (A) Co-localisation of MCAM with vinculin in Colo239F-WT3.1 cells, **(B)** Colo239F-LA3.1 cells, and **(C)** Colo239F-YA3.1 cells. No co-localisation was apparent between MCAM and vinculin. Images at 600 x magnification, scale bar = 50 µM.

4.2.11 β1-integrin expression in Colo239F cells

Previously, it has been reported that β1-integrin surface expression may be downregulated upon MCAM transfection into melanoma cell lines (Alais et al. 2001; Dye 2007). This finding, in addition to the differences seen when MCAM positive and negative Colo239F cells were plated on collagenI and IV, lead us to explore β1-integrin cell surface expression in the Colo239F cell series.

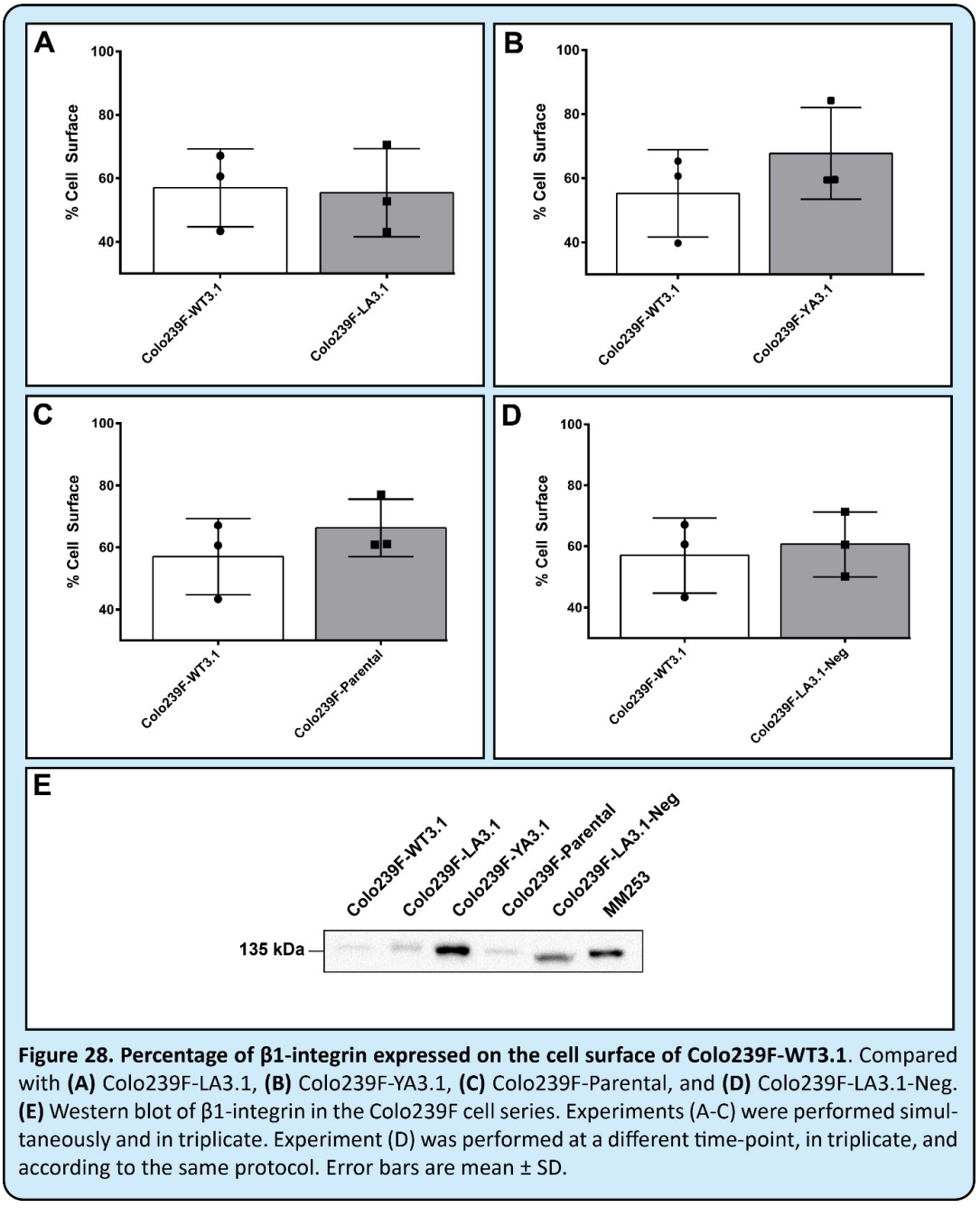

Figure 28. Percentage of β1-integrin expressed on the cell surface of Colo239F-WT3.1. Compared with **(A)** Colo239F-LA3.1, **(B)** Colo239F-YA3.1, **(C)** Colo239F-Parental, and **(D)** Colo239F-LA3.1-Neg. **(E)** Western blot of β1-integrin in the Colo239F cell series. Experiments (A-C) were performed simultaneously and in triplicate. Experiment (D) was performed at a different time-point, in triplicate, and according to the same protocol. Error bars are mean ± SD.

Interestingly, both Western blot analyses showed that β1-integrin expression appeared highest in Colo239F-YA3.1, however, the flow cytometry data is highly variable forthese cells (Fig. 28B). Furthermore, the Western blot results indicate a far greater increase ofexpression in Colo239F-YA3.1 than the flow cytometry data and Total expression and surface expression mean fluorescent intensity (MFI) are listed in Table 14. While no significant differences were noted, the mean cell surface expression of β1-integrin was slightly lower in MCAM-expressing cells compared to MCAM-negative (Fig. 28A D, Table 11). suggest that the Colo239F- YA3.1 cells express more β1-integrin than the MCAM-negative cells (Fig. 28E). These data remain to be confirmed.

Table 14. β1-Integrin expression in Colo239F cell populations.

Experiment	Cells	Cell Surface(MFI)	Total (MFI)	% MCAM on cell surface
1	**Colo239F-WT3.1**	10053.33 ± 1097.44	17865.83 ± 1402.05	57.0%
	Colo239F-LA3.1	8948 ± 1179.66	16370.67 ± 1163.32	55.4%
	Colo239F-Parental	11282.67 ± 1258.84	17045.33 ± 1087.04	66.3%
	Colo239F-LA3.1-Neg	10229.17 ± 1155.53	16956.5 ± 974.35	60.7%
2	**Colo239F-WT3.1**	7872.83 ± 4849.21	17361.83 ± 1759.13	43.1%
	Colo239F-YA3.1	6726.33 ± 4631.74	16425.83 ± 924.07	42.6%

The geometric mean fluorescence intensity (MFI) for β1-integrin shown for non-permeabilised cells (cell surface) and permeabilised cells (total). Experiment 1 and 2 were performed in triplicate at different time points due to cell availability. Data shown as mean ± SD.

4.3 Discussion

4.3.1 Changes in cell morphology and cell-ECM interactions in MCAM-positive cells

The second aim of this project was to functionally characterise the Colo239F cell series. Specifically, there were two fundamental questions of interest: whether MCAM expression in the Colo239F cells produced phenotypic characteristics consistent with previous literature, and whether the di-leucine and tyrosine mutants displayed changes in phenotype when compared to the WT-expressing cells.

Enforced expression of CAMs is commonly accompanied by a change in cell morphology. Forinstance, integrin expression levels are known to affect the shape and spreading of cells on various substrates (Khalili and

Ahmad 2015). Interestingly, enforced expression of MCAM has also been linked tomorphological changes in melanoma cells. Transfection of MCAM into the human melanoma SB2 and KW4 cell lines produced morphological changes, as well as in Chinese hamster ovary (CHO) epithelial cells (Dye 2007). However, other studies of this type have not described morphological changes associated with enforced expression of MCAM in melanoma (Johnson et al. 1997; Xie et al. 1997).Furthermore, previous data generated in our laboratory indicated MCAM appears to modulate cell morphology and spreading on certain ECM surfaces, including collagen I, IV and laminin-111 (laminin 1) and 332(laminin 5) (Dye 2007).

Here, the introduction of WT and mutant MCAM to the Colo239F cell line appeared to produce morphological changes. The adherent parental cell line has a characteristic fibroblastic morphology, typically displaying a bipolar elongated shape (visible in Fig. 11C). The cells transduced with WT MCAM appeared to retract, measuring significantly shorter on average than the other cells. While the Colo239F-WT3.1 cells were significantly shorter thanthe MCAM negative parental cell line, the overall area of the cells did not display as marked a change (Fig. 11A-B). This suggests that cells might be becoming wider or rounder as they retract. Interestingly, when transduced with WT MCAM, the KW4 melanoma cell line and CHO epithelial cell line were also reported to retract and become smaller and more rounded.However, in the same study, the SB2 cells displayed the opposite change (Dye 2007). This suggests that the effect MCAM expression has on cell shape is also a function of the levels of other CAMs expressed by these cells, e.g. integrins.

Furthermore, the MT transduced cell populations both displayed significantly increased cell length in comparison to WT-expressing and MCAM-negative Colo239F cells (Fig. 11A-B). Thisis a novel finding that may indicate loss/gain-of-function effects resulting from the mutations introduced in MCAM. Interestingly, it suggests the observed changes in morphology in MCAM positive cells may be driven, at least in part, by the cytoplasmic tail of MCAM. In addition, the MT and MCAM-negative cells grew in a manner comparatively like the parental Colo239F cell line. When grown to confluence they tended to spread over the top of each other in a tangled network, not forming a consistent monolayer. In contrast, the Colo239F- WT3.1 cells grew in “islands” of cells in which many cells had not spread and instead adhered to the top of these islands, and which remained attached after multiple rounds of washing with PBS (data not shown). This may indicate that cells expressing WT MCAM display higherhomotypic adhesion. To explore this, network-forming assays and aggregation assays were performed, however, neither could be optimised for the Colo239F cell series. Further experimentation into the adhesive preferences of this cell series is required.

Interestingly, significant changes in spreading behaviour on collagen type I, type IV, and laminin I were observed. In these assays, the cells were plated in serum free media, so the only interaction explored was between cell surface molecules and the purified matrix. Colo239F-YA3.1 and Colo239F-Parental (MCAM negative/low) displayed the highestproportion of spread cells, and a greater mean length of spread cells on collagen type I and IV. Colo239F-YA3.1 also had the greatest length under normal culture conditions (e.g. 10% serum) and displayed the smallest average cell height among the cells analysed. Cell spreading behaviour

on laminin 1 was most similar for Colo239F-WT3.1 and Colo239F-YA3.1; while the Colo239F-LA3.1 cells behaved similarly to Col239F parental and the negative control cells. Taken together, these data suggest the MCAM WT expression is associated withslower spreading on collagen type I and IV, and that this effect is reversed if MCAM containsthe Y641A mutation. In contrast, expression of WT and Y641A MCAM appears to enhance cell spreading on laminin I compared to MCAM negative cells; and this effect is lost in cells expressing MCAM containing the LL623-642AA mutation. All cells spread well on fibronectin.

Previous studies exploring the effect of MCAM on spreading behaviour in melanoma cells have reported conflicting results. One study found that MCAM expression had no effect on cell spreading on collagen type I or fibronectin (Xie et al. 1997), whereas another described reduced adhesion on vitronectin in cells expressing avian MCAM (HEMCAM) (Alais et al. 2001). Finally, work in ourlaboratory found that MCAM expression was linked to delayed spreading in cells on collagentype I and IV, with no differences seen for fibronectin and vitronectin (Dye 2007). However, all of these studies reported that MCAM-positive cells displayed delayed spreading and a roundedmorphology on laminin-111 (laminin-1) in comparison to MCAM-negative cells (Alais et al. 2001; Dye 2007; Xie et al. 1997). However, when spreading of ovarian cells was explored on collagen types I and IV, laminin 1,and fibronectin, the authors reported that MCAM expression was positively associated withspreading on all matrices, and that silencing MCAM resulted in reduced cell spreading on these substrates, as well as decreased invasion through Matrigel (Wu et al. 2012).

The mechanism by which MCAM may affect cell spreading is not entirely clear. One study reported that expression of the avian homolog of MCAM downregulated laminin-binding β1-integrin receptors (α3β1 α6β1, α7β1) on the cell surface, resulting in delayed spreading on this substrate (Alais et al. 2001). β1 integrin expression was explored in the Colo293F cell series, but by flow cytometry β1 expression appeared similar across all cell lines, although the proportion of total β1 expressed on the cell surface was higher in the Colo239F-Parental and Colo239F-LA3.1-neg cells. By western blot, the cell populations appeared to have similar (low) levels of β1 integrin except Colo239F-LA3.1-neg and Colo239F-YA3.1, which showed bands of higher intensity (YA > neg). These data need further investigation as it is difficult to reconcile the differences seen between the flow cytometry and immunoblot analyses; and it is difficult to draw any conclusions. Based on the data to date, however, there does not appear to be any association between β1 expression levels and cell spreading behaviour. Nor is there any evidence that MCAM binds any of the matrix proteins tested in this study, although it is known to bind laminin-411 and laminin-421 (laminin 8 and 9, respectively) (Flanagan et al. 2012; Ishikawa et al. 2014). Furthermore, laminin-322 (laminin 5) has been linked to melanoma migration (Seftor et al. 2001) and laminin-511 (laminin 10) is known to interact with the related IgSF member BCAM (Vainionpää et al. 2006).

Cell morphology is modulated by an array of different protein interactions, commonly involving the cytoskeleton and cytoskeletal elements, as well as adhesion molecules (Khalili and Ahmad 2015). These interactions will be discussed in more detail in the section below regarding cell migration. Briefly, however, the KKGK motif in the cytoplasmic tail of MCAM may be important in interpreting our observations. This motif interacts with and recruits the actin binding ERM proteins, promoting the formation of microvilli (Luo et al. 2012). However, a recent study found that the Y641 residue of MCAM (which we are investigating as a potential endocytosismotif) is phosphorylated following growth factor (VEGF) stimulation. This leads to a conformational change in the cytoplasmic domain of MCAM, which exposes the KKGK motif (Jouve et al. 2013). Our mutation, Y641A, may mimic the conformational changes that result from phosphorylation, unmask the KKGK site and lead to an upregulation of interactions between MCAM, the ERM proteins and the cytoskeleton. This is consistent with the enhanced spreading seen in the Colo239F-YA3.1 cells compared to Colo239F-WT3.1 and Colo239F LA3.1 cells on some matrices. How this model is reconciled to our observation that transfection of MCAM-WT into the Colo239F cells is generally associated with reduced spreading compared to parental cells is not yet clear. In addition, the Colo239F-LA3.1-neg cells may not be the most appropriate control cells, given they differ from the Colo239F parental cells in a number of assays.

To further clarify changes in the cytoskeleton following MCAM transfection, F-actin and vinculin/paxillin staining could be performed to observe cytoskeletal filaments and focal adhesions in Colo239F cells as they spread on various ECM substrates.

4.3.2 MCAM and proliferation

The WT MCAM-expressing cells displayed a faster growth rate than the Colo239F-Parental, Colo239F-YA3.1 and Colo239F-LA3.1 cells, however, the only significant change was after the ~120 h mark, where the Colo239F-WT3.1 cells continued to proliferate, while the others appeared to plateau (Fig. 12). This may reflect that Colo239F-WT3.1 cells are smaller, formed islands and showed some vertical growth (i.e. a lack of contact inhibition), whereas the othercells were more spread out when grown on standard tissue culture plastic. However, the MCAM-negative Colo239F-LA3.1-Neg cells displayed an almost identical growth rate to Colo239F-WT3.1. This may mean that the change in growth rate was an artefact of the transduction and selection process. As mentioned above, the Colo239F-WT3 cell populationalso produced some conflicting data in the spreading assay and further exploration of this population and analyses of other control cells is required to clarify these findings.

Proliferation following 120 hours was not investigated because by this time in the assay, cells were ~100% confluent and proliferation may have been inhibited by the size of the tissue culture vessel, contact inhibition and nutrient supply (although media was changed regularly). This could be explored by seeding a lower

number of cells or using a larger tissue culture vessel. However, previous data generated in the laboratory indicates the most relevant data is cell doubling time whilst cells are in exponential growth phase between ~48 and 120 hours, which is shown in Figure 12E.

The literature surrounding MCAM-induced changes in proliferation are conflicting. For instance, enforced expression of MCAM has been associated with an increase in proliferation (Alais et al. 2001; Kang et al. 2006) and MCAM has been linked to proliferative signalling cascades (Jiang et al. 2012). However, other studies have reported that no significant changes in proliferation resulting from enforced MCAM expression (Alais et al. 2001; Satyamoorthy et al. 2001). This suggests that proliferative phenotype is likely to be determined more by the complete genomic and proteomic features of a particular cell line, than by the expression of an individual protein such as MCAM.

In addition, MCAM expression may have an enhanced effect on proliferation when cells are stimulated with specific growth factors rather than standard serum conditions. For example, Xu et al (2019) found that growth factor stimulation lead to phosphorylation of Y641 in endothelial cells and allowed the KKGK motif to bind to Rictor, mediating the interaction of MCAM with the mTORC2 complex. CD146-mediated mTORC2 activation was found to promote cell proliferation and survival (Xu et al. 2019). Growth factor stimulation may be an area to explore in MCAM WT, MT and negative cells, although it is not yet clear from the literature how Rictor and ERM proteins binding the KKGK motif in MCAM is coordinated. Nor it is clearif MCAM-mediated mTORC2 activation occurs in melanoma cells as well as endothelial cells.

As each of the experiments were done separately with reference to the WT cell line, we could not compare between them. No experiment was performed comparing the parental to the transduced cell lines for several reasons. Firstly, the primary aim of these experiments was to compare the WT MCAM cell line to the cell lines expressing mutant endocytosis motifs. Secondly, the parental cell line had a low level of native MCAM expression, hence the creation of and comparison to the MCAM-neg cell line. Finally, these experiments involved direct cell counting (which was chosen in preference to metabolic-based assays, to remove the potential confounder of metabolic differences, which was not the focus of these assays).Direct cell counting is labour and time intensive and we believe the most accurate results were produced by using a “batch approach”. However, further investigations could use an assay such as AQueous One Cell Proliferation Assay (understanding its limitations as a metabolic based assay). AQueous One is a higher throughput technique that will allow a comparison of all cells simultaneously. In addition, cell death could be explored using an Annexin-V based assay; as direct counting and metabolic assays provide information on total cell number only and do not measure cell death. This would add information, as some cells may be dying as others are proliferating.

4.3.3 Mutations in the cytoplasmic tail of MCAM promote rear-directed cell migration

Wound-healing assays, Transwell assays, and random cell tracking were attempted to investigate the migratory phenotype of the Colo239F cell series. Unfortunately, the growth pattern of Colo239F cell line rendered the wound-healing assay inappropriate for these cells, as they do not grow in a monolayer. Furthermore, due to time restraints, only preliminary data were obtained for the Transwell assays (data not shown).

Random cell tracking was therefore the primary assessment of migratory phenotype in thesecells. Using live cell imaging, cells were visualised and tracked for up to 18 h in ten fields of view. This generated a full picture of the behaviour of these cells under normal cell culture conditions. Distance travelled was measured by two metrics. Firstly, distance was calculated along the path the cell travelled, and secondly, distance was calculated from starting point to end point along a straight line (directional migration). The Colo239F-WT3.1 cells exhibitedboth the lowest total distance of migration as well as the least sustained directional migration. This correlates with data from one study which reported a reduction in migrationin MCAM-positive versus MCAM-negative melanoma and epithelial cell lines (Dye 2007). In contrast, the Colo239F-YA3.1 and Colo239F-LA3.1 cells exhibited a greater distance travelled and a greater extent of directional migration than both the Colo239F-WT3.1 and MCAM-negative lines (Fig. 12).

MCAM has been linked to increased migration in melanoma cell lines via multiple lines of evidence. For instance, VEGF signalling is known to induce FAK activation and increase trans- endothelial migration. Furthermore, MCAM knockdown was found to reduce this effect (Jouve et al. 2015). An anti-MCAM antibody significantly reduced tumour cell migration on a laminin-421 matrix (Ishikawa et al. 2014). MCAM is also reported to activate RhoA via interactions with moesin in protrusions, leading to increased migration (Luo et al. 2012). The reduction in cell movement seen here in cells transduced with WT MCAM is therefore largely at odds with the literature. It is possible the different growth pattern seen in cells expressing WT MCAM (that is, the propensity to grown in tight clusters, see Figure 11) compared to parental Colo239F, may mean our analysis of cell movement using random cell tracking, does not accurately reflect the ability of these cells to migrate and invade. Thus, other assays measuring cell migration and invasion are required to explore this further. For example, a transwell assay using Matrigel and a chemotactic agent will measure invasion (rather than just cell motility), which may provide more informative data. Other methods that could be used include live cell imaging using a chemoattractant to induce directional migration; and three dimensional spheroid invasion models, which may better recapitulate a tumour environment. Interestingly, the increase in directional migration in cells expressing MT MCAM, comparedto WT MCAM, is consistent with previous data generated in our laboratory in the SB2 melanoma cells.

Another mechanism describing a role for MCAM in melanoma migration is the WRAMP structure (discussed in detail in Chapter 1, Section 1.6.1.5). As described by Connacher et al.2017, the WRAMP structure forms transiently at the rear of the cell, defines the direction ofcellular migration, and then disintegrates, reforming at the new rear when the cell changes direction (Connacher et al. 2017). While the WRAMP structure occurs intermittently in the Colo239F-WT3.1 cells, it occurs with far greater frequency in the cells expressing MT compared to WT MCAM (~5 % vs 40%). This suggests that either the recruitment of MCAM to WRAMP, or formation of the WRAMP structure itself is mediated, at least in part, by the intracellular tail of MCAM; and that mutations in this region affect this process. The significant increase in sustained directional migration observed in the Colo239F-LA3.1, and to a lesser extent in the Colo239F-YA3.1 cells, might be explained by either enhanced formation or increased stability of the WRAMP structure. If the WRAMP structure is more stable in the mutant Colo239F-LA3.1 and Colo239F-YA3.1 cells, then the cells could be expected to travel further in one direction.

To investigate this further, cells were treated with lithium chloride (an agonist of canonical Wnt signalling) and stained for MCAM and components of WRAMP to determine whether Wnt stimulation may induce similar levels of WRAMP formation in the Colo239F-WT3.1 cells,compared to unstimulated mutant cells. These experiments produced inconclusive results (data not shown) and requires further optimisation. Stimulating cells using exogenous Wnt5a, as performed in previous studies of WRAMP, may shed light on this hypothesis (Witze et al. 2013).

Wang et al. (2015) recently reported that Wnt5-mediated localisation of MCAM to the WRAMP structure is mediated by de-palmitoylation of MCAM at residue C590. Mutation of this residue to a glycine inhibited palmitoylation and increased trafficking of MCAM to WRAMP in the absence of Wnt5a stimulation, leading to the hypothesis that depalmitoylation of MCAM is required for WRAMP formation (Wang et al. 2015). Palmitoylation functions as a lipid anchor which embeds proteins in the cell membrane, and the cyclical nature of palmitoylation and depalmitoylation has a function in protein trafficking and relocalisation (Guan and Fierke 2011). Due to the location of the palmitoylated residue in the intracellular tail of MCAM, it is possible that in WT MCAM, the KKGK motif is masked and prevented from binding its interaction partners. As discussed above, the KKGK motif is believed to interact with ERM proteins and Rictor. However, in the model proposed by Wang et al (2015), depalmitoylation of C590 reveals the KKGK motif, to enable interaction with Cop1β, which is thought to mediate retrograde transport of MCAM from the Golgi to the WRAMP (Witze et al. 2013).

It is also possible that the mutations introduced into MCAM in this study interfere with palmitoylation. It may be that depalmitoylation induces trafficking of MCAM to the rear of the cell, and palmitoylation then traffics MCAM back to the membrane. If palmitoylation of the mutated protein is less effective, this might explain the pooling of MCAM at the WRAMPstructure observed in this study.

Exploring the role of palmitoylation and depalmitoylation in the trafficking of MCAM was beyond the scope of this study but presents an intriguing hypothesis for the formation of theWRAMP structure, as well as the general function of MCAM in melanoma. Moreover, it wouldbe interesting to explore whether the tyrosine phosphorylation-induced conformational change of the cytoplasmic tail, as described by Xu et al. (2019) also modulates palmitoylation/depalmitoylation of MCAM (Xu et al. 2019). Reciprocal regulation of phosphorylation and palmitoylation has been described for the dopamine transporter (DAT), a transmembrane protein that is responsible for re-uptake of dopamine at the pre-synaptic membrane (Moritz et al. 2015). This study found that high phosphorylation/low palmitoylation was associated with reduced dopamine transport, while low phosphorylation/high palmitoylationincreased transport velocity (Moritz et al. 2015). A further unexplored question raised by this and previousstudies is whether or not MCAM-negative cells can still generate WRAMP. In other words, isWRAMP MCAM-dependant or can it occur independently? This could be explored using the Colo239F cell series. Although the parental cell line has very low levels of MCAM, we did undertake a cell sort to isolate an MCAM negative subpopulation.

As previously discussed, the WRAMP structure contains many proteins integral to cytoskeletal and microtubule dynamics. Witze et al. described a cassette of proteins which co-localised with MCAM in the WRAMP structure, including F-actin, Cop1β, and calnexin (Witze et al. 2013). After noting polarised MCAM pooling in the mutant MCAM-expressing Colo239F cells, some proteins of the WRAMP interactome were selected for staining experiments to explore whether the intracellular MCAM pool was indeed the WRAMP structure. As F-actin co-localised consistently and strongly with MCAM in this pool, it is highlylikely that this is the same or similar to the WRAMP structure. A major finding of this study isthat both moesin and β1-integrin localised to the WRAMP structure in Colo239F cells (Figs. 18, 19). This finding is consistent with previous studies in melanoma. For instance, the ERULSstructure, is a rear-polarised event which involves ezrin (an ERM protein), F-actin, myosin light-chain, and β1-integrin (Lorentzen et al. 2011). Furthermore, moesin was reported to co-localise with F- actin and myosin IIB in a similar rear-polarised structure associated with RhoA signalling andincreased migration (Estecha et al. 2009).

Another major finding, which conflicts with the current literature, is that both calnexin and Cop1β failed to co-localise with either MCAM or at the WRAMP structure. This suggests that under the experimental conditions of this study, neither Cop1β nor the cortical ER are involvedin WRAMP formation. In the two papers on WRAMP published by Witze et al., exogenous Wnt5a was utilised to stimulate the formation of WRAMP. Under these conditions, calnexin(a marker for the ER) co-localised with the WRAMP structure. Here, calnexin staining produced whole-cell punctate staining with no clearly identifiable features except a conspicuous lack of calnexin staining within the WRAMP structure (Fig. 22). Furthermore, they reported that treatment of the cells with Brefeldin A (which blocks the recruitment of Cop1 to vesicles), as well as RNAi knockdown of Cop1β, resulted in the blocking of the formation of the WRAMP structure (Witze et al. 2013). Our findings suggest that WRAMP formation may be able to occur independently of these components in Wnt5a-unstimulated

cells. Based onthe results obtained from this study, and those discussed in the few papers published which discuss the WRAMP structure, there appear to be two possibilities. Firstly, the structure identified in this study is indeed WRAMP, but without Wnt5a stimulation, the ER is not recruited. Alternatively, it is possible that what we observed is not the WRAMP structure, and is a related structure resulting in a polarised pool of MCAM, F-actin, moesin, and β1- integrin (such as the ERULS).

Developing a Colo239F cell series expressing GFP-tagged WT and mutant MCAM may be beneficial for investigating these possibilities as well as determining the role of the dileucineand tyrosine motif in WRAMP formation, using live cell imaging. Furthermore, such an experiment, combined with exploring spreading behaviour on different matrix substrates, orfollowing Wnt5a treatment, may shed more light on the dynamic distribution of MCAM during cell migration in melanoma.

A previous hypothesis explaining why WT MCAM expression may result in reduced motility in melanoma cells in some assays, is that MCAM shifts the focus of cell adhesion from the cell-ECM interactions toward cell-cell interactions (Dye 2007). This hypothesis was formed on the basis of increased network formation in Matrigel network-forming assays, as well as a delayin wound closure and spreading on various matrix substrates (Dye 2007). To explore this hypothesis,network-forming assays and aggregation assays were attempted in this study, to determine whether the Colo239F cell series expressing MCAM exhibited a bias towards cell-cell interactions over cell-ECM. However, the Colo239F cells failed to produce networks on Matrigel at various cell concentrations (data not shown). Furthermore, while aggregation assays were attempted, data produced were unreliable and highly variable, and so were excluded from this report. The growth pattern of Colo239F-WT3.1 cells under normal cell culture, however, suggests that these cells have a preference for cell-cell interactions compared to parental Colo239F cells or cells expressing MT MCAM. That is, they displayed a tendency to grow vertically and adhere to the top of islands of cells, whereas the other cellsappeared more spread, even at high confluency. Further investigation into the preference and mechanism of cell-cell versus cell-ECM interactions is required in the parental and MCAM-expressing Colo239F cells, which may shed more light on the migratory phenotype.

4.3.4 Potential role of MCAM in cell protrusions and cell polarisation

MCAM co-localised strongly with F-actin and moesin in front-directed cellular extensions in the MCAM-transduced Colo239F cells (Fig. 20). Previous studies have reported similar findings where MCAM is expressed at cell protrusions and co-localises with the actin-binding proteins moesin and ezrin (Luo et al. 2012). Interestingly, MCAM is reported to interact directly with phosphorylated moesin, recruit RhoGDI1, induce RhoA activation, and thereby promote melanoma migration (Luo et al. 2012). Additionally, moesin changes localisation within the cell following knockdown of MCAM, and MCAM and moesin fail to co-co-localise when moesin lacks its FERM domain, which also results in decreased cell migration (Luo et al. 2012). MCAM is also

frequently noted to be highly expressed at the leading edge of breast cancer cell lines (Zeng et al. 2012), as well as endothelial progenitor cells (EPCs) where it co-localises with FAK and promotes migration (Kebir et al. 2010). Finally, MCAM is known to produce longer, more numerous microvilli in lymphocytes,potentially via interactions between MCAM and the cytoskeleton (Guezguez et al. 2007).

Cell protrusions constitute an important step in cell adhesion and migration and may represent another mechanism whereby MCAM is involved in the migration of melanoma cells. The co-localisation of MCAM, moesin, and F-actin, and the known interaction betweenMCAM and moesin, suggests that moesin facilitates interaction of MCAM with the cytoskeleton, potentially enabling cytoskeletal remodelling. The mechanism behind this interaction needs to be explored in further depth, as well as exploring other interaction partners of MCAM (including IQGAP1, ezrin, radixin, or hShroom1). Since the cytoplasmic tailof MCAM is so highly conserved between species, it is possible that the role MCAM plays in normal and metastatic function occurs primarily through signalling or interactions with othermolecules via this domain, rather than classical cell adhesion.

Here, MCAM was also found to co-localise with F-actin, moesin, and Cop1β in filament-like structures which extended longitudinally at the apical surface of Colo239F cells (Figs. 24, 25).Most often, these structures appeared in duplicate and ran bilaterally from front to end of the cell either side of the nucleus. These structures resemble actomyosin stress fibres, whichextend between focal adhesions at the front and rear of the cell. Why MCAM is present in these structures remains uncertain. However, the presence of moesin may indicate that it isacting as a linker between MCAM and the cytoskeleton. Furthermore, the surprising presence of Cop1β may indicate that MCAM is being trafficked to or along these filaments, as Cop1β is known to interact directly with the KKGK motif in the cytoplasmic tail of MCAM and is thought to mediate retrograde trafficking of MCAM (Witze et al. 2013).

Generally, cell migration follows four broad steps: protrusions at or extension of the leadingedge of the cell; formation of focal adhesions; translocation of the cell body toward the leading edge; and detachment of adhesions at the trailing edge (Kuo 2013). After the formation offocal adhesions via integrins and other CAMs, cytoskeletal filaments are formed between adhesions at the leading and trailing edge of the cell. These fibres anchor the cell and allow mechanotransduction of force through the cell, driving it forward (Kuo 2013). Interestingly, MCAMhas been implicated in two out of four of these steps – at the leading edge of the cell in protrusions, and along the stress fibres, which promote cell movement by contractile forces.To explore whether MCAM was present in focal adhesions, co-staining was performed between MCAM and vinculin (a marker for focal adhesions and cell-ECM interaction points) (Fig. 26). However, the staining resulted in a widespread punctate pattern, such that individual focal adhesions could not be identified. Previously, MCAM cross-linking has been reported to result in the phosphorylation of paxillin, a protein involved in forming focal adhesions (Anfosso et al. 1998). As paxillin also localises in focal adhesions, exploring paxillin staining in conjunction with vinculin staining may be beneficial. Phorbol Myristate Acetate (PMA)stimulation, which

activates protein kinase C (PCK), was found to increase focal adhesion formation (potentially through activation of focal adhesion kinase) in the SB2 melanoma cellsin our laboratory, and this approach could also be used in the Colo239F cells expressing WT and MT MCAM.

Furthermore, as mentioned above, MCAM co-localises with focal adhesion kinase (FAK) in EPCs (Kebir et al. 2010). However, in Madin-Darby Canine Kidney (MDCK) cells, MCAM was absent in both adherens junctions and focal adhesions (Guezguez et al. 2007). Exploring the role of talin and Filamin A mightbe beneficial, as both of these proteins are known to link cell surface receptors such as integrins to the actin cytoskeleton at focal adhesions (Kuo 2013). Furthermore, they are reported to be part of the WRAMP interactome and may shed light on the formation and mechanismof WRAMP (Witze et al. 2013).

4.3.5 Interaction between MCAM and β1-integrin

Previously, it has been hypothesised that MCAM modulates β1-integrin expression or activity on the surface of melanoma cells. As mentioned previously, HEMCAM (chicken MCAM) has been shown to downregulate β1-integrin (Alais et al. 2001), and in human SB2 cells a similar effect has been hypothesized (Dye 2007). In addition, co-immunofluorescence experiments performed in our laboratory show significant co-localization of MCAM and β1 integrin in SB melanoma cells (unpublished data).

The potential interaction between MCAM and β1-integrin was explored here via flow cytometry, immunofluorescence and Western blotting; however, our experiments focused broadly on the surface expression of the β1 integrin subunit and did not differentiate between isoforms or explore activity levels. Furthermore, the considerable variation in MFI between flow cytometry experiments suggests that β1-integrins undergo rapid trafficking. These fluctuations may be part of the normal regulation of surface β1-integrins in these cell lines. Additionally, the Western blot and flow cytometry data only weakly complement eachother. These experiments need to be repeated to confirm expression levels. Co-immunoprecipitation experiments were performed between MCAM and β1-integrin, and preliminary results indicate a possibility of interaction between these molecules (data not shown). However, these data were not convincing, and the experiment needs to be optimized and repeated. A full investigation into β1-integrin expression and activity was beyond the scope of this study, but our results indicate the possibility of interaction between β1-integrin and MCAM.

4.4 Conclusion

Colo239F cells expressing MCAM displayed significant changes in morphology compared to MCAM-negative cells. WT MCAM expression was associated with cells becoming shorter andsmaller on tissue culture plastic,

while cells expressing MCAM containing sorting motif mutants were significantly longer. The mutant MCAM Colo239F cells were also more mobileand demonstrated increased directional migration compared to MCAM WT-expressing cells in a random migration assay. Furthermore, while proliferation appears to be largely unchanged by MCAM expression, spreading behavior was different between the cells. On laminin I, MCAM-expressing cells spread faster than MCAM-negative cells, especially those expressing Y641A MCAM, which also displayed a significant increase in cell length on this substrate. While differences were not as clear on collagen I or IV, the tyrosine mutant- expressing cells displayed faster spreading (compared with other MCAM-positive cells) and longest cell morphology; indicating that spreading in the Colo239F cell line is modulated by the intracellular tail of MCAM. An alternative explanation is that the increase in β1-integrin expression seen in the Colo239F-YA3.1 cells facilitiates the increased spreading, since β1- integrins are the primary mediator of cell adhesion on these substrates. However, this hypothesis fails to account for the fast spreading seen by Colo239F-Parental cells on collagenwhile appearing to have relatively low β1-integrin expression, according to Western blot results.

Furthermore, MCAM appears to be involved in three seemingly distinct processes of cell migration: the WRAMP structure, cell protrusions, and the actomyosin stress fibres. We hypothesize that in the Colo239F-LA3.1 and Colo239F-YA3.1 cells, the WRAMP structure is more stable or resistant to breakdown, resulting in the increase of directional migration seenin these cells. Interestingly, the presence of moesin and F-actin in all three of these structures suggests that MCAM is interacting with the cytoskeleton through interactions with moesin, which is consistent with previous literature. Finally, the significant co-localisation of MCAM with β1-integrin, including both being present in the WRAMP structure, suggests that these two molecules may be interacting.

CHAPTER V:

Recycling and Sorting of MCAM

5.1 Introduction

As previously described, MCAM is likely to be involved in migration and is present at both theleading edge of cell in cell protrusions (Luo et al. 2012) and in the WRAMP structure at the rear of the cell (Witze et al. 2008). For MCAM to play a role in spreading and migration, we hypothesize that MCAM must be maintained on the cell surface. Furthermore, MCAM may be recycled from the trailing edge to leading edge of the cell during cell movement and directed to the WRAMP structure. Despite its importance in the biology and progression of melanoma metastasis, very little is known about how MCAM is internalised, recycled, or sorted throughout the cell.

The two putative endocytosis motifs of the intracellular tail of MCAM explored in this thesisare thought to be involved in the internalisation and sorting of proteins to endosomal and lysosomal compartments. Previously, the dileucine motif was linked to basolateral targetingof MCAM in endothelial cells (Guezguez et al. 2006). In this study, MCAM was found to co-localise with E- cadherin at the basal membrane. However, following knock-out of the dileucine motif, MCAM-L targeted to the apical membrane, along with MCAM-S (Guezguez et al. 2006). Witze et al. 2013 described a dynamin-dependent process whereby MCAM was internalised following Wnt5a stimulation (Witze et al. 2013). However, as dynamin is involved in both clathrin- and caveolin-mediated endocytosis (Doherty and McMahon 2009), this provided little insight into the process of MCAM internalisation.However, MCAM is reported to be at least partially endocytosed by a clathrin-mediated pathway, as revealed by hypertonic sucrose treatment of melanoma cells (Dye 2007).

The recycling of plasma membrane proteins begins with endocytosis, summarised in Fig. 4 (Chapter 1). Following the endocytosis of membrane receptors, the receptor-containing vesicles are trafficked to early endosomes. Briefly, vesicles containing internalised receptorsfuse with early endosomes, which mature into late endosomes and finally lysosomes, where it is believed the receptor is degraded. However, receptors can be rescued from lysosomal degradation at multiple points in the endosomal system and recycled to the cell surface (Grant and Donaldson 2009). If the cargo is to be recycled, it is subsequently trafficked from early endosomes either: directly back to the cell surface; to recycling endosomes for re-expression; to the Golgi via retrogradetransport; or to the nucleus (Xu et al. 2017). The Rab4-mediated short-loop recycling pathway recycles receptors from early endosomes to the cell surface, while receptors can also be trafficked torecycling endosomes, and subsequently to the cell surface, via the Rab11-mediated long-loop pathway (Grant and Donaldson 2009). Furthermore, receptors can be sorted and recycled from endosomes to the golgi apparatus via retrograde transport.

Studies in our laboratories indicate MCAM co-localises partially with Rab4, Rab5 and Rab11 in melanoma (George 2017). One previous study also found that MCAM is present in Rab5- and Rab7-marked endosomal fractions, suggesting the protein is at least partially sorted through these compartments in macrophages (Luo et al. 2017). Furthermore, MCAM is trafficked via Rab7/RhoB- mediated multi-vesicular bodies (late

endosomes) to the WRAMP structure (Witze et al. 2013). This suggests that MCAM sorting/recycling may be mediated, at least in part, by Rab7. Late endosomes mature into lysosomes wherein the contained molecule is degraded (Rink et al. 2005). Interestingly, transport can also occur between Rab7-marked late endosomes and the trans-Golgi network, suggesting the existence of a rescue pathway (Carroll et al. 2001; Pfeffer 2009). Molecules known to be involved in the bi-directional traffic between the endosomes and Golgi include receptors,lipids, and toxins (Progida and Bakke 2016). MCAM is also reported to co-localise with lysosomes, especially MT MCAM containing Y641G and L623P mutations (George 2017), suggesting that these mutations target MCAM to a degradative pathway.

Rab7 is directly involved with retromer function, acting as an accessory protein for vesicle interactions. Briefly, retromer is described as a "master regulator" of endosomal sorting (Burd and Cullen 2014). It is made up of two protein complexes: the cargo-selective complex (CSC), consisting of VPS26, VPS29, and VPS35, and a second complex consisting of sorting nexins which mediates membrane deformation/cargo binding (Seaman 2012). Three versions of retromer have been identified: SNX-BAR-retromer, consisting of the CSC and a heterodimer of SNX1/2 and SNX5/6; SNX3-retromer; and SNX27-retromer (Burd and Cullen 2014). Retromer is described in more detail in Section 1.5.7 and Figure 5. It has been hypothesised that Rab7 and retromer are involved in late endosome trafficking (Pfeffer 2009). Interestingly, retromer isKol a primary regulator of early endosome to TGN retrograde trafficking (Progida and Bakke 2016), and sorting nexins also individually regulate endosome to TGN sorting, to some extent (Burd and Cullen 2014).

Witze et al. 2013 described the co-localisation of ER marker calnexin with MCAM in the WRAMP structure, suggesting involvement of the ER in WRAMP formation and function (Witze et al. 2013). Furthermore, they described direct interaction between MCAM and Cop1β (a retrograde-transport mediator) suggesting that MCAM was trafficked from the Golgi to the ER. Indeed, following Cop1 knockout, MCAM co-localised strongly with the Golgi body in melanoma cells.Furthermore, the presence of MCAM inside late endosomes (MVBs) reported by this paper provides further supporting evidence and suggests a unique link between MCAM and a retrograde transport sorting pathway (Witze et al. 2013).

Considering the complexity of the endosomal system, it is possible that MCAM undergoes sorting via different pathways. This chapter explores the co-localisation of MCAM with endosomal markers to help determine how MCAM is sorted and recycled in the Colo239F cell line. Previous unpublished data in SB2 melanoma cells expressing Y641G and L623P MT MCAM, as well as protein stability prediction software results (Table 10), suggest that mutantMCAM may be targeted to a degradative pathway. Furthermore, the potential involvement of retromer and sorting nexins was explored via mRNA expression screening, to determine whether these proteins were expressed in melanoma cells and which may warrant further investigation in MCAM recycling and sorting in melanoma.

5.2 Results

5.2.1 LL623-624AA and Y641A do not affect cell surface expression of MCAM in the Colo239F cell lineG

To further investigate the roles of the tyrosine and dileucine motifs in MCAM internalisationand recycling, flow cytometry assays were performed to measure the proportion of MCAM expressed on the cell surface, compared to total MCAM expression, of each cell line. While findings were non-significant, it appears that the Colo239F-WT3.1 cells had slightly less cell surface expression as a percentage of the total than the mutant cells, especially Colo239F- YA3.1 (Fig. 29). Unfortunately, there was significant experiment variation for the Colo239F- WT3.1 and Colo239F-YA3.1 cells, and more replicates are required to investigate these data.The average mean fluorescent intensity (MFI) for total cell and cell surface MCAM for each cell line is displayed in Table 15. Experiment 1 and 2 were performed at separate time points.

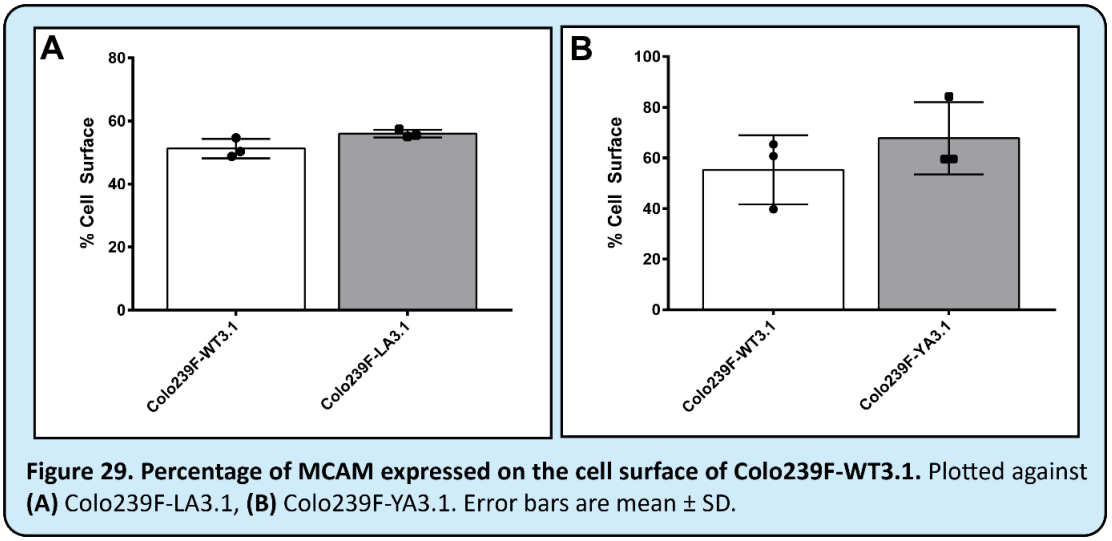

Figure 29. Percentage of MCAM expressed on the cell surface of Colo239F-WT3.1. Plotted against **(A)** Colo239F-LA3.1, **(B)** Colo239F-YA3.1. Error bars are mean ± SD.

Table 15. MCAM expression in Colo239F cells.

Experiment	Cells	Cell Surface (MFI)	Total (MFI)	Mean % cell surface MCAM
1	**Colo239F-WT3.1**	26149 ± 2346	51364 ± 6950	51%
	Colo239F-LA3.1	28378 ± 6459	50845 ± 12199	56%
2	**Colo239F-WT3.1**	22905 ± 8942	40683 ± 11632	56%
	Colo239F-YA3.1	30520 ± 8152	44524 ± 6243	69%

The geometric mean fluorescence intensity (MFI) for MCAM shown for non-permeabilised cells (cell surface) and permeabilised cells (total). Experiment 1 and 2 were performed in triplicate at different time points due to sample number. Data shown as mean ± SD.

5.2.2 MCAM does not co-localise with the Golgi body or lysosomes

To explore the localisation of MCAM within the cell, co-staining experiments were performed. Interestingly, no or limited co-localisation was apparent between MCAM and theGolgi, as visualised using an antibody against Golgin97 (Fig. 30A). As the mutations introduced into the MCAM-LA and MCAM-YA sequences were predicted to be destabilising by *in silico* analyses (Table 9, Section 3.3.5), it was hypothesised that the mutant MCAM protein may be targeted to the lysosomes. However, co-staining experiments between MCAM and Lamp-2 (a lysosomal marker) also produced no evidence of co-localisation (Fig. 30B).

5.2.3 Partial co-localisation between MCAM and endosomes

To further explore the localisation of MCAM within Colo239F cells, and to explore whether MCAM might be recycled throughout the cell via the endosomal sorting system, co-staining experiments were also performed between MCAM, Rab4 (early endosomes), Rab7 (late endosomes), Rab11 (recycling endosomes), and VPS35. MCAM displayed no co-localisation with VPS35, although apparent nuclear localisation of VPS35 is unexpected and may indicatefurther optimisation of this antibody is required (Fig. 31B). There was limited co-localisationwith Rab4 and Rab11 in a minority of cells (Fig. 30A, white arrow; Fig 30B). Interestingly, MCAM showed significant levels of co-localisation with Rab7, a marker for late endosomes (Fig. 32). This effect appears to be more pronounced in the Colo239F-WT3.1 cells comparedto the cells expressing MT MCAM, Colo239F-LA3.1 and Colo239F-YA3.1 (Fig. 32A).

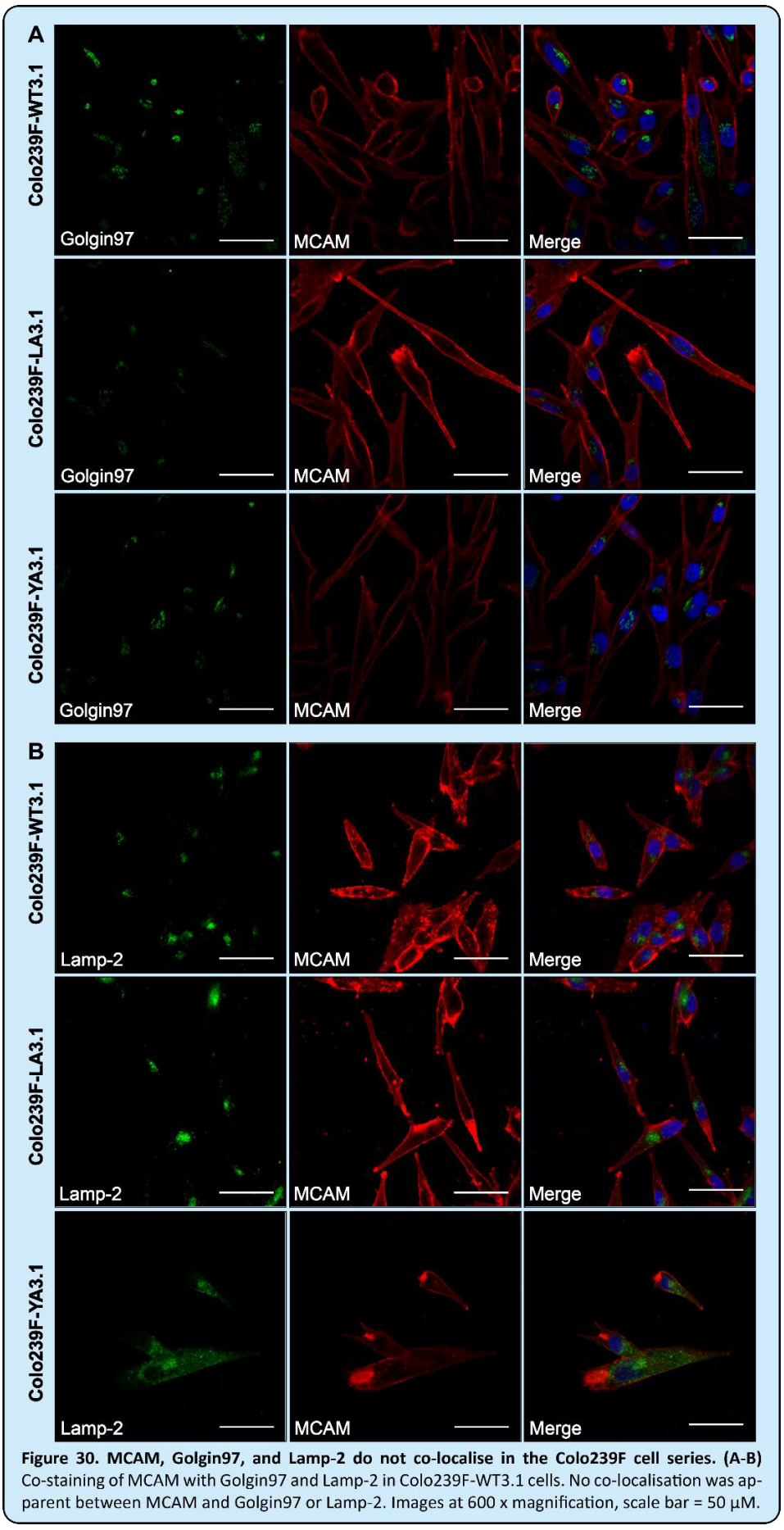

Figure 30. MCAM, Golgin97, and Lamp-2 do not co-localise in the Colo239F cell series. (A-B) Co-staining of MCAM with Golgin97 and Lamp-2 in Colo239F-WT3.1 cells. No co-localisation was apparent between MCAM and Golgin97 or Lamp-2. Images at 600 x magnification, scale bar = 50 µM.

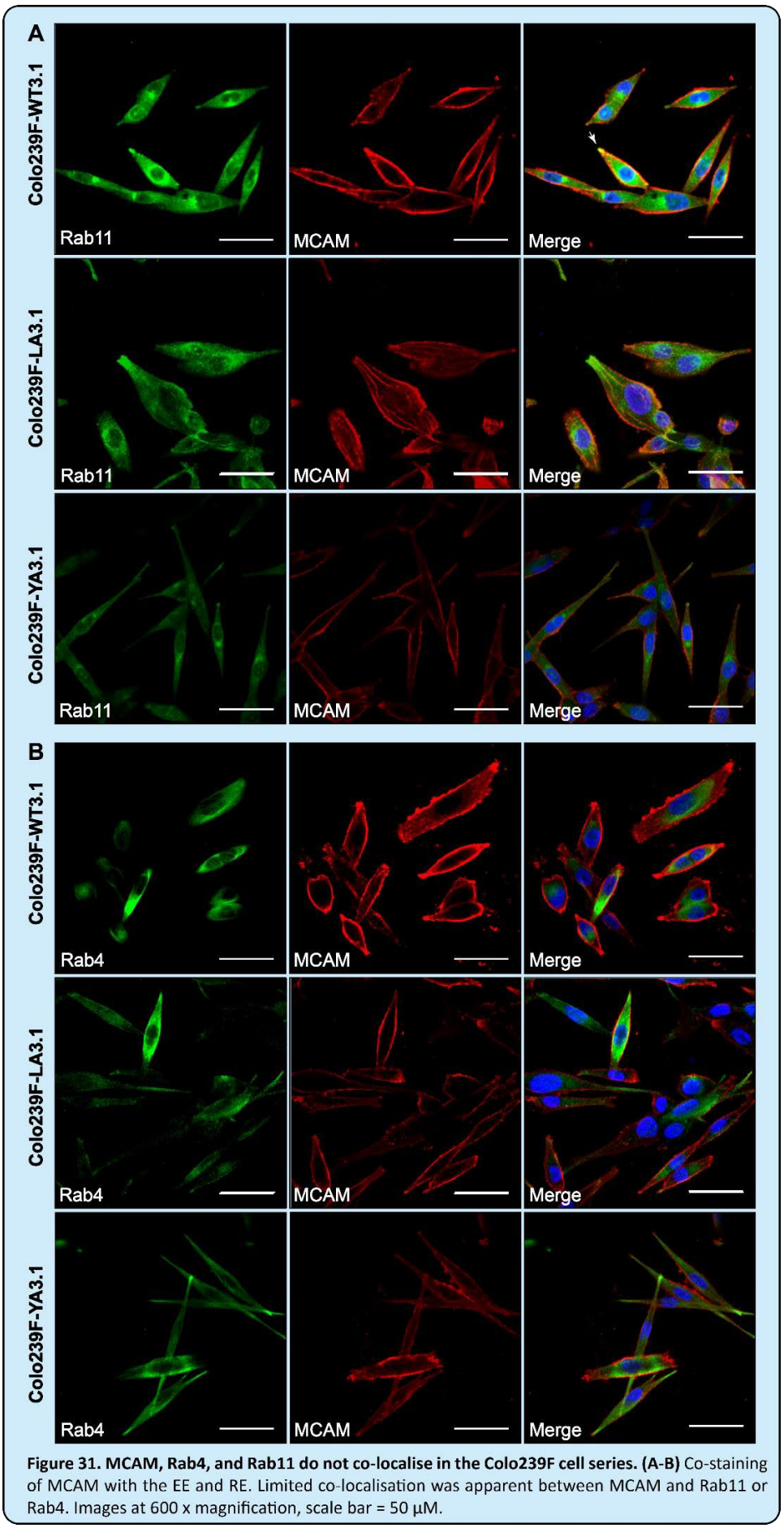

Figure 31. MCAM, Rab4, and Rab11 do not co-localise in the Colo239F cell series. (A-B) Co-staining of MCAM with the EE and RE. Limited co-localisation was apparent between MCAM and Rab11 or Rab4. Images at 600 x magnification, scale bar = 50 µM.

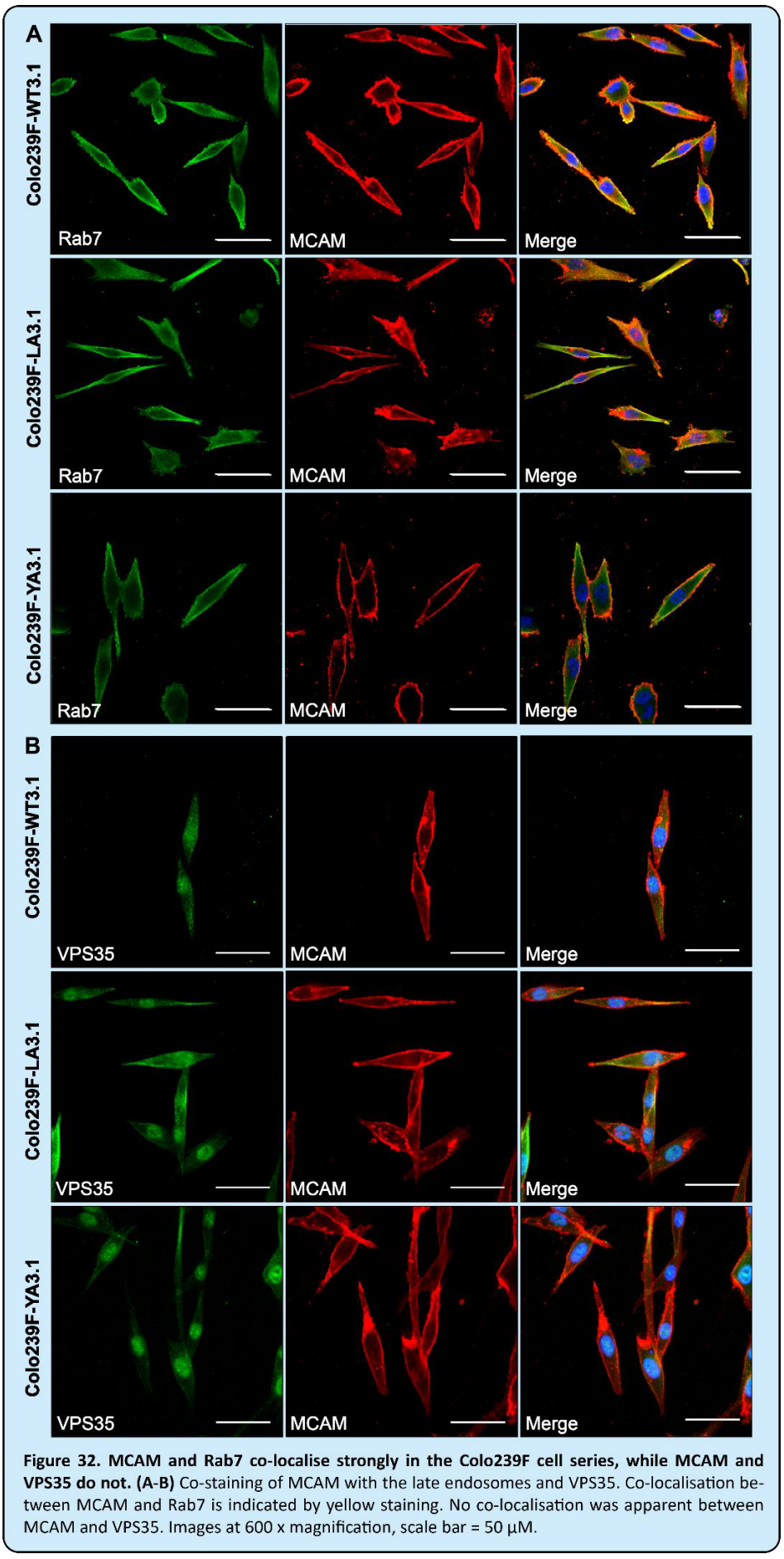

Figure 32. MCAM and Rab7 co-localise strongly in the Colo239F cell series, while MCAM and VPS35 do not. (A-B) Co-staining of MCAM with the late endosomes and VPS35. Co-localisation between MCAM and Rab7 is indicated by yellow staining. No co-localisation was apparent between MCAM and VPS35. Images at 600 x magnification, scale bar = 50 µM.

5.2.4 Sorting nexin and retromer gene expression in melanoma cell lines

Sorting nexin and retromer gene expression was explored for 14 SNX and retromer-associated genes in a range of melanoma cell lines. Genes analysed were *SNX1-6*, *SNX17*, *SNX27*, *SNX31*, *VPS26A*, *VPS26B*, *VPS29*, *VPS35*, and *RAB7A*; and control genes were succinate dehydrogenase complex subunit A (*SDHA*), TATA-binding protein (*TBP*) and glyceraldehyde 3-phosphate dehydrogenase (*GAPDH*). Data analyses and normalisation is described in Section 2.17 and efficiency data shown in Appendix 2. All genes except *SNX31* were found to be expressed in every melanoma cell line analysed (Figs. 33, 34). The SB2 cell line (derived from a primary melanoma and MCAM negative) was the least metastatic cell line analysed, and in the absence of melanocytes, was chosen as a control against which fold changes were calculated. The metastatic melanoma cell lines analysed were MM253, MM96L, SKMEL28, A2058, and Colo239F, all of which are MCAM positive except Colo239F. Five biological replicates were analysed for each cell line per gene. Table 11 and Figures 28 and 29 displays the average fold change and confidence intervals for each gene for each cell population.

The mean fold changes for *SNX1-6* generally indicated a trend for upregulation for every melanoma cell line, although in most cases this was not statistically significant. The MM96L and A2058 cell lines displayed a high level of variance in *SNX1*, making it difficult to draw anyconclusions (Fig. 33A-F). *SNX2* and *SNX6* expression was significantly upregulated in the Colo239F cell line (Fig. 34B, F) ($p \leq 0.05$). Some cell lines displayed marginal mean upregulation due to what may be an outlier, as four out of five replicates indicated gene downregulation, such as the A2058 cell line for *SNX3* (Fig. 33C). Hence, both a dot plot and table of averages were included to provide a better overview of the data. Interestingly, *SNX17*and *SNX27* expression was largely downregulated, except for the MM253 cell line (for SNX27), and the Colo239F cell line (for both *SNX17* and *SNX27*) (Fig. 33G, H). The A2058 cell line displayed a high level of variation between replicates for many of the genes analysed, suggesting that these data could benefit from repeat experiments with new replicates.

Once again, the retromer-associated proteins analysed generally indicated a trend towards increased expression in metastatic melanoma cell lines compared to the SB2 cell line. For *VPS26A*, all cell lines except A2058 showed increased expression (Fig. 33A), while for *VPS26B* all cell lines showed increased expression except for SKMEL28. (Fig. 34B). A similar trend was seen in *VPS29*, with only SKMEL28 showing downregulated expression (Fig. 34C). *VPS35* showed more variation between cell lines, with SKMEL28 and A2058 being slightly downregulated while the other cell lines were slightly upregulated (Fig. 34D). *Rab7a* was most interesting. While these genes were upregulated in all cell lines compared to against the SB2 cell line, only the MM253 and MM96L cell lines displayed statistically significant upregulation ($p \leq 0.01$, $p \leq 0.05$ respectively) (Fig. 34E).

Table 16. Fold changes for sorting nexin and retromer-associated genes expressed by melanoma cell lines.

Gene	SKMEL28	MM253	MM96L	A2058	Colo239F
SNX1	1.08 (0.30, 1.86)	5.26 (-3.53, 14.06)	1.70 (-2.07, 5.45)	1.04 (-1.39, 3.47)	3.26 (-0.32, 6.85)
SNX2	8.80 (0.21, 17.40)	10.84 (-7.34, 29.06)	20.23 (-15.69, 56.15)	4.87 (-2.44, 12.19)	27.54 (-3.23, 58.30)
SNX3	0.82 (-0.14, 1.78)	4.97 (1.58, 8.35)	1.81 (-0.16, 3.79)	1.17 (-0.89, 3.23)	2.78 (0.34, 5.23)
SNX4	1.76 (-0.46, 3.97)	5.16 (-0.37,10.68)	3.64 (-1.15, 8.43)	2.89 (-1.27, 7.05)	3.70 (0.32, 7.07)
SNX5	2.89 (1.57, 4.19)	8.82 (-4.18, 21.83)	3.80 (-3.62, 11.20)	1.09 (-0.25, 2.43)	7.77 (-2.31, 17.86)
SNX6	0.96 (0.58, 1.35)	2.48 (-0.11, 5.08)	2.86 (-1.79, 7.50)	1.83 (-0.86, 4.51)	19.32 (4.67, 33.96)
SNX17	0.38 (0.02, 0.75)	3.25 (-2.49, 8.98)	0.35 (-0.05, 0.75)	0.17 (-0.21, 0.55)	2.97 (1.09, 4.85)
SNX27	0.21 (0.12, 0.31)	0.81 (0.17, 1.44)	0.75 (0.08, 1.41)	0.31 (-0.09, 0.72)	1.39 (0.46, 2.32)
VPS26A	1.79 (-0.92, 4.50)	6.14 (-1.79, 14.08)	3.77 (-1.54, 9.09)	0.88 (-0.05, 1.80)	3.60 (-0.87, 8.07)
VPS26B	0.91 (0.07, 1.74)	4.44 (-2.23, 11.14)	2.41 (-0.59, 5.42)	1.53 (-1.60, 4.65)	4.93 (-1.07, 10.93)
VPS29	0.73 (-0.20, 1.67)	3.06 (-1.9, 8.01)	1.80 (-0.03, 6.63)	0.97 (-0.97, 2.90)	3.93 (0.67, 7.19)
VPS35	0.51 (-0.17, 1.19)	1.09 (0.29, 1.89)	1.50 (-0.01, 3.01)	0.67 (-0.51, 1.85)	2.14 (0.14, 4.14)
RAB7A	3.47 (-0.04, 6.99)	20.29 (-8.12, 48.71)	9.00 (-3.50, 21.50)	2.17 (0.19, 4.15)	6.58 (-0.69, 13.85)

Data analysed against the SB2 cell line and presented as mean (lower 95% confidence interval limit, upper 95% confidence interval limit).

Figure 31 presents these data as averages of biological replicates for each cell line plotted foreach gene. Viewed like this, it is apparent that all genes analysed appear to be slightly upregulated on average in metastatic melanoma (compared to the primary melanoma, SB2)except for *SNX17* and *SNX27*, which are downregulated (Fig. 35A, B). Furthermore, *SNX2* and *RAB7A* appear to be upregulated to the highest extent (Fig. 35). However, variation there was considerable variation between biological replicates for some cell lines and therefore, these data should be interpreted with caution.

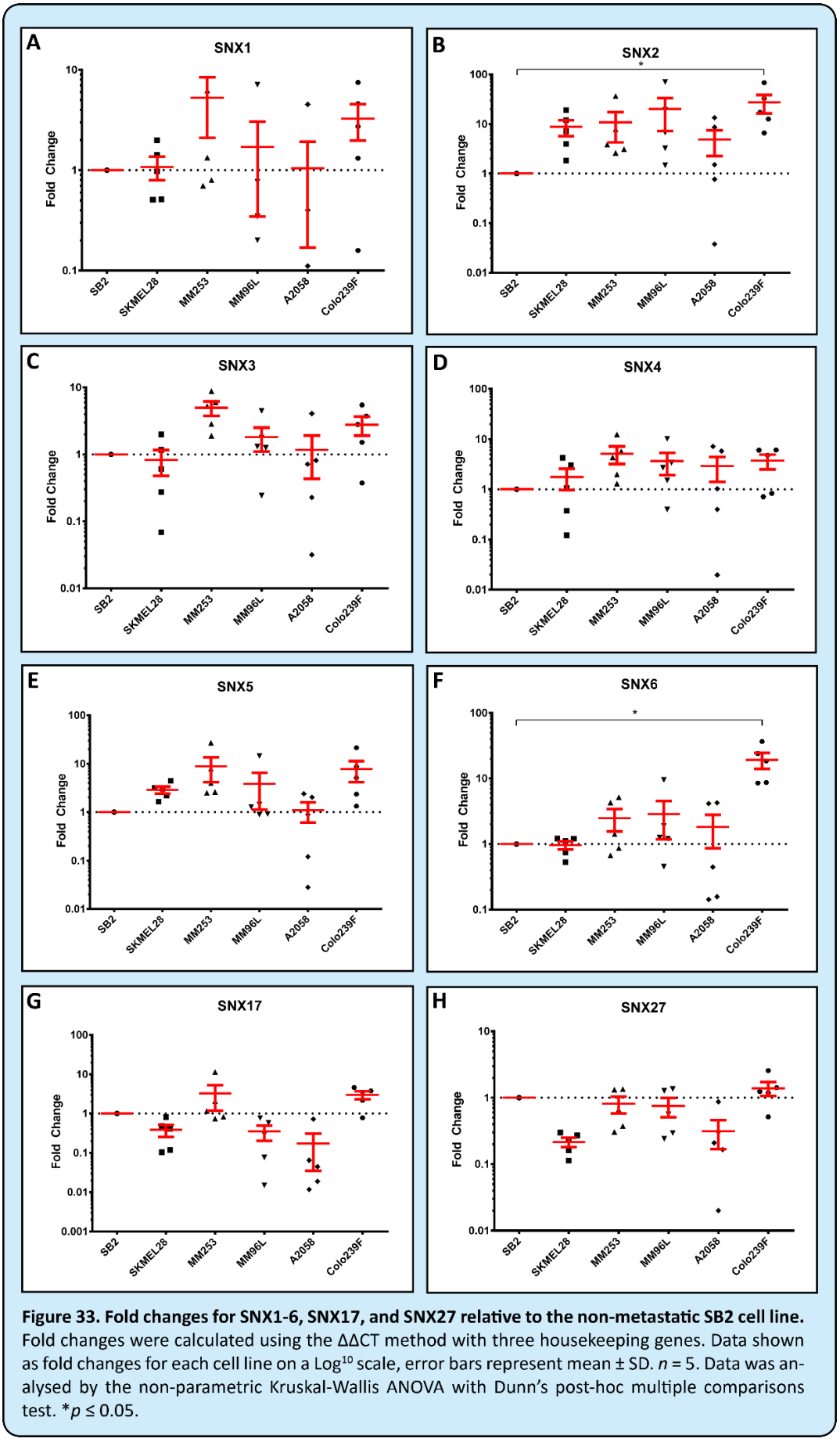

Figure 33. Fold changes for SNX1-6, SNX17, and SNX27 relative to the non-metastatic SB2 cell line. Fold changes were calculated using the ΔΔCT method with three housekeeping genes. Data shown as fold changes for each cell line on a Log^{10} scale, error bars represent mean ± SD. $n = 5$. Data was analysed by the non-parametric Kruskal-Wallis ANOVA with Dunn's post-hoc multiple comparisons test. *$p \leq 0.05$.

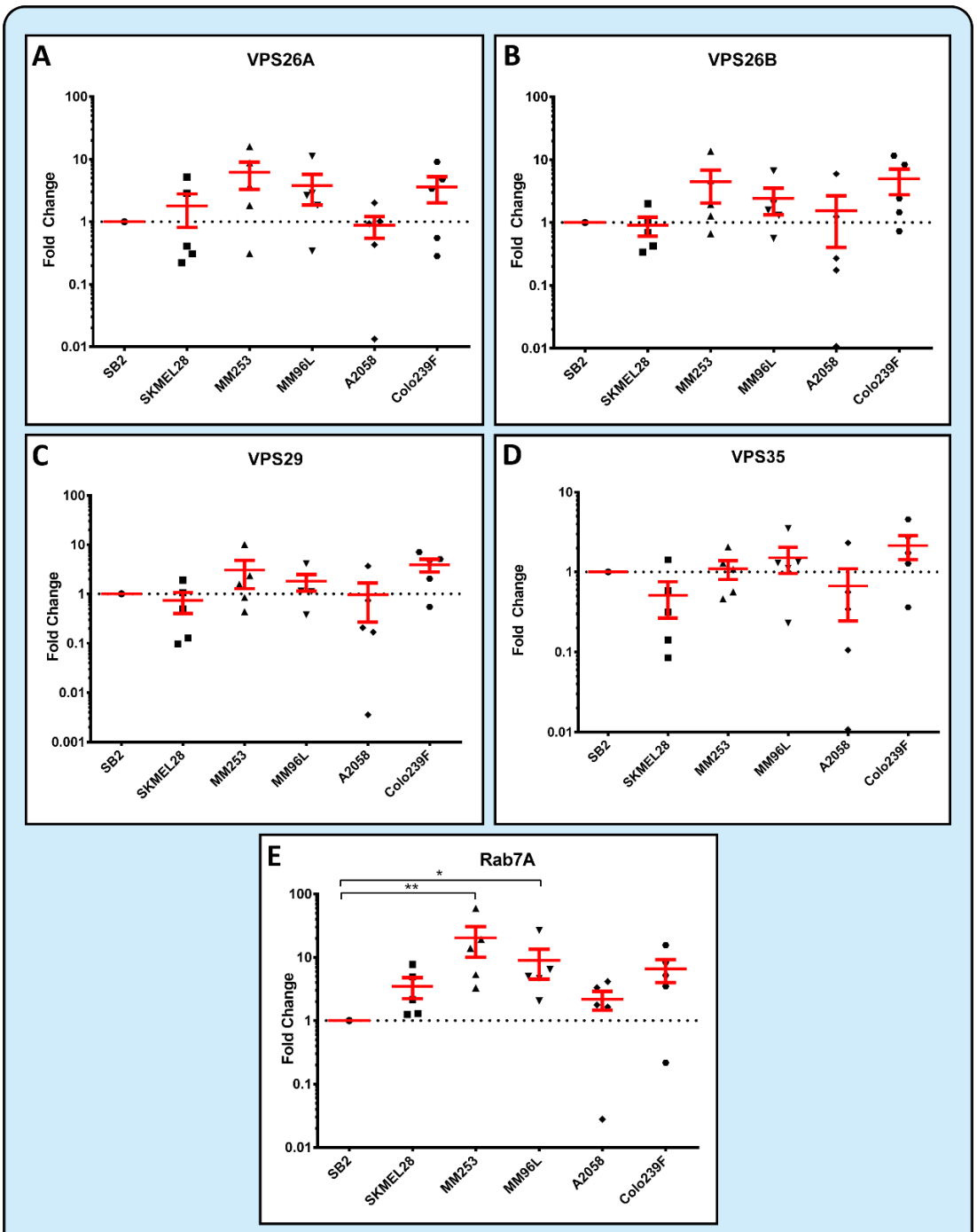

Figure 34. Fold changes for VPS26A/B, VPS29, VPS35, and RAB7A relative to the non-metastatic SB2 cell line. Fold changes were calculated using the ΔΔCT method with three housekeeping genes. Data shown as fold changes for each cell line on a Log^{10} scale, error bars represent mean ± SD. *n* = 5. Data was analysed by the non-parametric Kruskal-Wallis ANOVA with Dunn's post-hoc multiple comparisons test. *$p \leq 0.05$, **$p \leq 0.01$.

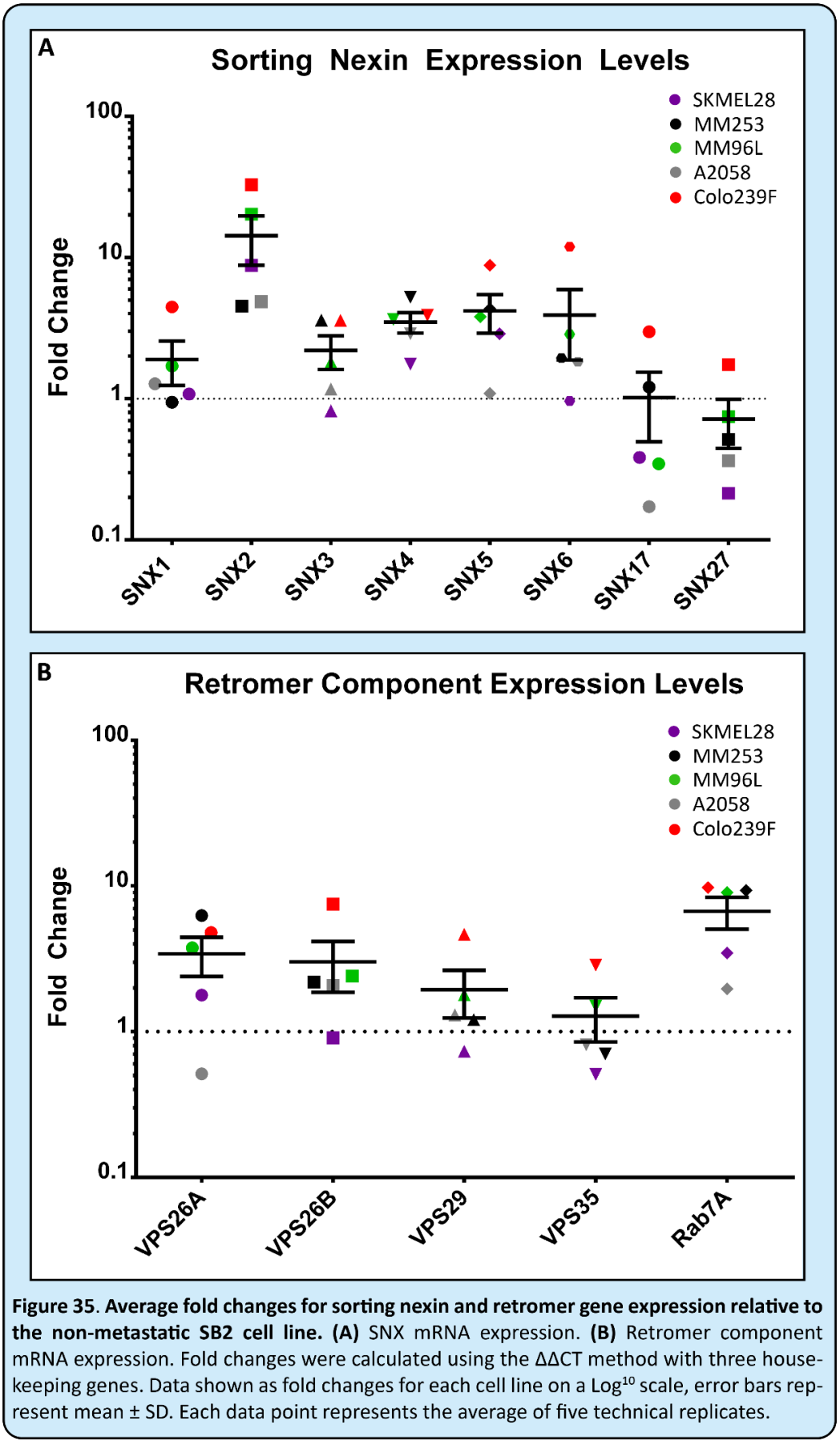

Figure 35. Average fold changes for sorting nexin and retromer gene expression relative to the non-metastatic SB2 cell line. (A) SNX mRNA expression. **(B)** Retromer component mRNA expression. Fold changes were calculated using the ΔΔCT method with three housekeeping genes. Data shown as fold changes for each cell line on a Log^{10} scale, error bars represent mean ± SD. Each data point represents the average of five technical replicates.

5.2.5 Rab7a and VPS35 protein expression in melanoma cell lines

Western blots were performed to compare protein expression of VPS35 and Rab7a with gene expression, in the melanoma cell lines which were explored via qPCR. Interestingly, there was some differences observed between protein and gene expression. The MM253, MM96L, and Colo239F cell lines appeared not to have detectable levels of VPS35 protein, although MM96L and Colo239F cells had slightly elevated expression of *VPS35* compared to SB2 at the mRNA level. Further, the Colo239F cell line appeared to have undetectable Rab7a in the lysate despite having strong gene expression. However, this experiment was only performed once due to time restraints and therefore may represent experimental error. Only a subset of the molecules analysed by qPCR were explored via Western blot, due to time and budget constraints.

The immunoblot was performed using equal amounts of lysate (assessed by BCA, 20 µg of each lysate was loaded)

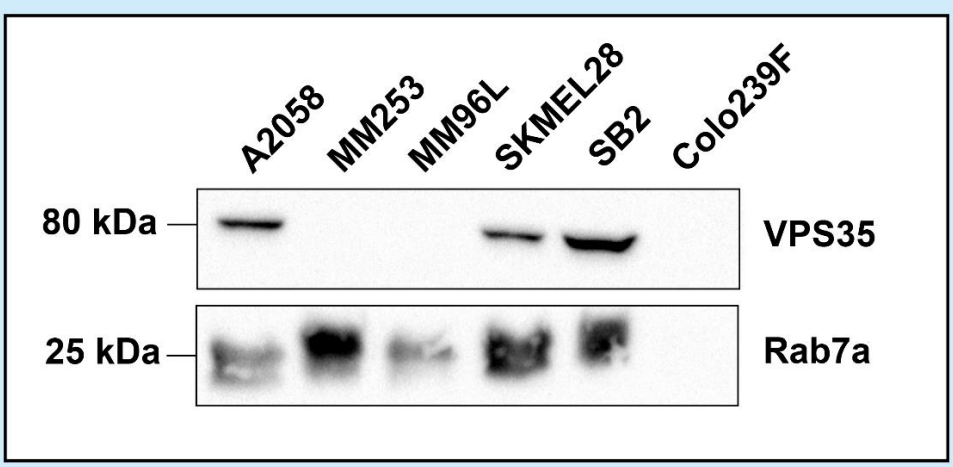

Figure 36. Western blot showing Rab7a and VPS35 protein expression in six melanoma cell lines.

5.3 Discussion

5.3.1 MCAM recycling and sub-cellular localisation

Previous studies in our laboratory using the SB2 cell series indicated that the ratio of cell surface:total MCAM differed in cells expressing WT vs MT MCAM, with cells expressing MCAM containing a mutation in the di-leucine motif showing intracellular accumulation, potentially localising within the TGN or lysosomes (Dye 2007). Thus, we explored this in the Colo239F cell series.

Interestingly, the ratio of cell surface: total expression of MCAM was similar in all the Colo239F-MCAM positive cells, regardless of whether they expressed WT MCAM or MCAM containing the Y641A or LL623-624AA mutation. Colo239F-YA3.1 displayed a slightly higher level of surface MCAM (as well as surface: total ratio) compared to the other cell lines, but this was not statistically significant. This suggests that WT and MT MCAM were internalised and recycled throughout the cell in a similar manner in the Colo239F cells, and that neither of the two putative endocytosis motifs investigated are required for MCAM expression to be maintained on the cell surface (Fig. 29, Table 15).

Flow cytometry antibody-feeding based recycling assays (Arancibia-Carcamo et al. 2006) were then attempted, to determine whether there was any alteration in the rate of MCAM recycling between cells expressing WT or MT MCAM. These assays involved staining the outside of cells with an anti-MCAM antibody on ice and then placing cells at 37^{o}C for variable lengths of time to allow internalisation. Cells were then removed from the incubator and stained with secondary antibody to detect antibody remaining on the cell surface. However, these assays were highly variable, and the data were unreliable. Another cell surface labelling method that could be used to explore MCAM internalisation and recycling is cell-surface biotinylation using a cleavable biotin label (Arancibia-Carcamo et al. 2006). In addition, more information about the recycling pathway of MCAM could be gained by using chemical inhibitors such as primaquine, which inhibits recycling of endocytosed proteins to the plasma membrane (van Weert et al. 2000); or by the transfection of dominant negative proteins. For example, overexpression of Dynamin 1 K44A mutant constructs inhibits clathrin mediated endocytosis; and either wild type or dominant negative Rab proteins could be over-expressed to identify the role of specific endosomal compartments in MCAM recycling (Arancibia-Carcamo et al. 2006).

To further explore potential recycling pathways of MCAM, its cellular localisation was explored by co-immunofluorescent staining of MCAM with markers of early, recycling and late endosomes, the lysosome, the TGN and the ER.

Rab proteins are part of the superfamily of Ras-like GTPases and are known to regulate almost all parts of the cellular sorting machinery, including cargo recruitment, coat assembly,vesicle budding, motor machinery recruitment, vesicle transport along cytoskeletal filaments, vesicle tethering, and vesicle fusion with target

membranes (Guerra and Bucci 2016; Progida and Bakke 2016). Rabsfunction by cycling between an inactive, GDP-bound state, and an active, GTP-bound state (Progida and Bakke 2016). As described above, Rab proteins enter the endosomal pathway at different points, meaning each Rab generally localises to particular endosomal compartments. Rab4 and Rab5 are markers for the early endosome and regulate endocytosis and early endosome formation (Naslavsky and Caplan 2018; Progida and Bakke 2016). Rab7a is a marker of late endosomes and regulates the maturation of early to late endosomes, and then to lysosomes (Guerra and Bucci 2016). Rab9 also co-localises with late endosomes and lysosomes, helps maintain their proper morphology and may, withRab7b, contribute to retrograde transport from late endosomes to the TGN (Progida and Bakke 2016). Rab11 is a marker for recycling endosomes, as well as partially being present in the TGN and vesicles that leave the Golgi (Welz et al. 2014).

Here, we found that MCAM does not significantly co-localise with the early or recycling endosomes (identified by Rab 5 and Rab 4 staining, respectively), suggesting that the amountof MCAM passing through these vesicles may be low, or transient. Rab4 mediates a fast recycling pathway through which cell surface molecules are rapidly recycled to the cell surface from early endosomes (Grant and Donaldson 2009). The limited co-localisation of MCAM with Rab4 suggests that under our experimental conditions, Rab4 only partially regulates MCAM recycling, or MCAM is only transiently present in early endosomes in small amounts. Rab11 marks recycling endosomes and mediates the long-loop recycling pathway by which receptors are taken back to the cell surface (Grant and Donaldson 2009). Likewise, the limited co-localisation seen here between MCAM and Rab11 suggests that either MCAM is present in recycling endosomes only in small amounts, or that MCAM is only partially recycled via the long-loop pathway.

Interestingly, MCAM in the Colo239F cells strongly co-localises with late endosomes (Rab7), suggesting that intracellular MCAM resides in this compartment. As described, there is a known retrograde recycling pathway for some receptors from the late endosomes to the Golgi body (Progida and Bakke 2016). Furthermore, Witze et al. 2013 described a mechanism by which MCAM istrafficked through late endosomes to the WRAMP structure (Witze et al. 2013). Thus, we explored co- localisation of MCAM with the TGN using the Golgin97 antibody (Huotari and Helenius 2011). Considering the co- localisation of MCAM with Rab7 but not with Lamp-2 (lysosomes), it is interesting that there is also no co-localisation with the TGN. It could be hypothesized that if MCAM is rescued from a lysosomal degradation pathway, then it is being sorted into a retrograde transport pathway to the TGN. However, the lack of co-localisation with the Golgi/TGN suggests this hypothesis is incorrect. Alternatively, MCAM may be targeted to the TGN and rapidly sorted into a recycling pathway, such that immunofluorescent staining at a single time point is not sufficient to observe co-localisation between MCAM and these compartments. Performing co-immunofluorescent staining with MCAM and Rab7b antibodies may help ameliorate this gap in knowledge, as Rab7b localises to and mediates retrograde trafficking between the late endosomes and TGN (Guerra and Bucci 2016).

Witze et al. 2013 also described a mechanism by which Cop1β mediated retrograde transportof MCAM from the Golgi to the ER (Witze et al. 2013). Cop1β generally recognises its cargo via an intracellular di-lysine motif (KKxx), such as the KKGK motif present in the intracellular domain of MCAM (Arakel and Schwappach 2018). This may explain the lack of co-localisation seen for MCAM and the Golgi. MCAM may be rescued from late endosomes and traffic quickly through the Golgi to the ER. However, in our experiments, MCAM also displayed no co-localisation with Calnexin, a marker of the ER.

These data partially conflicts with previous work done by our group in MCAM-transfected human SB2 melanoma cells, where MCAM was found to frequently co-localise with Rab5, Rab11, and Lamp-1 (George 2017). In the SB2 cell series, cells expressing di-leucine MT MCAM showed significant co-localisation with a marker of the TGN. This suggests that there may be cell line specific differences in the way MCAM is recycled through the cell. In addition, the di-leucine mutant expressed in the SB2 cells is a leucine to proline mutation, whereas the mutation used in this study was leucine to alanine, which is a more neutral mutation. Given the data generated in the Colo239F cells, the co-localisation of MCAM with Rab7 in the SB2 cell series is an area that requires investigation.

Future experiments could also involve exploring MCAM recycling in cell lines that naturally express MCAM. This was not performed in this thesis, as the primary focus was the comparison of WT vs MT MCAM; due to the previous data generated in the laboratory in the SB2 cells series. In addition, melanoma cells could be transiently transfected with constructs to fluorescently label MCAM and components of the recycling machinery, which would allow real time imaging of MCAM intracellular trafficking.

Other molecules of interest in recycling are the adaptor proteins, which are involved in bidirectional transport between the endosomes and the TGN (Progida and Bakke 2016). For instance, AP-1 and AP-4 mediate TGN-to-endosome transport, AP-2 is primarily involved in clathrin-mediated endocytosis and AP-3 regulates trafficking to lysosomal compartments (Progida and Bakke 2016). AP-5 is more recently described and appears to mediate endosomal/lysosomal homeostasis (Progida and Bakke 2016). Therefore, it may be beneficial to study any potential role for adaptor proteins in the cellular sorting of MCAM. Some preliminary work in our laboratory has found limited co-localisationof MCAM with AP-2 in SB2 MCAM positive cells; but this requires confirmation.

Stress fibres have been previously described to be important for receptor recycling, such as in the case of C-C chemokine receptor type 5 (CCR5). CCR5 internalisation and recycling was found to be regulated by the Rho-dependant activation of Rab GTPases and actin polymerisation into stress fibres (Mueller and Strange 2004). We found that MCAM co-localised with F-actin, moesin, and Cop1β in parallel bilateral structures resembling stress fibres (Figs. 24, 25, Chapter IV). This is also reminiscent of the sorting pathway described by Witze et al. 2013 whereby MCAM is trafficked via Rab4/RhoA-mediated late endosomes as well as Cop1β-

mediated retrograde transport (Witze et al. 2013). This indicates that MCAM may be sorted along cytoskeletal filaments, however, this hypothesis requires further study.

5.3.2 Retromer, sorting nexins, and associated proteins in melanoma

The co-localisation of MCAM and Rab7 suggests a potential role for retromer/SNXs in sortingMCAM through the endosomal system. Considering the sparsity of literature surrounding retromer and SNXs in melanoma, initial investigation was via a broad approach, exploring mRNA expression in melanoma.

For analysis, six cell lines were chosen: four native MCAM-expressing metastatic melanoma cell lines (MM253, MM96L, SKMEL28, and A2058), and two MCAM-negative cell lines (SB2 and Colo239F). Fourteen SNX and retromer genes were chosen for analysis, based on their central role in retromer function: *SNX1-6*, *SNX17*, *SNX27*, *SNX31*, *VPS26A*, *VPS26B*, *VPS29*,*VPS35*, and *RAB7A*. Interestingly, *SNX31* has been described as an oncogene in melanoma, driving metastasis (Hodis et al. 2012). Unfortunately, however, *SNX31* expression has previously been foundto be lost in cell culture of melanoma (Tseng et al. 2014). Indeed, we found no mRNA expression of two isoforms of *SNX31* in our melanoma cell lines (data not shown). Fold change analysis was performed relative to gene expression in the SB2 primary melanoma cell line, as normal melanocytes were not available.

As mentioned above, retromer and the sorting nexins are important in endosome-to-TGN and endosome-to-plasma-membrane transport (Burd and Cullen 2014). Interestingly, almost all genes analysed were upregulated in the more metastatic melanoma cell lines, with *SNX2* and *RAB7A* showingthe clearest pattern of upregulation. Only *SNX17* and *SNX27* were downregulated in metastatic melanoma cell lines (Fig. 35). There were also cell line specific trends in expression levels. For instance, the SKMEL28 cell line consistently displayed expression levels at or near the lowest of the cell lines, while the Colo239F cell line consistently displayed the highest expression levels (Fig. 35). Since the expression of SNX genes in melanoma cell lines has not previously been investigated, the significance of these findings is unknown. However, the increased expression of retromer and associated molecules in metastatic melanoma is consistent with the crucial role of the retromer in intracellular trafficking and with recent publications exploring sorting nexins in other malignancies. For example, recent data implicates changes in SNX1 expression in gastric cancer (Zhan et al. 2018), SNX10 in colorectal cancer (Zhang et al. 2020) and SNX27 in breast cancer (Sharma et al. 2020; Zhang, Li, et al. 2019). As previously mentioned, SNX17 and SNX31 have received the most attention in melanoma, and are believed to regulate β1 integrin surface expression through binding to the NPxY motif in the β1 integrin cytoplasmic domain (Tseng et al. 2014).

The increased expression of *SNX2* and *RAB7A* may represent the upregulation of important pathways in malignant melanoma. SNX2 forms part of the SNX-BAR heterodimer,which mediates membrane deformation in retromer binding (Burd and Cullen 2014), although this function of SNX2 is thought to be redundant and interchangeable with SNX1 (Schwarz et al. 2002).

Most interesting is perhaps the significant upregulation of *RAB7A* in the malignant melanoma cells we screened. Rab7a has been identified as a key driver in melanoma metastasis as part of an "endo-lysosomal" gene cluster. However, Rab7a expression is not constant throughout melanoma progression – with higher levels during early melanoma progression associated with a proliferative phenotype, and lower levels associated with invasion (Alonso-Curbelo et al. 2014). As most of the cell lines in our analysis are metastatic this is very interesting, as it might be expected that Rab7 mRNA levels would decrease in these cells, relative to a non-invasive melanoma (e.g.SB2 cells). The addition of a melanocyte cell line to this panel may help reconcile some of the differences observed here.

The significant co-localisation of MCAM with Rab7 in MCAM-transduced Colo239F cells (Fig 32A), may represent an upregulation of lysosomal rescue pathways in metastatic melanoma, including the rescue of MCAM from late endosomes. Interestingly, the Rab7a western blot performed on the melanoma cell lines analysed by qPCR, suggests that the Colo239F cell line expressed no Rab7 protein (Fig. 36) - however, it was successfully detected by both immunofluorescence and qPCR. Whilst there may be differences in mRNA and protein levels,it is difficult to reconcile the differences between immunofluorescence and western blot data. Due to time restraints, only one replicate of this experiment was performed and so the lack of Rab7 in the immunoblot for the Colo239F cell line may represent experimental error. The immunoblot will be repeated using fresh cell lysates and an appropriate loading control, such as Revert total protein stain.

We also investigated potential co-localization between VPS35 and MCAM. Although VPS35 did not show any upregulation at the mRNA level, as a core component of retromer we were interested to explore its intracellular localisation and any potential co-localisation with MCAM. We found no evidence of co-localisation between VPS35 and MCAM. However, we did see a significant amount of nuclear localisation of VPS35, which is inconsistent with its known location and role in the cell. This suggests this antibody requires further optimisationbefore drawing further conclusions.

The other genes showing notable differences in expression between control and metastatic melanoma were *SNX17* and *SXN27*, which were both downregulated. SNX17 recycles plasma membrane receptors to the cell surface, including β1-integrin. SNX17 has been shown to interact with β1-integrin via interactions between its FERM domain and the tyrosine motif in the intracellular tail of β1-integrin (Rabouille 2017; Steinberg et al. 2012). β1-integrin contains an NxxY-conforming tyrosine motif while MCAM contains a YIDL tyrosine motif, indicating that SNX17/SNX27 may not interact directly with MCAM. SNX17 was downregulated in three out of five melanoma cell lines analysed, however, it was slightly upregulated in the Colo239F-Parental cell line, in comparison to the SB2 cell line (Fig. 34).

Interestingly, β1-integrin cell surface expression was highly variable in the Colo239F cell lines generated in this study, but also showed significant co-localisation with MCAM (Fig. 20, 28), although we were unable to determine a direct interaction between these two molecules via co-immunoprecipitation. Furthermore, as

discussed in Chapter IV, it has been hypothesised that MCAM is associated with downregulation/ inactivation of cell surface β1-integrin in both human and avian models (Alais et al. 2001; Dye 2007). β1-integrin mRNA expression levels in the MCAM-expressing Colo239F cell lines was not explored but may provide additional insight into correlation between MCAM and β1-integrin expression. However, total protein content, as measured by flow cytometry, indicated no significant differences in β1-integrin expression among the Colo239 cell series. Indeed, only Colo239F-YA3.1 displayed a slight increase in β1-integrin expression. Interestingly, by Western blot, the Colo239F-YA3.1 cell line appeared to have a greater level of total β1-integrin (Fig. 28).

5.4 Conclusion

Colo239F cell lines expressing either WT or MT MCAM showed similar proportions of cell surface MCAM expression compared to total cell expression. Indeed, the proportion of cell surface expression may be slightly higher in cells expressing MT MCAM (particularly the tyrosine Y641A mutation). This differs to that seen in the SB2 cells, where cells expressing MT MCAM showed a smaller proportion of cell surface (relative to total) expression. This suggests that neither the dileucine nor tyrosine motifs significantly affect MCAM endocytosis and recycling in the Colo239F cells.

Further exploration of recycling pathways in the Colo239F cells expressing either WT or MT MCAM displayed no co-localisation of MCAM with the Golgi body, ER, or lysosomes,and only limited co-localisation with Rab4 and Rab11. However, MCAM co-localised strongly with Rab7, especially in Colo239F-WT3.1 cells. Together these data suggest that MCAM is localised to late endosomes within the Colo239F cell line, and only to a limited degree in early and recycling endosomes. It is possible that MCAM contained in late endosomes avoids a degradative pathway, and is instead trafficked through the cell to the WRAMP structure. However, it is unlikely that MCAM is recycled to any great extent via either the Rab4- mediated short-loop, or Rab11-mediated long-loop pathways in the Colo239F cells.

Finally, components of the retromer appear to be highly expressed in metastatic melanoma, especially *SNX2* and *RAB7A*. However, *SNX17* and *SNX27* appear to be largely downregulated. This may affect β1-integrin expression in these cell lines, as the FERM domain of SNX17 is known to bind the NxxY motif of β1-integrin. Whether this is also associated with MCAM expression is unknown, although we have seen significant localization of β1-integrin and MCAM in many melanoma cells. We were unable to explore protein expression for the majority of the retromer components, but as previously mentioned, Rab7 protein was highly expressed and showed strong co-localization with MCAM. This is in contrast to VPS35, which showed no co-localization with MCAM in our hands. Protein expression levels of other sorting nexins and retromer components needs to be explored to determine the validity of the mRNA expression data.

CHAPTER VI:

Conclusion

6.0 Conclusion

The major outcomes of this study included:

1. The generation of Colo239F melanoma cell populations expressing WT, LL623- 624AA-MCAM, Y641A-MCAM, and control MCAM negative cells, via lentiviral transduction and cell sorting.
2. Characterisation of the metastatic phenotype of melanoma cells expressing WT andMT MCAM using *in vitro* assays. This included exploring differences in cell morphology, proliferation, migration, and cell spreading on different substrates. Primarily, data presented here suggests that cells expressing MCAM containing the LL623-624AA and Y641A mutations showed an increase in sustained directional migration and differences in spreading behaviour compared to cells expressing WT MCAM, but no differences in proliferation.
3. Determining the subcellular localisation of WT and MT MCAM, as well as its co-localisation with important cellular markers. Interestingly, we found that MCAM consistently co-localised with F-actin, moesin, and β1-integrin in putative stress fibres, the WRAMP structure, and cell protrusions, indicating three potentially distinct mechanistic roles for MCAM in cell migration and morphology.
4. Investigating whether WT or MT MCAM expression was associated with, or altered the expression of other cell surface molecules, including β1-integrin. It was determined the expression levels and proportion of intracellular and cell surface MCAM and β1-integrin were largely unaltered by the LL623-624AA and Y641A mutations.
5. Exploring the ways in which MCAM may be endocytosed and recycled throughout the cell, including any potential role for retromer and sorting nexins in this process. The primary results from these investigations suggest that the disruptive mutations do not affect MCAM stability, despite conflicting results from predictive software. Further, it appears that *SNX31* expression is lost in cell culture, while *SNX2* and *Rab7a* may be upregulated in metastatic melanoma. The role of the retromer and associated proteins in MCAM recycling remains unclear.

The data presented in this study suggest that the two putative endocytosis motifs in the intracellular tail of MCAM - the dileucine and tyrosine motifs – are integral to certain aspects of MCAM function, and dispensable for others. Expression of LL623-624A- and Y641A-MCAM in Colo239F cells was associated with an increase in directional migration, increased occurrence of the WRAMP structure, alterations in spreading behaviour on various substrates, and differences in morphology. However, there were no differences in proliferation, or levels of intracellular and surface MCAM expression in the WT vs MT MCAM expressing cells. All MCAM expressing cells showed co-localisation of MCAM with moesin, F-actin, and β1-integrin in the WRAMP structure. Furthermore, all MCAM expressing cells also displayed co-localisation of MCAM with moesin and F-actin in cell protrusions, and with moesin, F-actin, and Cop1β in actomyosin stress fibres. This

suggests three potential mechanisms by which MCAM may contribute to melanoma migration, none of which require functional dileucine or tyrosine motifs.

We propose that the LL623-624AA and Y641A mutations enhance the stability of the WRAMP structure in Colo239F cells - potentially by reducing recycling of MCAM back to the cell surface or into a different sorting pathway. Further, the occurrence and increased stability ofthe WRAMP structure may explain the increase in their occurrence in the MT MCAM expressing cell lines, as well as their increased sustained directional migration. In addition, the increase in WRAMP-associated MCAM may affect growth morphology; with cells expressing WT MCAM showing higher homotypic cell adhesion, while MT MCAM expressing cells demonstrate lower cell adhesion and higher cell mobility.

An area requiring further investigation is the interaction of MCAM with the cytoskeleton. It has become clear that MCAM is an important cytoskeletal modulator and it has been shownto have direct interactions with several cytoskeletal linkers including moesin, ezrin, radixin, hShroom1, and IQGAP1 (Dye et al. 2009; Luo et al. 2012; Witze et al. 2013). The co-localisation of MCAM at both cell protrusions, and within what appear to be actomyosin stress fibres, with moesin, F-actin, and Cop1β, suggests a mechanistic role of MCAM in cell migration and morphology. The presence of Cop1β may also indicate the trafficking of MCAM throughout the cell along cytoskeletal scaffolds. Experiments to highlight precisely how MCAM interacts with these molecules, andwhat mechanistic role it plays (if any), will be important to understanding the basic function of MCAM, and may produce novel targets for melanoma therapy.

Interestingly, MCAM appeared to have little to no effect on β1-integrin expression. Previously it has been hypothesised that MCAM reduces β1-integrin cell surface expression or activity (Dye 2007; George 2017). Here, we found that there was little difference in β1-integrin surface expression across the Colo239F cell series, except for a potential increase in expression in the Colo239F-YA3.1 cells. However, we did not explore integrin activity levels in these cells. The increased spreading speed and cell length in Colo239F-YA3.1 cells compared to WT MCAM expressing cells may be explained by increased β1-integrin expression or activation. It is also possible, however, that the Y641A mutation causes a conformational change in the intracellular tail of MCAM, analogous to the change proposed to occur via phosphorylation of the tyrosine motif (Xu et al. 2019). Indeed, the Y641A mutation may be producing a more activated state of MCAM, which might explain the differences in phenotype.

Finally, data presented here in relation to the recycling of MCAM are inconclusive but potentially hint at how MCAM is trafficked throughout the cell. Interestingly, neither WT norMT MCAM expressing cells displayed co-localisation with lysosomal markers, as would be expected by the results from the structural stability prediction software. Indeed, both WT and MT MCAM appeared to only partially localise in Rab5-marked early endosomes and Rab11- marked recycling endosomes. Instead, MCAM largely co-localised with Rab7a, a marker for late endosomes which mediates early-to-late endosome and late endosome-to-lysosome

maturation. This suggests that MCAM is largely pooling within late endosomes, and avoids the canonical lysosomal degradation pathway. This is consistent with the proposed mechanism described by Witze et al. 2013 by which MCAM is trafficked in MVBs from the cell surface to the WRAMP structure (Alonso-Curbelo et al. 2014).

Furthermore, five melanoma cell lines were confirmed to constitutively express retromer core component and sorting nexin genes. Gene expression for retromer was largely upregulated in metastatic melanoma, compared with a non-metastatic cell line. However, both *SNX17* and *SNX27* were downregulated in metastatic melanoma. Furthermore, no co-localisation was noted between MCAM and VPS35; suggesting that MCAM is not sorted via retromer in the Colo239F cell line. The role of retromer in melanoma is poorly understood and requires further investigation.

There are a number of limitations of the study and areas that require further experimentation. These include confirmation of the cell proliferation data (comparing all cell lines simultaneously); and further exploration of the cell migration data using additional chemotactic assays. The potential interaction between MCAM and β1-integrin remains to be clarified, as our co-immunoprecipitation experiments were unsuccessful. In addition, the relative proportion of WT and MT MCAM cells expressing the WRAMP structure, and whether Wnt5a signaling affects this, would significantly add to this study.

In summary, the tyrosine and dileucine motifs in the intracellular tail of MCAM appear to have several important but potentially redundant roles in contributing to the metastatic phenotype of melanoma cells. Further elucidating the role of MCAM, and its various interaction partners, in the WRAMP mechanism may lead to unique therapies to combat melanoma invasion and metastasis. Another area of interest is the KKGK motif in the intracellular tail of MCAM, which is reported to interact with a number of different proteins, including moesin, Cop1β and Rictor (Witze et al. 2013; Xu et al. 2019); all of which may be influenced by the dileucineand tyrosine motifs. In particular, exploring whether palmitoylation, phosphorylation or other modifications affect the conformation or interactions of the intracellular tail is worth further investigation.

7.0 References

Abdel-Malek, Z., I. Suzuki, A. Tada, S. Im, and C. Akcali. 1999. "The Melanocortin-1 Receptor and Human Pigmentation." *Ann N Y Acad Sci* 885: 117-33. https://doi.org/10.1111/j.1749-6632.1999.tb08669.x.

Abdel-Malek, Z., V. B. Swope, I. Suzuki, C. Akcali, M. D. Harriger, S. T. Boyce, K. Urabe, and V. J. Hearing. 1995. "Mitogenic and Melanogenic Stimulation of Normal Human Melanocytes by Melanotropic Peptides." *Proceedings of the National Academy of Sciences of the United States of America* 92 (5): 1789-1793. https://doi.org/10.1073/pnas.92.5.1789.

Adair, T.H., and J.P. Montani. 2010. "Angiogenesis."

Adzhubei, I. A., S. Schmidt, L. Peshkin, V. E. Ramensky, A. Gerasimova, P. Bork, A. S. Kondrashov, and S. R. Sunyaev. 2010. "A Method and Server for Predicting Damaging Missense Mutations." *Nat Methods* 7 (4): 248-9. https://doi.org/10.1038/nmeth0410-248.

Aguilar, Rubén Claudio, and Beverly Wendland. 2005. "Endocytosis of Membrane Receptors: Two Pathways Are Better Than One." *Proceedings of the National Academy of Sciences of the United States of America* 102 (8): 2679. https://doi.org/10.1073/pnas.0500213102.

Alais, S., N. Allioli, C. Pujades, J. L. Duband, O. Vainio, B. A. Imhof, and D. Dunon. 2001. "Hemcam/Cd146 Downregulates Cell Surface Expression of Beta1 Integrins." *J Cell Sci* 114 (Pt 10): 1847-59.

Aldovini, D., F. Demichelis, C. Doglioni, D. Di Vizio, E. Galligioni, S. Brugnara, B. Zeni et al. 2006. "M-Cam Expression as Marker of Poor Prognosis in Epithelial Ovarian Cancer." *Int J Cancer* 119 (8): 1920-6. https://doi.org/10.1002/ijc.22082.

Alford, Deborah, and Joyce Taylor-Papadimitriou. 1996. "Cell Adhesion Molecules in the Normal and Cancerous Mammary Gland." *Journal of Mammary Gland Biology and Neoplasia* 1 (2): 207-218. https://doi.org/10.1007/BF02013644.

Alonso-Curbelo, D., E. Riveiro-Falkenbach, E. Perez-Guijarro, M. Cifdaloz, P. Karras, L. Osterloh, D. Megias et al. 2014. "Rab7 Controls Melanoma Progression by Exploiting a Lineage-Specific Wiring of the Endolysosomal Pathway." *Cancer Cell* 26 (1): 61-76. https://doi.org/10.1016/j.ccr.2014.04.030.

Anfosso, F., N. Bardin, V. Frances, E. Vivier, L. Camoin-Jau, J. Sampol, and F. Dignat-George. 1998. "Activation of Human Endothelial Cells Via S-Endo-1 Antigen (Cd146) Stimulates the Tyrosine Phosphorylation of Focal Adhesion Kinase P125(Fak)." *J Biol Chem* 273 (41): 26852-6. https://doi.org/10.1074/jbc.273.41.26852.

Arakel, E. C., and B. Schwappach. 2018. "Formation of Copi-Coated Vesicles at a Glance." *J Cell Sci* 131 (5). https://doi.org/10.1242/jcs.209890.

Arancibia-Carcamo, I. L., B. P. Fairfax, S. J. Moss, and J. T. Kittler. 2006. "Studying the Localization, Surface Stability and Endocytosis of Neurotransmitter Receptors by Antibody Labeling and Biotinylation Approaches." In *The Dynamic Synapse: Molecular Methods in Ionotropic Receptor Biology* ed., edited by J. T. Kittler and S. J. Moss. Boca Raton (FL). https://www.ncbi.nlm.nih.gov/pubmed/21204477.

Australian Institute of Health and Welfare. 2016. 'Skin Cancer in Australia.', Canberra: AIHW.

Bardin, N., F. Anfosso, J. M. Masse, E. Cramer, F. Sabatier, A. Le Bivic, J. Sampol, and F. Dignat-George. 2001. "Identification of Cd146 as a Component of the Endothelial Junction Involved in the Control of Cell-Cell Cohesion." *Blood* 98 (13): 3677-84. https://doi.org/10.1182/blood.v98.13.3677.

Bardin, N., M. Blot-Chabaud, N. Despoix, A. Kebir, K. Harhouri, J. P. Arsanto, L. Espinosa et al. 2009. "Cd146 and Its Soluble Form Regulate Monocyte Transendothelial Migration." *Arterioscler Thromb Vasc Biol* 29 (5): 746-53. https://doi.org/10.1161/atvbaha.108.183251.

Bardin, N., V. Frances, V. Combes, J. Sampol, and F. Dignat-George. 1998. "Cd146: Biosynthesis and Production of a Soluble Form in Human Cultured Endothelial Cells." *FEBS Lett* 421 (1): 12-4. https://doi.org/10.1016/s0014-5793(97)01455-5.

Bardin, N., F. George, M. Mutin, C. Brisson, N. Horschowski, V. Francés, G. Lesauie, and J. Sampol. 1996. "S-Endo 1, a Pan-Endothelial Monoclonal Antibody Recognizing a Novel Human Endothelial Antigen." *Tissue Antigens* 48 (5): 531-539. https://doi.org/10.1111/j.1399-0039.1996.tb02666.x.

Bardin, N., V. Moal, F. Anfosso, L. Daniel, P. Brunet, J. Sampol, and F. Dignat George. 2003. "Soluble Cd146, a Novel Endothelial Marker, Is Increased in Physiopathological Settings Linked to Endothelial Junctional Alteration." *Thromb Haemost* 90 (5): 915-20. https://doi.org/10.1160/th02-11-0285.

Beadling, C., E. Jacobson-Dunlop, F. S. Hodi, C. Le, A. Warrick, J. Patterson, A. Town et al. 2008. "Kit Gene Mutations and Copy Number in Melanoma Subtypes." *Clin Cancer Res* 14 (21): 6821-8. https://doi.org/10.1158/1078-0432.Ccr-08-0575.

Bittner, M., P. Meltzer, Y. Chen, Y. Jiang, E. Seftor, M. Hendrix, M. Radmacher et al. 2000. "Molecular Classification of Cutaneous Malignant Melanoma by Gene Expression Profiling." *Nature* 406 (6795): 536-40. https://doi.org/10.1038/35020115.

Boneberg, E. M., H. Illges, D. F. Legler, and G. Furstenberger. 2009. "Soluble Cd146 Is Generated by Ectodomain Shedding of Membrane Cd146 in a Calcium-Induced, Matrix Metalloprotease-Dependent Process." *Microvasc Res* 78 (3): 325-31. https://doi.org/10.1016/j.mvr.2009.06.012.

Bonifacino, J. S., and L. M. Traub. 2003. "Signals for Sorting of Transmembrane Proteins to Endosomes and Lysosomes." *Annu Rev Biochem* 72: 395-447. https://doi.org/10.1146/annurev.biochem.72.121801.161800.

Boulaiz, H., J. A. Marchal, J. Prados, C. Melguizo, and A. Aranega. 2005. "Non-Viral and Viral Vectors for Gene Therapy." *Cell Mol Biol (Noisy-le-grand)* 51 (1): 3-22.

Breuer, J., E. Korpos, M. J. Hannocks, T. Schneider-Hohendorf, J. Song, L. Zondler, S. Herich et al. 2018. "Blockade of Mcam/Cd146 Impedes Cns Infiltration of T Cells over the Choroid Plexus." *J Neuroinflammation* 15 (1): 236. https://doi.org/10.1186/s12974-018-1276-4.

Bu, P., J. Zhuang, J. Feng, D. Yang, X. Shen, and X. Yan. 2007. "Visualization of Cd146 Dimerization and Its Regulation in Living Cells." *Biochim Biophys Acta* 1773 (4): 513-20. https://doi.org/10.1016/j.bbamcr.2007.01.009.

Buchanan, Tyler, Afsaneh Amouzegar, and Jason J. Luke. 2021. "Next-Generation Immunotherapy Approaches in Melanoma." *Current Oncology Reports* 23 (10): 116. https://doi.org/10.1007/s11912-021-01104-z.

Burd, C., and P. J. Cullen. 2014. "Retromer: A Master Conductor of Endosome Sorting." *Cold Spring Harb Perspect Biol* 6 (2). https://doi.org/10.1101/cshperspect.a016774.

Campbell, I. D., and M. J. Humphries. 2011. "Integrin Structure, Activation, and Interactions." *Cold Spring Harb Perspect Biol* 3 (3). https://doi.org/10.1101/cshperspect.a004994.

Capriotti, E., P. Fariselli, R. Calabrese, and R. Casadio. 2005. "Predicting Protein Stability Changes from Sequences Using Support Vector Machines." *Bioinformatics* 21 Suppl 2: ii54-8. https://doi.org/10.1093/bioinformatics/bti1109.

Carroll, K. S., J. Hanna, I. Simon, J. Krise, P. Barbero, and S. R. Pfeffer. 2001. "Role of Rab9 Gtpase in Facilitating Receptor Recruitment by Tip47." *Science* 292 (5520): 1373-6. https://doi.org/10.1126/science.1056791.

Chaffer, Christine L., and Robert A. Weinberg. 2011. "A Perspective on Cancer Cell Metastasis." *Science* 331 (6024): 1559. https://doi.org/10.1126/science.1203543.

Chappell, William H., Linda S. Steelman, Jacquelyn M. Long, Ruth C. Kempf, Stephen L. Abrams, Richard A. Franklin, Jörg Bäsecke et al. 2011. "Ras/Raf/Mek/Erk and Pi3k/Pten/Akt/Mtor Inhibitors: Rationale and Importance to Inhibiting These Pathways in Human Health." *Oncotarget* 2 (3): 135-164. https://doi.org/10.18632/oncotarget.240.

Chiriboga, L., S. Meehan, I. Osman, M. Glick, G. de la Cruz, B. S. Howell, G. Friedman-Jimenez, R. J. Schneider, and S. Jamal. 2016. "Endothelin-1 in the Tumor Microenvironment Correlates with Melanoma Invasion." *Melanoma Res* 26 (3): 236-44. https://doi.org/10.1097/cmr.0000000000000235.

Choi, Yongwook, and Agnes P. Chan. 2015. "Provean Web Server: A Tool to Predict the Functional Effect of Amino Acid Substitutions and Indels." *Bioinformatics* 31 (16): 2745-2747. https://doi.org/10.1093/bioinformatics/btv195.

Cohen, C., A. Zavala-Pompa, J. H. Sequeira, M. Shoji, D. G. Sexton, G. Cotsonis, F. Cerimele, B. Govindarajan, N. Macaron, and J. L. Arbiser. 2002. "Mitogen-Actived Protein Kinase Activation Is an Early Event in Melanoma Progression." *Clin Cancer Res* 8 (12): 3728-33.

Cohen, M. B., T. L. Griebling, C. A. Ahaghotu, O. W. Rokhlin, and J. S. Ross. 1997. "Cellular Adhesion Molecules in Urologic Malignancies." *Am J Clin Pathol* 107 (1): 56-63. https://doi.org/10.1093/ajcp/107.1.56.

Colomb, F., W. Wang, D. Simpson, M. Zafar, R. Beynon, J. M. Rhodes, and L. G. Yu. 2017. "Galectin-3 Interacts with the Cell-Surface Glycoprotein Cd146 (Mcam, Muc18) and Induces Secretion of Metastasis-Promoting Cytokines from Vascular Endothelial Cells." *J Biol Chem* 292 (20): 8381-8389. https://doi.org/10.1074/jbc.M117.783431.

Conibear, E., and N. G. Davis. 2010. "Palmitoylation and Depalmitoylation Dynamics at a Glance." *J Cell Sci* 123 (Pt 23): 4007-10. https://doi.org/10.1242/jcs.059287.

Connacher, M. K., J. W. Tay, and N. G. Ahn. 2017. "Rear-Polarized Wnt5a-Receptor-Actin-Myosin-Polarity (Wramp) Structures Promote the Speed and Persistence of Directional Cell Migration." *Mol Biol Cell* 28 (14): 1924-1936. https://doi.org/10.1091/mbc.E16-12-0875.

Cramer, L. P. 2010. "Forming the Cell Rear First: Breaking Cell Symmetry to Trigger Directed Cell Migration." *Nat Cell Biol* 12 (7): 628-32. https://doi.org/10.1038/ncb0710-628.

Cullen, P. J., and H. C. Korswagen. 2011. "Sorting Nexins Provide Diversity for Retromer-Dependent Trafficking Events." *Nat Cell Biol* 14 (1): 29-37. https://doi.org/10.1038/ncb2374.

Curtin, J. A., J. Fridlyand, T. Kageshita, H. N. Patel, K. J. Busam, H. Kutzner, K. H. Cho et al. 2005. "Distinct Sets of Genetic Alterations in Melanoma." *N Engl J Med* 353 (20): 2135-47. https://doi.org/10.1056/NEJMoa050092.

D'Onofrio, M. F., S. Brezillon, T. Baranek, C. Perreau, P. J. Roughley, F. X. Maquart, and Y. Wegrowski. 2008. "Identification of Beta1 Integrin as Mediator of Melanoma Cell Adhesion to Lumican." *Biochem Biophys Res Commun* 365 (2): 266-72. https://doi.org/10.1016/j.bbrc.2007.10.155.

Da Forno, P. D., J. H. Pringle, P. Hutchinson, J. Osborn, Q. Huang, L. Potter, R. A. Hancox, A. Fletcher, and G. S. Saldanha. 2008. "Wnt5a Expression Increases During Melanoma Progression and Correlates with Outcome." *Clin Cancer Res* 14 (18): 5825-32. https://doi.org/10.1158/1078-0432.Ccr-07-5104.

De Pascalis, Chiara, and Sandrine Etienne-Manneville. 2017. "Single and Collective Cell Migration: The Mechanics of Adhesions." *Mol Biol Cell* 28 (14): 1833-1846. https://doi.org/10.1091/mbc.E17-03-0134.

Despoix, N., T. Walzer, N. Jouve, M. Blot-Chabaud, N. Bardin, P. Paul, L. Lyonnet, E. Vivier, F. Dignat-George, and F. Vely. 2008. "Mouse Cd146/Mcam Is a Marker of Natural Killer Cell Maturation." *Eur J Immunol* 38 (10): 2855-64. https://doi.org/10.1002/eji.200838469.

Dewing, D., M. Emmett, and R. Pritchard Jones. 2012. "The Roles of Angiogenesis in Malignant Melanoma: Trends in Basic Science Research over the Last 100 Years." *ISRN Oncol* 2012: 546927. https://doi.org/10.5402/2012/546927.

Dissanayake, S. K., M. Wade, C. E. Johnson, M. P. O'Connell, P. D. Leotlela, A. D. French, K. V. Shah et al. 2007. "The Wnt5a/Protein Kinase C Pathway Mediates Motility in Melanoma Cells Via the Inhibition of Metastasis Suppressors and Initiation of an Epithelial to Mesenchymal Transition." *J Biol Chem* 282 (23): 17259-71. https://doi.org/10.1074/jbc.M700075200.

Doherty, G. J., and H. T. McMahon. 2009. "Mechanisms of Endocytosis." *Annu Rev Biochem* 78: 857-902. https://doi.org/10.1146/annurev.biochem.78.081307.110540.

Dominguez, R., and K. C. Holmes. 2011. "Actin Structure and Function." *Annu Rev Biophys* 40: 169-86. https://doi.org/10.1146/annurev-biophys-042910-155359.

Duesberg, P., R. Stindl, and R. Hehlmann. 2001. "Origin of Multidrug Resistance in Cells with and without Multidrug Resistance Genes: Chromosome Reassortments Catalyzed by Aneuploidy." *Proceedings of the National Academy of Sciences of the United States of America* 98 (20): 11283-8. https://doi.org/10.1073/pnas.201398998.

Duggan, Máire A., William F. Anderson, Sean Altekruse, Lynne Penberthy, and Mark E. Sherman. 2016. "The Surveillance, Epidemiology, and End Results (Seer) Program and Pathology: Toward Strengthening the Critical Relationship." *The American journal of surgical pathology* 40 (12): e94-e102. https://doi.org/10.1097/PAS.0000000000000749.

Dye, D. E. 2007. "The Role of Mcam in Melanoma and Metastasis."

Dye, D. E., S. Karlen, B. Rohrbach, O. Staub, L. R. Braathen, K. A. Eidne, and D. R. Coombe. 2009. "Hshroom1 Links a Membrane Bound Protein to the Actin Cytoskeleton." *Cell Mol Life Sci* 66 (4): 681-96. https://doi.org/10.1007/s00018-009-8645-1.

Dye, Danielle E., Sandra Medic, Mel Ziman, and Deirdre R. Coombe. 2013. "Melanoma Biomolecules: Independently Identified but Functionally Intertwined." *Frontiers in oncology* 3: 252-252. https://doi.org/10.3389/fonc.2013.00252.
Eggermont, A. M., and J. M. Kirkwood. 2004. "Re-Evaluating the Role of Dacarbazine in Metastatic Melanoma: What Have We Learned in 30 Years?" *Eur J Cancer* 40 (12): 1825-36. https://doi.org/10.1016/j.ejca.2004.04.030.
Elbashir, S. M., J. Harborth, W. Lendeckel, A. Yalcin, K. Weber, and T. Tuschl. 2001. "Duplexes of 21-Nucleotide Rnas Mediate Rna Interference in Cultured Mammalian Cells." *Nature* 411 (6836): 494-8. https://doi.org/10.1038/35078107.
Elder, David E. 2006. "Pathology of Melanoma." *Clinical Cancer Research* 12 (7): 2308s. https://doi.org/10.1158/1078-0432.CCR-05-2504.
Ellgaard, L., and A. Helenius. 2003. "Quality Control in the Endoplasmic Reticulum." *Nat Rev Mol Cell Biol* 4 (3): 181-91. https://doi.org/10.1038/nrm1052.
Elshal, M. F., S. S. Khan, N. Raghavachari, Y. Takahashi, J. Barb, J. J. Bailey, P. J. Munson, M. A. Solomon, R. L. Danner, and J. P. McCoy, Jr. 2007. "A Unique Population of Effector Memory Lymphocytes Identified by Cd146 Having a Distinct Immunophenotypic and Genomic Profile." *BMC Immunol* 8: 29. https://doi.org/10.1186/1471-2172-8-29.
Elshal, Mohamed F., Sameena S. Khan, Yoshiyuki Takahashi, Michael A. Solomon, and J. Philip McCoy. 2005. "Cd146 (Mel-Cam), an Adhesion Marker of Endothelial Cells, Is a Novel Marker of Lymphocyte Subset Activation in Normal Peripheral Blood." *Blood* 106 (8): 2923. https://doi.org/10.1182/blood-2005-06-2307.
Espagnolle, N., F. Guilloton, F. Deschaseaux, M. Gadelorge, L. Sensebe, and P. Bourin. 2014. "Cd146 Expression on Mesenchymal Stem Cells Is Associated with Their Vascular Smooth Muscle Commitment." *J Cell Mol Med* 18 (1): 104-14. https://doi.org/10.1111/jcmm.12168.
Estecha, Ana, Lorena Sánchez-Martín, Amaya Puig-Kröger, Rubén A. Bartolomé, Joaquín Teixidó, Rafael Samaniego, and Paloma Sánchez-Mateos. 2009. "Moesin Orchestrates Cortical Polarity of Melanoma Tumour Cells to Initiate 3d Invasion." *J Cell Sci* 122 (19): 3492. https://doi.org/10.1242/jcs.053157.
Falzone, Luca, Rossella Salemi, Salvatore Travali, Aurora Scalisi, James A. McCubrey, Saverio Candido, and Massimo Libra. 2016. "Mmp-9 Overexpression Is Associated with Intragenic Hypermethylation of Mmp9 Gene in Melanoma." *Aging* 8 (5): 933-944. https://doi.org/10.18632/aging.100951.
Farahani, E., H. K. Patra, J. R. Jangamreddy, I. Rashedi, M. Kawalec, R. K. Rao Pariti, P. Batakis, and E. Wiechec. 2014. "Cell Adhesion Molecules and Their Relation to (Cancer) Cell Stemness." *Carcinogenesis* 35 (4): 747-59. https://doi.org/10.1093/carcin/bgu045.
Fayazi, M., M. Salehnia, and S. Ziaei. 2015. "Differentiation of Human Cd146-Positive Endometrial Stem Cells to Adipogenic-, Osteogenic-, Neural Progenitor-, and Glial-Like Cells." *In Vitro Cell Dev Biol Anim* 51 (4): 408-14. https://doi.org/10.1007/s11626-014-9842-2.
Ferlay, J., I. Soerjomataram, R. Dikshit, S. Eser, C. Mathers, M. Rebelo, D. M. Parkin, D. Forman, and F. Bray. 2015. "Cancer Incidence and Mortality Worldwide: Sources, Methods and Major Patterns in Globocan 2012." *Int J Cancer* 136 (5): E359-86. https://doi.org/10.1002/ijc.29210.
Flanagan, K., K. Fitzgerald, J. Baker, K. Regnstrom, S. Gardai, F. Bard, S. Mocci et al. 2012. "Laminin-411 Is a Vascular Ligand for Mcam and Facilitates Th17 Cell Entry into the Cns." *PLoS One* 7 (7): e40443. https://doi.org/10.1371/journal.pone.0040443.
Franker, Mariella A. M., and Casper C. Hoogenraad. 2013. "Microtubule-Based Transport – Basic Mechanisms, Traffic Rules and Role in Neurological Pathogenesis." *J Cell Sci* 126 (11): 2319. https://doi.org/10.1242/jcs.115030.
Gao, Qian, Junfeng Zhang, Xiumei Wang, Ying Liu, Rongqiao He, Xingfeng Liu, Fei Wang et al. 2017. "The Signalling Receptor Mcam Coordinates Apical-Basal Polarity and Planar Cell Polarity During Morphogenesis." *Nature Communications* 8: 15279. https://doi.org/10.1038/ncomms15279
Garcia, S., J. P. Dales, E. Charafe-Jauffret, S. Carpentier-Meunier, L. Andrac-Meyer, J. Jacquemier, C. Andonian et al. 2007. "Poor Prognosis in Breast Carcinomas Correlates with Increased Expression of Targetable Cd146 and C-Met and with Proteomic Basal-Like Phenotype." *Hum Pathol* 38 (6): 830-41. https://doi.org/10.1016/j.humpath.2006.11.015.

George, T. 2017. "Recycling of Melanoma Cell Adhesion Molecule in Melanoma Metastasis." School of Biomedical Science Curtin University. Perth.
Gershenwald, J. E., R. A. Scolyer, K. R. Hess, V. K. Sondak, G. V. Long, M. I. Ross, A. J. Lazar et al. 2017. "Melanoma Staging: Evidence-Based Changes in the American Joint Committee on Cancer Eighth Edition Cancer Staging Manual." *CA Cancer J Clin* 67 (6): 472-492. https://doi.org/10.3322/caac.21409.
Gloster, H. M., Jr., and D. G. Brodland. 1996. "The Epidemiology of Skin Cancer." *Dermatol Surg* 22 (3): 217-26. https://doi.org/10.1111/j.1524-4725.1996.tb00312.x.
Gong, C., J. Shen, Z. Fang, L. Qiao, R. Feng, X. Lin, and S. Li. 2018. "Abnormally Expressed Junb Transactivated by Il-6/Stat3 Signaling Promotes Uveal Melanoma Aggressiveness Via Epithelial-Mesenchymal Transition." *Biosci Rep* 38 (4). https://doi.org/10.1042/BSR20180532.
Grant, Barth D., and Julie G. Donaldson. 2009. "Pathways and Mechanisms of Endocytic Recycling." *Nat Rev Mol Cell Biol* 10 (9): 597-608. https://doi.org/10.1038/nrm2755.
Gray-Schopfer, V., C. Wellbrock, and R. Marais. 2007. "Melanoma Biology and New Targeted Therapy." *Nature* 445 (7130): 851-7. https://doi.org/10.1038/nature05661.
Griffin, M., D. Scotto, D. H. Josephs, S. Mele, S. Crescioli, H. J. Bax, G. Pellizzari et al. 2017. "Braf Inhibitors: Resistance and the Promise of Combination Treatments for Melanoma." *Oncotarget* 8 (44): 78174-78192. https://doi.org/10.18632/oncotarget.19836.
Guan, Xiaomu, and Carol A. Fierke. 2011. "Understanding Protein Palmitoylation: Biological Significance and Enzymology." *Science China. Chemistry* 54 (12): 1888-1897. https://doi.org/10.1007/s11426-011-4428-2.
Guarneri, Claudio, Valentina Bevelacqua, Jerry Polesel, Luca Falzone, Patrizia S. Cannavò, Demetrios A. Spandidos, Grazia Malaponte, and Massimo Libra. 2017. "Nf-Kb Inhibition Is Associated with Opn/Mmp-9 Downregulation in Cutaneous Melanoma." *Oncology reports* 37 (2): 737-746. https://doi.org/10.3892/or.2017.5362.
Guerra, F., and C. Bucci. 2016. "Multiple Roles of the Small Gtpase Rab7." *Cells* 5 (3). https://doi.org/10.3390/cells5030034.
Guezguez, Borhane, Pascale Vigneron, Sandrine Alais, Thierry Jaffredo, Julie Gavard, René-Marc Mège, and Dominique Dunon. 2006. "A Dileucine Motif Targets Mcam-L Cell Adhesion Molecule to the Basolateral Membrane in Mdck Cells." *FEBS Lett* 580 (15): 3649-3656. https://doi.org/https://doi.org/10.1016/j.febslet.2006.05.048.
Guezguez, Borhane, Pascale Vigneron, Nathalie Lamerant, Claudine Kieda, Thierry Jaffredo, and Dominique Dunon. 2007. "Dual Role of Melanoma Cell Adhesion Molecule (Mcam)/Cd146 in Lymphocyte Endothelium Interaction: Mcam/Cd146 Promotes Rolling Via Microvilli Induction in Lymphocyte and Is an Endothelial Adhesion Receptor." *The Journal of Immunology* 179 (10): 6673. https://doi.org/10.4049/jimmunol.179.10.6673.
Hahn, K., R. DeBiasio, and D. L. Taylor. 1992. "Patterns of Elevated Free Calcium and Calmodulin Activation in Living Cells." *Nature* 359 (6397): 736-8. https://doi.org/10.1038/359736a0.
Halt, K. J., H. E. Parssinen, S. M. Junttila, U. Saarela, S. Sims-Lucas, P. Koivunen, J. Myllyharju, S. Quaggin, I. N. Skovorodkin, and S. J. Vainio. 2016. "Cd146(+) Cells Are Essential for Kidney Vasculature Development." *Kidney Int* 90 (2): 311-324. https://doi.org/10.1016/j.kint.2016.02.021.
Hamill, Kevin J., Kristina Kligys, Susan B. Hopkinson, and Jonathan C. R. Jones. 2009. "Laminin Deposition in the Extracellular Matrix: A Complex Picture Emerges." *J Cell Sci* 122 (24): 4409. https://doi.org/10.1242/jcs.041095.
Han, Y. P., T. L. Tuan, H. Wu, M. Hughes, and W. L. Garner. 2001. "Tnf-Alpha Stimulates Activation of Pro-Mmp2 in Human Skin through Nf-(Kappa)B Mediated Induction of Mt1-Mmp." *J Cell Sci* 114 (Pt 1): 131-139. https://www.ncbi.nlm.nih.gov/pubmed/11112697.
Handolias, D., R. Salemi, W. Murray, A. Tan, W. Liu, A. Viros, A. Dobrovic, J. Kelly, and G. A. McArthur. 2010. "Mutations in Kit Occur at Low Frequency in Melanomas Arising from Anatomical Sites Associated with Chronic and Intermittent Sun Exposure." *Pigment Cell Melanoma Res* 23 (2): 210-5. https://doi.org/10.1111/j.1755-148X.2010.00671.x.
Harhouri, K., A. Kebir, B. Guillet, A. Foucault-Bertaud, S. Voytenko, M. D. Piercecchi-Marti, C. Berenguer et al. 2010. "Soluble Cd146 Displays Angiogenic Properties and Promotes Neovascularization in

Experimental Hind-Limb Ischemia." *Blood* 115 (18): 3843-51. https://doi.org/10.1182/blood-2009-06-229591.
Harterink, M., F. Port, M. J. Lorenowicz, I. J. McGough, M. Silhankova, M. C. Betist, J. R. T. van Weering et al. 2011. "A Snx3-Dependent Retromer Pathway Mediates Retrograde Transport of the Wnt Sorting Receptor Wntless and Is Required for Wnt Secretion." *Nat Cell Biol* 13 (8): 914-923. https://doi.org/10.1038/ncb2281.
He, J., Q. Yang, and L. J. Chang. 2005. "Dynamic DNA Methylation and Histone Modifications Contribute to Lentiviral Transgene Silencing in Murine Embryonic Carcinoma Cells." *J Virol* 79 (21): 13497-508. https://doi.org/10.1128/jvi.79.21.13497-13508.2005.
Hemmings, B. A., and D. F. Restuccia. 2012. "Pi3k-Pkb/Akt Pathway." *Cold Spring Harb Perspect Biol* 4 (9): a011189. https://doi.org/10.1101/cshperspect.a011189.
Henriksen, K., and M. A. Karsdal. 2016. "Chapter 1 - Type I Collagen." In *Biochemistry of Collagens, Laminins and Elastin* ed., edited by Morten A. Karsdal, 1-11. Academic Press. https://doi.org/https://doi.org/10.1016/B978-0-12-809847-9.00001-5.
Hiroi, Satoshi, Yasuhiro Tsukamoto, Fumihiko Sasaki, Naomasa Miki, and Eiichi Taira. 2003. "Involvement of Gicerin, a Cell Adhesion Molecule, in Development and Regeneration of Chick Sciatic Nerve." *FEBS Lett* 554 (3): 311-314. https://doi.org/https://doi.org/10.1016/S0014-5793(03)01176-1.
Hodis, Eran, Ian R. Watson, Gregory V. Kryukov, Stefan T. Arold, Marcin Imielinski, Jean-Philippe Theurillat, Elizabeth Nickerson et al. 2012. "A Landscape of Driver Mutations in Melanoma." *Cell* 150 (2): 251-263. https://doi.org/10.1016/j.cell.2012.06.024.
Hofmann, A., B. Kessler, S. Ewerling, A. Kabermann, G. Brem, E. Wolf, and A. Pfeifer. 2006. "Epigenetic Regulation of Lentiviral Transgene Vectors in a Large Animal Model." *Mol Ther* 13 (1): 59-66. https://doi.org/10.1016/j.ymthe.2005.07.685.
Holmes, David I. R., and Ian Zachary. 2005. "The Vascular Endothelial Growth Factor (Vegf) Family: Angiogenic Factors in Health and Disease." *Genome biology* 6 (2): 209-209. https://doi.org/10.1186/gb-2005-6-2-209.
Homrich, Mirka, Ingo Gotthard, Hilke Wobst, and Simone Diestel. 2015. "Cell Adhesion Molecules and Ubiquitination-Functions and Significance." *Biology* 5 (1): 1. https://doi.org/10.3390/biology5010001.
Howe, Grant A., and Christina L. Addison. 2012. "B1 Integrin: An Emerging Player in the Modulation of Tumorigenesis and Response to Therapy." *Cell adhesion & migration* 6 (2): 71-77. https://doi.org/10.4161/cam.20077.
Huang, L. T., M. M. Gromiha, and S. Y. Ho. 2007. "Iptree-Stab: Interpretable Decision Tree Based Method for Predicting Protein Stability Changes Upon Mutations." *Bioinformatics* 23 (10): 1292-3. https://doi.org/10.1093/bioinformatics/btm100.
Huotari, J., and A. Helenius. 2011. "Endosome Maturation." *EMBO J* 30 (17): 3481-500. https://doi.org/10.1038/emboj.2011.286.
Huttenlocher, Anna, and Alan Rick Horwitz. 2011. "Integrins in Cell Migration." *Cold Spring Harb Perspect Biol* 3 (9): a005074-a005074. https://doi.org/10.1101/cshperspect.a005074.
Imbert, A. M., C. Garulli, E. Choquet, M. Koubi, M. Aurrand-Lions, and C. Chabannon. 2012. "Cd146 Expression in Human Breast Cancer Cell Lines Induces Phenotypic and Functional Changes Observed in Epithelial to Mesenchymal Transition." *PLoS One* 7 (8): e43752. https://doi.org/10.1371/journal.pone.0043752.
Ishikawa, T., Z. Wondimu, Y. Oikawa, G. Gentilcore, R. Kiessling, S. Egyhazi Brage, J. Hansson, and M. Patarroyo. 2014. "Laminins 411 and 421 Differentially Promote Tumor Cell Migration Via Alpha6beta1 Integrin and Mcam (Cd146)." *Matrix Biol* 38: 69-83. https://doi.org/10.1016/j.matbio.2014.06.002.
Iversen, Nina, Baard Birkenes, Kari Torsdalen, and Srdjan Djurovic. 2005. "Electroporation by Nucleofector Is the Best Nonviral Transfection Technique in Human Endothelial and Smooth Muscle Cells." *Genetic vaccines and therapy* 3 (1): 2-2. https://doi.org/10.1186/1479-0556-3-2.
Jiang, G., L. Zhang, Q. Zhu, D. Bai, C. Zhang, and X. Wang. 2016. "Cd146 Promotes Metastasis and Predicts Poor Prognosis of Hepatocellular Carcinoma." *J Exp Clin Cancer Res* 35: 38. https://doi.org/10.1186/s13046-016-0313-3.

Jiang, T., J. Zhuang, H. Duan, Y. Luo, Q. Zeng, K. Fan, H. Yan et al. 2012. "Cd146 Is a Coreceptor for Vegfr-2 in Tumor Angiogenesis." *Blood* 120 (11): 2330-9. https://doi.org/10.1182/blood-2012-01-406108.
Johannes, L., and V. Popoff. 2008. "Tracing the Retrograde Route in Protein Trafficking." *Cell* 135 (7): 1175-87. https://doi.org/10.1016/j.cell.2008.12.009.
Johnson, J. P., M. Bar-Eli, B. Jansen, and E. Markhof. 1997. "Melanoma Progression-Associated Glycoprotein Muc18/Mcam Mediates Homotypic Cell Adhesion through Interaction with a Heterophilic Ligand." *Int J Cancer* 73 (5): 769-74. https://doi.org/10.1002/(sici)1097-0215(19971127)73:5<769::aid-ijc26>3.0.co;2-#.
Jouve, N., R. Bachelier, N. Despoix, M. G. Blin, M. K. Matinzadeh, S. Poitevin, M. Aurrand-Lions et al. 2015. "Cd146 Mediates Vegf-Induced Melanoma Cell Extravasation through Fak Activation." *Int J Cancer* 137 (1): 50-60. https://doi.org/10.1002/ijc.29370.
Jouve, Nathalie, Nicolas Despoix, Marion Espeli, Laurent Gauthier, Sophie Cypowyj, Karim Fallague, Claudine Schiff, Françoise Dignat-George, Frédéric Vély, and Aurélie S. Leroyer. 2013. "The Involvement of Cd146 and Its Novel Ligand Galectin-1 in Apoptotic Regulation of Endothelial Cells." *J Biol Chem* 288 (4): 2571-2579. https://doi.org/10.1074/jbc.M112.418848.
Kaksonen, M., and A. Roux. 2018. "Mechanisms of Clathrin-Mediated Endocytosis." *Nat Rev Mol Cell Biol* 19 (5): 313-326. https://doi.org/10.1038/nrm.2017.132.
Kamiguchi, H., and V. Lemmon. 1997. "Neural Cell Adhesion Molecule L1: Signaling Pathways and Growth Cone Motility." *J Neurosci Res* 49 (1): 1-8.
Kamiyama, T., H. Watanabe, M. Iijima, A. Miyazaki, and S. Iwamoto. 2012. "Coexpression of Ccr6 and Cd146 (Mcam) Is a Marker of Effector Memory T-Helper 17 Cells." *J Dermatol* 39 (10): 838-42. https://doi.org/10.1111/j.1346-8138.2012.01544.x.
Kang, Y., F. Wang, J. Feng, D. Yang, X. Yang, and X. Yan. 2006. "Knockdown of Cd146 Reduces the Migration and Proliferation of Human Endothelial Cells." *Cell Res* 16 (3): 313-8. https://doi.org/10.1038/sj.cr.7310039.
Karlen, Stéphane, and Lasse R. Braathen. 2000. "Role of the Initiator Element in the Regulation of the Melanoma Cell Adhesion Molecule Gene." *Journal of Investigative Dermatology* 115 (4): 668-673. https://doi.org/https://doi.org/10.1046/j.1523-1747.2000.00100.x.
Kawauchi, T. 2012. "Cell Adhesion and Its Endocytic Regulation in Cell Migration During Neural Development and Cancer Metastasis." *Int J Mol Sci* 13 (4): 4564-90. https://doi.org/10.3390/ijms13044564.
Kebir, A., K. Harhouri, B. Guillet, J. W. Liu, A. Foucault-Bertaud, E. Lamy, E. Kaspi et al. 2010. "Cd146 Short Isoform Increases the Proangiogenic Potential of Endothelial Progenitor Cells in Vitro and in Vivo." *Circ Res* 107 (1): 66-75. https://doi.org/10.1161/circresaha.109.213827.
Khalili, A. A., and M. R. Ahmad. 2015. "A Review of Cell Adhesion Studies for Biomedical and Biological Applications." *Int J Mol Sci* 16 (8): 18149-84. https://doi.org/10.3390/ijms160818149.
Kohlhapp, F. J., and H. L. Kaufman. 2016. "Molecular Pathways: Mechanism of Action for Talimogene Laherparepvec, a New Oncolytic Virus Immunotherapy." *Clin Cancer Res* 22 (5): 1048-54. https://doi.org/10.1158/1078-0432.CCR-15-2667.
Kosary, C. L., S. F. Altekruse, J. Ruhl, R. Lee, and L. Dickie. 2014. "Clinical and Prognostic Factors for Melanoma of the Skin Using Seer Registries: Collaborative Stage Data Collection System, Version 1 and Version 2." *Cancer* 120 Suppl 23: 3807-14. https://doi.org/10.1002/cncr.29050.
Kramer, R. H., M. Vu, Y. F. Cheng, and D. M. Ramos. 1991. "Integrin Expression in Malignant Melanoma." *Cancer Metastasis Rev* 10 (1): 49-59.
Krauthammer, Michael, Yong Kong, Byung Hak Ha, Perry Evans, Antonella Bacchiocchi, James P. McCusker, Elaine Cheng et al. 2012. "Exome Sequencing Identifies Recurrent Somatic Rac1 Mutations in Melanoma." *Nature genetics* 44 (9): 1006-1014. https://doi.org/10.1038/ng.2359.
Kristiansen, G., Y. Yu, K. Schluns, C. Sers, M. Dietel, and I. Petersen. 2003. "Expression of the Cell Adhesion Molecule Cd146/Mcam in Non-Small Cell Lung Cancer." *Anal Cell Pathol* 25 (2): 77-81.
Kuo, Jean-Cheng. 2013. "Mechanotransduction at Focal Adhesions: Integrating Cytoskeletal Mechanics in Migrating Cells." *J Cell Mol Med* 17 (6): 704-712. https://doi.org/10.1111/jcmm.12054.
Kuske, M. D. A., and J. P. Johnson. 1999. "Assignment of the Human Melanoma Cell Adhesion Molecule Gene (Mcam) to Chromosome 11 Band Q23.3 by Radiation Hybrid Mapping." *Cytogenetic and Genome Research* 87 (3-4): 258-258. https://doi.org/10.1159/000015439.

Larkin, J., V. Chiarion-Sileni, R. Gonzalez, J. J. Grob, C. L. Cowey, C. D. Lao, D. Schadendorf et al. 2015. "Combined Nivolumab and Ipilimumab or Monotherapy in Untreated Melanoma." *N Engl J Med* 373 (1): 23-34. https://doi.org/10.1056/NEJMoa1504030.

Larkin, J., V. Chiarion-Sileni, R. Gonzalez, J. J. Grob, P. Rutkowski, C. D. Lao, C. L. Cowey et al. 2019. "Five-Year Survival with Combined Nivolumab and Ipilimumab in Advanced Melanoma." *N Engl J Med* 381 (16): 1535-1546. https://doi.org/10.1056/NEJMoa1910836.

Lee, C. S., C. M. Thomas, and K. E. Ng. 2017. "An Overview of the Changing Landscape of Treatment for Advanced Melanoma." *Pharmacotherapy* 37 (3): 319-333. https://doi.org/10.1002/phar.1895.

Lee, K. R., J. S. Lee, Y. R. Kim, I. G. Song, and E. K. Hong. 2014. "Polysaccharide from Inonotus Obliquus Inhibits Migration and Invasion in B16-F10 Cells by Suppressing Mmp-2 and Mmp-9 Via Downregulation of Nf-Kappab Signaling Pathway." *Oncology reports* 31 (5): 2447-53. https://doi.org/10.3892/or.2014.3103.

Lehmann, J. M., B. Holzmann, E. W. Breitbart, P. Schmiegelow, G. Riethmuller, and J. P. Johnson. 1987. "Discrimination between Benign and Malignant Cells of Melanocytic Lineage by Two Novel Antigens, a Glycoprotein with a Molecular Weight of 113,000 and a Protein with a Molecular Weight of 76,000." *Cancer Res* 47 (3): 841-5.

Lehmann, J. M., G. Riethmuller, and J. P. Johnson. 1989. "Muc18, a Marker of Tumor Progression in Human Melanoma, Shows Sequence Similarity to the Neural Cell Adhesion Molecules of the Immunoglobulin Superfamily." *Proceedings of the National Academy of Sciences of the United States of America* 86 (24): 9891-5. https://doi.org/10.1073/pnas.86.24.9891.

Lei, Xing, Ce-Wen Guan, Yang Song, and Huan Wang. 2015. "The Multifaceted Role of Cd146/Mcam in the Promotion of Melanoma Progression." *Cancer cell international* 15 (1): 3-3. https://doi.org/10.1186/s12935-014-0147-z.

Leonardi, G. C., L. Falzone, R. Salemi, A. Zanghi, D. A. Spandidos, J. A. McCubrey, S. Candido, and M. Libra. 2018. "Cutaneous Melanoma: From Pathogenesis to Therapy (Review)." *Int J Oncol* 52 (4): 1071-1080. https://doi.org/10.3892/ijo.2018.4287.

Lerner, A. B., and J. S. McGuire. 1964. "Melanocyte-Stimulating Hormone and Adrenocorticotrophic Hormone. Their Relation to Pigmentation." *N Engl J Med* 270: 539-46. https://doi.org/10.1056/nejm196403122701101.

Li, G., J. Kalabis, X. Xu, F. Meier, M. Oka, T. Bogenrieder, and M. Herlyn. 2003. "Reciprocal Regulation of Melcam and Akt in Human Melanoma." *Oncogene* 22 (44): 6891-9. https://doi.org/10.1038/sj.onc.1206819.

Li, Yan, Jin-Ming Yu, Xue-Mei Zhan, Li-Li Liu, Ning Jin, and Yan-Xia Zhang. 2014. "Correlation of Cd146 Expression and Clinicopathological Characteristics in Esophageal Squamous Cell Carcinoma." *Oncology letters* 8 (2): 859-863. https://doi.org/10.3892/ol.2014.2227.

Liang, Y. K., Zeng, Y. S. Xiao, Y. Wu, Y. X. Ouyang, M. Chen, Y. C. Li et al. 2017. "Mcam/Cd146 Promotes Tamoxifen Resistance in Breast Cancer Cells through Induction of Epithelial-Mesenchymal Transition, Decreased Eralpha Expression and Akt Activation." *Cancer Lett* 386: 65-76. https://doi.org/10.1016/j.canlet.2016.11.004.

Linos, E., S. M. Swetter, M. G. Cockburn, G. A. Colditz, and C. A. Clarke. 2009. "Increasing Burden of Melanoma in the United States." *J Invest Dermatol* 129 (7): 1666-74. https://doi.org/10.1038/jid.2008.423.

Liu, J., M. Fukunaga-Kalabis, L. Li, and M. Herlyn. 2014. "Developmental Pathways Activated in Melanocytes and Melanoma." *Arch Biochem Biophys* 563: 13-21. https://doi.org/10.1016/j.abb.2014.07.023.

Liu, J. W., J. K. Nagpal, C. Jeronimo, J. E. Lee, R. Henrique, M. S. Kim, K. L. Ostrow et al. 2008. "Hypermethylation of Mcam Gene Is Associated with Advanced Tumor Stage in Prostate Cancer." *Prostate* 68 (4): 418-26. https://doi.org/10.1002/pros.20709.

Liu, Wen-Fang, Shu-Rong Ji, Jian-Jun Sun, Yi Zhang, Zhong-Yan Liu, Ai-Bin Liang, and Hua-Zong Zeng. 2012. "Cd146 Expression Correlates with Epithelial-Mesenchymal Transition Markers and a Poor Prognosis in Gastric Cancer." *Int J Mol Sci* 13 (5): 6399-6406. https://doi.org/10.3390/ijms13056399.

Long, GV, R Dummer, A Ribas, I Puzanov, A VanderWalde, RHI Andtbacka, O Olivier Michielin et al. 2016. "Efficacy Analysis of Masterkey-265 Phase 1b Study of Talimogene Laherparepvec (T-Vec) and

Pembrolizumab (Pembro) for Unresectable Stage Iiib-Iv Melanoma." *Journal of Clinical Oncology* 34 (15_suppl): 9568-9568. https://doi.org/10.1200/JCO.2016.34.15_suppl.9568.

López-Ferrando, Víctor, Andrea Gazzo, Xavier de la Cruz, Modesto Orozco, and Josep Ll Gelpí. 2017. "Pmut: A Web-Based Tool for the Annotation of Pathological Variants on Proteins, 2017 Update." *Nucleic acids research* 45 (W1): W222-W228. https://doi.org/10.1093/nar/gkx313.

Lorentzen, A., J. Bamber, A. Sadok, I. Elson-Schwab, and C. J. Marshall. 2011. "An Ezrin-Rich, Rigid Uropod-Like Structure Directs Movement of Amoeboid Blebbing Cells." *J Cell Sci* 124 (Pt 8): 1256-67. https://doi.org/10.1242/jcs.074849.

Luca, M., B. Hunt, C. D. Bucana, J. P. Johnson, I. J. Fidler, and M. Bar-Eli. 1993. "Direct Correlation between Muc18 Expression and Metastatic Potential of Human Melanoma Cells." *Melanoma Res* 3 (1): 35-41. https://doi.org/10.1097/00008390-199304000-00006.

Luo, Y., H. Duan, Y. Qian, L. Feng, Z. Wu, F. Wang, J. Feng, D. Yang, Z. Qin, and X. Yan. 2017. "Macrophagic Cd146 Promotes Foam Cell Formation and Retention During Atherosclerosis." *Cell Res* 27 (3): 352-372. https://doi.org/10.1038/cr.2017.8.

Luo, Y., C. Zheng, J. Zhang, D. Lu, J. Zhuang, S. Xing, J. Feng, D. Yang, and X. Yan. 2012. "Recognition of Cd146 as an Erm-Binding Protein Offers Novel Mechanisms for Melanoma Cell Migration." *Oncogene* 31 (3): 306-21. https://doi.org/10.1038/onc.2011.244.

Ma, X., J. Liu, J. Wu, X. Yan, P. Wu, Y. Liu, S. Li et al. 2010. "Synergistic Killing Effect between Vorinostat and Target of Cd146 in Malignant Cells." *Clin Cancer Res* 16 (21): 5165-76. https://doi.org/10.1158/1078-0432.Ccr-09-3174.

Maertens, Ophélia, Bryan Johnson, Pablo Hollstein, Dennie T. Frederick, Zachary A. Cooper, Ludwine Messiaen, Roderick T. Bronson et al. 2013. "Elucidating Distinct Roles for Nf1 in Melanomagenesis." *Cancer discovery* 3 (3): 338-349. https://doi.org/10.1158/2159-8290.CD-12-0313.

Markowska, A. I., K. C. Jefferies, and N. Panjwani. 2011. "Galectin-3 Protein Modulates Cell Surface Expression and Activation of Vascular Endothelial Growth Factor Receptor 2 in Human Endothelial Cells." *J Biol Chem* 286 (34): 29913-21. https://doi.org/10.1074/jbc.M111.226423.

Mayor, Satyajit, Robert G. Parton, and Julie G. Donaldson. 2014. "Clathrin-Independent Pathways of Endocytosis." *Cold Spring Harb Perspect Biol* 6 (6): a016758. https://doi.org/10.1101/cshperspect.a016758.

McGary, E. C., A. Heimberger, L. Mills, K. Weber, G. W. Thomas, M. Shtivelband, D. C. Lev, and M. Bar-Eli. 2003. "A Fully Human Antimelanoma Cellular Adhesion Molecule/Muc18 Antibody Inhibits Spontaneous Pulmonary Metastasis of Osteosarcoma Cells in Vivo." *Clin Cancer Res* 9 (17): 6560-6.

McNally, K. E., and P. J. Cullen. 2018. "Endosomal Retrieval of Cargo: Retromer Is Not Alone." *Trends Cell Biol* 28 (10): 807-822. https://doi.org/10.1016/j.tcb.2018.06.005.

McNally, Kerrie E., Rebecca Faulkner, Florian Steinberg, Matthew Gallon, Rajesh Ghai, David Pim, Paul Langton et al. 2017. "Retriever Is a Multiprotein Complex for Retromer-Independent Endosomal Cargo Recycling." *Nat Cell Biol* 19 (10): 1214-1225. https://doi.org/10.1038/ncb3610.

Melnikova, Vladislava O., Krishnakumar Balasubramanian, Gabriel J. Villares, Andrey S. Dobroff, Maya Zigler, Hua Wang, Frederik Petersson et al. 2009. "Crosstalk between Protease-Activated Receptor 1 and Platelet-Activating Factor Receptor Regulates Melanoma Cell Adhesion Molecule (Mcam/Muc18) Expression and Melanoma Metastasis." *J Biol Chem* 284 (42): 28845-28855. https://doi.org/10.1074/jbc.M109.042150.

Miller, A. J., and M. C. Mihm, Jr. 2006. "Melanoma." *N Engl J Med* 355 (1): 51-65. https://doi.org/10.1056/NEJMra052166.

Milone, Michael C., and Una O'Doherty. 2018. "Clinical Use of Lentiviral Vectors." *Leukemia* 32 (7): 1529-1541. https://doi.org/10.1038/s41375-018-0106-0.

Minana, R., J. M. Duran, M. Tomas, J. Renau-Piqueras, and C. Guerri. 2001. "Neural Cell Adhesion Molecule Is Endocytosed Via a Clathrin-Dependent Pathway." *Eur J Neurosci* 13 (4): 749-56. https://doi.org/10.1046/j.0953-816x.2000.01439.x.

Mintz-Weber, C. S., and J. P. Johnson. 2000. "Identification of the Elements Regulating the Expression of the Cell Adhesion Molecule Mcam/Muc18. Loss of Ap-2 Is Not Required for Mcam Expression in Melanoma Cell Lines." *J Biol Chem* 275 (44): 34672-80. https://doi.org/10.1074/jbc.M003812200.

Molhoek, K. R., G. Erdag, J. K. Rasamny, C. Murphy, D. Deacon, J. W. Patterson, C. L. Slingluff, Jr., and D. L. Brautigan. 2011. "Vegfr-2 Expression in Human Melanoma: Revised Assessment." *Int J Cancer* 129 (12): 2807-15. https://doi.org/10.1002/ijc.25963.

Moore, G. E., L. K. Woods, L. A. Quinn, R. T. Morgan, and T. U. Semple. 1980. "Characterization of Cell Lines from Four Undifferentiated Human Malignancies." *Cancer* 45 (9): 2311-23. https://doi.org/10.1002/1097-0142(19800501)45:9<2311::aid-cncr2820450914>3.0.co;2-w.

Moreno-Fortuny, Artal, Laricia Bragg, Giulio Cossu, and Urmas Roostalu. 2017. "Mcam Contributes to the Establishment of Cell Autonomous Polarity in Myogenic and Chondrogenic Differentiation." *Biology open* 6 (11): 1592-1601. https://doi.org/10.1242/bio.027771.

Moritz, A. E., D. E. Rastedt, D. J. Stanislowski, M. Shetty, M. A. Smith, R. A. Vaughan, and J. D. Foster. 2015. "Reciprocal Phosphorylation and Palmitoylation Control Dopamine Transporter Kinetics." *J Biol Chem* 290 (48): 29095-105. https://doi.org/10.1074/jbc.M115.667055.

Moro, N., C. Mauch, and P. Zigrino. 2014. "Metalloproteinases in Melanoma." *Eur J Cell Biol* 93 (1-2): 23-9. https://doi.org/10.1016/j.ejcb.2014.01.002.

Mueller, A., and P. G. Strange. 2004. "Mechanisms of Internalization and Recycling of the Chemokine Receptor, Ccr5." *Eur J Biochem* 271 (2): 243-52. https://doi.org/10.1046/j.1432-1033.2003.03918.x.

Naslavsky, N., and S. Caplan. 2018. "The Enigmatic Endosome - Sorting the Ins and Outs of Endocytic Trafficking." *J Cell Sci* 131 (13). https://doi.org/10.1242/jcs.216499.

Nodomi, S., K. Umeda, S. Saida, T. Kinehara, T. Hamabata, T. Daifu, I. Kato et al. 2016. "Cd146 Is a Novel Marker for Highly Tumorigenic Cells and a Potential Therapeutic Target in Malignant Rhabdoid Tumor." *Oncogene* 35 (40): 5317-5327. https://doi.org/10.1038/onc.2016.72.

Oka, S., H. Uramoto, Y. Chikaishi, and F. Tanaka. 2012. "The Expression of Cd146 Predicts a Poor Overall Survival in Patients with Adenocarcinoma of the Lung." *Anticancer Res* 32 (3): 861-4.

Ouhtit, Allal, Mohammed E. Abdraboh, Andrew D. Hollenbach, Hatem Zayed, and Madhwa H. G. Raj. 2017. "Cd146, a Novel Target of Cd44-Signaling, Suppresses Breast Tumor Cell Invasion." *Cell communication and signaling : CCS* 15 (1): 45-45. https://doi.org/10.1186/s12964-017-0200-3.

Pankov, Roumen, and Kenneth M. Yamada. 2002. "Fibronectin at a Glance." *J Cell Sci* 115 (20): 3861. https://doi.org/10.1242/jcs.00059.

Pasquier, E., N. Bardin, L. De Saint Martin, M. T. Le Martelot, C. Bohec, S. Roche, D. Mottier, and F. Dignat-George. 2005. "The First Assessment of Soluble Cd146 in Women with Unexplained Pregnancy Loss. A New Insight?" *Thromb Haemost* 94 (6): 1280-4.

Pearl, R. A., M. D. Pacifico, P. I. Richman, G. D. Wilson, and R. Grover. 2008. "Stratification of Patients by Melanoma Cell Adhesion Molecule (Mcam) Expression on the Basis of Risk: Implications for Sentinel Lymph Node Biopsy." *J Plast Reconstr Aesthet Surg* 61 (3): 265-71. https://doi.org/10.1016/j.bjps.2007.04.010.

Petrie, R. J., A. D. Doyle, and K. M. Yamada. 2009. "Random Versus Directionally Persistent Cell Migration." *Nat Rev Mol Cell Biol* 10 (8): 538-49. https://doi.org/10.1038/nrm2729.

Pfeffer, S. R. 2009. "Multiple Routes of Protein Transport from Endosomes to the Trans Golgi Network." *FEBS Lett* 583 (23): 3811-6. https://doi.org/10.1016/j.febslet.2009.10.075.

Pickl, W. F., O. Majdic, G. F. Fischer, P. Petzelbauer, I. Faé, M. Waclavicek, J. Stöckl et al. 1997. "Muc18/Mcam (Cd146), an Activation Antigen of Human T Lymphocytes." *The Journal of Immunology* 158 (5): 2107. http://www.jimmunol.org/content/158/5/2107.abstract.

Progida, C., and O. Bakke. 2016. "Bidirectional Traffic between the Golgi and the Endosomes - Machineries and Regulation." *J Cell Sci* 129 (21): 3971-3982. https://doi.org/10.1242/jcs.185702.

Rabouille, C. 2017. "Retriever Fetches Integrins from Endosomes." *Nat Cell Biol* 19 (10): 1144-1146. https://doi.org/10.1038/ncb3612.

Rapanotti, Maria Cristina, Elena Campione, Giulia Spallone, Augusto Orlandi, Sergio Bernardini, and Luca Bianchi. 2017. "Minimal Residual Disease in Melanoma: Circulating Melanoma Cells and Predictive Role of Mcam/Muc18/Melcam/Cd146." *Cell Death Discovery* 3: 17005. https://doi.org/10.1038/cddiscovery.2017.5.

Ricard-Blum, Sylvie. 2011. "The Collagen Family." *Cold Spring Harb Perspect Biol* 3 (1): a004978-a004978. https://doi.org/10.1101/cshperspect.a004978.

Ridley, Anne J., Martin A. Schwartz, Keith Burridge, Richard A. Firtel, Mark H. Ginsberg, Gary Borisy, J. Thomas Parsons, and Alan Rick Horwitz. 2003. "Cell Migration: Integrating Signals from Front to Back." *Science* 302 (5651): 1704. https://doi.org/10.1126/science.1092053.

Rigel, D. S., and J. A. Carucci. 2000. "Malignant Melanoma: Prevention, Early Detection, and Treatment in the 21st Century." *CA Cancer J Clin* 50 (4): 215-36; quiz 237-40. https://doi.org/10.3322/canjclin.50.4.215.

Rink, J., E. Ghigo, Y. Kalaidzidis, and M. Zerial. 2005. "Rab Conversion as a Mechanism of Progression from Early to Late Endosomes." *Cell* 122 (5): 735-49. https://doi.org/10.1016/j.cell.2005.06.043.

Rossi, S., M. Cordella, C. Tabolacci, G. Nassa, D. D'Arcangelo, C. Senatore, P. Pagnotto et al. 2018. "Tnf-Alpha and Metalloproteases as Key Players in Melanoma Cells Aggressiveness." *J Exp Clin Cancer Res* 37 (1): 326. https://doi.org/10.1186/s13046-018-0982-1.

Rummel, M. M., C. Sers, and J. P. Johnson. 1996. "Phorbol Ester and Cyclic Amp-Mediated Regulation of the Melanoma-Associated Cell Adhesion Molecule Muc18/Mcam." *Cancer Res* 56 (9): 2218-23.

Russell, Katie C., Donald G. Phinney, Michelle R. Lacey, Bonnie L. Barrilleaux, Kristin E. Meyertholen, and Kim C. O'Connor. 2010. "In Vitro High-Capacity Assay to Quantify the Clonal Heterogeneity in Trilineage Potential of Mesenchymal Stem Cells Reveals a Complex Hierarchy of Lineage Commitment." *STEM CELLS* 28 (4): 788-798. https://doi.org/10.1002/stem.312.

Sacchetti, Benedetto, Alessia Funari, Stefano Michienzi, Silvia Di Cesare, Stefania Piersanti, Isabella Saggio, Enrico Tagliafico et al. 2007. "Self-Renewing Osteoprogenitors in Bone Marrow Sinusoids Can Organize a Hematopoietic Microenvironment." *Cell* 131 (2): 324-336. https://doi.org/https://doi.org/10.1016/j.cell.2007.08.025.

Salemi, R., L. Falzone, G. Madonna, J. Polesel, D. Cina, D. Mallardo, P. A. Ascierto, M. Libra, and S. Candido. 2018. "Mmp-9 as a Candidate Marker of Response to Braf Inhibitors in Melanoma Patients with Braf(V600e) Mutation Detected in Circulating-Free DNA." *Front Pharmacol* 9: 856. https://doi.org/10.3389/fphar.2018.00856.

Sand, J. M. B., F. Genovese, and M. A. Karsdal. 2016. "Chapter 4 - Type Iv Collagen." In *Biochemistry of Collagens, Laminins and Elastin* ed., edited by Morten A. Karsdal, 31-41. Academic Press. https://doi.org/https://doi.org/10.1016/B978-0-12-809847-9.00004-0.

Sandri, S., F. Faiao-Flores, M. Tiago, P. C. Pennacchi, R. R. Massaro, D. K. Alves-Fernandes, G. N. Berardinelli et al. 2016. "Vemurafenib Resistance Increases Melanoma Invasiveness and Modulates the Tumor Microenvironment by Mmp-2 Upregulation." *Pharmacol Res* 111: 523-533. https://doi.org/10.1016/j.phrs.2016.07.017.

Sandru, A., S. Voinea, E. Panaitescu, and A. Blidaru. 2014. "Survival Rates of Patients with Metastatic Malignant Melanoma." *J Med Life* 7 (4): 572-6. https://www.ncbi.nlm.nih.gov/pubmed/25713625.

Satyamoorthy, K., J. Muyrers, F. Meier, D. Patel, and M. Herlyn. 2001. "Mel-Cam-Specific Genetic Suppressor Elements Inhibit Melanoma Growth and Invasion through Loss of Gap Junctional Communication." *Oncogene* 20 (34): 4676-84. https://doi.org/10.1038/sj.onc.1204616.

Schepers, Ute, and Thomas Kolter. 2001. "Rna Interference: A New Way to Analyze Protein Function." *Angewandte Chemie International Edition* 40 (13): 2437-2439. https://doi.org/10.1002/1521-3773(20010702)40:13<2437::AID-ANIE2437>3.0.CO;2-R.

Schiano, C., V. Grimaldi, A. Casamassimi, T. Infante, A. Esposito, A. Giovane, and C. Napoli. 2012. "Different Expression of Cd146 in Human Normal and Osteosarcoma Cell Lines." *Med Oncol* 29 (4): 2998-3002. https://doi.org/10.1007/s12032-012-0158-3.

Schlagbauer-Wadl, Hermine, Burkhard Jansen, Markus Müller, Peter Polterauer, Klaus Wolff, Hans-Georg Eichler, Hubert Pehamberger, Edith Konakand, and Judith P. Johnson. 1999. "Influence of Muc18/Mcam/Cd146 Expression on Human Melanoma Growth and Metastasis in Scid Mice." *Int J Cancer* 81 (6): 951-955. https://doi.org/10.1002/(SICI)1097-0215(19990611)81:6<951::AID-IJC18>3.0.CO;2-V.

Schmittgen, Thomas D., and Kenneth J. Livak. 2008. "Analyzing Real-Time Pcr Data by the Comparative Ct Method." *Nature Protocols* 3: 1101. https://doi.org/10.1038/nprot.2008.73.

Schwarz, D. G., C. T. Griffin, E. A. Schneider, D. Yee, and T. Magnuson. 2002. "Genetic Analysis of Sorting Nexins 1 and 2 Reveals a Redundant and Essential Function in Mice." *Mol Biol Cell* 13 (10): 3588-600. https://doi.org/10.1091/mbc.e02-03-0145.

Seaman, M. N. 2012. "The Retromer Complex - Endosomal Protein Recycling and Beyond." *J Cell Sci* 125 (Pt 20): 4693-702. https://doi.org/10.1242/jcs.103440.

Seftor, R. E., E. A. Seftor, N. Koshikawa, P. S. Meltzer, L. M. Gardner, M. Bilban, W. G. Stetler-Stevenson, V. Quaranta, and M. J. Hendrix. 2001. "Cooperative Interactions of Laminin 5 Gamma2 Chain, Matrix Metalloproteinase-2, and Membrane Type-1-Matrix/Metalloproteinase Are Required for Mimicry of Embryonic Vasculogenesis by Aggressive Melanoma." *Cancer Res* 61 (17): 6322-7.

Seidel, J. A., A. Otsuka, and K. Kabashima. 2018. "Anti-Pd-1 and Anti-Ctla-4 Therapies in Cancer: Mechanisms of Action, Efficacy, and Limitations." *Frontiers in oncology* 8: 86. https://doi.org/10.3389/fonc.2018.00086.

Sers, C., K. Kirsch, U. Rothbächer, G. Riethmüller, and J. P. Johnson. 1993. "Genomic Organization of the Melanoma-Associated Glycoprotein Muc18: Implications for the Evolution of the Immunoglobulin Domains." *Proceedings of the National Academy of Sciences of the United States of America* 90 (18): 8514-8518. https://doi.org/10.1073/pnas.90.18.8514.

Seyfried, T. N., and L. C. Huysentruyt. 2013. "On the Origin of Cancer Metastasis." *Crit Rev Oncog* 18 (1-2): 43-73.

Sharma, P., S. Parveen, L. V. Shah, M. Mukherjee, Y. Kalaidzidis, A. J. Kozielski, R. Rosato, J. C. Chang, and S. Datta. 2020. "Snx27-Retromer Assembly Recycles Mt1-Mmp to Invadopodia and Promotes Breast Cancer Metastasis." *The Journal of cell biology* 219 (1). https://doi.org/10.1083/jcb.201812098.

Shih, I. M., D. E. Elder, D. Speicher, J. P. Johnson, and M. Herlyn. 1994. "Isolation and Functional Characterization of the A32 Melanoma-Associated Antigen." *Cancer Res* 54 (9): 2514-20.

Shih, I. M., and R. J. Kurman. 1996. "Expression of Melanoma Cell Adhesion Molecule in Intermediate Trophoblast." *Lab Invest* 75 (3): 377-88.

Shih, I., T. Wang, T. Wu, R. J. Kurman, and J. D. Gearhart. 1998. "Expression of Mel-Cam in Implantation Site Intermediate Trophoblastic Cell Line, Ist-1, Limits Its Migration on Uterine Smooth Muscle Cells." *J Cell Sci* 111 (17): 2655. http://jcs.biologists.org/content/111/17/2655.abstract.

Shih, L. M., M. Y. Hsu, J. P. Palazzo, and M. Herlyn. 1997. "The Cell-Cell Adhesion Receptor Mel-Cam Acts as a Tumor Suppressor in Breast Carcinoma." *Am J Pathol* 151 (3): 745-51.

Shihab, H. A., J. Gough, M. Mort, D. N. Cooper, I. N. Day, and T. R. Gaunt. 2014. "Ranking Non-Synonymous Single Nucleotide Polymorphisms Based on Disease Concepts." *Hum Genomics* 8: 11. https://doi.org/10.1186/1479-7364-8-11.

Smith, K. 2001. "Theoretical Mechanisms in Targeted and Random Integration of Transgene DNA." *Reprod Nutr Dev* 41 (6): 465-85.

So, Ju-Hoon, Sung-Kook Hong, Hyun-Taek Kim, Seung-Hyun Jung, Mi-Sun Lee, Jung-Hwa Choi, Young-Ki Bae, Tetsuhiro Kudoh, Ji-Hun Kim, and Cheol-Hee Kim. 2010. "Gicerin/Cd146 Is Involved in Zebrafish Cardiovascular Development and Tumor Angiogenesis." *Genes to Cells* 15 (11): 1099-1110. https://doi.org/10.1111/j.1365-2443.2010.01448.x.

Solinet, S., K. Mahmud, S. F. Stewman, K. Ben El Kadhi, B. Decelle, L. Talje, A. Ma, B. H. Kwok, and S. Carreno. 2013. "The Actin-Binding Erm Protein Moesin Binds to and Stabilizes Microtubules at the Cell Cortex." *The Journal of cell biology* 202 (2): 251-60. https://doi.org/10.1083/jcb.201304052.

Stalin, J., K. Harhouri, L. Hubert, P. Garrigue, M. Nollet, A. Essaadi, A. Muller et al. 2016. "Soluble Cd146 Boosts Therapeutic Effect of Endothelial Progenitors through Proteolytic Processing of Short Cd146 Isoform." *Cardiovasc Res* 111 (3): 240-51. https://doi.org/10.1093/cvr/cvw096.

Stalin, J., K. Harhouri, L. Hubert, C. Subrini, D. Lafitte, J. C. Lissitzky, N. Elganfoud et al. 2013. "Soluble Melanoma Cell Adhesion Molecule (Smcam/Scd146) Promotes Angiogenic Effects on Endothelial Progenitor Cells through Angiomotin." *J Biol Chem* 288 (13): 8991-9000. https://doi.org/10.1074/jbc.M112.446518.

Stalin, J., L. Vivancos, N. Bardin, F. Dignat-George, and M. Blot-Chabaud. 2017. "Mcam and Its Isoforms as Novel Targets in Angiogenesis Research and Therapy." *Physiologic and Pathologic Angiogenesis* Signalling Mechanisms and Targeted Therapy.

Steinberg, F., M. Gallon, M. Winfield, E. C. Thomas, A. J. Bell, K. J. Heesom, J. M. Tavare, and P. J. Cullen. 2013. "A Global Analysis of Snx27-Retromer Assembly and Cargo Specificity Reveals a Function in Glucose and Metal Ion Transport." *Nat Cell Biol* 15 (5): 461-71. https://doi.org/10.1038/ncb2721.

Steinberg, F., K. J. Heesom, M. D. Bass, and P. J. Cullen. 2012. "Snx17 Protects Integrins from Degradation by Sorting between Lysosomal and Recycling Pathways." *The Journal of cell biology* 197 (2): 219-30. https://doi.org/10.1083/jcb.201111121.

Taira, E., T. Nagino, H. Taniura, N. Takaha, C. H. Kim, C. H. Kuo, B. S. Li, H. Higuchi, and N. Miki. 1995. "Expression and Functional Analysis of a Novel Isoform of Gicerin, an Immunoglobulin Superfamily Cell Adhesion Molecule." *J Biol Chem* 270 (48): 28681-7. https://doi.org/10.1074/jbc.270.48.28681.

Taira, E., T. Nagino, Y. Tsukamoto, S. Okumura, O. Muraoka, F. Sakuma, and N. Miki. 1999. "Cytoplasmic Domain Is Not Essential for the Cell Adhesion Activities of Gicerin, an Ig-Superfamily Molecule." *Exp Cell Res* 253 (2): 697-703. https://doi.org/10.1006/excr.1999.4713.

Taira, E., N. Takaha, H. Taniura, C. H. Kim, and N. Miki. 1994. "Molecular Cloning and Functional Expression of Gicerin, a Novel Cell Adhesion Molecule That Binds to Neurite Outgrowth Factor." *Neuron* 12 (4): 861-72.

Taira, Eiichi, Keiko Kohama, Yasuhiro Tsukamoto, Shigeki Okumura, and Naomasa Miki. 2004. "Characterization of Gicerin/Muc18/Cd146 in the Rat Nervous System." *Journal of Cellular Physiology* 198 (3): 377-387. https://doi.org/10.1002/jcp.10413.

Taira, Eiichi, Keiko Kohama, Yasuhiro Tsukamoto, Shigeki Okumura, and Naomasa Miki. 2005. "Gicerin/Cd146 Is Involved in Neurite Extension of Ngf-Treated Pc12 Cells." *Journal of Cellular Physiology* 204 (2): 632-637. https://doi.org/10.1002/jcp.20365.

Taira, Eiichi, Tomoko Nagino, Yasuhiro Tsukamoto, Yun Ding, Sadashige Sakuma, and Naomasa Miki. 1998. "Neurite Promotion from Ciliary Ganglion Neurons by Gicerin." *Neurochemistry International* 32 (1): 23-29. https://doi.org/https://doi.org/10.1016/S0197-0186(97)00049-1.

Tang, X., X. Chen, Y. Xu, Y. Qiao, X. Zhang, Y. Wang, Y. Guan, F. Sun, and J. Wang. 2015. "Cd166 Positively Regulates Mcam Via Inhibition to Ubiquitin E3 Ligases Smurf1 and Betatrcp through Pi3k/Akt and C-Raf/Mek/Erk Signaling in Bel-7402 Hepatocellular Carcinoma Cells." *Cell Signal* 27 (9): 1694-702. https://doi.org/10.1016/j.cellsig.2015.05.006.

Tate, J. G., S. Bamford, H. C. Jubb, Z. Sondka, D. M. Beare, N. Bindal, H. Boutselakis et al. 2019. "Cosmic: The Catalogue of Somatic Mutations in Cancer." *Nucleic acids research* 47 (D1): D941-D947. https://doi.org/10.1093/nar/gky1015.

Tavtigian, Sean V., Graham B. Byrnes, David E. Goldgar, and Alun Thomas. 2008. "Classification of Rare Missense Substitutions, Using Risk Surfaces, with Genetic- and Molecular-Epidemiology Applications." *Human mutation* 29 (11): 1342-1354. https://doi.org/10.1002/humu.20896.

Temkin, P., B. Lauffer, S. Jager, P. Cimermancic, N. J. Krogan, and M. von Zastrow. 2011. "Snx27 Mediates Retromer Tubule Entry and Endosome-to-Plasma Membrane Trafficking of Signalling Receptors." *Nat Cell Biol* 13 (6): 715-21. https://doi.org/10.1038/ncb2252.

Testa, U., G. Castelli, and E. Pelosi. 2017. "Melanoma: Genetic Abnormalities, Tumor Progression, Clonal Evolution and Tumor Initiating Cells." *Med Sci (Basel)* 5 (4). https://doi.org/10.3390/medsci5040028.

Thelen, K., T. Georg, S. Bertuch, P. Zelina, and G. E. Pollerberg. 2008. "Ubiquitination and Endocytosis of Cell Adhesion Molecule Dm-Grasp Regulate Its Cell Surface Presence and Affect Its Role for Axon Navigation." *J Biol Chem* 283 (47): 32792-801. https://doi.org/10.1074/jbc.M805896200.

Theveneau, Eric, and Roberto Mayor. 2012. "Cadherins in Collective Cell Migration of Mesenchymal Cells." *Current opinion in cell biology* 24 (5): 677-684. https://doi.org/10.1016/j.ceb.2012.08.002.

Tian, B., Y. Zhang, and N. Li. 2013. "Cd146 Protein as a Marker to Predict Postoperative Liver Metastasis in Colorectal Cancer." *Cancer Biother Radiopharm* 28 (6): 466-70. https://doi.org/10.1089/cbr.2012.1426.

Tormin, Ariane, Ou Li, Jan Claas Brune, Stuart Walsh, Birgit Schütz, Mats Ehinger, Nicholas Ditzel, Moustapha Kassem, and Stefan Scheding. 2011. "Cd146 Expression on Primary Nonhematopoietic Bone Marrow Stem Cells Is Correlated with in Situ Localization." *Blood* 117 (19): 5067-5077. https://doi.org/10.1182/blood-2010-08-304287.

Tsatmali, M., J. Ancans, and A. J. Thody. 2002. "Melanocyte Function and Its Control by Melanocortin Peptides." *J Histochem Cytochem* 50 (2): 125-33. https://doi.org/10.1177/002215540205000201.

Tseng, H. Y., N. Thorausch, T. Ziegler, A. Meves, R. Fassler, and R. T. Bottcher. 2014. "Sorting Nexin 31 Binds Multiple Beta Integrin Cytoplasmic Domains and Regulates Beta1 Integrin Surface Levels and Stability." *J Mol Biol* 426 (18): 3180-3194. https://doi.org/10.1016/j.jmb.2014.07.003.

Tu, Tao, Chunxia Zhang, Huiwen Yan, Yongting Luo, Ruirui Kong, Pushuai Wen, Zhongde Ye et al. 2015. "Cd146 Acts as a Novel Receptor for Netrin-1 in Promoting Angiogenesis and Vascular Development." *Cell Res* 25 (3): 275-287. https://doi.org/10.1038/cr.2015.15.

Tugues, S., S. Koch, L. Gualandi, X. Li, and L. Claesson-Welsh. 2011. "Vascular Endothelial Growth Factors and Receptors: Anti-Angiogenic Therapy in the Treatment of Cancer." *Mol Aspects Med* 32 (2): 88-111. https://doi.org/10.1016/j.mam.2011.04.004.

Vagnozzi, A. N., and D. Pratico. 2019. "Endosomal Sorting and Trafficking, the Retromer Complex and Neurodegeneration." *Mol Psychiatry* 24 (6): 857-868. https://doi.org/10.1038/s41380-018-0221-3.

Vainio, O., D. Dunon, F. Aïssi, J. P. Dangy, K. M. McNagny, and B. A. Imhof. 1996. "Hemcam, an Adhesion Molecule Expressed by C-Kit+ Hemopoietic Progenitors." *The Journal of cell biology* 135 (6 Pt 1): 1655-1668. https://doi.org/10.1083/jcb.135.6.1655.

Vainionpää, Noora, Yamato Kikkawa, Kari Lounatmaa, Jeffrey H. Miner, Patricia Rousselle, and Ismo Virtanen. 2006. "Laminin-10 and Lutheran Blood Group Glycoproteins in Adhesion of Human Endothelial Cells." *American Journal of Physiology-Cell Physiology* 290 (3): C764-C775. https://doi.org/10.1152/ajpcell.00285.2005.

van Weert, A. W., H. J. Geuze, B. Groothuis, and W. Stoorvogel. 2000. "Primaquine Interferes with Membrane Recycling from Endosomes to the Plasma Membrane through a Direct Interaction with Endosomes Which Does Not Involve Neutralisation of Endosomal Ph nor Osmotic Swelling of Endosomes." *Eur J Cell Biol* 79 (6): 394-9. https://doi.org/10.1078/0171-9335-00062.

Wai Wong, C., D. E. Dye, and D. R. Coombe. 2012. "The Role of Immunoglobulin Superfamily Cell Adhesion Molecules in Cancer Metastasis." *Int J Cell Biol* 2012: 340296. https://doi.org/10.1155/2012/340296.

Wang, P., Y. Luo, H. Duan, S. Xing, J. Zhang, D. Lu, J. Feng, D. Yang, L. Song, and X. Yan. 2013. "Microrna 329 Suppresses Angiogenesis by Targeting Cd146." *Molecular and cellular biology* 33 (18): 3689-99. https://doi.org/10.1128/MCB.00343-13.

Wang, W., K. B. Runkle, S. M. Terkowski, R. I. Ekaireb, and E. S. Witze. 2015. "Protein Depalmitoylation Is Induced by Wnt5a and Promotes Polarized Cell Behavior." *J Biol Chem* 290 (25): 15707-16. https://doi.org/10.1074/jbc.M115.639609.

Wang, Y. F., C. C. Jiang, K. A. Kiejda, S. Gillespie, X. D. Zhang, and P. Hersey. 2007. "Apoptosis Induction in Human Melanoma Cells by Inhibition of Mek Is Caspase-Independent and Mediated by the Bcl-2 Family Members Puma, Bim, and Mcl-1." *Clin Cancer Res* 13 (16): 4934-42. https://doi.org/10.1158/1078-0432.Ccr-07-0665.

Wang, Z., Q. Xu, N. Zhang, X. Du, G. Xu, and X. Yan. 2020. "Cd146, from a Melanoma Cell Adhesion Molecule to a Signaling Receptor." *Signal Transduct Target Ther* 5 (1): 148. https://doi.org/10.1038/s41392-020-00259-8.

Watson-Hurst, K., and D. Becker. 2006. "The Role of N-Cadherin, Mcam and Beta3 Integrin in Melanoma Progression, Proliferation, Migration and Invasion." *Cancer Biol Ther* 5 (10): 1375-82. https://doi.org/10.4161/cbt.5.10.3241.

Weeraratna, Ashani T., Yuan Jiang, Galen Hostetter, Kevin Rosenblatt, Paul Duray, Michael Bittner, and Jeffrey M. Trent. 2002. "Wnt5a Signaling Directly Affects Cell Motility and Invasion of Metastatic Melanoma." *Cancer Cell* 1 (3): 279-288. https://doi.org/https://doi.org/10.1016/S1535-6108(02)00045-4.

Welz, T., J. Wellbourne-Wood, and E. Kerkhoff. 2014. "Orchestration of Cell Surface Proteins by Rab11." *Trends Cell Biol* 24 (7): 407-15. https://doi.org/10.1016/j.tcb.2014.02.004.

Weninger, W., M. Rendl, M. Mildner, C. Mayer, J. Ban, A. Geusau, G. Bayer, A. Tanew, O. Majdic, and E. Tschachler. 2000. "Keratinocytes Express the Cd146 (Muc18/S-Endo) Antigen in Tissue Culture and During Inflammatory Skin Diseases." *J Invest Dermatol* 115 (2): 219-24. https://doi.org/10.1046/j.1523-1747.2000.00039.x.

Whittaker, S. R., J. P. Theurillat, E. Van Allen, N. Wagle, J. Hsiao, G. S. Cowley, D. Schadendorf, D. E. Root, and L. A. Garraway. 2013. "A Genome-Scale Rna Interference Screen Implicates Nf1 Loss in Resistance to Raf Inhibition." *Cancer discovery* 3 (3): 350-62. https://doi.org/10.1158/2159-8290.Cd-12-0470.

Witze, E. S., M. K. Connacher, S. Houel, M. P. Schwartz, M. K. Morphew, L. Reid, D. B. Sacks, K. S. Anseth, and N. G. Ahn. 2013. "Wnt5a Directs Polarized Calcium Gradients by Recruiting Cortical

Endoplasmic Reticulum to the Cell Trailing Edge." *Dev Cell* 26 (6): 645-57. https://doi.org/10.1016/j.devcel.2013.08.019.
Witze, E. S., E. S. Litman, G. M. Argast, R. T. Moon, and N. G. Ahn. 2008. "Wnt5a Control of Cell Polarity and Directional Movement by Polarized Redistribution of Adhesion Receptors." *Science* 320 (5874): 365-9. https://doi.org/10.1126/science.1151250.
Wu, G. J., M. W. Wu, C. Wang, and Y. Liu. 2011. "Enforced Expression of Metcam/Muc18 Increases Tumorigenesis of Human Prostate Cancer Lncap Cells in Nude Mice." *J Urol* 185 (4): 1504-12. https://doi.org/10.1016/j.juro.2010.11.052.
Wu, G. J., M. W. Wu, S. W. Wang, Z. Liu, P. Qu, Q. Peng, H. Yang et al. 2001. "Isolation and Characterization of the Major Form of Human Muc18 Cdna Gene and Correlation of Muc18 over-Expression in Prostate Cancer Cell Lines and Tissues with Malignant Progression." *Gene* 279 (1): 17-31. https://doi.org/10.1016/s0378-1119(01)00736-3.
Wu, Z., Z. Wu, J. Li, X. Yang, Y. Wang, Y. Yu, J. Ye, C. Xu, W. Qin, and Z. Zhang. 2012. "Mcam Is a Novel Metastasis Marker and Regulates Spreading, Apoptosis and Invasion of Ovarian Cancer Cells." *Tumour Biol* 33 (5): 1619-28. https://doi.org/10.1007/s13277-012-0417-0.
Xie, S., M. Luca, S. Huang, M. Gutman, R. Reich, J. P. Johnson, and M. Bar-Eli. 1997. "Expression of Mcam/Muc18 by Human Melanoma Cells Leads to Increased Tumor Growth and Metastasis." *Cancer Res* 57 (11): 2295-303.
Xu, Jinping, Wei Wang, Yvonne Kapila, Jeffrey Lotz, and Sunil Kapila. 2009. "Multiple Differentiation Capacity of Stro-1+/Cd146+ Pdl Mesenchymal Progenitor Cells." *Stem cells and development* 18 (3): 487-496. https://doi.org/10.1089/scd.2008.0113.
Xu, Wenyi, Huijuan Hua, Yueh-Ho Chiu, Guannan Li, Huihan Zhi, Zhengquan Yu, Fazheng Ren, Yongting Luo, and Wei Cui. 2019. "Cd146 Regulates Growth Factor-Induced Mtorc2 Activity Independent of the Pi3k and Mtorc1 Pathways." *Cell Reports* 29 (5): 1311-1322.e5. https://doi.org/10.1016/j.celrep.2019.09.047.
Xu, Yanjie, Jixiang Xia, Suxuan Liu, Sam Stein, Cueto Ramon, Hang Xi, Luqiao Wang et al. 2017. "Endocytosis and Membrane Receptor Internalization: Implication of F-Bar Protein Carom." *Frontiers in bioscience (Landmark edition)* 22: 1439-1457. https://doi.org/10.2741/4552.
Yadav, L., N. Puri, V. Rastogi, P. Satpute, and V. Sharma. 2015. "Tumour Angiogenesis and Angiogenic Inhibitors: A Review." *J Clin Diagn Res* 9 (6): Xe01-xe05. https://doi.org/10.7860/jcdr/2015/12016.6135.
Yan, Xiyun, Yun Lin, Dongling Yang, Yi Shen, Mei Yuan, Zhiqiang Zhang, Peiyu Li et al. 2003. "A Novel Anti-Cd146 Monoclonal Antibody, Aa98, Inhibits Angiogenesis and Tumor Growth." *Blood* 102 (1): 184. https://doi.org/10.1182/blood-2002-04-1004.
Yang, H., S. Wang, Z. Liu, M. H. Wu, B. McAlpine, J. Ansel, C. Armstrong, and G. Wu. 2001. "Isolation and Characterization of Mouse Muc18 Cdna Gene, and Correlation of Muc18 Expression in Mouse Melanoma Cell Lines with Metastatic Ability." *Gene* 265 (1-2): 133-45. https://doi.org/10.1016/s0378-1119(01)00349-3.
Ye, Zhongde, Chunxia Zhang, Tao Tu, Min Sun, Dan Liu, Di Lu, Jing Feng, Dongling Yang, Feng Liu, and Xiyun Yan. 2013. "Wnt5a Uses Cd146 as a Receptor to Regulate Cell Motility and Convergent Extension." *Nature Communications* 4: 2803. https://doi.org/10.1038/ncomms3803

https://www.nature.com/articles/ncomms3803#supplementary-information.
Zabouo, Gwladys, Anne-Marie Imbert, Jocelyne Jacquemier, Pascal Finetti, Thomas Moreau, Benjamin Esterni, Daniel Birnbaum, François Bertucci, and Christian Chabannon. 2009. "Cd146 Expression Is Associated with a Poor Prognosis in Human Breast Tumors and with Enhanced Motility in Breast Cancer Cell Lines." *Breast Cancer Research* 11 (1): R1. https://doi.org/10.1186/bcr2215.
Zeng, Ping, Hai Li, Pei-Hua Lu, Li-Na Zhou, Min Tang, Chao-Ying Liu, and Min-Bin Chen. 2017. "Prognostic Value of Cd146 in Solid Tumor: A Systematic Review and Meta-Analysis." *Scientific Reports* 7 (1): 4223. https://doi.org/10.1038/s41598-017-01061-3.
Zeng, Q., Z. Wu, H. Duan, X. Jiang, T. Tu, D. Lu, Y. Luo et al. 2014. "Impaired Tumor Angiogenesis and Vegf-Induced Pathway in Endothelial Cd146 Knockout Mice." *Protein Cell* 5 (6): 445-56. https://doi.org/10.1007/s13238-014-0047-y.

Zeng, Qiqun, Weidong Li, Di Lu, Zhenzhen Wu, Hongxia Duan, Yongting Luo, Jing Feng, Dongling Yang, Li Fu, and Xiyun Yan. 2012. "Cd146, an Epithelial-Mesenchymal Transition Inducer, Is Associated with Triple-Negative Breast Cancer." *Proceedings of the National Academy of Sciences* 109 (4): 1127. https://doi.org/10.1073/pnas.1111053108.

Zhan, X. Y., Y. Zhang, E. Zhai, Q. Y. Zhu, and Y. He. 2018. "Sorting Nexin-1 Is a Candidate Tumor Suppressor and Potential Prognostic Marker in Gastric Cancer." *PeerJ* 6: e4829. https://doi.org/10.7717/peerj.4829.

Zhang, F., S. I. Thornhill, S. J. Howe, M. Ulaganathan, A. Schambach, J. Sinclair, C. Kinnon, H. B. Gaspar, M. Antoniou, and A. J. Thrasher. 2007. "Lentiviral Vectors Containing an Enhancer-Less Ubiquitously Acting Chromatin Opening Element (Ucoe) Provide Highly Reproducible and Stable Transgene Expression in Hematopoietic Cells." *Blood* 110 (5): 1448-57. https://doi.org/10.1182/blood-2006-12-060814.

Zhang, Hongfeng, Timothy Huang, Yujuan Hong, Weijie Yang, Xian Zhang, Hong Luo, Huaxi Xu, and Xin Wang. 2018. "The Retromer Complex and Sorting Nexins in Neurodegenerative Diseases." *Frontiers in aging neuroscience* 10: 79-79. https://doi.org/10.3389/fnagi.2018.00079.

Zhang, J., K. Li, Y. Zhang, R. Lu, S. Wu, J. Tang, Y. Xia, and J. Sun. 2019. "Deletion of Sorting Nexin 27 Suppresses Proliferation in Highly Aggressive Breast Cancer Mda-Mb-231 Cells in Vitro and in Vivo." *BMC Cancer* 19 (1): 555. https://doi.org/10.1186/s12885-019-5769-z.

Zhang, P., Y. Wu, T. Y. Belenkaya, and X. Lin. 2011. "Snx3 Controls Wingless/Wnt Secretion through Regulating Retromer-Dependent Recycling of Wntless." *Cell Res* 21 (12): 1677-90. https://doi.org/10.1038/cr.2011.167.

Zhang, S., Z. Yang, W. Bao, L. Liu, Y. You, X. Wang, L. Shao et al. 2020. "Snx10 (Sorting Nexin 10) Inhibits Colorectal Cancer Initiation and Progression by Controlling Autophagic Degradation of Src." *Autophagy* 16 (4): 735-749. https://doi.org/10.1080/15548627.2019.1632122.

Zhang, X., Z. Wang, Y. Kang, X. Li, X. Ma, and L. Ma. 2014. "Mcam Expression Is Associated with Poor Prognosis in Non-Small Cell Lung Cancer." *Clin Transl Oncol* 16 (2): 178-83. https://doi.org/10.1007/s12094-013-1057-6.

Zhang, Z., M. C. Miller, X. Xu, C. Song, F. Zhang, Y. Zheng, Y. Zhou, G. Tai, and K. H. Mayo. 2019. "Nmr-Based Insight into Galectin-3 Binding to Endothelial Cell Adhesion Molecule Cd146: Evidence for Noncanonical Interactions with the Lectin's Crd Beta-Sandwich F-Face." *Glycobiology* 29 (8): 608-618. https://doi.org/10.1093/glycob/cwz036.

Zhang, Z., Y. Zheng, H. Wang, Y. Zhou, and G. Tai. 2018. "Cd146 Interacts with Galectin-3 to Mediate Endothelial Cell Migration." *FEBS Lett* 592 (11): 1817-1828. https://doi.org/10.1002/1873-3468.13083.

Zhang, Z., S. Zhu, Y. Yang, X. Ma, and S. Guo. 2015. "Matrix Metalloproteinase-12 Expression Is Increased in Cutaneous Melanoma and Associated with Tumor Aggressiveness." *Tumour Biol* 36 (11): 8593-600. https://doi.org/10.1007/s13277-015-3622-9.

Zheng, B., K. Ohuchida, Y. Chijiiwa, M. Zhao, Y. Mizuuchi, L. Cui, K. Horioka et al. 2016. "Cd146 Attenuation in Cancer-Associated Fibroblasts Promotes Pancreatic Cancer Progression." *Mol Carcinog* 55 (11): 1560-1572. https://doi.org/10.1002/mc.22409.

Zheng, C., Y. Qiu, Q. Zeng, Y. Zhang, D. Lu, D. Yang, J. Feng, and X. Yan. 2009. "Endothelial Cd146 Is Required for in Vitro Tumor-Induced Angiogenesis: The Role of a Disulfide Bond in Signaling and Dimerization." *Int J Biochem Cell Biol* 41 (11): 2163-72. https://doi.org/10.1016/j.biocel.2009.03.014.

Zhou, Yun, He Huang, Lin-Jing Yuan, Ying Xiong, Xin Huang, Jia-Xin Lin, and Min Zheng. 2015. "Cd146 as an Adverse Prognostic Factor in Uterine Sarcoma." *European journal of medical research* 20 (1): 67-67. https://doi.org/10.1186/s40001-015-0160-2.

Zhuang, J., T. Jiang, D. Lu, Y. Luo, C. Zheng, J. Feng, D. Yang, C. Chen, and X. Yan. 2010. "Nadph Oxidase 4 Mediates Reactive Oxygen Species Induction of Cd146 Dimerization in Vegf Signal Transduction." *Free Radic Biol Med* 49 (2): 227-36. https://doi.org/10.1016/j.freeradbiomed.2010.04.007.

Zigler, M., G. J. Villares, A. S. Dobroff, H. Wang, L. Huang, R. R. Braeuer, T. Kamiya et al. 2011. "Expression of Id-1 Is Regulated by Mcam/Muc18: A Missing Link in Melanoma Progression." *Cancer Res* 71 (10): 3494-504. https://doi.org/10.1158/0008-5472.Can-10-3555.

Zoni, Eugenio, Letizia Astrologo, Charlotte K. Y. Ng, Salvatore Piscuoglio, Janine Melsen, Joël Grosjean, Irena Klima et al. 2019. "Therapeutic Targeting of Cd146/Mcam Reduces Bone Metastasis in Prostate Cancer." *Molecular Cancer Research* 17 (5): 1049. https://doi.org/10.1158/1541-7786.MCR-18-1220.

8.0 APPENDICES

8.1 Appendix 1: MCAM mRNA and protein sequence

8.1.2 MCAM mRNA Sequence

NCBI accession number NM_006500

```
   1 acttgcgtct cgccctccgg ccaagcatgg ggcttcccag gctggtctgcgccttcttgc
  61 tcgccgcctg ctgctgctgt cctcgcgtcg cgggtgtgcc cggagaggctgagcagcctg
 121 cgcctgagct ggtggaggtg gaagtgggca gcacagccct tctgaagtgcggcctctccc
 181 agtcccaagg caacctcagc catgtcgact ggttttctgt ccacaaggagaagcggacgc
 241 tcatcttccg tgtgcgccag ggccagggcc agagcgaacc tggggagtacgagcagcggc
 301 tcagcctcca ggacagaggg gctactctgg ccctgactca agtcacccccaagacgagc
 361 gcatcttctt gtgccagggc aagcgccctc ggtcccagga gtaccgcatccagctccgcg
 421 tctacaaagc tccggaggag ccaaacatcc aggtcaaccc cctgggcatccctgtgaaca
 481 gtaaggagcc tgaggaggtc gctacctgtg tagggaggaa cgggtaccccattcctcaag
 541 tcatctggta caagaatggc cggcctctga aggaggagaa gaaccgggtccacattcagt
 601 cgtcccagac tgtggagtcg agtggtttgt acaccttgca gagtattctgaaggcacagc
 661 tggttaaaga agacaaagat gcccagtttt actgtgagct caactaccggctgcccagtg
 721 ggaaccacat gaaggagtcc agggaagtca ccgtccctgt tttctacccgacagaaaaag
 781 tgtggctgga agtggagccc gtgggaatgc tgaaggaagg ggaccgcgtggaaatcaggt
 841 gtttggctga tggcaaccct ccaccacact tcagcatcag caagcagaaccccagcacca
 901 gggaggcaga ggaagagaca accaacgaca acggggtcct ggtgctggagcctgcccgga
 961 aggaacacag tgggcgctat gaatgtcagg cctggaactt ggacaccatgatatcgctgc
1021 tgagtgaacc acaggaacta ctggtgaact atgtgtctga cgtccgagtgagtcccgcag
1081 cccctgagag acaggaaggc agcagcctca ccctgacctg tgaggcagagagtagccagg
1141 acctcgagtt ccagtggctg agagaagaga cagaccaggt gctggaaaggggggcctgtgc
1201 ttcagttgca tgacctgaaa cgggaggcag gaggcggcta tcgctgcgtggcgtctgtgc
1261 ccagcatacc cggcctgaac cgcacacagc tggtcaagct ggccatttttggccccccctt
```

1321 ggatggcatt caaggagagg aaggtgtggg tgaaagagaa tatggtgttgaatctgtctt

1381 gtgaagcgtc agggcacccc cggcccacca tctcctggaa cgtcaacggcacggcaagtg

1441 aacaagacca agatccacag cgagtcctga gcaccctgaa tgtcctcgtgaccccggagc

1501 tgttggagac aggtgttgaa tgcacggcct ccaacgacct gggcaaaaacaccagcatcc

1561 tcttcctgga gctggtcaat ttaaccaccc tcacaccaga ctccaacacaaccactggcc

1621 tcagcacttc cactgccagt cctcatacca gagccaacag cacctccacagagagaaagc

1681 tgccggagcc ggagagccgg ggcgtggtca tcgtggctgt gattgtgtgcatcctggtcc

1741 tggcggtgct gggcgctgtc ctctatttcc tctataagaa gggcaagctgccgtgcaggc

1801 gctcagggaa gcaggagatc acgctgcccc cgtctcgtaa gaccgaacttgtagttgaag

1861 ttaagtcaga taagctccca gaagagatgg gcctcctgca gggcagcagcggtgacaaga

1921 gggctccggg agaccaggga gagaaataca tcgatctgag gcattagccccgaatcactt

1981 cagctccctt ccctgcctgg accattccca gctccctgct cactcttctctcagccaaag

2041 cctccaaagg gactagagag aagcctcctg ctcccctcac ctgcacacccccctttcagag

2101 ggccactggg ttaggacctg aggacctcac ttggccctgc aagccgcttttcagggacca

2161 gtccaccacc atctcctcca cgttgagtga agctcatccc aagcaaggagccccagtctc

2221 ccgagcgggt aggagagttt cttgcagaac gtgtttttttc tttacacacattatggctgt

2281 aaatacctgg ctcctgccag cagctgagct gggtagcctc tctgagctggtttcctgccc

2341 caaaggctgg cttccaccat ccaggtgcac cactgaagtg aggacacaccggagccaggc

2401 gcctgctcat gttgaagtgc gctgttcaca cccgctccgg agagcaccccagcggcatcc

2461 agaagcagct gcagtgttgc tgccaccacc ctcctgctcg cctcttcaaagtctcctgtg

2521 acatttttttc tttggtcaga agccaggaac tggtgtcatt ccttaaaagatacgtgccgg

2581 ggccaggtgt ggtggctcac gcctgtaatc ccagcacttt gggaggccgaggcgggcgga

2641 tcacaaagtc aggacgagac catcctggct aacacggtga aaccctgtctctactaaaaa

2701 tacaaaaaaa aattagctag gcgtagtggt tggcacctat agtcccagctactcggaagg

2761 ctgaagcagg agaatggtat gaatccagga ggtggagctt gcagtgagccgagaccgtgc

2821 cactgcactc cagcctgggc aacacagcga gactccgtct cgaggaaaaaaaaagaaaag

2881 acgcgtacct gcggtgagga agctgggcgc tgttttcgag ttcaggtgaattagcctcaa

2941 tccccgtgtt cacttgctcc catagccctc ttgatggatc acgtaaaactgaaaggcagc

3001 ggggagcaga caaagatgag gtctacactg tccttcatgg ggattaaagctatggttata

3061 ttagcaccaa acttctacaa accaagctca gggccccaac cctagaagggcccaaatgag

```
3121 agaatggtac ttagggatgg aaaacggggc ctggctagag cttcgggtgtgtgtgtctgt
3181 ctgtgtgtat gcatacatat gtgtgtatat atggttttgt caggtgtgtaaatttgcaaa
3241 ttgtttcctt tatatatgta tgtatatata tatatgaaaa tatatatatatatgaaaaat
3301 aaagcttaat tgtcccagaa aatcatacat tgctttttta ttctacatgggtaccacagg
3361 aacctggggg cctgtgaaac tacaaccaaa aggcacacaa aaccgtttccagttggcagc
3421 agagatcagg ggttacctct gcttctgagc aaatggctca agctctaccagagcagacag
3481 ctaccctact tttcagcagc aaaacgtccc gtatgacgca gcacgaagggcctggcaggc
3541 tgttagcagg agctatgtcc cttcctatcg tttccgtcca ctt
```

8.1.2 MCAM protein Sequence

NCBI accession number NP_006491.1

MGLPRLVCAFLLAACCCCPRVAGVPGEAEQPAPELVEVEVGSTALLKCGLSQSQGNLSHVDWFSVHKE
KRTLIFRVRQGQGQSEPGEYEQRLSLQDRGATLALTQVTPQDERIFLCQGKRPRSQEYRIQLRVYKAPEE
PNIQVNPLGIPVNSKEPEEVATCVGRNGYPIPQVIWYKNGRPLKEEKNRVHIQSSQTVESSGLYTLQSILK
AQLVKEDKDAQFYCELNYRLPSGNHMKESREVTVPVFYPTEKVWLEVEPVGMLKEGDRVEIRCLADGN
PPPHFSISKQNPSTREAEEETTNDNGVLVLEPARKEHSGRYECQAWNLDTMISLLSEPQELLVNYVSDVR
VSPAAPERQEGSSLTLTCEAESSQDLEFQWLREETDQVLERGPVLQLHDLKREAGGGYRCVASVPSIPGL
NRTQLVKLAIFGPPWMAFKERKVWVKENMVLNLSCEASGHPRPTISWNVNGTASEQDQDPQRVLSTL
NVLVTPELLETGVECTASNDLGKNTSILFLELVNLTTLTPDSNTTTGLSTSTASPHTRANSTSTERKLPEPES
RGVVIVAVIVCILVLAVLGAVLYFLYKKGKLPCRRSGKQEITLPPSRKTELVVEVKSDKLPEEMGLLQGSSG
DKRAPGDQGEKYIDLRH

8.2 Appendix 2: qPCR Efficiency Calculations

Appendix 2. qPCR efficiency calculations.

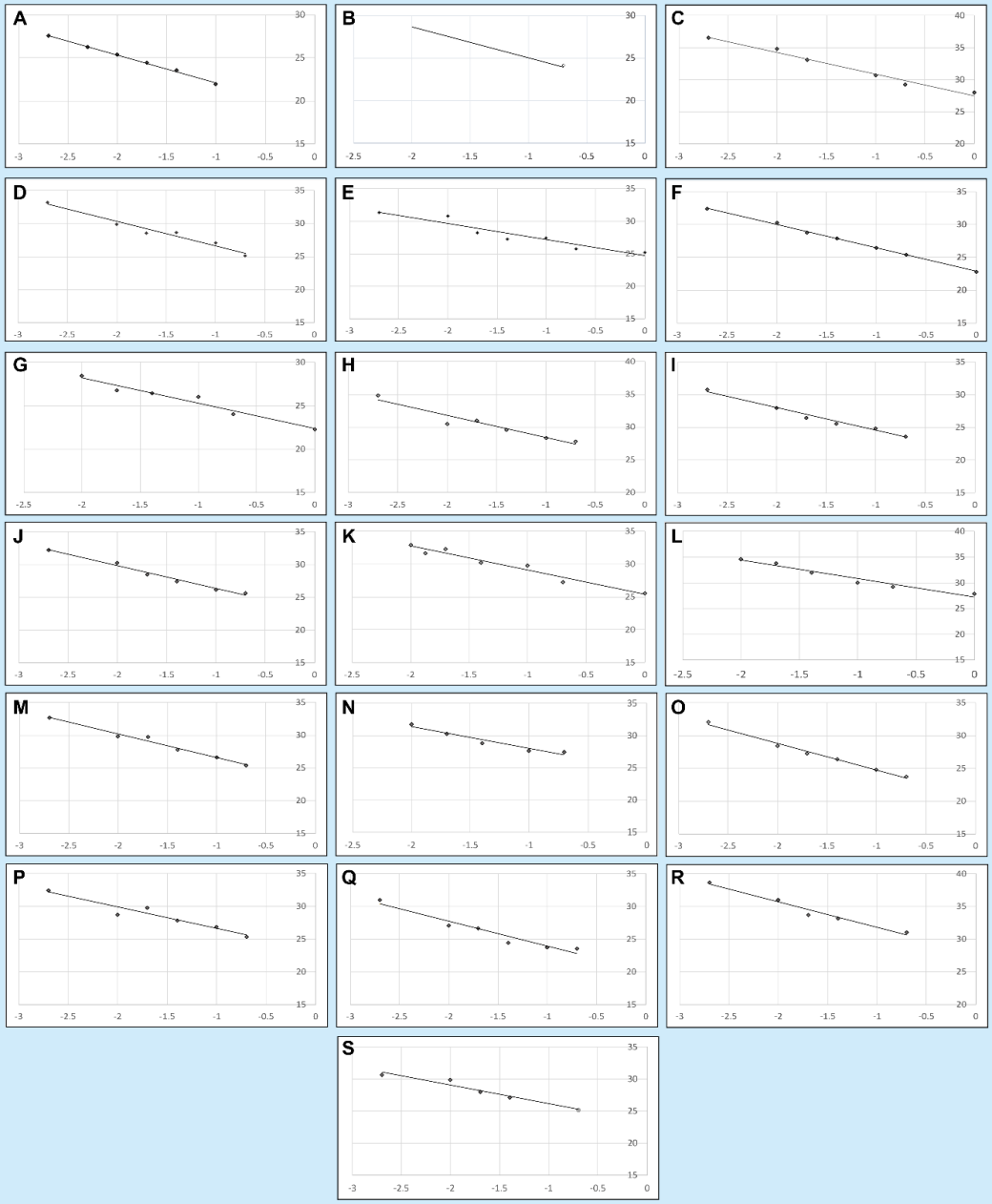

Appendix 2. qPCR primer efficiency graphs. (A) ACTAB **(B)** GAPDH **(C)** TBP **(D)** SDHA **(E)** SNX1 **(F)** SNX2 **(G)** SNX3 **(H)** SNX4 **(I)** SNX5 **(J)** SNX6 **(K)** SNX17 **(L)** SNX18 **(M)** VPS26A **(N)** VPS26B **(O)** VPS29 **(P)** VPS35 **(Q)** RAB7A **(R)** MCAM-S **(S)** MCAM-L. Y axis = PCR cycle number, X axis = log scale dilution factor.